

THE DEVELOPMENT OF CHEMICAL TOOLS
FOR INVESTIGATING THE FUNCTIONAL ROLES OF
THE POLY(ADP-RIBOSE) POLYMERASE (PARP) FAMILY

By

Rory Kyle Morgan

A DISSERTATION

Presented to the Department of Physiology & Pharmacology
and the Oregon Health & Science University

School of Medicine

in partial fulfillment of the requirements for the degree of

Doctor of Philosophy

August 2017

School of Medicine

Oregon Health & Science University

CERTIFICATE OF APPROVAL

This is to certify that the PhD dissertation of

Rory Kyle Morgan

has been approved

Michael Cohen, Ph.D. (Mentor)

Thomas Scanlan, Ph.D. (Committee Chair)

Kimberly Beatty, Ph.D. (Member)

David Farrens, Ph.D. (Member)

Xiangshu Xiao, Ph.D. (Member)

TABLE OF CONTENTS

Chapter 1: Introduction	1
Summary	2
ADP-ribosylation	3
NAD ⁺ -consuming Enzymes	3
ADPr Overview	4
A History of Mono-ADPr and Bacterial Toxins	5
Mammalian ADPr: Ecto-ARTs and PARPs	7
The PARP Family	8
PARP Classification	9
A Focus on Mono-ADPr PARP Biology	10
Chemical Tools for Studying PARPs	12
Identifying Protein Targets of Individual PARPs	12
A Chemical Genetics Strategy for Identifying Protein Targets	14
Detecting Cellular ADPr	17
Developing Selective Inhibitors of Individual PARP Family Members	18
A Chemical Genetics Strategy for Selective Inhibition of PARPs	21
Rational Design Strategies for Selective Inhibition of PARPs	22
Dissertation Overview	24
Chapter 2: Development of Orthogonal NAD⁺ Analogue-Engineered PARP Pairs	26
Abstract	27
Introduction	28
Results and Discussion	30
Part I: Development of a chemical genetics strategy for the poly-ADPr subclass of PARPs	30
PARP1 can be engineered with a unique inhibitor-sensitizing mutation within the nicotinamide-binding site	33

A C-5-ethyl-modified NAD ⁺ analogue (5-Et-6-a-NAD ⁺) is selectively used by engineered poly-ADPr PARPs	34
Orthogonal NAD ⁺ analogue-engineered poly-ADPr PARP pairs can be used to identify family-member specific PARP protein targets	37
Part II: Development of a chemical genetics strategy for the mono-ADPr subclass of PARPs	37
C-5-substituted 6-a-NAD ⁺ analogues are not used by ‘ceiling’ position mutants of PARP10	39
A C-5-benzyl-substituted 6-a-NAD ⁺ analogue is selectively used by a ‘floor’ position mutant in PARP10	40
Mutating the floor position in other mono-ADPr PARPs confers sensitivity with 5-Bn-6-a-NAD ⁺	41
Orthogonal NAD ⁺ analogue-engineered mono-ADPr PARP pairs can be used to identify family-member specific PARP protein targets	43
Conclusions and Future Directions	43
Experimental	45
Chemical Synthesis	45
Other Methods	59
Chapter 3: A Clickable Aminooxy Probe for Monitoring Cellular ADP-ribosylation	65
Abstract	66
Introduction	67
Results and Discussion	67
Design of a clickable aminooxy probe for detection of ADP-ribosylated acidic residues	67
AO-alkyne reacts with an aldehyde on Glu/Asp-ADP-ribose to form an oxime	68
An aldehyde exists at the C1'-position of Glu/Asp-ADP-ribose capable of reacting with aminooxy probes.....	70
Functional studies with aminooxy probes support a previously reported model of MacroD-mediated reversal of Glu/Asp-ADP-ribose	73
AO-alkyne detects PARP10 automodification in cells	74
AO-alkyne detects automodification of PARP11 on acidic residues	76
AO-alkyne detects stimulus-induced endogenous ADP-ribosylation.....	77
An improved 2,4-dimethoxyaniline catalyst for detecting protein ADPr using AO-alkyne	79
Conclusions and Future Directions	80

Experimental	83
Chemical Synthesis	83
Other Methods	85
Chapter 4: Development of a Chemical Genetics Strategy for Selective Inhibition of PARP10	93
Abstract	94
Introduction	95
Results and Discussion	96
Structural data guides the design of a chemical genetics strategy.....	96
Synthesis of C-7 substituted dihydroisoquinolin-1(2 <i>H</i>)-ones.....	98
C-7 substituted dq analogues are selective for LG-PARP10.....	99
A 7-Br substituted dq compound selectively inhibits full-length PARP10 ...	102
PARP10 L926G mutation does not perturb activity in cells	103
A 7-iodo substituted dq compound exhibits similar selectivity	104
Transfer of bromo group to different inhibitor scaffolds maintains selectivity	105
Selectivity of compounds observed in vitro does not translate in cells	106
Conclusions and Future Directions	108
Experimental	110
Chemical Synthesis	110
Other Methods	119
Chapter 5: Rational Design Strategies for Selective Inhibition of PARP10	125
Abstract	126
Introduction	127
Results and Discussion	128
Strategy 1: Targeting a hydrophobic subpocket within the nicotinamide-binding site of PARP10	128
A 6-phenyl substituted dq compound is selective for PARP10 over PARP11	131
Meta-position modifications at the 6-position phenyl group of dq increase selectivity for PARP10 over PARP11	133
Combined 5- and 6-position modifications on dq further increase selectivity for PARP10 over PARP11	134
Substitution of 6-position phenyl group for a pyridinyl group on dq increases solubility while still maintaining PARP10 selectivity	134

A 6-position trifluoromethyl-modified pyridinyl group on dq is the most selective modification for PARP10	135
Compound 5.22 inhibits PARP10 auto-ADP-ribosylation in cells	138
Compound 5.22 is >10-fold selective for PARP10 with activity in cells	139
Strategy 2: Targeting a noncatalytic, nonconserved cysteine residue on the D-loop of PARP10.....	140
An <i>N</i> -(2-ethyl)acrylamide-substituted mq probe is potent toward PARP10	143
Conclusions and Future Directions	143
Experimental	146
Chemistry Methods	146
Other Methods	165
Chapter 6: Concluding Remarks	171
References	176
Appendix A: Protocol for Detecting Protein ADP-ribosylation Using a Clickable Aminooxy Probe	193
Appendix B: Table of IC₅₀ Values for Additional dq Compounds	201
Appendix C: ¹H and ¹³C NMR Spectra	203

Acknowledgments

The path of graduate school is long and arduous, often amounting to more failures than successes. A strong support network is critical for pushing past the bumps in the road to emerge successful on the other side. I was taught in graduate school that all data is good data, whether or not it supports our hypothesis. Something can be gleaned from every experiment. I would like to thank my graduate advisor Mike Cohen for teaching me this philosophy. His determination and attention to scientific detail has shown me how to persevere even when projects appear to have come to a standstill. Being his first graduate student, I am thankful for his belief in my abilities and making me think in a way that pushes scientific boundaries.

I would also like to thank my lab members, both past and present. As the first and only graduate student in the lab, I would like to thank Ian, Jeff, and Haihong for guiding me along the way. Jeff taught me the ins and outs of cell culture and microscopy, both techniques that were very new to me. Haihong offered her medicinal chemistry expertise, and on many occasions, always knew just the right conditions to optimize a reaction or purification. I want to especially thank Ian, who took me under his wing, and taught me a vast amount of molecular biology and biochemistry techniques. I have become a well-rounded scientist from our insightful discussions and collaborations. His techniques and tricks will stay with me as I enter into my next scientific chapter. I would also like to thank Madison for her time in the lab. She was willing to do anything, even when cloning projects were thrown at her from every direction.

I would also like to thank the current members of the lab for their constant support and willingness to help. I would to thank Ilsa for her determination and hard-work. I greatly appreciate her vast amount of protein preps and assay optimization to move both our projects forward. I would like to thank Anke for her willingness to help with anything, especially cell culture, assays, and always following up on our orders. I would like to thank Kelsie for bringing a much-needed energy to the lab. Her laugh always brought a smile to everyone's face even when experiments were not necessarily cooperating that day.

I would like thank the members of my dissertation advisory committee: Prof. Tom Scanlan, Prof. Kimberly Beatty, and Prof. Dave Farrens, for their mentorship and guidance. I would also like to thank Prof. Xiangshu Xiao for serving on my defense committee. Graduate school can be an isolating experience, but their belief and constant support allowed to me push forward.

I would like to thank my ARCS donors Dick and Deanne Rubinstein and Bob and Kathleen Ames for their continued support and conviction in my dissertation studies. It was a pleasure having somebody cheer me along the way and truly believe in my research.

I am thankful for my family, who has always believed in my decisions. I am most grateful for my partner, Ryan. He has supported me when experiments have failed and my motivation has faded. He has the uncanny ability to make me smile in any situation. He is my best cheerleader and always reminds me of my potential even when my judgment may be clouded. I am truly grateful for his patience, support, and encouragement throughout my dissertation studies.

List of Figures and Schemes

Figure 1-1. ADP-ribosylation (ADPr) is the transfer of ADP-ribose onto amino acids (X = Asp, Glu, Arg, Lys, Cys, Ser, Asn) of target proteins.....	5
Figure 1-2. Steric complementation chemical genetics strategy (bump-hole approach).	15
Figure 1-3. PARP inhibitors approved by the FDA.....	19
Figure 2-1. Schematic for the design of modified NAD ⁺ analogs that are preferentially utilized by engineered PARPs.....	30
Figure 2-2. (a) The key residue, K903, in PARP1 near the C-5 position of 3-methoxybenzamide. (b) Sequence alignment of the nicotinamide binding site of the poly-ADPr PARPs.....	31
Scheme 2-1. Synthesis of C-5 substituted nicotinamide analogs 2.3 , 2.5 , and 2.6	32
Scheme 2-2. Synthesis of C-5 substituted nicotinamide analogs 2.7 and 2.8	32
Scheme 2-3. Synthesis of 6-a-NAD ⁺	33
Figure 2-3. Comparative inhibition of WT-PARP1 and KA-PARP1 by select nicotinamide analogues.....	34
Scheme 2-4. Synthesis of 5-Et-6-a-NAD ⁺ (2.1)	35
Figure 2-4. Orthogonal auto-ADPr of sensitized PARPs using modified NAD ⁺ variants.	36
Figure 2-5. Poly-ADPr and mono-ADPr PARPs differ at key amino acid residues.	38
Figure 2-6. Profiling of PARP10 variants with NAD ⁺ analogues.....	40
Figure 2-7. Lysate labeling by IG-PARP10 or IG-PARP11 in the presence of 5-Bn-6-a-NAD ⁺	42

Scheme 3-1. Synthesis of AO-alkyne (3.1)	68
Figure 3-1. AO-alkyne, a clickable aminooxy probe that can detect ADPr of acidic amino acids	69
Figure 3-2. PARP10 _{cat} and PARP15 _{cat} -mediated ADP-ribosylation of SRPK2 <i>in vitro</i> is detected by 3.1 following click conjugation with rhodamine-azide.....	70
Figure 3-3. AO-alkyne reveals an unanticipated mechanism of ADPr on acidic residues. (a) Proposed mechanism of PARP catalyzed ADPr of acidic residues	71
Figure 3-4. AO-alkyne detects auto-ADPr of PARP10 in cells	74
Figure 3-5. Labeling of ADP-ribosylated GFP-PARP10 by 3.1 is most efficient with PDA catalysis.	75
Figure 3-6. Detection of PARP11 activity in cells with 3.1	77
Figure 3-7. AO-alkyne detects ADP-ribose modification catalyzed by endogenous PARPs activated during oxidative stress	78
Figure 3-8. Optimized labeling conditions for detection of auto-ADPr of GFP-PARP10 in HEK293T cells using AO-alkyne and DMA	79
Figure 3-9. Quantification of PARP10 labeling under glycohydrolase knockout U-2 OS cell lines.....	82
Figure 4-1. A chemical genetics strategy for generating selective inhibitors of PARP10.....	97
Figure 4-2. LG-PAPR10 _{cat} exhibits similar activity to WT-PARP10 _{cat}	98
Scheme 4-1. Synthesis of analogue 4.2 via intramolecular aromatic substitution reaction.....	99
Scheme 4-2. Syntheses of analogues 4.3 – 4.8 via Schmidt reaction	99
Figure 4-3. C-7 substituted dq analogues selectively inhibit LG-PARP10 _{cat}	100

Figure 4-4. Screening of C7-substituted dq analogues against WT-PARP10 _{cat}	101
Figure 4-5. Screening of C7-substituted dq analogues against WT-PARP1	102
Figure 4-6. 7-Br-dq (4.4) selectively inhibits the auto-ADPr activity of full-length LG-PARP10.....	103
Figure 4-7. Cellular auto-ADPr activity of GFP-tagged full-length LG-PARP10 is similar to WT-PARP10, as measured in cells using AO-alkyne.....	104
Scheme 4-3. Synthesis of 7-I-dq analogue 4.12	104
Scheme 4-4. Synthesis of 7-Br-5-Me-dq (4.15).....	105
Scheme 4-5. Synthesis of 8-Br-TIL (4.18).....	106
Figure 4-8. Compounds 4.15 and 4.18 do not maintain selectivity for full-length LG-PARP10 versus WT-PARP10 in cells	107
Figure 5-1. Rational design of a selective inhibitor of PARP10 based on a 3,4-dihydroisoquinolin-1(2 <i>H</i>)-one scaffold	129
Scheme 5-1. Synthesis of 3,4-dihydroisoquinolin-1(2 <i>H</i>)-ones with modifications at the 5- and 6-position	131
Figure 5-2. Compound 5.22 inhibits PARP10-dependent ADPr in cells.....	139
Figure 5-3. Development of electrophilic probes targeting C907 of PARP10 ..	140
Figure 5-4. Potential second generation electrophilic probe for selective inhibition of PARP10.....	145

List of Tables

Table 4-1. C-7 substituted dq analogues selectively inhibit the engineered PARP10 mutant, LG-PARP10 _{cat}	101
Table 4-2. Bromo-substituted analogues selectively inhibit the engineered PARP10 mutant, LG-PARP10 _{cat}	106
Table 5-1. <i>In vitro</i> IC ₅₀ values for selected 5- and 6-substituted dq compounds against PARP10 _{cat} and PARP11	132
Table 5-2. <i>In vitro</i> IC ₅₀ values for 5.20 – 5.24 against PARP10 _{cat} and PARP11	136
Table 5-3. Selectivity profile of 5.22 against PARP family members	137
Table B-1. Approximate IC ₅₀ values for additional dq compounds not appearing in Chapter 5	201

Abstract

The poly(ADP-ribose) polymerase (PARP) family catalyzes the post-translational modification known as ADP-ribosylation (ADPr) from donor molecule nicotinamide adenine dinucleotide (NAD^+). The PARP family consists of 17 members (in humans) based upon a conserved catalytic domain. The family is further divided based on whether they catalyze mono-ADPr, the transfer of a single ADP-ribose to protein targets, or poly-ADPr, the transfer of additional ADP-ribose units onto the initial ADP-ribose modification. The poly-ADPr PARPs have been extensively studied, most notably PARP1 and PARP2, for their involvement in DNA damage recognition and repair. The mono-ADPr PARPs have only recently been investigated in various roles throughout the cell. Their study has been limited mostly to knockdown techniques to identify cellular phenotypes. These genetic approaches remove the PARP from the cellular system and do not provide the ability to identify specific targets of PARPs, nor do they allow a dynamic study of PARP biology. They also preclude the ability to connect PARP catalytic activity to a given process without ruling out other domain features within PARPs.

In my dissertation research, I developed chemical tools to circumvent the current limitations that are preventing a detailed study of mono-ADPr PARP biology. Previous studies to identify targets of PARPs can only detect global ADP-ribosylation; whereas, I have synthesized modified NAD^+ analogues that are selectively used by engineered PARPs. These orthogonal NAD^+ analogue-engineered PARP pairs can be used to identify direct protein targets of a single

PARP among the entire PARP family, enabling the connection of an observed PARP phenotype to a specific ADP-ribosylated protein target (Chapter 2). Previous methods to identify cellular ADPr rely on techniques that must be applied post-lysis or on fixed cells. I have developed a chemical probe that can be delivered to cells to provide a snapshot of ADPr levels in a given time window, which is more physiologically relevant than previously used methods (Chapter 3). Lastly, I developed chemical probes that can be used to modulate the activity of a specific PARP among the entire PARP family. I utilized a chemical genetics strategy to engineer PARP10 to use an orthogonal chemical probe that is not used by other wild-type PARPs (Chapter 4). I also implemented rational design strategies to target regions within the active site of PARP10 with small-molecule probes to achieve selective inhibition (Chapter 5). These chemical tools will provide a platform for future studies of PARP biology, and in particular, illuminate the specific roles of the understudied mono-ADPr PARP subclass.

Chapter 1: Introduction

Summary

The posttranslational modification (PTM) of amino acids provides dynamic changes in protein function to regulate cellular processes. PTMs have been discovered that elicit changes in protein activity (e.g., phosphorylation), folding (e.g., glycosylation), and localization within the cell (e.g., lipidation). Recently, the PTM known as ADP-ribosylation (ADPr), specifically ADPr catalyzed by the poly(ADP)-ribose (PARP) family, has received much attention for its role in various stress responses throughout the cell. PARPs have also been implicated in several disease states such as cancer, inflammation, and neurodegeneration, highlighting them as targets for therapeutic intervention.¹

The study of ADPr and the PARP enzymes has been slow in comparison to other PTMs such as phosphorylation catalyzed by kinases. The nature of ADPr has made it difficult to study. In particular, the labile, heterogeneous, and charged character of ADPr has prevented a clear understanding of its function. In addition, due to the presence of multiple active PARP family members in a cell at a given time, determining the contributions from a single PARP have proven challenging. Inhibitor development to study the function of PARPs has also been hindered due to the highly conserved nature of the catalytic transferase domain. The design of chemical tools to study the PARP family would greatly aid the study and understanding of ADPr and the contributions of individual PARP family members.

In the remaining sections of this chapter, I will give a brief overview of the history of ADPr and the classification of the PARP family of enzymes. I will focus

on the current limitations to study ADPr and highlight techniques that have been used to study other PTMs and the enzymes involved (e.g., kinases, methyltransferases, acetyltransferases, etc.). Particular attention will be given to recent chemical biology techniques, as these will form the foundation of my dissertation. I will end with a discussion on inhibitor development for the PARP family and suitable strategies for obtaining selective inhibition for individual PARP family members.

ADP-ribosylation

Nicotinamide adenine dinucleotide (NAD^+) is an essential metabolite that is central to many biochemical processes across many kingdoms of life. NAD^+ serves a crucial role in oxidoreductase reactions during catabolism where it receives electrons during beta oxidation, glycolysis, and the citric acid cycle, converting from its oxidized (NAD^+) to reduced state (NADH^+).² In addition to its role as an electron carrier, NAD^+ is also a substrate for diverse classes of enzymes. In these reactions, NAD^+ is directly consumed by its conversion or transfer to a substrate protein, which is in contrast to its electron shuttling role in oxidoreductase reactions where NAD^+ undergoes reversible oxidation state changes.²

NAD^+ -consuming Enzymes

The consumption of NAD^+ has been observed for three classes of enzymes found in humans. The first class of NAD^+ -consuming enzymes includes

the silent information regulator 2 (Sir2) proteins, or sirtuins, which catalyze NAD⁺-dependent deacetylation.³ In this reaction, sirtuins utilize NAD⁺ to deacetylate lysine residues, producing nicotinamide and the metabolite 2'-O-acetyl-ADP-ribose in the process.⁴ A second class of NAD⁺-consuming enzymes are the cyclic ADP-ribose synthases, which produce and hydrolyze the Ca²⁺-mobilizing second messenger cyclic ADP-ribose from NAD⁺.⁵ The last class of enzymes includes the ADP-ribosyltransferases (ARTs), which includes the PARPs. ARTs catalyze ADPr, or the transfer of the ADP-ribose group of NAD⁺ onto amino acids in proteins, resulting in the release of nicotinamide (**Figure 1-1**). Of all the enzymatic reactions that consume NAD⁺, only ADPr results in a post-translational modification of proteins, highlighting a distinct role for NAD⁺ in the regulation of protein targets and signaling pathways in the cell.

ADPr Overview

ADPr can be divided into two forms: mono-ADPr, the transfer of a single ADP-ribose group onto amino acids in target proteins; and poly-ADPr, in which the initial ADP-ribose is modified with additional ADP-ribose groups to produce branched polymers known as poly(ADP-ribose) (PAR) (**Figure 1-1**).⁶ Known amino acid acceptors of ADPr in eukaryotic cells include lysine, arginine, glutamate, aspartate, cysteine, serine, and asparagine.⁷ ADPr can activate or inhibit the activity of the target protein as well as facilitate protein-protein interactions through domains that bind the ADP-ribose modification. ADPr is a reversible modification, and distinct enzymes degrade PAR and remove ADP-

ribose based on the amino acid modified, returning target proteins to their native state.¹

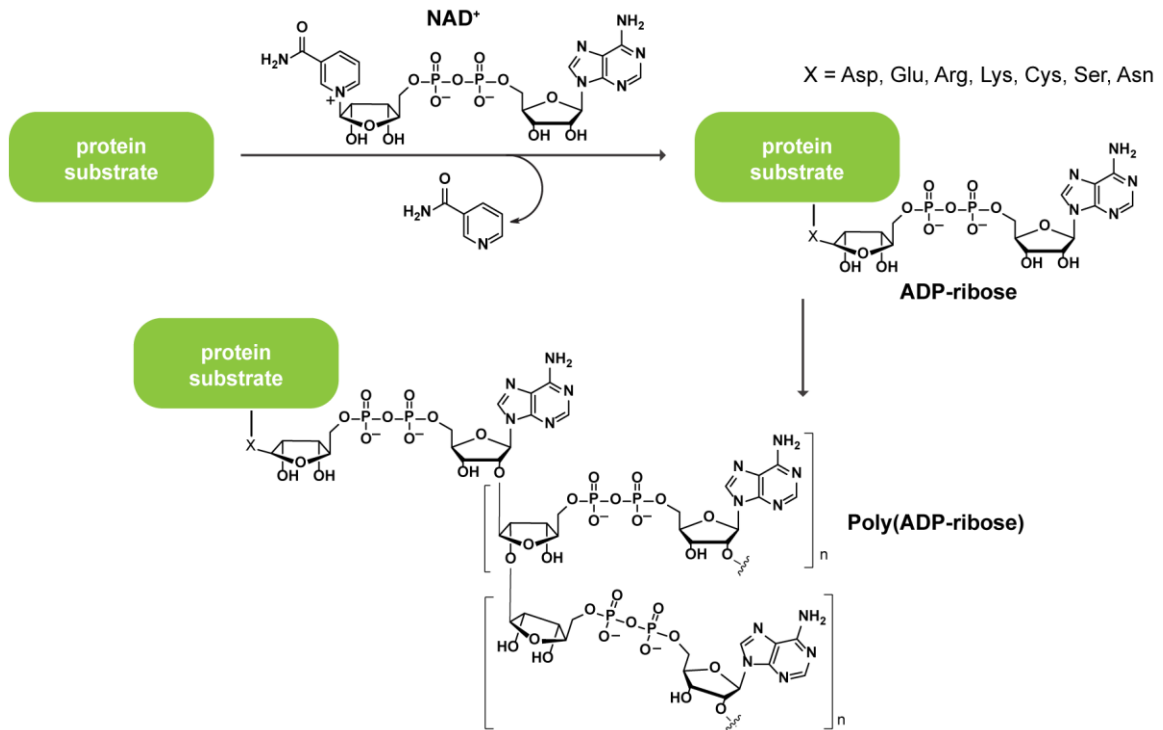


Figure 1-1. ADP-ribosylation (ADPr) is the transfer of ADP-ribose onto amino acid side chains of target proteins, releasing nicotinamide in the process. The initial ADP-ribose group can be further modified to produce poly(ADP-ribose) (PAR) in both linear and branched forms.

A History of Mono-ADPr and Bacterial Toxins

Mono-ADPr reactions were originally identified in bacterial pathophysiology, catalyzed by toxins associated with diphtheria, pertussis, cholera, and some clostridial diseases. Two of the more well-known classes of toxins with ADPr activity include diphtheria toxin (DT) and cholera toxin (CT). DT was discovered in 1888 after examining sterile cultures isolated from *Corynebacterium diphtheria*. Injection of filtrates into animals resulted in lesions characteristic of diphtheria, leading to the eventual correlation of DT as the

causative agent of diphtheria infection.⁸ DT was later discovered to be a secreted protein produced by a phage of *C. diphtheria*.⁹ The holotoxin consists of three distinct domains: an N-terminal catalytic domain with mono-ADPr activity, a central translocation domain, and a C-terminal receptor-binding domain.¹⁰ DT binds to the ubiquitously expressed heparin binding epidermal growth factor (HB-EGF) receptor and is internalized by the host via endocytosis.¹¹ DT then catalyzes specific mono-ADPr of elongation factor 2 (EF2) at diphthamide residue 715,¹² which, in turn, prevents association of EF2 to proteins involved in translation and effectively blocks host cell protein synthesis.¹³ The death of cells lining the back of the throat due to inhibited protein translation leads to the characteristic lesions observed with diphtheria infection.

CT was predicted to be a secreted toxin about the same time as DT,¹⁴ but it was not until 1959 that CT was identified. The injection of sterile culture filtrate of *Vibrio cholera* into rat intestines yielded a watery fluid accumulation similar to the disease pathology of *V. cholera* infection.¹⁵ CT consists of a catalytic mono-ADPr domain and an associated pentameric binding domain.¹⁰ CT toxin binds to the ganglioside GM1 on the membrane of intestinal epithelia cells, stimulating endocytosis and delivery into the cytosol.¹⁶ The catalytic domain is activated by binding to the small GTPase ADP-ribosylation factor (ARF)¹⁷ and catalyzes mono-ADPr of an arginine residue in the G_α subunit of G_s (G stimulatory).^{18,19} ADPr locks G_s in a GTP-bound state, which causes constitutive activation of adenylyl cyclase and increased levels of cAMP,¹⁸ followed by activation of protein kinase A and stimulation of chloride ion efflux channel. This CT-induced signaling

results in the secretion of ions and water into the intestinal lumen, causing the characteristic watery diarrhea associated with cholera infection. The mono-ADPr toxins DT and CT found in bacteria share homology to distinct classes of enzymes found in humans, suggesting an evolutionary link between bacterial and human ADPr.

Mammalian ADPr: Ecto-ARTs and PARPs

ADPr in mammals is catalyzed by two major classes of enzymes: 1) the extracellular membrane-associated ARTs (ecto-ARTs) and 2) the mammalian poly(ADP-ribose) polymerases (PARPs). Mammalian ecto-ARTs are a family of structurally related enzymes that are either expressed at the cell surface or secreted extracellularly. This class of enzymes shares sequence homology to, and functionality with, CT and catalyzes mono-ADPr of arginine residues. Ecto-ARTs provide regulation of membrane receptors in the extracellular compartment for cell communication, especially during tissue injury.²⁰

The second class of enzymes known as PARPs were identified in the early 2000s based on sequence similarity to DT.²¹ As opposed to ecto-ARTs, PARPs are intracellular ARTs and can either catalyze mono-ADPr or poly-ADPr at a variety of amino acid residues. Recently, a proposal was made to reclassify the ecto-ARTs and PARPs based on their catalytic reaction and structural features.²² Ecto-ARTs are also referred to as ARTCs (C = cholera toxin-like), whereas PARPs are also referred to as ARTDs (D = diphtheria toxin-like). The new nomenclature is also based upon differences in a key catalytic triad motif

within the active sites of the two enzyme classes. The R-S-E (Arg-Ser-Glu) triad is found in ARTCs, and the H-Y-E/ Φ (His-Tyr-Glu/ Φ , where Φ = hydrophobic residue) is found in ARTDs. As this new nomenclature takes time to become incorporated into the field, the more commonly used PARP nomenclature will be used throughout this dissertation.

The PARP Family

The PARP family consists of 17 members in humans based on a conserved catalytic domain with homology to DT.²² The founding member of the PARP family, PARP1, was first noted in 1963 for its ability to synthesize a novel biopolymer in vertebrate cells,²³ later identified as PAR. Most early work was focused on PARP1 and its well-known role in DNA damage detection and repair. It was not until more than 30 years later that the second member of the family, PARP2, was discovered when residual poly-ADPr activity remained in fibroblasts isolated from PARP1^{-/-} mice, which was attributed to PARP2 activity.²⁴ More recently, the identification of the remaining PARP family members was discovered based on sequence alignment of the conserved PARP catalytic domain.^{25,21} PARPs have emerged as major regulators of diverse cellular processes, and many are being pursued as therapeutic targets for the treatment of diseases such as cancer.²⁶

PARP Classification

PARPs have been classified according to different structural features and ADPr reactions that they catalyze.^{21,27} PARPs can be classified based upon their structural domains and functions: the DNA-dependent PARPs (PARPs 1, 2, and 3); the tankyrases (PARPs 5a and 5b); the CCCH (Cys-Cys-Cys-His) zinc finger-containing and WWE (Trp-Trp-Glu) PAR-binding domain-containing PARPs (PARPs 7, 12, 13.1, 13.2); and the PAR-binding macrodomain-containing “macro” PARPs (PARPs 9, 14, and 15).

The PARP family can also be classified according to catalytic ADPr activities: mono-ADPr, poly-ADPr, or inactive.²⁷ The mono-ADPr PARPs include PARPs 3, 4, 6, 8, 10, 12, and 14-16. The poly-ADPr PARPs include PARPs 1, 2, 5a, and 5b. No enzymatic activity has been described for PARP 9 and PARP13 until a recent report which showed that PARP9 can mono-ADPr ubiquitin when bound to the E3 ligase DTx3L,²⁸ suggesting that specific binding partners of PARPs could have dramatic effects on modulating PARP activity.

The PARP family can also be further categorized based upon a conserved catalytic triad motif: H-Y-E/ Φ .²² The histidine and tyrosine residues are required for proper orientation of NAD⁺ within the active site. The third residue varies throughout the PARP family. The glutamate can be found in PARPs 1-5a,b (H-Y-E PARPs) and was originally believed to impart poly-ADPr activity to these PARPs. Although PARPs 3 and 4 contain a glutamate, they lack poly-ADPr activity and are considered mono-ADPr PARPs,²⁷ suggesting that additional structural features are important for poly-ADPr activity. The remaining active

PARPs 6-8, 10-12, 14-16 (H-Y- Φ PARPs) contain a hydrophobic residue (isoleucine, leucine, or tyrosine) at the third position of the residue and all exhibit mono-ADPr activity. These observed structural differences in the H-Y-E and H-Y- Φ subclasses of PARPs will be useful for guiding the development of a chemical genetics strategy for identifying protein targets of PARPs (Chapter 2) in addition to guiding inhibitor development for the PARP family (Chapters 4 and 5).

A Focus on Mono-ADPr PARP Biology

The historical focus of the PARP field has largely been on the poly-ADPr subclass. PARP1 and PARP2 are the most widely studied PARPs for their well-known involvement in DNA repair recognition and repair.^{29,30} PARPs 5a and 5b (the tankyrases) have also been well studied for their involvement in telomere maintenance, Wnt/ β -catenin signaling, mitosis, and insulin signaling.³¹

My dissertation research focused on the much less studied mono-ADPr subclass of PARPs. The PARP family contains more mono-ADPr enzymes compared to poly-ADPr enzymes, highlighting the need to better understand this subclass of PARPs in order to gain a complete picture of PARP family function. Seminal studies were recently conducted that characterized the cellular localization and knockdown phenotypes of mono-ADPr PARPs.³² The studies found that a large majority of the PARPs localize to the cytoplasm, while some localize to distinct subcellular organelles (e.g., Golgi, centrosome, focal adhesions). In addition, some mono-ADPr PARPs showed cell cycle-dependent shuttling from the nucleus to cytoplasm. The knockdown phenotypes of the

mono-ADPr ranged from defects in mitosis (PARP 7), actin cytoskeletal regulation (PARPs 9 and 14), and membrane morphology (PARPs 8 and 16). Defects in viability were also observed for PARPs 8 and 14. These studies highlight the important roles that the mono-ADPr PARPs play in cellular physiology and have spurred increased interest in their biology.

The biology of the mono-ADPr PARPs has only recently just been investigated in the last decade. The mono-ADPr PARPs have been implicated in a variety of biological processes in the cell. PARP16 has been shown to regulate the unfolded protein response by modulating the activity of key endoplasmic reticulum sensors PERK and IRE1 α .³³ PARP10 has been implicated as an attenuator of NF- κ B signaling.³⁴ PARP6 is required for proper neuronal development in the hippocampus.³⁵ Additionally, PARP14 and PARP15 are proposed to be involved in host-virus conflicts mediated through their macrodomains.³⁶ While these studies connect mono-ADPr PARPs to specific biological processes, the mechanistic details of how these PARPs elicit their action remain unknown. Most studies provide only preliminary evidence connecting mono-ADPr PARPs to a given phenotype or signaling pathway. Subsequent studies were hindered due to the lack of chemical tools to further dissect the roles that these mono-ADPr PARPs are playing. The development of chemical tools for investigating the functional roles of PARPs, in general, will circumvent limitations that are currently preventing a detailed investigation into the cellular functions of the mono-ADPr PARP subclass.

Chemical Tools for Studying PARPs

There are currently three predominant limitations in the field that are preventing a detailed study of PARP function. The first limitation is the ability to identify protein targets of individual PARP members among the entire family. Secondly, the methods used to detect cellular ADPr, and in particular mono-ADPr, are lacking. Finally, there is a dearth of selective inhibitors for individual PARP members that can be used to probe the specific functions of a single PARP without confounding results from inhibition of other PARPs. In the next sections, I will discuss the current state of the PARP field in the following areas: 1) identifying protein targets of PARPs, 2) detecting cellular ADPr, and 3) developing selective inhibitors for PARP family members. I will also introduce the techniques that I use to help circumvent these three limitations in the field.

Identifying Protein Targets of Individual PARPs

Determining the direct protein targets of individual PARPs will greatly aid in the understanding of the functions of PARPs and inform potential therapeutic strategies for their inhibition. One of the limitations in the study of PARP biology is the ability to identify the protein targets of a specific PARP. This limitation can be attributed to the expression of multiple active PARP family members in a cell at a given time.³⁷ Many PARPs also exhibit compensatory functions,³⁸ making it difficult to determine the individual contribution of a single PARP among related enzymes that share common protein targets.

Current methods to identify ADP-ribosylated targets only provide a global view of ADPr and cannot decipher protein targets labeled by a specific PARP. The most widely used methods for detection of protein targets of PARPs rely on antibodies or antibody-like fusion proteins that bind specifically to the ADP-ribose modification. For many decades, the anti-PAR monoclonal antibody known as 10H³⁹ was the main method used to immunoprecipitate poly-ADP-ribosylated protein targets for subsequent identification using tandem mass spectrometry (MS) techniques. More recently, ADP-ribose-binding domains (ARBDs) have been used to capture ADP-ribosylated protein targets. In particular, the macrodomains, globular domains of ~130-190 amino acids, are ARBDs that bind to an ADP-ribose monomer or the terminal ADP-ribose moiety in a PAR chain. The macrodomain from the archaebacterial protein Af1521 has been successfully used to identify proteome-wide ADP-ribosylated protein targets.^{40–42}

There have also been chemical methods to capture ADP-ribosylated protein targets following digestion using boronate affinity chromatography, in which the diol moiety of ADP-ribose forms an ester linkage with the boronate resin.⁴³ The ADP-ribosylated peptides can then be eluted using hydroxylamine, which cleaves at the ester bond between the ADP-ribose modification and an acidic residue (Glu or Asp). The resulting mass change (+15.0109) of the peptide due to conversion to the hydroxamic acid species can be detected during MS analysis to identify the protein target.

Analogues of NAD⁺ have also been used to identify targets of ADPr that contain a handle that can be used in subsequent pull-down techniques. The

analogues 6-biotin-NAD⁺ and 6-alkyne-NAD⁺ contain a biotin or alkyne handle, respectively, on the *N*⁶-position of the adenosine moiety of NAD⁺. This handle is transferred to the protein target during ADPr. It was shown as a proof of principle that DT could use biotinylated NAD⁺ as a substrate to incorporate ADP-ribose into the target EF2, and subsequent pull down using streptavidin beads isolated the modified EF2 from cellular extracts.⁴⁴ The alkyne-tagged NAD⁺ was used to label protein targets of PARP1, and following click conjugation of biotin-azide and streptavidin enrichment, the protein targets were isolated and identified using mass spectrometry.⁴⁵ These NAD⁺ analogues provide a method to isolate and identify protein targets of PARPs, but like the previous methods described, they lack the ability to differentiate protein targets from a single PARP among the entire PARP family, especially in conditions in which all PARP family members are present (e.g., in a cellular lysate).

A Chemical Genetics Strategy for Identifying Protein Targets

Previous work has shown that the identification of protein targets from highly conserved enzyme families can be accomplished using a chemical genetics strategy. In this method, specificity of an enzyme for its substrate is conferred by introduction of new interactions between an engineered enzyme and substrate pair that are not present in the native system.

One such strategy involves steric complementation (also known as a 'bump-hole' approach). The substrate is modified with a large, bulky modification ('bump') that can only be accommodated by extra space ('hole') in the binding

pocket of the enzyme, which is created by site-directed mutagenesis (**Figure 1-2**).^{46,47} A common strategy is to substitute bulky hydrophobic residues (e.g., phenylalanine, tyrosine, isoleucine, valine, or methionine) with smaller amino acid residues (e.g., alanine or glycine). The modification on the substrate creates a steric clash with the native enzyme, creating an orthogonal engineered enzyme-modified substrate pair that can be used to identify direct targets of the engineered enzyme.⁴⁷

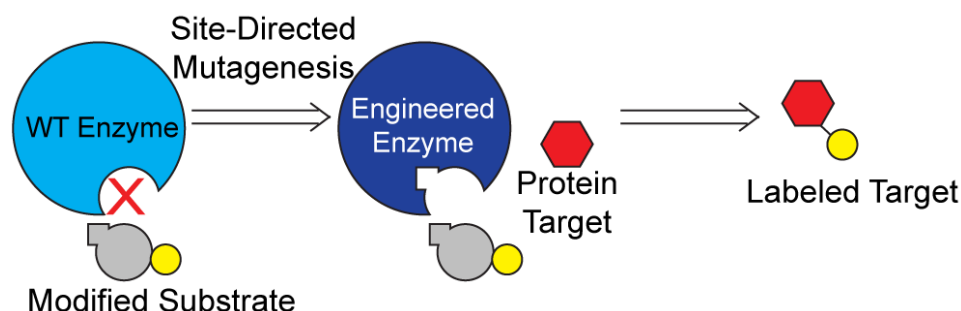


Figure 1-2. Steric complementation chemical genetics strategy ('bump-hole' approach). A bulky hydrophobic residue is substituted with a smaller amino acid to accommodate a steric modification on the substrate. The modification creates a steric clash with WT enzymes, creating an orthogonal engineered enzyme-modified substrate pair to identify labeled protein targets.

The bump-hole concept was first demonstrated by Schreiber and colleagues to engineer the binding pocket of the cyclophilin receptor to accommodate a modified cyclosporine ligand.⁴⁸ They used the bump-hole approach for modulating protein-protein interactions.

However, the work of Shokat and colleagues pioneered the bump-hole method for identifying protein targets of specific kinase. The identification of targets for a single kinase is a necessary step toward deciphering the biological role of an individual kinase among the >500 kinases in the human proteome. In early work, Shokat and colleagues engineered the protein tyrosine kinase v-Src

to utilize an ATP analogue containing a cyclopentyl group at the N^6 -position of adenosine (N^6 -(cyclopentyl)-ATP).⁴⁹ Importantly, the N^6 -cyclopentyl-ATP was not accepted by any wild-type kinases when incubated in cellular lysates, demonstrating the orthogonality of their approach. This seminal study led to the future optimization of an N^6 -benzyl-ATP⁵⁰ that could be widely used by engineered kinases with mutations ('holes') at the conserved hydrophobic "gatekeeper" residue.⁵¹ The N^6 -benzyl-ATP has been used to identify novel cytoskeletal targets of vSrc involved in the control of actin assembly⁵² A further refinement of the method involved the introduction of λ -thiophosphate to the ATP analogues, which allowed for the specific enrichment of thiophosphate-modified proteins using iodoacetyl-agarose. They identified >70 substrates of the human Cdk1-cyclin B complex.⁵³ This technique has been widely used to identify specific protein targets of individual kinases and reveal important insight into kinase-controlled biology.

Given the success of the bump-hole strategy with kinases, many other enzyme families have been engineered to accommodate modified substrates.⁴⁷ The bump-hole strategy has been applied to the >100 member methyltransferase (MT) family, which use S-adenosyl-L-methionone (SAM) for methylation of nucleic acids, proteins, and small molecules.⁵⁴ Luo and coworkers were instrumental in engineering MTs. They discovered a conserved tyrosine gatekeeper residue that, similar to the kinase family, when mutated created a "hole" for a bulky allyl-substituted SAM analogue.⁵⁵ Wild-type MTs were unable to use the bulky SAM analogue, demonstrating the orthogonality of their approach.

Additionally, the bump-hole approach has been applied to the acetyltransferase (KAT) family by modification of acetyl-CoA for use by engineered KATs.^{56,57} Many other enzyme families have been amenable to the bump-hole approach to engineer substrate specificity for understanding family-member specific biology.⁴⁷ Due to the powerful utility of this method for deciphering the contribution of individual enzymes in largely conserved enzyme families, the bump-hole approach will serve as the foundation for identifying direct protein targets of PARPs, as discussed in Chapter 2.

Detecting Cellular ADPr

The detection of cellular ADPr has been mainly limited to techniques that can be applied post-lysis or post-fixation of cells. These methods include many of the strategies described for identifying protein targets of PARPs (vide supra). Briefly, antibodies for PAR or antibody-like fusion proteins can be used for immunofluorescent applications on fixed cells. Additionally, NAD⁺ analogues such as 6-a-NAD⁺ can be used for ADPr followed by click conjugation with azide reporters, but these analogues must be applied in cellular lysates due to the cellular impermeability of the highly charged NAD⁺ molecule. There have been methods to allow NAD⁺ analogues access to the inside of the cell that rely on transient permeabilization of the cellular membrane with detergents⁵⁸ or feeding of the *N*⁶-propargyl adenosine precursor for metabolic incorporation into ADP-ribosylated proteins.⁵⁹ These approaches may impart toxicity due to

permeabilization or require long incubation periods for incorporation that could obscure the levels or restrict the dynamic measurement of ADPr.

These methods prevent the study of the dynamic nature of ADPr or do not maintain the compartmentalization of proteins that exists in intact eukaryotic cells. Methods to provide a snapshot of ADPr levels in a cell at a given time do not exist. The development of chemical probes to circumvent these limitations and provide detection of ADPr in intact cells will be discussed in Chapter 3.

Developing Selective Inhibitors of Individual PARP Family Members

The development of inhibitors targeting PARP1 began in the 1980s by medicinal chemistry groups in academia and biotechnology/pharmaceutical companies. The surge in interest was spurred in the mid-2000s by the finding that PARP1 inhibition could serve as a chemosensitizer in combination with cytotoxic agents to induce DNA damage and kill rapidly dividing cancer cells.⁶⁰ It was also discovered that PARP1 inhibitors could be used as a single-agent therapy for tumor types that are deficient in certain DNA repair mechanisms such as double strand break repair (e.g., mutations in the BRCA1 and BRCA2 genes)^{61,62} in a phenomenon known as synthetic lethality.⁶³

More than 30 years of medicinal chemistry efforts have resulted in several PARP1 clinical candidates. Within the last few years, three of these candidates have been approved by the FDA as cancer therapeutics (**Figure 1-3**). In December 2014, olaparib (AstraZeneca) was approved for use as a single-agent therapy for germline BRCA-mutated advanced ovarian cancers. Two years later,

the FDA also granted rucaparib (Clovis Oncology) accelerated approval as a therapy for patients with advanced ovarian cancers. The following year, niraparib (Tesaro, Inc.) was approved for the maintenance treatment of patients with recurrent epithelial ovarian, fallopian, and peritoneal cancer. The recent approvals by the FDA within the last few years highlight the potential of PARP inhibitors as therapeutics for certain cancers.

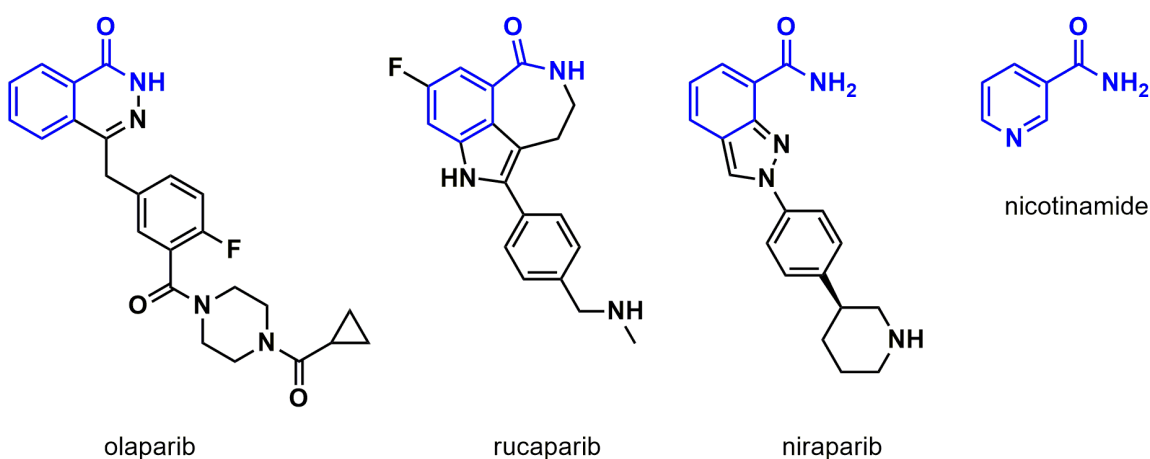


Figure 1-3. PARP1 inhibitors approved by the FDA. The inhibitors act by competing for NAD^+ in the PARP active site. The nicotinamide isostere for each inhibitor is highlighted in blue.

While early inhibitor development on PARP1 resulted in the FDA approval of drug candidates as treatments for certain cancers, many PARP inhibitors inhibit multiple members of the PARP family. Most PARP1 inhibitors also inhibit PARP2 due to their structural homology. However, whether these inhibitors could also inhibit other PARP family members was still unknown. A study in 2012 profiled 185 known PARP inhibitors, both clinical candidates (some now FDA-approved drugs) as well as research probes, in an assay that measured binding to 13 of 17 catalytic domains of the PARP family.⁶⁴ A large majority of inhibitors

bound to multiple members of the PARP family, demonstrating that many PARP inhibitors are unselective and share inhibitory profiles. In particular, both FDA-approved inhibitors olaparib and rucaparib bind tightly to additional PARP family members besides the originally designated PARP1 and PARP2. While the polypharmacology is observed to be poly-ADPr subclass specific, the therapeutic effect of this pan-selectivity is not known.

A follow-up study measured inhibition of several PARP inhibitors in an activity assay across the PARP family,⁶⁵ as opposed to the binding assay used previously. The study confirmed the prior observation that both olaparib and rucaparib are unselective. Olaparib only exhibited ~15-20-fold selectivity for PARP1 and -2 over other family members, while rucaparib showed far less selectivity across other family members. These selectivity studies demonstrate that most PARP inhibitors are broadly effective against many members of the PARP family. Most PARP inhibitors are nicotinamide mimics that target the highly conserved PARP NAD⁺-binding pocket,⁶⁶ which can explain the observed polypharmacology. While inhibition of multiple PARP family members may be advantageous for certain clinical applications such as cancers where the combined inhibition of PARP-controlled pathways could have synergistic effects, these unselective inhibitors make poor probes to decipher specific biology connected to a single PARP enzyme.

A Chemical Genetics Strategy for Selective Inhibition of PARPs

Obtaining selective inhibition of a single enzyme among the entire family can be obtained using a chemical genetics strategy. The bump-hole approach (vide supra) has been applied to inhibitor scaffolds (instead of substrates) to obtain selective inhibition of an engineered enzyme (**Figure 1-2**).⁴⁷ Importantly, the modification on the inhibitor scaffold prevents binding to wild-type enzymes to provide an orthogonal engineered enzyme-“bumped” inhibitor pair for studying the biology of a single enzyme within the family.

Shokat and coworkers established a basis for modulating kinase activity using engineered kinases and inhibitors containing bulky substituents that occupy the pocket formed by mutating the kinase gatekeeper residue.⁵¹ To date, this strategy has been applied successfully to more than 80 kinases from different subfamilies including Src kinases, cyclin-dependent kinases, and calmodulin-dependent kinases.⁶⁷ The chemical genetics strategy has been instrumental in connecting specific kinase activity to biological processes such as CaMKII α in learning and memory⁶⁸ and Cdk1 (Cdc28) in cell-cycle regulation.⁵¹ The rapid modulation of enzyme activity using the chemical genetics strategy is advantageous to avoid gene compensation that can occur with knockdown techniques. In a study using an engineered Pho85 kinase and an orthogonal inhibitor, an unexpected role of Pho85 in glucose metabolism was established that was not seen in previous knockdown studies of Pho85 because of an adaptation in gene expression over the time required for knockdown.⁶⁹

I used chemical genetics to achieve selective inhibition of a single enzyme among highly conserved enzyme families. This enabled me to achieve selective inhibition of a single PARP among the entire family (Chapter 4). The focus will be on the inhibition of the mono-ADPr subclass of PARPs, specifically PARP10, because there has been limited effort to selectively inhibit this subclass.

Rational Design Strategies for Selective Inhibition of PARPs

The design of PARP inhibitors has been mostly focused on targeting the nicotinamide pocket of the active site, as this pocket makes favorable interactions with small molecules containing a nicotinamide isostere such as a benzamide.⁷⁰ The nicotinamide pocket is a highly conserved structural feature among the PARP family, which has prevented inhibitor selectivity.^{64,65} There has been some success in the design of selective inhibitors for PARP1/PARP2 (e.g., veliparib/ABT-888)⁷¹ as well as the tankyrases (PARPs 5a/5b).⁷²⁻⁷⁴ However, the design of selective inhibitors targeting the mono-ADPr subclass of PARPs has only recently been reported. Progress in the design of selective inhibitors of both PARP10 and PARP14 is preliminary, as many of the reported inhibitors display modest to no selectivity, or the PARP family selectivity profile is unknown.⁷⁵⁻⁷⁹

The PARP field would benefit greatly from a toolbox of selective inhibitors targeting specific members of the mono-ADPr subclass. In order to obtain selective inhibition, subtle differences in the structural features of individual PARP enzymes must be considered to introduce favorable interactions that impart selectivity. I envisioned two strategies that take advantage of differing

structural features of the PARP family: 1) targeting key catalytic residue differences within the nicotinamide binding site to achieve selectivity between the H-Y-E and H-Y- Φ subclasses (see PARP Classification section, page 9); and 2) targeting variable D-loop residues that cover the NAD⁺-binding site.

There is a key catalytic triad difference within the nicotinamide-binding site of PARPs that divides the PARP family into the H-Y-E and H-Y- Φ (Φ = hydrophobic) subclasses.²² I hypothesized that the difference in the last residue could be utilized to obtain selectivity between the subclasses of PARPs. Hydrophobic groups that could potentially clash with the glutamate of the poly-ADPr PARPs may be favored for the mono-ADPr PARPs. Additionally, the hydrophobic residue in the H-Y- Φ subclass varies between a leucine, isoleucine, or tyrosine, suggesting that additional selectivity could be obtained within the H-Y- Φ by targeting these residue differences.

The D-loop has been identified as having a high degree of sequence variability among the PARP family, highlighting this feature as a strategy for targeting.^{64,80} The D-loop is a loop of variable size within the PARP family that encloses the NAD⁺ substrate in the active site. Many cocrystal structures of inhibitor-bound PARPs have shown missing electron density for parts of the flexible D-loop.^{81,82} This suggests that specific interactions could be made between the inhibitor and that D-loop to potentially stabilize the D-loop and impart selectivity among PARPs. The D-loop also contains nonconserved cysteine residues for a subset of PARP family members, which could potentially be targeted with electrophilic inhibitors to achieve irreversible inhibition as a

means for achieving selectivity. This strategy of targeting cysteine residues has been applied successfully to the kinase and protease families to achieve selectivity among highly conserved enzyme families.⁸³ I will describe preliminary results on the development of electrophilic inhibitors targeting a D-loop cysteine residue of PARP10.

As there has been limited progress in the design of selective inhibitors for the mono-ADPr subclass of PARPs, these rational design strategies will be implemented to provide chemical probes that can be used to study the biology of mono-ADPr PARPs (Chapter 5).

Dissertation Overview

The predominant goal of my dissertation research was the development of chemical tools to investigate the functional roles of PARP family members. A particular focus was on the mono-ADPr subclass of PARPs because much less is known about this subclass despite being connected to important cellular signaling pathways involved in disease. The current methods to study mono-ADPr PARP biology are limited, which has prevented a comprehensive understanding of their targets and downstream signaling pathways. First, I developed modified NAD⁺ analogues that are selectively used by engineered PARPs (Chapter 2). Collaborating with Dr. Ian Carter O'Connell, these orthogonal NAD⁺ analogue-engineered PARP pairs were used to identify specific protein targets of a single PARP among the entire PARP family. Next, I developed chemical probes for detecting cellular ADPr (Chapter 3). My method

allows for the detection of cellular mono-ADPr, which has been hindered since the discovery of the enzymes that catalyze mono-ADPr. The probes also revealed an unanticipated mechanism for ADP-ribosylation, which has important implications for how ADPr is recognized and reversed in the cell. Then, I developed chemical probes for achieving selective inhibition of mono-ADPr PARP family members. I used both chemical genetics (Chapter 4) and rational design strategies (Chapter 5) that will guide future development of probes that can be used for studying mono-ADPr PARP biology. Overall, the methods that I have developed will help to circumvent the limitations in the field will enable future studies on the roles that PARPs are playing in the cell. My work positions PARP biologists to advance our knowledge of ADPr as well as highlight the PARP family as critical regulators of cellular physiology and pathophysiology.

Chapter 2: Development of Orthogonal NAD⁺ Analogue-Engineered PARP Pairs

Ian Carter-O'Connell, Haihong Jin, **Rory K. Morgan**, and Michael S. Cohen

Portions of this chapter were originally published in *J. Am. Chem. Soc.* on April 9, 2014 in volume 136, issue 14, pages 5201 - 5204 (Copyright © 2014 American Chemical Society)⁸⁴ and in *Cell Rep.* on January 7, 2016 in volume 14, issue 3, pages 621 – 631 (Copyright © 2016 The Authors. Published by Elsevier Inc.).⁸⁵ Both publications have been adapted for this dissertation and reprinted with permission. I designed and synthesized the nicotinamide and NAD⁺ analogues in close collaboration with Dr. Haihong Jin. Dr. Ian Carter O'Connell performed all molecular biology, cell biology, and target identification presented in this chapter.

Abstract

The posttranslational modification ADP-ribosylation (ADPr) plays a major role in the regulation of cellular processes in both normal physiology and pathophysiology. ADPr is catalyzed by the poly(ADP-ribose) polymerase (PARP) enzyme family, which can be divided into two subclasses: those that catalyze poly-ADPr (PARPs 1, 2, 5a,b) and those that catalyze mono-ADPr (PARPs 3, 4, 6-8, 10-12, 14-16). The study of the PARP enzyme family has been hindered by the ability to identify direct protein targets of individual PARP family members because they all share the same substrate, nicotinamide adenine dinucleotide (NAD⁺). Here we describe a chemical genetics strategy for the design of orthogonal NAD⁺ analogue-engineered PARP pairs that can be used to identify protein targets of individual PARPs. We synthesized orthogonal NAD⁺ analogues that are used by engineered PARPs from both subclasses. In the case of the poly-ADPr subclass, a C-5-ethyl substituted NAD⁺ analogue (5-Et-6-a-NAD⁺) was selectively used by poly-ADPr PARPs with a lysine to alanine mutation at the 'ceiling' position within the nicotinamide binding site. On the other hand, for the mono-ADPr subclass of PARPs, a C-5-benzyl substituted NAD⁺ (5-Bn-6-a-NAD⁺) was selectively used by mono-ADPr PARPs containing an isoleucine to glycine mutation at the 'floor' position within the nicotinamide binding site. These orthogonal NAD⁺ analogue-engineered PARP pairs are powerful tools for identifying direct protein targets of individual PARP family members, which will guide future studies to further understand the cellular functions of PARPs.

Introduction

ADP-ribosylation (ADPr) is a post-translational modification that plays a major role in a wide array of cellular processes (e.g., energy metabolism, transcription, and genomic maintenance).³⁰ In humans, ADP-ribose transfer is catalyzed by a family of 17 poly(ADP-ribose) polymerases (PARPs, also known as ARTDs) that share a conserved catalytic domain.²² PARPs catalyze the transfer of the ADP-ribose moiety from nicotinamide adenine dinucleotide (NAD⁺) to their target proteins.⁸⁶ The PARP family has been recently sub-classified based on the ability of the individual PARP enzymes to catalyze the transfer of a single ADP-ribose unit (mono-ADPr PARPs: PARPs 3, 4, 6-8, 10-12, 14-16) or multiple ADP-ribose units (poly-ADPr PARPs: PARPs 1, 2, 5a,b) onto target proteins.²²

The identification of protein targets of individual PARP family members has been challenging due to both the functional redundancy among the PARPs and the concurrent expression of multiple PARPs in a cell at any given time. For example, PARP1 is the best understood PARP family member for its involvement in stress signaling. While studies have identified protein targets of ADPr in stress signaling pathways,^{41,43} it is not entirely clear if these are direct targets of PARP1 or other PARPs with overlapping target specificities or shared expression profiles. Further, many of the PARPs that catalyze mono-ADPr, which is a large majority of the PARP family, are not as well understood as the poly-ADPr subclass of PARPs. This can be mainly attributed to the lack of chemical tools that has prevented the identification of direct protein targets for individual PARP

family members. There exists non-radioactive NAD⁺ derivatives, such as 6-biotin-NAD⁺⁴⁴ and 6-alkyne-NAD⁺ (6-a-NAD⁺),⁴⁵ for use in copper-catalyzed click conjugation to azide reporters, but these have only been useful for identifying targets of ADPr on a global scale. These NAD⁺ derivatives are unable to identify the direct protein targets of individual PARPs since they are substrates for all PARPs. The identification of direct targets for each PARP family member would greatly facilitate the understanding of the functional roles for each of these individual enzymes.

To address this challenge, we sought a chemical genetic approach for identifying the direct protein targets of PARPs. We decided to adapt a “bump-hole” technique that was originally used to study engineered kinase-modified ATP pairs.⁵¹ This method has been used not only to identify the targets of kinases,⁸⁷ but has been widely adapted to study substrate targeting for multiple post-translational modifications (e.g., acetylation,⁵⁶ methylation,⁸⁸) and to incorporate non-natural amino acids via modified aminoacyl-tRNA synthetases.^{89,90} We envisioned that a unique hydrophobic pocket could be engineered in the nicotinamide-binding site of PARPs such that they could bind an orthogonal NAD⁺ variant containing a substituent at the C-5 position on the nicotinamide moiety of NAD⁺. This orthogonal NAD⁺ variant would also contain an alkyne tag at the N⁶-position on the adenosine moiety for copper-catalyzed click conjugation to a biotin-azide probe (**Figure 2-1**). We hypothesized that a substituent (e.g. alkyl or benzyl) at the C-5 position on the nicotinamide moiety would be sufficient to exclude the orthogonal NAD⁺ variant from the active site of

wild-type PARPs. We first implemented this chemical genetics strategy for the poly-ADPr subclass (Part I), which then guided the strategy for the mono-ADPr subclass (Part II).

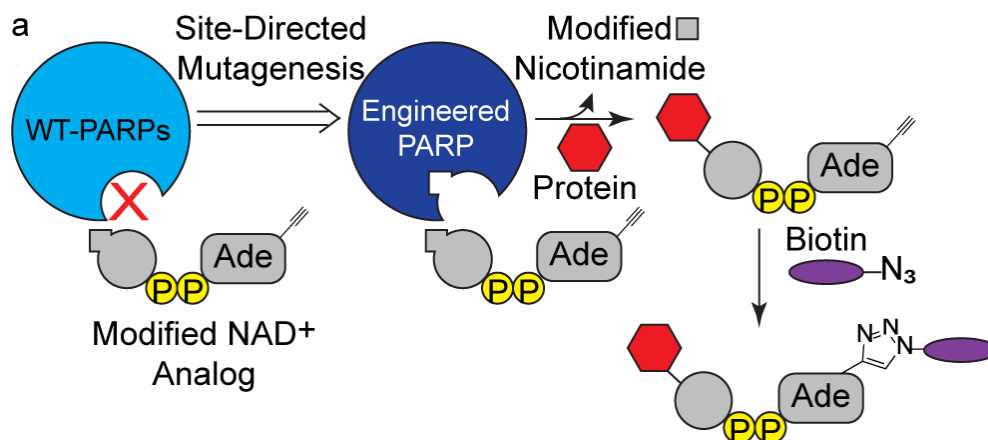


Figure 2-1. Schematic for the design of modified NAD⁺ analogs that are preferentially utilized by engineered PARPs. P: phosphate, Ade: adenine.

Results and Discussion

Part I: Development of a chemical genetics strategy for the poly-ADPr subclass of PARPs

We first identified a position within the poly-ADPr PARP nicotinamide-binding site that we could mutate to a smaller amino acid to create a hydrophobic pocket that would accommodate orthogonal NAD⁺ variants containing a substituent at the C-5 position. Multiple crystal structures are available for the poly-ADPr sub-class of PARPs bound to nicotinamide analogues, providing a guide for mutagenesis of residues within the nicotinamide binding site.^{91–93} The crystal structure of PARP1 bound to the nicotinamide analogue 3-methoxybenzamide (PDB ID: 3PAX)⁹¹ reveals a lysine residue (K903) that forms van der Waals contacts with the C-5 position of the benzamide ring (**Figure 2-**

2a). While we considered other positions within the active site, we focused on lysine 903 (K903) since it is conserved throughout the poly-ADPr PARP subclass, thus providing a potentially general strategy for identifying the direct targets of poly-ADPr PARPs (**Figure 2-2b**). Due to its established, well-characterized enzymatic activity,^{94,95} we began by engineering PARP1.

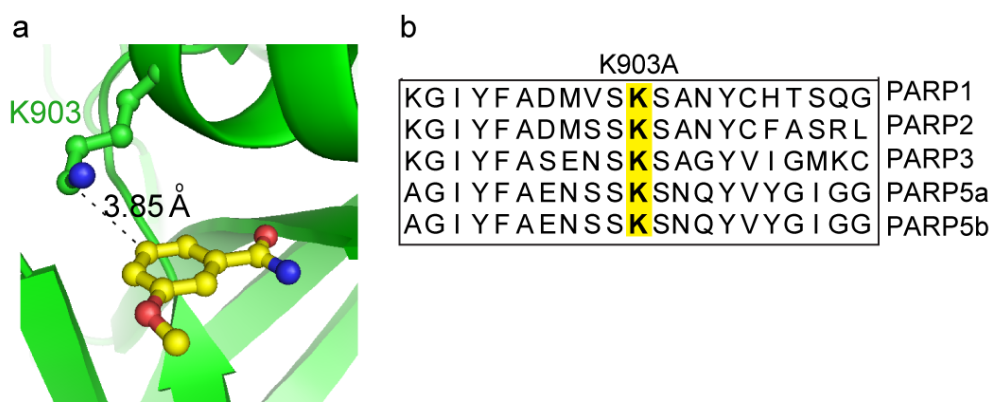
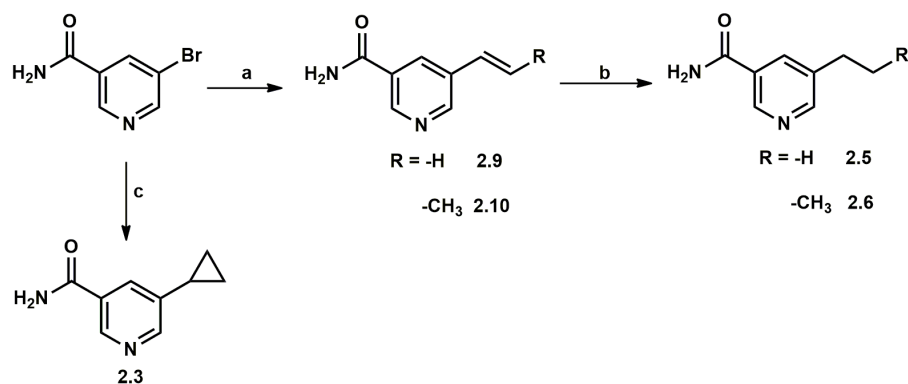


Figure 2-2. (a) The key residue, K903, in PARP1 (green), is within 3.85 Å of the C-5 position of 3-methoxybenzamide (yellow) (PDB ID: 3PAX).⁹¹ (b) Sequence alignment of the nicotinamide binding site of the poly-ADPr PARPs, highlighting K903 (PARP1).

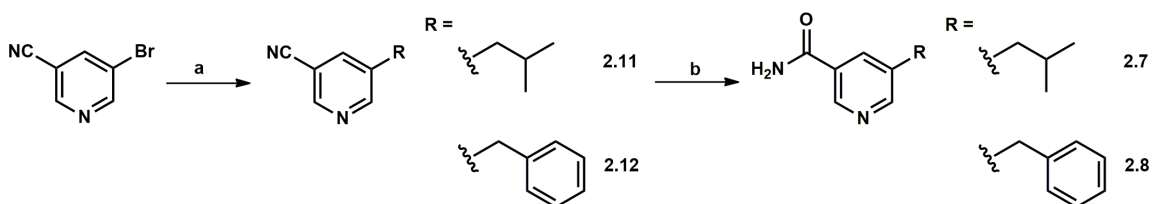
To accommodate substituents at the C-5 position of the nicotinamide ring, we mutated K903 to an alanine (K903A). Rather than starting with a synthetically challenging orthogonal NAD⁺ variant, we reasoned that we could first test simple nicotinamide analogues as inhibitors, since nicotinamide and the nicotinamide nucleotide of NAD⁺ bind in the same orientation in the active site of PARPs. We therefore synthesized a small panel of nicotinamide analogues containing various substituents at the C-5 position (**Figure 2-3a**). A C-5-cyclopropyl nicotinamide analogue **2.3** was synthesized using a Suzuki cross-coupling of cyclopropylboronic acid and 5-bromonicotinamide. C-5-substituted ethyl (**2.3**) and propyl (**2.6**) nicotinamide analogues were prepared with Suzuki couplings of the

corresponding alkenyl trifluoroborates and 5-bromonicotinamide followed by catalytic transfer hydrogenation using triethylsilane as a hydrogen source⁹⁶ (**Scheme 2-1**).



Scheme 2-1. Synthesis of C-5 substituted nicotinamide analogs 2.3, 2.5, and 2.6. Reagents and conditions: a. potassium vinyltrifluoroborate (for 2.9) or potassium *trans*-1-propenyl trifluoroborate (for 2.10), Cs₂CO₃, 1 mol % PdCl₂(PPh₃)₂, ACN/H₂O (10:1) (93 – 95% yield); b. triethylsilane (TES), 10 mol% Pd-C, MeOH (82 – 91% yield); c. cyclopropylboronic acid, PdCl₂(dppf), K₂CO₃, dioxane/H₂O (4:1) (84% yield).

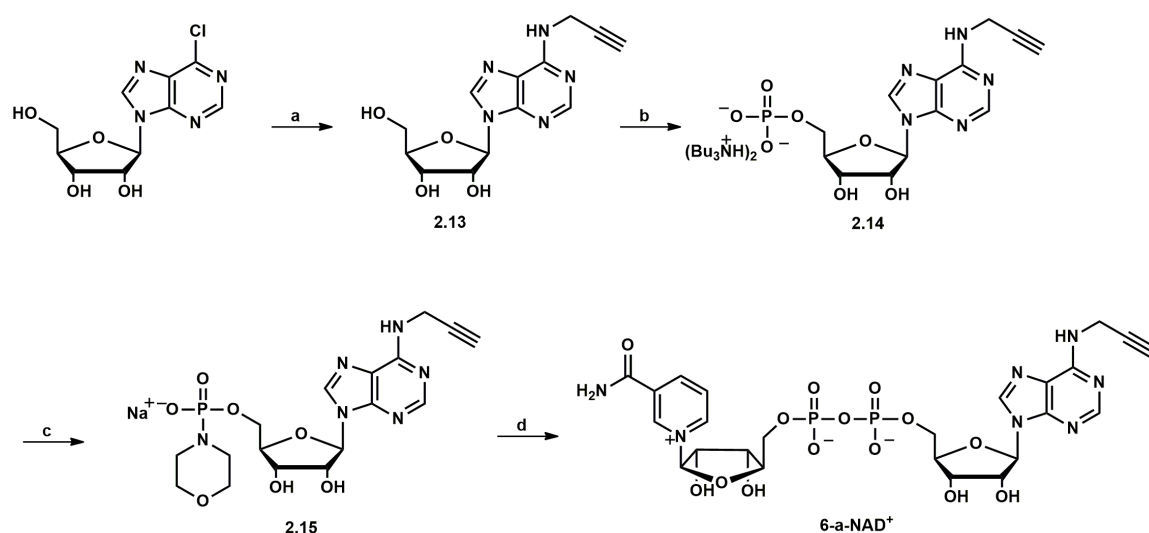
C-5-substituted isobutyl (**2.7**) and benzyl (**2.8**) nicotinamide analogues were synthesized using Negishi couplings with the corresponding organozinc bromide species and 5-bromonicotinonitrile. Hydrolysis of the nitrile group using a polymer-supported hydroxide ion resin yielded nicotinamide analogues **2.7** and **2.8**.



Scheme 2-2. Synthesis of C-5 substituted nicotinamide analogs 2.7 and 2.8. Reagents and conditions: a. organozinc bromide (isobutyl or benzyl), PdCl₂(dppf) (for 2.11) or Pd(PPh₃)₄ (for 2.12), THF (41% yield for 2.11, 84% yield for 2.12); (b) Amberlite IRA 410 resin (hydroxide form), MeOH/H₂O (1:1) (72 – 82% yield).

PARP1 can be engineered with a unique inhibitor-sensitizing mutation within the nicotinamide-binding site

To determine if nicotinamide analogs with substituents at the C-5 position are more selective for K903A PARP1 (KA-PARP1) than for wild-type PARP1 (WT-PARP1), we monitored ADP-ribose transfer to the PARP1 target, Histone H1.⁹⁷



Scheme 2-3. Synthesis of 6-a-NAD⁺. Reagents and conditions: a. propargylamine, DIPEA, EtOH (60% yield); b. trimethyl phosphate, H₂O, then POCl₃ (51% yield); (c) morpholine, PPh₃, Aldrich thiol-2, DMSO (92% yield); d. β-NMN, MnCl₂, MgSO₄, formamide (40% yield).

We used a previously described clickable NAD⁺ derivative, 6-a-NAD⁺, which contains an alkyne at the N-6 position of the adenosine ring that can be conjugated to an azide reporter via click chemistry for monitoring ADPr.⁴⁵ We reported an improved synthesis of 6-a-NAD⁺ utilizing an N⁶-adenosine monophosphate morpholidate intermediate for coupling to β-nicotinamide mononucleotide (β-NMN) with MnCl₂ to yield 6-a-NAD⁺ (**Scheme 2-3**).

We sought a C-5-substituted nicotinamide analog that was at least 10-fold more selective for KA-PARP1 compared to WT-PARP1. We found that all C-5-substituted nicotinamide analogs were more selective for KA-PARP1 than for WT-PARP1 (**Figure 2-3b**). The most potent and selective analog of KA-PARP1 was 5-ethyl-nicotinamide **2.5** ($IC_{50} = 165 \pm 11 \mu M$), with 14-fold selectivity over WT-PARP1 ($IC_{50} = 2359 \pm 368 \mu M$) (**Figure 2-3b**). Together, these results demonstrate that PARP1 can be engineered to create a unique, inhibitor-sensitizing mutation in the nicotinamide-binding site.

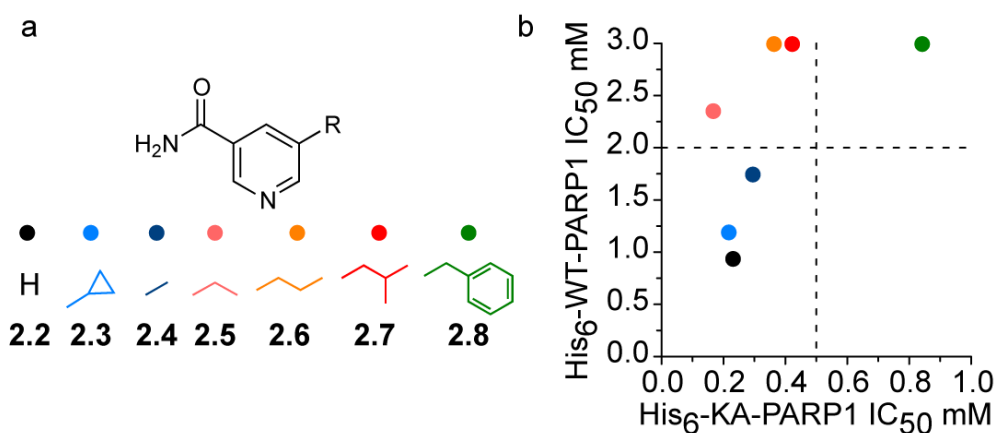
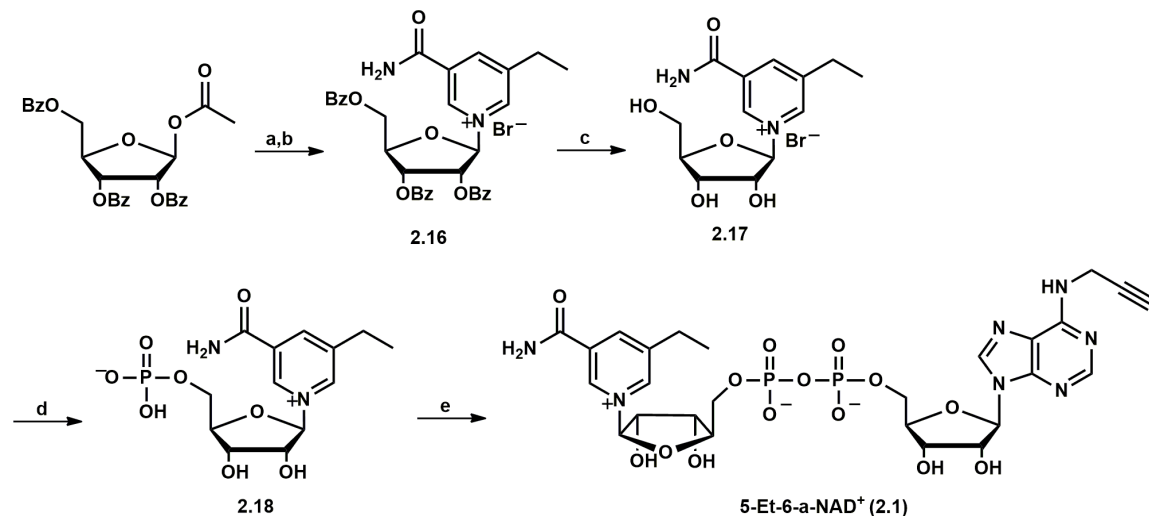


Figure 2-3. Comparative inhibition of WT-PARP1 and KA-PARP1 by select nicotinamide analogues. (a) C-5 substituted nicotinamide analogues. (b) IC_{50} values (mM) for each analogues are plotted comparing the WT-PARP1 (y-axis) and KA-PARP1 (x-axis) variants.

A C-5-ethyl-modified NAD⁺ analogue (5-Et-6-a-NAD⁺) is selectively used by engineered poly-ADPr PARPs

We next sought to prepare an orthogonal NAD⁺ variant that would be a substrate for KA-PARP1, but not WT-PARP1. Guided by the results of our inhibitor studies, we synthesized the orthogonal NAD⁺ variant, 5-Et-6-a-NAD⁺

(**2.1**), which contains an ethyl substituent at the C-5 position of the nicotinamide ring and an alkyne at the N^6 position of the adenosine ring (**Scheme 2-4**).



Scheme 2-4. Synthesis of 5-Et-6-a-NAD⁺ (**2.1**). Reagents and conditions: a. HBr (33 wt% in acetic acid), toluene (67% yield); b. **2.5**, ACN; d. 7 N NH₃ in MeOH (71% yield); d. POCl₃, trimethyl phosphate, H₂O (74% yield); e. **2.15**, MnCl₂, MgSO₄, formamide (31% yield).

To investigate the substrate specificity of 5-Et-6-a-NAD⁺, we monitored auto-ADPr of WT- and KA-PARP1 by click conjugation to a biotin-azide reporter. Incubation of KA-PARP1 with increasing concentrations of 5-Et-6-a-NAD⁺ resulted in auto-ADPr of KA-PARP1 (Figure 3a). By contrast, no modification of WT-PARP1 was detected by up to 250 μ M 5-Et-6-a-NAD⁺ (**Figure 2-4a**).

To further establish the generalizability of our approach, we next sought to determine if our engineered PARP enzyme–5-Et-6-a-NAD⁺ pair could work for other poly-ADPr PARP family members. We focused on PARP2 and PARP5b (also known as Tankyrase 2) because of their well-characterized enzymatic activity. Similar to WT-PARP1, no modification of WT-PARP2 and WT-PARP5b was detected up to 250 μ M 5-Et-6-a-NAD⁺ (**Figure 2-4b,c**).

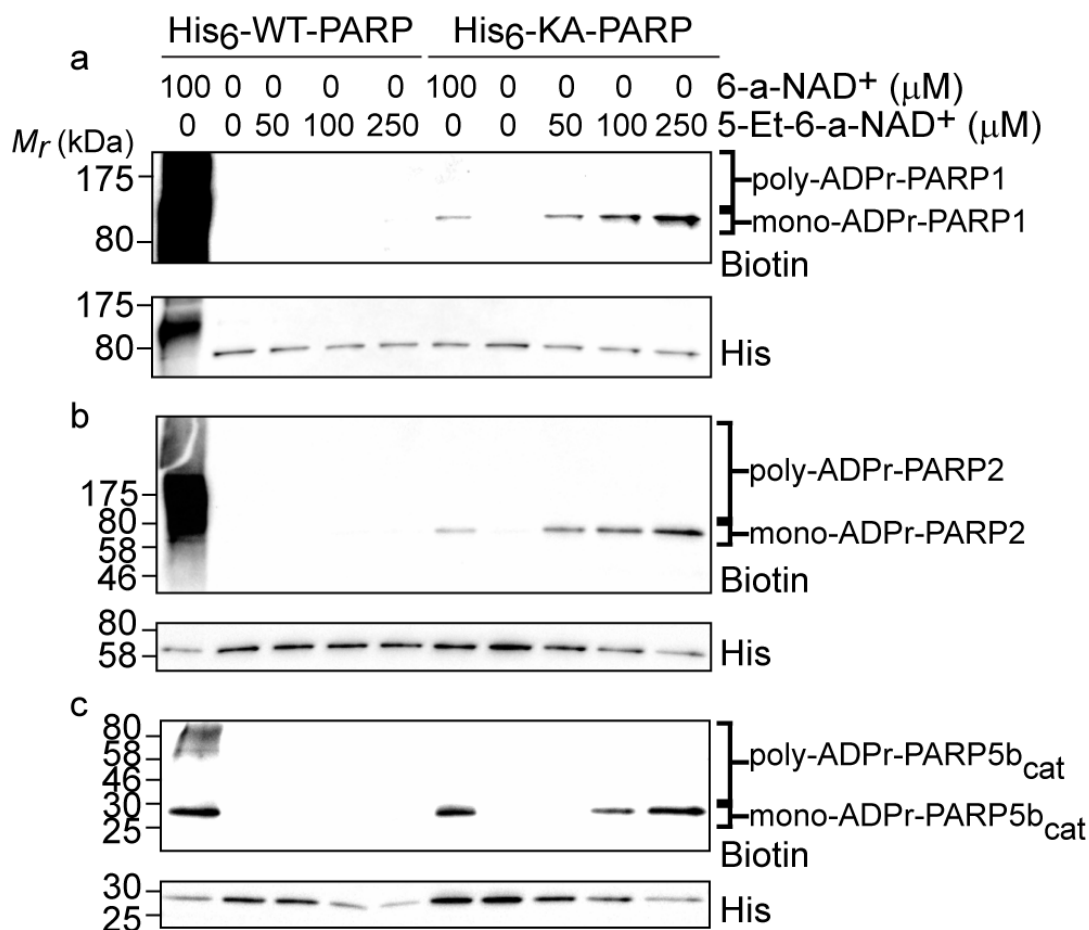


Figure 2-4. Orthogonal auto-ADPr of sensitized PARPs using modified NAD⁺ variants. The concentration of NAD⁺ analog is indicated. Samples were subjected to immunoblot detection with streptavidin (Biotin) to detect modified protein. His-tag (His) detection served as a loading control. Poly-ADPr and mono-ADPr modified fractions are indicated. (a) PARP1. (b) PARP2. (c) PARP5b.

Mutation of the conserved lysine in the nicotinamide binding pocket of PARP2 and PARP5b to alanine (KA-PARP2 and KA-PARP5b, respectively) conferred sensitivity to 5-Et-6-a-NAD⁺, as evidenced by the single biotinylated band at the molecular weight of the KA-PARPs (**Figure 2-4b,c**). Taken together, these experiments demonstrate that we have successfully created a poly-ADPr PARP-wide engineered enzyme–modified substrate pair.

Orthogonal NAD⁺ analogue-engineered poly-ADPr PARP pairs can be used to identify family-member specific PARP protein targets

In summary, simple C-5-substituted nicotinamide analogues were synthesized and shown to be selective inhibitors of the engineered PARP1 mutant, KA-PARP1. These inhibitors guided the design of the orthogonal NAD⁺ variant, 5-Et-6-a-NAD⁺, which was selectively used by engineered KA-PARPs, PARP1, PARP2, and PARP5b in auto-ADPr reactions. In subsequent studies, both KA-PARP1 and KA-PARP2 were used in combination with 5-Et-6-a-NAD⁺ in nuclear extracts followed by affinity purification and tandem mass spectrometry to identify 42 direct PARP1 targets and 301 direct PARP2 targets,⁸⁴ validating this method as a powerful strategy to identify specific protein targets of poly-ADPr PARP family members.

Part II: Development of a chemical genetics strategy for the mono-ADPr subclass of PARPs

We demonstrated that a chemical genetics strategy could be implemented for the poly-ADPr PARPs, but we wanted to extend this strategy to the less-understood mono-ADPr PARPs to provide a technique for identifying protein targets of this subclass. In the previous strategy for the poly-ADPr PARPs, we found that mutating a lysine residue (referred to as the 'ceiling' position) to a smaller alanine residue created a unique pocket that could accommodate 5-Et-6-a-NAD⁺. The analogous ceiling position in the mono-ADPr PARPs, however, is

not a lysine, but is replaced by a leucine (PARP10, 16), an isoleucine (PARP6, 8), or a tyrosine (PARP7, 11, 12, 14, 15) (**Figure 2-5a**).

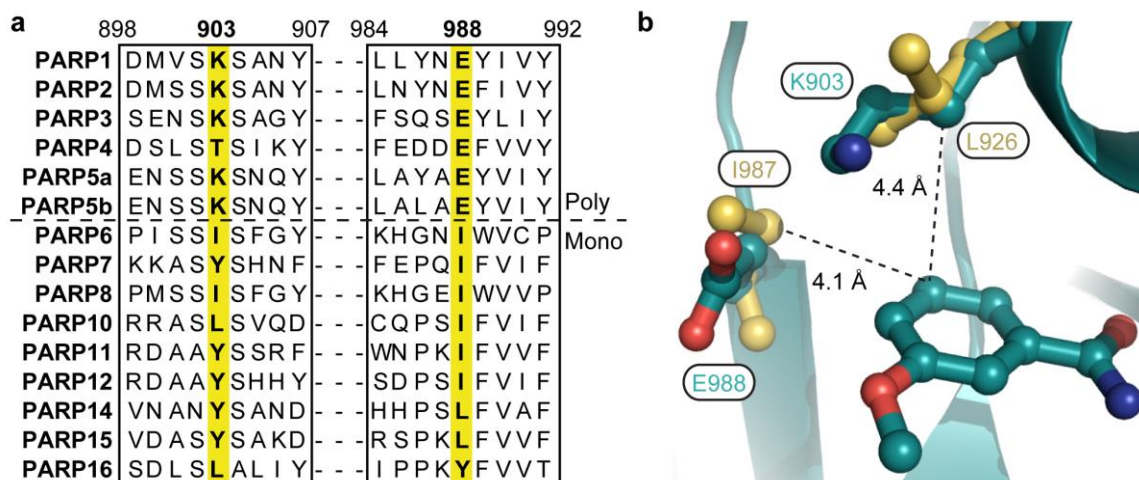


Figure 2-5. Poly-ADPr and mono-ADPr PARPs differ at key amino acid residues. **(a)** Sequence alignment of the nicotinamide binding site of poly-ADPr PARPs and the mono-ADPr PARPs. Number reflects the amino acid position in PARP1. **(b)** Overlay of crystal structures of PARP1_{cat} (dark blue) (PDB ID: 3PAX)⁹¹ and PARP10_{cat} (PDB ID: 3HKV) showing the nicotinamide binding sites. The distance between the key amino acids identified in PARP10 (L926 and I987) and the C-5 position of 3-methoxybenzamide are indicated.

Examination of the crystal structures of 3-aminobenzamide-bound PARP10 (PDB ID: 3HKV) and PARP1 (PDB ID: 3PAX)⁹¹ revealed that L926 of PARP10 occupies a similar space as K903 in PARP1 (**Figure 2-5b**). We hypothesized that mutation of L926 (human PARP10 numbering) in the ceiling position of PARP10 to a smaller amino acid (e.g., alanine or glycine), as in Part I, could accommodate NAD⁺ analogues with modifications at the C-5 position of the nicotinamide ring.

C-5-substituted 6-a-NAD⁺ analogues are not used by ‘ceiling’ position mutants of PARP10

We prepared the corresponding alanine and glycine mutants (L926A/G) within the catalytic domain of PARP10 (PARP10_{cat}) and profiled these mutants for their ability to use 5-Et-6-a-NAD⁺ as well as additional NAD⁺ analogues with modifications at the C-5 position of the nicotinamide ring (e.g., methyl, propyl, isobutyl, or benzyl). These additional NAD⁺ analogues were prepared as previously described in Part I (**Scheme 2-4**), but the C-5-ethyl modified β -NMN precursor **2.18** was replaced with the corresponding C-5-methyl, propyl, isobutyl, or benzyl modified β -NMN precursor to yield 5-Me-6-a-NAD⁺, 5-Pr-6-a-NAD⁺, 5-iBu-6-a-NAD⁺, and 5-Bn-6-a-NAD⁺, respectively.

We monitored L926A- and L926G-PARP10_{cat}-mediated ADPr of the known substrate SRSF protein kinase 2 (SRPK2)^{98,99} in the presence of the NAD⁺ analogues followed by click conjugation with rhodamine-azide and subsequent in-gel fluorescence as a readout of activity (**Figure 2-6a**). The control compound 6-a-NAD⁺ was used as a substrate to ADP-ribosylate SRPK2 by WT-PARP10_{cat}, and to a lesser extent by L926A- and L926G-PARP10_{cat} (**Figure 2-6b,c**). Modified analogues 5-Me-6-a-NAD⁺ and 5-Et-6-a-NAD⁺ were used by L926G-PARP10_{cat}, but to a very low degree (only 5% ADPr activity compared to WT-PARP10_{cat} activity with 6-a-NAD⁺). Based on these results, we sought to find an alternative position within the nicotinamide-binding site of PARP10 that when mutated to a smaller residue could confer sensitivity to modified NAD⁺ analogues.

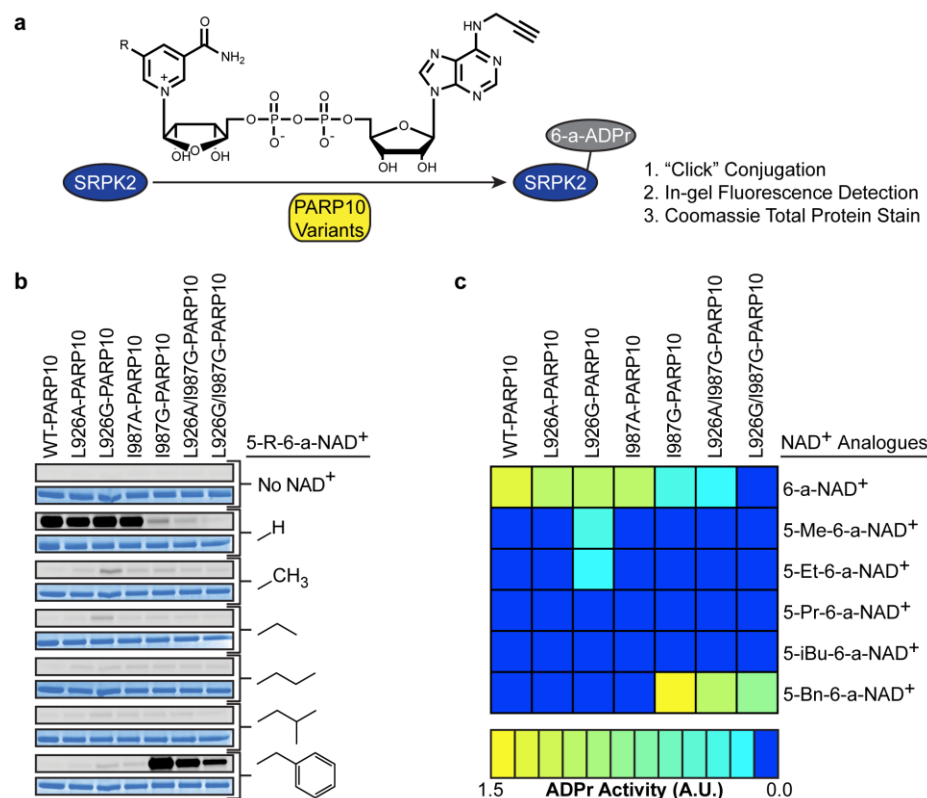


Figure 2-6. Profiling of PARP10 variants with NAD⁺ analogues. **(a)** PARP10 variants were incubated with SRPK2 in the presence of individual NAD⁺ analogues. Modified SRPK2 was subjected to click conjugation with rhodamine-azide, and ADPr levels were quantified using in-gel fluorescence. **(b)** Results from profiling of PARP10 variants with NAD⁺ analogues. For each analogue tested, the gel was first imaged to detect ADP-ribosylated SRPK2 after click conjugation with rhodamine azide (top gel) and then stained with Coomassie to detect total SRPK2 (bottom gel). **(c)** Quantification of global ADPr efficiency normalized against the total protein for the engineered pairs tested in **(b)**.

A C-5-benzyl-substituted 6-a-NAD⁺ analogue is selectively used by a 'floor' position mutant in PARP10

We reexamined the crystal structure of PARP10 and hypothesized that I987 (human PARP10 numbering) in the 'floor' position could be engineered to confer sensitivity to modified NAD⁺ analogues (**Figure 2-5b**). I987 makes Van der Waals contacts with the C-5 position of the benzamide ring of 3-aminobenzamide and is also well-conserved among the mono-ADPr subclass (**Figure 2-5a**), suggesting that that this strategy could be applied across the

mono-ADPr subclass of PARPs. We prepared the corresponding alanine and glycine I987 mutants of PARP10 and profiled their activity with the panel of C-5 substituted 6-a-NAD⁺ analogues as substrates. We found the 5-Bn-6-a-NAD⁺ was used efficiently by I987G-PARP10_{cat} (~140% ADPr activity compared to WT-PARP10_{cat} with 6-a-NAD⁺, **Figure 2-6b,c**); however, 6-a-NAD⁺ was a poor substrate for I987G-PARP10_{cat} (~5% ADPr activity compared to WT-PARP10_{cat} with 6-a-NAD⁺, **Figure 2-6b,c**). These results taken together demonstrate that mutating I987 in the floor position of PARP10 results in an orthogonal switch in substrate specificity from 6-a-NAD⁺ to 5-Bn-6-a-NAD⁺.

Mutating the floor position in other mono-ADPr PARPs confers sensitivity with 5-Bn-6-a-NAD⁺

We next sought to determine whether the mutation could be applied to the full-length enzyme in PARP10. We also wanted to determine whether the mutation could be applied to another mono-ADPr PARP. We chose PARP11 because, in addition to an isoleucine at the floor position (I313, PARP11 numbering), it has a tyrosine at the PARP10-L926 ceiling position, which would allow us to determine the generalizability of the strategy with mono-ADPr PARPs with differing residues at the ceiling position (**Figure 2-5a**). We generated the corresponding isoleucine to glycine mutants in GFP-tagged full-length PARP10 (IG-PARP10) and PARP11 (IG-PARP11) and compared their ADPr activity in HEK293T lysates. Treatment of lysates from IG-PARP10- and IG-PARP11-

transfected cells with 5-Bn-6-a-NAD⁺ (100 μ M) resulted in labeling for both engineered PARPs (**Figure 2-7**).

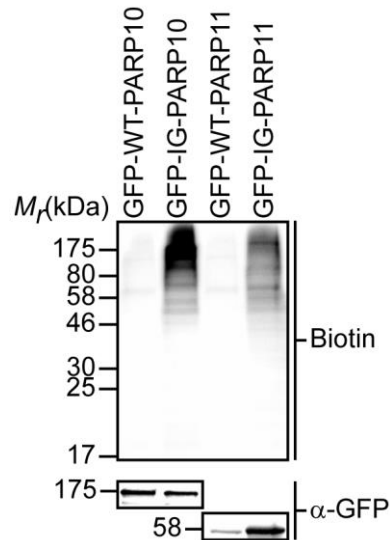


Figure 2-7. Lysate labeling by IG-PARP10 or IG-PARP11 in the presence of 5-Bn-6-a-NAD⁺. HEK293T cells were transfected with either WT- or IG-PARP10 or PARP11, and the resulting lysate was incubated for 2 h in the presence of 5-Bn-6-a-NAD⁺ (100 μ M). Lysates were subjected to click conjugation with biotin-azide, and the ADPr of direct protein targets was observed using streptavidin-HRP (Biotin). The faint bands in the WT-PARP lanes corresponds to endogenous biotinylated proteins. Expression of each PARP was confirmed using via immunoblot detection of GFP.

Minimal background labeling was detected in lysates expressing either WT-PARP10 or PARP11, highlighting the ability of endogenous and non-engineered PARPs to use 5-Bn-6-a-NAD⁺ as a substrate for ADPr. The protein banding patterns for IG-PARP10 and IG-PARP11 are distinct, demonstrating that the target specificities of PARP10 and PARP11 differ in the cell. These results confirm that PARP10 and PARP11 label family-member-specific proteins.

Orthogonal NAD⁺ analogue-engineered mono-ADPr PARP pairs can be used to identify family-member specific PARP protein targets

In summary, we engineered mono-ADPr PARPs to use a C-5 substituted 6-a-NAD⁺ analogue. In contrast to the poly-ADPr PARPs, mutating the ceiling position (L926) in mono-ADPr PARP10 did not enable the use of C-5 substituted 6-a-NAD⁺ analogues. Ultimately, mutating the floor position (I987) to a glycine in PARP10 enabled the use of 5-Bn-6-a-NAD⁺ and loss of activity with 6-a-NAD⁺, demonstrating an orthogonal substrate switch. When the isoleucine to glycine floor mutation was translated to an additional mono-ADPr PARP, PARP11, a similar switch in substrate preference for 5-Bn-6-a-NAD⁺ was observed. Both IG-PARP10 and IG-PARP11 labeled distinct protein targets in lysates in the presence of 5-Bn-6-a-NAD⁺, demonstrating specific targeting preferences for these mono-ADPr PARPs. In subsequent studies, targets of both IG-PARP10 and IG-PARP11 were identified following immunoprecipitation and tandem mass spectrometry to reveal a large target set (140) for PARP10 with broad roles in mRNA metabolism, cellular metabolism, and protein transport; whereas a small target set (21) was identified for PARP11 with specific roles in nuclear membrane transport,⁸⁵ which is consistent with a previously identified role of PARP11 in nuclear envelope maintenance.¹⁰⁰

Conclusions and Future Directions

In this study, orthogonal NAD⁺ analogue-engineered PARP pairs were developed for both the poly-ADPr and mono-ADPr subclasses of PARPs.

Whereas engineering the 'ceiling' position in the poly-ADPr PARPs provided orthogonal substrate preference for 5-Et-6-a-NAD⁺, engineering the analogous position in the mono-ADPr subclass of PARPs did not follow a similar trend in substrate preference. Engineering a different residue, the 'floor' position, within the mono-ADPr subclass of PARPs, however, provided orthogonal substrate preference for 5-Bn-6-a-NAD⁺. The difference in substrate preference between the mono-ADPr and poly-ADPr subclasses could highlight important differences in how each subclass identifies and modifies substrate targets. Future structural studies with engineered PARPs from both subclasses and their corresponding orthogonal substrate could reveal how substrate switching occurs between the engineered PARP and wild-type counterpart. These studies could help to better understand the structural features that are necessary for target identification and modification by PARPs.

Future studies could also include implementation of the chemical genetics strategy to identify protein targets in a cellular system as opposed to a cell-free system. This would provide more relevant concentrations and activation states of target proteins in comparison to a cellular lysate, which is the current limitation of the approach due to the membrane impermeability of the NAD⁺ analogues. Future work on developing membrane permeable analogues that can be dosed to cell-lines containing engineered PARPs introduced through genome-editing techniques (e.g., CRISPR/Cas9) could greatly facilitate the understanding of the cellular functions of the PARP family under more physiologically relevant conditions and in response to certain stress stimuli.

Experimental

Chemical Synthesis

General. ^1H and ^{13}C NMR were recorded on a Bruker DPX spectrometer at 400 MHz and 100 MHz, respectively. Chemical shifts are reported as parts per million (ppm) downfield from an internal tetramethylsilane standard or solvent references. High-resolution mass spectra were acquired on a ThermoElectron LTQ-Orbitrap discovery high resolution mass spectrometer with a dedicated Accela HPLC system by Andrea DeBarber at the Bioanalytical MS facility, Portland State University. For air- and water-sensitive reactions, glassware was oven-dried prior to use and reactions were performed under argon. Dichloromethane, dimethylformamide, and tetrahydrofuran were dried using the solvent purification system manufactured by Glass Contour, Inc. (Laguna Beach, CA). All other solvents were of ACS chemical grade (Fisher Scientific) and used without further purification unless otherwise indicated. Commercially available starting reagents were used without further purification. Nicotinamide (**2.2**) (Sigma-Aldrich, >99.5%), 5-methylnicotinamide (**2.4**) (Alfa Aesar, 97%), and beta-nicotinamide mononucleotide (β -NMN) (Sigma-Aldrich, >95%) were used without further purification. Analytical thin-layer chromatography was performed with silica gel 60 F₂₅₄ glass plates (SiliCycle). Flash column chromatography was conducted with either pre-packed Redisep R_f normal/reverse phase columns (Teledyne ISCO) or self-packed columns containing 200-400 mesh silica gel (SiliCycle) on a Combiflash Companion purification system (Teledyne ISCO). High performance liquid chromatography (HPLC) was performed on a Varian

Prostar 210 (Agilent) with a flow rate of 20 ml/min using Polaris 5 C18-A columns (150 x 4.6 mm, 3 μ m -analytical, 150 x 21.2 mm, 5 μ m-preparative) (Agilent). HPLC analytical conditions: mobile phase (MP) A: 0.1% formic acid (aq), mobile phase (MP) B: 0.1% formic acid in acetonitrile (ACN); flow rate = 1.0 ml/min; condition **A**: 0 – 2 min: 0%B, 2 – 15 min: 0-100%B, 15 – 17 min: 100%B; condition **B**: 0 – 1 min: 0%B, 1 – 12 min: 0-40%B, 12 – 13 min: 40%B, 13 – 14 min: 0%B; UV-Vis detection: λ_1 = 254 nm, λ_2 = 280 nm. All final products were \geq 95% purity as assessed by this method. Retention times (t_R) and purity refer to UV detection at 220 nm.

5-cyclopropyl-nicotinamide (**2.3**): 5-bromo-nicotinamide (1.05g, 5mmol), cyclopropylboronic acid (558mg, 6.5mmol), K_2CO_3 (2.1g, 15 mmol), $PdCl_2(dppf)$ (204mg, 0.25mmol) were dissolved in dioxane (40 ml) and water (4 ml) in a pressure glass vessel. Ar gas was then bubbled through the solution for 15 min. The reaction vessel was sealed and stirred at 100°C for 8 h. The reaction mixture was then cooled to rt and quenched with saturated aq. NH_4Cl solution (25 ml). The layers were separated and the aq. layer was extracted with EtOAc (3 x 15 ml). The combined organic layers were dried over $MgSO_4$, filtered, and concentrated *in vacuo*. The crude product was purified via a Combiflash Companion system (24g Redisep R_f Normal Phase; MP A: hexanes, MP B: EtOAc; 0-2 min: 40%B, 2-14 min: 40-100%B, 14-29 min: 100%B). Fractions containing the desired product were pooled and concentrated *in vacuo* to yield the product off white solid (681 mg, 84%). 1H NMR (400 MHz, $CDCl_3$) δ 8.74 (d, J

= 2.1 Hz, 1H), 8.52 (d, J = 2.2 Hz, 1H), 7.74 (t, J = 2.1 Hz, 1H), 6.24 (br., 1H), 6.19 (br., 1H), 2.09-1.72 (m, 1H), 1.16-0.92 (m, 2H), 0.76 (dt, J =6.7, 4.8 Hz, 2H); ^{13}C NMR (100 MHz, CDCl_3) δ 167.96, 151.49, 145.10, 140.07, 132.07, 128.91, 13.06, 9.60.

5-vinyl-nicotinamide (**2.9**): 5-bromo-nicotinamide (1.05 g, 5 mmol), potassium vinyl trifluoroborate (871 mg, 6.5 mmol), Cs_2CO_3 (4.5g, 15 mmol) and $\text{PdCl}_2(\text{PPh}_3)_2$ (175 mg, 0.25 mmol) were added to a flask and evacuated/refilled with Ar gas (5x). The contents of the flask were suspended in ACN/ H_2O (10:1; 44 ml) and evacuated/refilled with Ar (5x) and stirred at 120°C for 1.5 h. The reaction was allowed to cool to rt and quenched with saturated aq. NH_4Cl solution (25 ml). The layers were separated and the aq. layer was extracted with EtOAc (3 x 15 ml). The combined organic layers were dried over Na_2SO_4 , filtered, and concentrated *in vacuo*. The crude product was purified via a Combiflash Companion system (24g Redisep R_f Normal Phase; MP A: hexanes, MP B: EtOAc; 0-2 min: 40%B, 2-14 min: 40-100%B, 14-29 min: 100%B). Fractions containing the desired product were pooled and concentrated *in vacuo* to yield the product as off white solid (700 mg, 95% yield). ^1H NMR (400 MHz, $\text{MeOD}-d_4$) δ 8.89 (d, J = 2.1 Hz, 1H), 8.70 (d, J = 2.1 Hz, 1H), 8.37 (t, J = 2.1 Hz, 1H), 6.83 (dd, J = 17.7, 11.0 Hz, 1H), 6.02 (d, J = 17.7 Hz, 1H), 5.49 (d, J = 11.1 Hz, 1H); ^{13}C NMR (100 MHz, $\text{MeOD}-d_4$) δ 169.67, 150.99, 148.38, 134.98, 133.58, 131.22, 131.22, 118.48.

5-ethyl-nicotinamide (2.5): 5-vinyl-nicotinamide **2.9** (550 mg, 3.7 mmol) was dissolved in anhydrous MeOH in a pressure vessel. 10% Pd/C (55 mg) was added and the reaction was stirred under H₂ gas at rt for 5 h. The reaction was filtered over a pad of Celite® 545 to remove Pd/C and the filtrate was concentrated *in vacuo*. The crude product was purified via a Combiflash Companion system (24g Redisep R_f Normal Phase; MP A: hexanes, MP B: EtOAc; 0-2 min: 40%B, 2-14 min: 40-100%B, 14-29 min: 100%B). Fractions containing the desired product were pooled and concentrated *in vacuo* to yield the product as an off white solid (500 mg, 91%). ¹H NMR (400 MHz, DMSO-*d*₆) δ 8.85 (s, 1H), 8.57 (s, 1H), 8.13 (s, 1H), 8.06 (s, 1H), 7.57 (s, 1H), 2.67 (q, *J* = 7.6 Hz, 2H), 1.22 (t, *J* = 7.6, 3H); ¹³C NMR (101 MHz, DMSO) 166.65, 151.56, 146.23, 138.68, 134.29, 129.38, 25.16, 15.16. LC-HRMS (ESI) *m/z* [M+H]⁺ calculated for C₈H₁₁N₂O⁺ 151.0859, found 151.0852.

trans-5-propenyl-nicotinamide (2.10): 5-bromo-nicotinamide (1.0 g, 5.0 mmol), potassium *trans*-1-propenyl trifluoroborate (961.9 mg, 6.5 mmol), PdCl₂(PPh₃)₂ (351 mg, 0.5 mmol), and Cs₂CO₃ (4.88g, 15.0 mmol) were added to a flask and evacuated/refilled with Ar gas (5x). The contents of the flask were suspended in ACN/H₂O (10:1; 44 ml) and evacuated/refilled with Ar (5x) and refluxed (100°C) for 3.5 h. LC analysis revealed consumption of the starting material. The reaction was allowed to cool to rt and quenched with saturated aq. NH₄Cl solution (25 ml). The layers were separated and the aq. layer was extracted with EtOAc (3 x 15 ml). The combined organic layers were dried over Na₂SO₄, filtered, and

concentrated *in vacuo*. The crude product was purified via a Combiflash Companion system (24g Redisep R_f Normal Phase; MP A: hexanes, MP B: EtOAc; 0-2 min: 40%B, 2-14 min: 40-100%B, 14-29 min: 100%B). Fractions containing the desired product were pooled and concentrated *in vacuo* to yield the product as a beige solid (750 mg, 93%). Condition **A**, t_R = 8.91 min. ¹H NMR (400 MHz, DMSO-*d*₆) δ 8.83 (d, J = 2.0 Hz, 1H), 8.68 (d, J = 2.1 Hz, 1H), 8.22 (t, J = 2.1 Hz, 1H), 8.15 (s, 1H), 7.60 (s, 1H), 6.69 – 6.29 (m, 2H), 1.89 (d, J = 5.1 Hz, 3H).

5-propyl-nicotinamide (2.6): *trans*-5-(prop-1-en-1-yl)nicotinamide **2.10** (467 mg, 2.88 mmol) was dissolved in MeOH (20 ml) in a pressure vessel. 10% Pd/C (93.4 mg) was suspended in the reaction mixture. Triethylsilane (Et₃SiH, 25.3 ml, 158.4 mmol) was added via syringe and the reaction was capped and stirred at rt for 43 h. ¹H NMR analysis of a small reaction aliquot revealed consumption of the starting material. The reaction was filtered over a pad of Celite® 545 to remove Pd/C and the filtrate was concentrated *in vacuo*. The residue was purified via a Combiflash Companion system (12g Redisep R_f Normal Phase; MPA: CH₂Cl₂, MPB: MeOH; 0-3 min: 0%B, 3-15 min: 0-30%B, 15-16 min: 30%B). Fractions containing the desired product were pooled and concentrated *in vacuo* to yield the product as an off-white solid (390 mg, 82%). Condition **A**, t_R = 8.54 min. ¹H NMR (400 MHz, DMSO-*d*₆) δ 8.85 (d, J = 2.1 Hz, 1H), 8.54 (d, J = 2.1 Hz, 1H), 8.12 (s, 1H), 8.03 (t, J = 2.2 Hz, 1H), 7.56 (s, 1H), 2.62 (t, J = 7.6 Hz, 2H), 1.62

(m, $J = 7.4$ Hz, 2H), 0.89 (t, $J = 7.3$ Hz, 3H). ^{13}C NMR (100 MHz, $\text{DMSO-}d_6$) δ 166.59, 151.93, 146.27, 137.06, 134.78, 129.31, 33.93, 23.66, 13.49.

5-isobutyl-nicotinonitrile (2.11): 5-bromo-nicotinonitrile (2.0 g, 10.9 mmol) and Pd(dppf)Cl_2 (400 mg, 0.55 mmol) were added to a flame-dried flask. The flask was evacuated and refilled with Ar gas (3x). Anhydrous THF (60 ml) was added via syringe along with isobutylzinc bromide (40.0 ml, 0.5 M in THF). The mixture was evacuated/refilled with Ar (4x) and heated at 85°C (reflux) for 3 h followed by overnight stirring at rt. LC analysis revealed consumption of the starting material. The reaction was quenched with saturated aqueous NH_4Cl (100 ml) and the layers were separated. The aq. layer was extracted with EtOAc (3 x 15 ml) and the organic layers were combined, dried over Na_2SO_4 , filtered, and concentrated *in vacuo*. The crude residue was purified via a Combiflash Companion system (24g RediSep R_f Normal Phase; MP A: hexanes, MP B: EtOAc; 0-2 min: 0%B, 2-15 min: 0-100%B, 15-17 min: 100%B). Fractions containing the desired product were pooled and concentrated *in vacuo* to yield the product as an amorphous off-white solid (710 mg, 41%). Condition **A**, $t_R = 13.37$ min. ^1H NMR (400 MHz, CDCl_3) δ 8.73 (d, $J = 2.0$ Hz, 1H), 8.61 (d, $J = 2.1$ Hz, 1H), 7.73 (t, $J = 2.1$ Hz, 1H), 2.54 (d, $J = 7.2$ Hz, 2H), 1.89 (m, $J = 13.6, 6.8$ Hz, 1H), 0.93 (d, $J = 6.6$ Hz, 6H).

5-isobutyl-nicotinamide (2.7): 5-isobutyl-nicotinonitrile **2.11** (594 mg, 3.7 mmol) was suspended in MeOH/ H_2O (1:1, 50 mL). Amberlite® IRA 410 resin (6.79g, -

OH form) was added. The resin was prepared previously by stirring Amberlite® IRA 410 resin (Cl⁻ form) in 10% NaOH solution (300 ml) for 3 h, followed by extensive rinsing of the resin with degassed H₂O until rinsate pH was neutral. The reaction was heated at reflux for 4.5 h. LC analysis revealed consumption of the starting material. The reaction was cooled to rt and filtered. The resin was rinsed thoroughly with MeOH (50 ml) and the filtrates were combined and concentrated *in vacuo*. The resulting residue was redissolved in EtOAc (50 ml) to yield two layers. The layers were separated and the aqueous layer was extracted with EtOAc (3 x 10 ml). The combined organic layers were dried over Na₂SO₄, filtered, and concentrated *in vacuo*. The solid was purified via a Combiflash Companion system (12g RediSep R_f Normal Phase; MP A: CH₂Cl₂, MP B: MeOH; 0-3 min: 0%B, 3-15 min: 0-30%B, 15-17 min: 30%B). Fractions containing the desired product were pooled and concentrated *in vacuo* to yield the product as a white solid (540 mg, 82%). Condition **A**, *t_R* = 9.52 min. ¹H NMR (400 MHz, DMSO-*d*₆) δ 8.86 (d, *J* = 2.1 Hz, 1H), 8.51 (d, *J* = 2.1 Hz, 1H), 8.12 (s, 1H), 8.01 (t, *J* = 2.2 Hz, 1H), 7.57 (s, 1H), 2.53 (d, 2H, obscured by solvent peak), 1.87 (m, *J* = 13.5, 6.8 Hz, 1H), 0.86 (d, *J* = 6.6 Hz, 6H). ¹³C NMR (100 MHz, DMSO-*d*₆) δ 166.57, 152.36, 146.31, 136.04, 135.33, 129.21, 41.10, 29.34, 21.96 (2C).

5-benzyl-nicotinonitrile (2.12): 5-bromonicotinonitrile (1.0 g, 5.5 mmol) and Pd(PPh₃)₄ (317 mg, 0.27 mmol) were added to a flame-dried flask. The flask was evacuated and refilled with Ar gas (3x). Anhydrous THF (30 ml) was added via

syringe along with benzylzinc bromide (21.9 ml, 0.5 M in THF). The mixture was evacuated/refilled with Ar (4x) and heated at 85°C (reflux) for 1.25 h. LC analysis revealed consumption of starting material. The reaction was quenched with saturated aqueous NH₄Cl (50 ml) and the layers were separated. The aqueous layer was extracted with EtOAc (3 x 10 ml) and the organic layers were combined, dried over Na₂SO₄, filtered, and concentrated *in vacuo*. The crude residue was purified via a Combiflash Companion system (24g RediSep R_f Gold Normal Phase; MP A: hexanes, MP B: EtOAc; 0-2 min: 0%B, 2-13 min: 0-100%B, 13-16min: 100%B). Fractions containing the desired product were pooled and concentrated *in vacuo* to yield the product as an amorphous light yellow solid (900 mg g, 84%). Condition **A**, *t_R* = 13.36 min. ¹H NMR (400 MHz, CDCl₃) δ 8.72 (dd, *J* = 13.0, 2.1 Hz, 2H), 7.71 (t, *J* = 2.1 Hz, 1H), 7.41 – 7.32 (m, 2H), 7.32 – 7.27 (m, 1H), 7.21 – 7.12 (m, 2H), 4.04 (s, 2H).

5-benzyl-nicotinamide (2.8): 5-benzyl-nicotinonitrile **2.12** (677 mg, 3.5 mmol) was suspended in MeOH/H₂O (1:1, 48 mL). Amberlite® IRA 410 resin (6.39g, ⁻OH form) was added. The resin was prepared previously by stirring Amberlite® IRA 410 resin (Cl⁻ form) in 10% NaOH solution (300 ml) for 3 h, followed by extensive rinsing of the resin with degassed H₂O until rinsate pH was neutral. The reaction was heated at reflux for 3 h. LC analysis revealed consumption of the starting material. The reaction was cooled to rt and filtered. The resin was rinsed thoroughly with MeOH (50 ml) and the filtrates were combined and concentrated *in vacuo*. The resulting solid was purified via a Combiflash Companion system

(12g RediSep R_f Normal Phase; MPA: CH₂Cl₂, MPB: MeOH; 0-2 min: 0%B, 2-13 min: 0-30%B, 13-15 min: 30%B). Fractions containing the desired product were pooled and concentrated *in vacuo* to yield the product as an off-white solid (0.53 g, 72%). Condition **A**, *t_R* = 10.41 min. ¹H NMR (400 MHz, DMSO-*d*₆) δ 8.86 (d, *J* = 2.1 Hz, 1H), 8.63 (d, *J* = 2.1 Hz, 1H), 8.13 (s, 1H), 8.04 (t, *J* = 2.2 Hz, 1H), 7.57 (s, 1H), 7.36 – 7.24 (m, 4H), 7.24 – 7.16 (m, 1H), 4.02 (s, 2H). ¹³C NMR (100 MHz, DMSO-*d*₆) δ 166.40, 152.04, 146.40, 140.19, 136.62, 135.27, 129.50, 128.75 (2C), 128.67 (2C), 126.35, 37.84.

6-alkyne-adenosine (2.13): 6-chloropurine riboside (1.0 g, 3.5 mmol) was added to absolute ethanol (15 ml) and heated to reflux. DIPEA (1.82 ml, 10.5 mmol) and propargylamine (0.67 ml, 10.5 mmol) were added and the mixture was refluxed for 2 h. LC analysis revealed consumption of the starting material. The reaction was cooled to rt and the precipitated product was filtered and washed with cold methanol to yield a white solid (637 mg, 60%). Condition **B**, *t_R* = 9.42 min. ¹H NMR (400 MHz, DMSO-*d*₆) δ 8.41 (s, 1H), 8.28 (s, 1H), 5.90 (d, *J* = 6.1 Hz, 1H), 5.46 (d, *J* = 6.1 Hz, 1H), 5.35 (dd, *J* = 7.0, 4.6 Hz, 1H), 5.20 (d, *J* = 4.6 Hz, 1H), 4.60 (q, *J* = 5.9 Hz, 1H), 4.25 (s, 2H), 4.15 (td, *J* = 4.8, 3.1 Hz, 1H), 3.96 (q, *J* = 3.5 Hz, 1H), 3.75 – 3.48 (m, 2H), 3.04 (t, *J* = 2.4 Hz, 1H).

6-alkyne-AMP (2.14): 6-alkyne adenosine **2.13** (500 mg, 1.64 mmol) was heated under vacuum at 60°C for 30 min and suspended in trimethyl phosphate (5.5 ml). H₂O (14.7 μl, 0.82 mmol) was added and the mixture was heated at 50 °C for 15

min with gradual clearing. The mixture was cooled to 0°C with an ice bath and POCl₃ (457 µl, 4.91 mmol) was added dropwise. The mixture was stirred at 0°C for 3 h. LC analysis revealed consumption of the starting material. The mixture was precipitated in cold Et₂O (150 ml) in an ice bath. The residue was dissolved in ice cold H₂O (6 ml) and stirred for 10 min. The reaction was immediately neutralized with 6N NaOH. The mixture was concentrated *in vacuo* and the solid was purified via ion-pairing reversed phase chromatography using a Combiflash Companion system (C18Aq 5.5g Redisep R_f; MP A: 10 mM tributylamine/30 mM acetic acid pH 4.4 (aq), MP B: methanol; 0-1 min: 0%B, 1-12 min: 0-50%B, 12-14 min: 100%B). Fractions containing desired product were pooled and concentrated *in vacuo* to yield the tributylammonium (TBA) salt of the product as a thick oil (632 mg, 51% yield). *t_R* = 7.63 min. ¹H NMR (400 MHz, D₂O) δ 8.54 (s, 1H), 8.26 (s, 1H), 6.09 (d, *J* = 5.9 Hz, 1H), 4.75 (t, *J* = 5.7 Hz, 1H, obscured by HOD peak), 4.47 (dd, *J* = 5.1, 3.4 Hz, 1H), 4.39 – 4.23 (m, 3H), 4.00 (dd, *J* = 4.5, 3.0 Hz, 2H), 3.15 – 3.00 (m, 12H), 2.59 (t, *J* = 2.4 Hz, 1H), 1.71 – 1.53 (m, 12H), 1.32 (m, *J* = 7.4 Hz, 12H), 0.89 (t, *J* = 7.4 Hz, 18H).

6-alkyne-AMP-morpholidate (2.15): 6-alkyne-AMP TBA salt **2.14** (371 mg, 0.49 mmol) was dissolved in anhydrous DMSO (2.2 mL) and coevaporated with anhydrous DMF (3 x 5 ml). The resulting residue was redissolved in additional anhydrous DMSO (1.75 ml) and the following were added in sequence: PPh₃ (687 mg, 2.62 mmol), morpholine (369 µl, 4.22 mmol), and 2,2'-dipyridyldisulfide (Aldrithiol) (577 mg, 2.62 mmol). The resulting yellow solution was stirred at rt

under Ar for 90 min. LC analysis revealed consumption of starting material. To the reaction was added 0.2 M NaI in acetonitrile (40 ml) dropwise to form a white precipitate (ppt). The mixture was centrifuged at 8,000g for 10 min at 4°C. The supernatant was decanted and the ppt was washed with ACN (5 ml) and centrifuged again using the same conditions. The ppt was washed with EtOAc (2 x 5 ml) or until the yellow color was removed. The ppt was redissolved in MeOH and concentrated *in vacuo* to yield the sodium salt of the product as a white solid (215 mg, 92%), which was used in subsequent coupling reactions without further purification. Condition **B**, t_R = 9.00 min. ^1H NMR (400 MHz, D_2O) δ 8.40 (s, 1H), 8.29 (s, 1H), 6.10 (d, J = 5.0 Hz, 1H), 4.83 – 4.80 (m, 1H, obscured by HOD peak), 4.52 (t, J = 4.8 Hz, 1H), 4.40 – 4.25 (m, 3H), 4.00 (ttt, J = 11.7, 8.5, 7.8, 3.8 Hz, 2H), 3.50 (t, J = 4.8 Hz, 4H), 2.86 (p, J = 4.9 Hz, 4H), 2.59 (t, J = 2.4 Hz, 1H). ^{13}C NMR (100 MHz, D_2O) δ 154.50, 153.33, 149.05, 119.80, 87.96, 84.36, 74.66, 70.87, 67.49, 64.40, 45.23, 30.81. LC-HRMS (ESI) m/z $[\text{M}+\text{H}+\text{Na}]^+$ calculated for $\text{C}_{17}\text{H}_{22}\text{N}_6\text{NaO}_7\text{P}$ 477.12580, observed 477.12626.

6-*a*-NAD⁺. 6-*a*-NAD⁺ was previously described;⁴⁵ however, we used a different synthetic procedure. 6-alkyne-AMP-morpholidate **2.15** (24 mg, 0.05 mmol), β -NMN (20 mg, 0.055 mmol), and MgSO_4 (12 mg, 0.1 mmol) were dissolved in a solution of MnCl_2 (0.38 ml, 0.2 M in formamide) at rt for 48 h. The reaction was then concentrated *in vacuo* and the crude product was purified via preparative HPLC (MP A: 0.1% formic acid (aq), MP B: 0.1% formic acid in ACN; 0-5 min: 0-10%B, 5-8 min: 10-15%B, 8-10 min: 15-20%B, 10-12 min: 20-50%B). Fractions

containing the desired product were pooled and concentrated *in vacuo* to yield the desired product (14 mg, 40% yield). ^1H NMR (400 MHz, D_2O) δ 9.34 (s, 1H), 9.18 (d, J = 6.3 Hz, 1H), 8.85 (d, J = 8.1 Hz, 1H), 8.53 (s, 1H), 8.34 (d, J = 0.8 Hz, 1H), 8.15 (m, 1H), 6.09 (d, J = 5.5 Hz, 2H), 4.73 (m, 1H), 4.47-4.53 (m, 3H), 4.41 (m, 2H), 4.33 (m, 3H), 4.19 (m, 3H), 2.70 (s, 1H).

*N'-(2,3,5-Tri-*o*-Benzoyl- β -D-ribofuranosyl)-3-aminocarbonyl-5-ethyl-pyridinium bromide (2.16)*: β -D-ribofuranose-acetate-2, 3, 5-tribenzoate (504 mg, 1 mmol) was dissolved in toluene (15 ml) and cooled to 0°C. HBr (33wt% in acetic acid) (368 mg, 1.5 mmol) was added dropwise and the reaction was stirred at 0°C for 2 h. 0.5 ml of the solution mixture was taken and evaporated to dryness for NMR analysis. In the ^1H NMR spectrum the anomeric proton for the β -form is a singlet at 6.6 ppm and a doublet at 6.9 ppm for the α -form. After the starting material was consumed and ^1H NMR confirmed the formation of the β -form, the reaction was concentrated *in vacuo*. The crude β -D-ribofuranose-bromo-2, 3, 5-tribenzoate product was azeotroped with toluene (3 x 20 ml) to remove remaining acetic acid and dried *in vacuo* for 2 h. Crude β -D-ribofuranose-bromo-2, 3, 5-tribenzoate and 5-ethyl nicotinamide **5** (91 mg, 0.6 mmol) was dissolved in ACN (40 ml). The reaction was stirred under Ar gas at rt for 2 days. The reaction was concentrated *in vacuo* (temperature kept below 35°C). The crude product was dissolved in CDCl_3 (2 ml) and ppt by adding ethyl ether (10 ml). The entire procedure was repeated three times to yield the desired product (270 mg, 67% yield), which was used in subsequent reactions without further purification. ^1H

NMR (400 MHz, CDCl₃) δ 10.66 (s, 1H), 10.43 (s, 1H), 8.95 (s, 1H), 8.87 (s, 1H), 8.47 (s, 1H), 8.08 (m, 4H), 8.01 (m, 2H), 7.68 – 7.54 (m, 3H), 7.53 – 7.34 (m, 6H), 6.08 – 5.89 (m, 2H), 5.86 – 5.71 (m, 1H), 5.14 – 5.00 (m, 2H), 4.93 – 4.79 (m, 1H), 2.66 (q, J = 7.6 Hz, 2H), 1.19 (t, J = 7.6, 3H). HRMS (ESI) m/z [M+H]⁺ calculated for C₃₄H₃₂N₂O₈⁺ 595.20749, found 595.20890.

N'-(β -D-ribofuranosyl)-3-aminocarbonyl-5-ethyl-pyridinium bromide (2.17): **2.16** (150 mg, 0.22 mmol) was dissolved in ammonia (15 mL, 7 N in MeOH) and the reaction was stirred at -10°C for 36 h. The reaction was concentrated *in vacuo* and the crude product was dissolved in MeOH (1 mL). Addition of ethyl ether (10 mL) resulted in ppt of the desired product. The procedure was repeated three times to yield the desired product as an off white powder (56 mg, 71% yield), which was used in subsequent reactions without further purification. Some epimerization was observed (~5-10% α -form was present as determined by ¹H NMR analysis). ¹H NMR (400 MHz, D₂O) δ 9.40 (s, 1H), 9.13 (s, 1H), 8.82 (d, J = 1.7 Hz, 1H), 6.19 (d, J = 4.1 Hz, 1H), 4.55 – 4.39 (m, 2H), 4.34 (t, J = 4.8 Hz, 1H), 4.07 – 4.03 (dd, 1H, J = 2.80 and 12.80 Hz, 1H), 3.91-3.87 (dd, 1H, J = 3.2 and 12.8 Hz, 1H), 2.96 (q, J = 7.6 Hz, 2H), 1.31 (t, J = 7.6 Hz, 3H). HRMS (ESI) m/z [M+H]⁺ calculated for C₁₃H₂₀N₂O₅⁺, 283.12885, found 283.12904.

5-ethyl-nicotinamide mononucleotide (2.18): **2.17** was dissolved in trimethylphosphate (0.18 mL) and the reaction was cooled to 0°C. POCl₃ (166 mg, 1.08 mmol) was added and the reaction was stirred at 0°C for 4 h. A few

drops H₂O was then added to quench the reaction. Trimethylphosphate was removed by extraction with ethyl ether (20 ml). The remaining trimethylphosphate was removed by a second extraction with THF (5 ml). The aq layer was concentrated *in vacuo*. The crude product was dissolved in H₂O (0.5 ml) and purified via two-step ion exchange chromatography (Dowex resin 1 x 2, formate resin, eluted with water; H⁺ resin, eluted with water). Fractions containing the desired product were pooled and concentrated *in vacuo* to yield the desired product (74 mg, 74% yield). ¹H NMR (400 MHz, D₂O) δ 9.31 (s, 1H), 9.06 (s, 1H), 8.84 (s, 1H), 6.14 (d, *J*=5.6 Hz, 1H), 4.56 (m, 1H), 4.43 (t, *J*=5.2 Hz, 1H), 4.41-4.40 (dd, *J*=5.0, 2.4 Hz, 1H), 4.29 (ddd, *J*=12.0, 4.4, 2.4 Hz, 1H), 4.13 (ddd, *J* = 11.9, 4.9, 2.1 Hz, 1H), 2.97 (q, *J*=7.6 Hz, 2H), 1.32 (t, *J*=7.6 Hz, 3H); ¹³C NMR (100 MHz, D₂O/ CD₃OD (9:1)) δ 167.05, 147.14, 146.59, 142.70, 138.02, 134.60, 100.99, 88.69, 78.78, 72.29, 65.11, 26.64, 14.58. HRMS (ESI) *m/z* [M+H]⁺ calculated for C₁₃H₂₀N₂O₈P⁺, 363.09518, found 363.09643.

5-Et-6-a-NAD⁺ (2.1): 6-alkyne-AMP-morpholidate **2.15** (24 mg, 0.05 mmol), 5-ethyl-nicotinamide mononucleotide **2.18** (20 mg, 0.055 mmol), and MgSO₄ (12 mg, 0.1 mmol) were dissolved in a solution of MnCl₂ (0.38 ml, 0.2 M in formamide) at rt for 48 h. The reaction was then concentrated *in vacuo* and the crude product was purified via preparative HPLC (MP A: 0.1% formic acid (aq), MP B: 0.1% formic acid in ACN; 0-5 min: 0-10%B, 5-8 min: 10-15%B, 8-10 min: 15-20%B, 10-12 min: 20-50%B). Fractions containing the desired product were pooled and concentrated *in vacuo* to yield the desired product (11 mg, 31%

yield). ^1H NMR (400 MHz, D_2O) δ 9.11 (s, 1H), 8.90 (s, 1H), 8.73 (s, 1H), 8.44 (s, 1H), 8.22 (s, 1H), 5.99 (dd, $J = 13.4, 5.5$ Hz, 2H), 4.71 (1H, overlapping with HOD peak), 4.48 (d, $J = 6.0$ Hz, 2H), 4.47 – 4.38 (m, 1H), 4.33 (s, 3H), 4.21 (s, 3H), 2.89 (q, $J = 7.6$ Hz, 2H), 2.65 (s, 1H), 1.27 (t, $J = 7.6$ Hz, 3H); ^{13}C NMR (100 MHz, D_2O) δ 165.72, 147.15, 146.61, 142.71, 137.95, 132.31, 100.91, 88.16, 84.97, 80.06, 78.59, 75.30, 73.67, 71.82, 71.27, 62.64, 26.60, 14.44. LC-HRMS (ESI) m/z $[\text{M}+\text{H}]^+$ calculated for $\text{C}_{26}\text{H}_{33}\text{N}_7\text{O}_{14}\text{P}_2^+$, 730.16389, found 730.16502.

Other Methods

Cell culture and reagents. HEK 293T cells were grown at 37°C and 5% CO_2 . Cells were passaged in DMEM + 10% FBS (Gibco) + penicillin/streptomycin (Invitrogen). Transient transfections of HEK293T cells with 20 μg of GFP-tagged expression vectors per 10-cm dish (~70% confluency) were performed using the CalPhos system (Clontech) according to manufacturer's instructions. Cells were lysed in HEPES buffer supplemented with cOmplete EDTA-free protease inhibitor (Roche), and cell debris was cleared by centrifugation at 14,000 $\times g$ for 5 min at 4 °C. Antibodies used for immunoblot detection were anti-His (His.H8, Pierce, 1:1,000) and goat anti-mouse IgG – HRP (Novex). Primary antibodies (stored at 1 mg/ml) were used at the indicated concentration and secondary antibodies at 1:5,000 for immunoblot assays. Streptavidin-HRP (Jackson ImmunoResearch) was stored at -20°C in a 50% glycerol mix (0.5 mg/ml) and was used at 1:5,000 for immunoblot assays.

Cloning and mutagenesis. The coding region for human PARP1 and PARP5b were obtained from the DNASU plasmid repository (PARP1: HsCD00040600, PARP5b: HsCD00080244)⁷. cDNA encoding mouse PARP2 was obtained from a cDNA library generated for this study. RNA was isolated from mouse embryonic brain tissue using the TRIzol® reagent (Invitrogen) protocol. 5 µg of isolated RNA was reverse transcribed with SuperScript® III Reverse Transcriptase (Invitrogen) to produce cDNA. Full-length PARP1 and PARP2 were PCR-amplified from cDNA using primers with non-complementary restriction enzyme sites located at the 5' and 3' ends. Primers for amplification of PARP5b were designed to amplify only the catalytic domain (residues 934-1166). Amplified products were cloned into pET-28b⁺ (Novagen) for expression. PARP10_{cat} was cloned as previously described.⁹⁹ Mutants were generated using the QuickChange® II XL site-directed mutagenesis kit (Agilent). Plasmids were sequenced from both the 5' and 3' direction to confirm the coding sequence.

Expression and purification of PARP1, PARP2, PARP5b_{cat}, and PARP10_{cat}.

PARP1 and PARP2 were expressed in the *Escherichia coli* BL21 pRARE2 strain (EMD Millipore). Cells were first cultured in LB media overnight at 225 rpm and 37°C in an Excella® E24 Incubator (New Brunswick Scientific). One liter of TB media (12 g Bacto Tryptone (BD Biosciences), 24 g Bacto Yeast Extract (BD Biosciences), 0.4% glycerol, 17 mM KH₂PO₄, 72 mM K₂HPO₄, 1% glucose, 100 µM ZnCl₂, 50 µg/ml kanamycin, 34 µg/ml chloramphenicol) was inoculated with the starting culture and grown to OD₆₀₀ = 0.8 – 1.0 at 225 rpm and 37°C. The

temperature was reduced to 16°C and expression was induced by adding isopropyl β -D-thiogalactoside (IPTG) to 0.4 mM. After incubation at 16°C for 18 – 24 h, cells were harvested by centrifugation at 6,000 g for 10 min. The cell pellet was re-suspended in lysis buffer (20 mM HEPES, pH 7.5, 1 mM β -mercaptoethanol (β -Me), 1 mM benzamidine, 0.2% NP-40, 0.2% TWEEN-20, 500 mM NaCl, 1 mM phenylmethylsulfonyl fluoride (PMSF), 8.3 mg/L DNase I (Roche)) at 4°C, subjected to cell disruption using a Sonifier 450 (Branson), and lysate was clarified by centrifugation at 12,000 g for 30 min at 4°C. Lysates were incubated with pre-washed Ni-NTA agarose resin (50% slurry, Qiagen) with end-over-end rotation at 4°C for 1 h. Following extensive washing with buffer B1+20 (20 mM HEPES, pH 7.5, 1 mM β -Me, 1 mM PMSF, 1 mM benzamidine, 500 mM NaCl, 20 mM imidazole) protein was eluted in buffer B1+400 (20 mM HEPES, pH 7.5, 1 mM β -Me, 500 mM NaCl, 400 mM imidazole) and diluted with an equal volume of buffer 3AB+400 (100 mM Tris-HCl, pH 7.5, 0.5 mM EDTA, 14 mM β -Me, 0.4 M NaCl). Eluate was then loaded to a pre-washed 3-aminobenzamide-sepharose 4B chromatography column by gravity flow. The column was washed with buffer 3AB+400 followed by an equal volume of buffer 3AB+800 (100 mM Tris-HCl, pH 7.5, 0.5 mM EDTA, 14 mM β -Me, 0.8 M NaCl) and protein was eluted in buffer 3AB+MetB (100 mM Tris-HCl, pH 7.5, 0.5 mM EDTA, 14 mM β -Me, 0.4 M NaCl, 2 mM 3-methoxybenzamide). Fractions containing PARP protein were collected and dialyzed to 50 mM Tris-HCl, pH 7.5, 0.1 mM EDTA, 1 mM β -Me, 0.4 M NaCl at 4°C. Protein concentrations were determined by Bradford assay with BSA standards and purity was assessed by PageBlue staining

(Pierce) after SDS-polyacrylamide gel electrophoresis (SDS-PAGE). $\geq 90\%$ purity was achieved for each of the PARP1 and PARP2 variants. PARP5b_{cat} was expressed as above, but was only purified using Ni-NTA agarose resin. $\geq 50\%$ purity was achieved for each of the PARP5b_{cat} variants. PARP10_{cat} WT and variants were expressed and purified as described previously.⁹⁹

Histone H1 plate assays. 250 ng of each PARP1 variant was pre-incubated with varying concentrations (0 - 2 mM) of nicotinamide (Sigma), 5-methylnicotinamide (Alfa Aesar), or various nicotinamide analogs in hB buffer (50 mM Tris-HCl, pH 8.0, 100 mM NaCl, 10 mM MgCl₂, 1 mM *tris*(2-carboxyethyl)phosphine (TCEP), 10 ng/ μ L activated DNA (Sigma)) in individual wells of an 8-well Histone H1 strip plate (Trevigen) at rt for 10 min. 6-a-NAD⁺ pre-incubated with an identical concentration of inhibitor in plate buffer was added to the PARP mix to a final concentration of 50 μ M. The reaction proceeded for 30 min at 30°C for the WT-PARP1 and 60 min for the mutants, the plate was washed thrice in 1X PBST (1x PBS, 1% triton X-100), thrice in 1X PBS, and click conjugation was performed in CB buffer (100 μ M biotin-PEG₃-azide, 100 μ M Tris[(1-benzyl-1*H*-1,2,3-triazol-4-yl)methyl]amine (TBTA, Sigma), 1 mM CuSO₄, 1 mM TCEP, 1X PBS) for 30 min at rt. The plates were washed thrice in 1X PBST, thrice in 1X PBS, and incubated with streptavidin-HRP in SH buffer (150 mM KPO₄, pH 7.5, 150 mM KCl, 300 ng/ μ L BSA, 30 mM β -Me) for 30 min at rt. The plates were washed thrice in 1X PBST, thrice in 1X PBS, and were developed using SureBlue™ TMB Microwell Peroxidase Substrate (KPL) for 2 – 5 min prior

to quenching with an equal volume of 1N HCl. Absorbance at 405 nm for each sample was read on a Fusion Universal Microplate Analyzer (Packard). Inhibitor dose-response curves were fit using linear regression in Prism 5 (GraphPad Software). The mean IC₅₀ was calculated from three independent assays.

Auto-modification assays. 300 ng of either the WT or KA variant of PARP1, PARP2, or PARP5b_{cat} were brought up in hB buffer – activated DNA was absent for assays involving PARP5b_{cat} – and automodification was initiated by adding an equal volume of either hB buffer, 6-a-NAD⁺, or 5-Et-6-a-NAD⁺ to a final concentration of either 0 μ M (hB), 50 μ M (5-Et-6-a-NAD⁺), 100 μ M (5-Et-6-a-NAD⁺ or 6-a-NAD⁺), or 250 μ M (5-Et-6-a-NAD⁺) modified NAD⁺ analog. Reactions proceeded for 1 h at 30°C, click conjugation was performed by spiking in a one-third volume of CBT buffer (1.5 mM Tris(3-hydroxypropyltriazolylmethyl)amine (THPTA, Sigma), 750 μ M CuSO₄, 300 μ M biotin-PEG₃-azide, 7.5 mM sodium ascorbate, 1X PBS) and reactions were left at rt for 1 h. Reactions were fractionated by SDS-PAGE and subsequent immunoblot analysis was performed using a ChemiDoc™ MP Imaging System (Bio-Rad). Each experiment was repeated at least twice, shown are representative images.

SRPK2 ADPr Assay. 1 μ M of each PARP10_{cat} variant was incubated with 3 μ M SRPK2 and 100 μ M of each modified NAD⁺ analogue for 2 h at 30 °C in a 20 μ L reaction volume consisting of 50 mM HEPES (pH 7.5), 100 mM NaCl, 10 mM

MgCl₂, and 0.5 mM TCEP. Click conjugation was performed with 1.5 mM THPTA, 750 μM CuSO₄, 300 μM sulforhodamine B-PEG₃-azide, and 7.5 mM sodium ascorbate in 1 x PBS for 1 h at room temperature. SRPK2 labeling was quantified using Image Lab v5.2 (Bio-Rad).

Chapter 3: A Clickable Aminoxy Probe for Monitoring Cellular ADP-ribosylation

Rory K. Morgan and Michael S. Cohen

Portions of this chapter were originally published in *ACS Chem. Bio.* on August 21, 2015 in volume 10, issue 8, pages 1778–1784 (Copyright © 2015, American Chemical Society)⁹⁹ and in *Methods Mol. Bio* published online on July 11, 2017 as part of Alexei V. Tulin (ed.), *Poly(ADP-Ribose) Polymerase: Methods and Protocols* (Copyright © Springer Science+Business Media LLC 2017).¹⁰¹ Both publications have been adapted for this dissertation and reprinted with permission.

Abstract

ADP-ribosylation (ADPr) is essential for cell function yet there is a dearth of methods for detecting this posttranslational modification in cells. Here, we describe a clickable aminooxy alkyne (AO-alkyne) probe that can detect cellular ADPr on acidic amino acids following Cu-catalyzed conjugation to an azide-containing reporter. Using AO-alkyne, we show that PARP10 and PARP11 are auto-ADP-ribosylated in cells. We also demonstrate that AO-alkyne can be used to monitor stimulus-induced ADPr in cells. Functional studies using AO-alkyne support a previously unknown mechanism for ADPr on acidic amino acids, wherein a glutamate or aspartate at the initial C1'-position of ADP-ribose transfers to the C2'-position. This new mechanism for ADPr has important implications for how glutamyl/aspartyl-ADP-ribose is recognized by proteins in cells.

Introduction

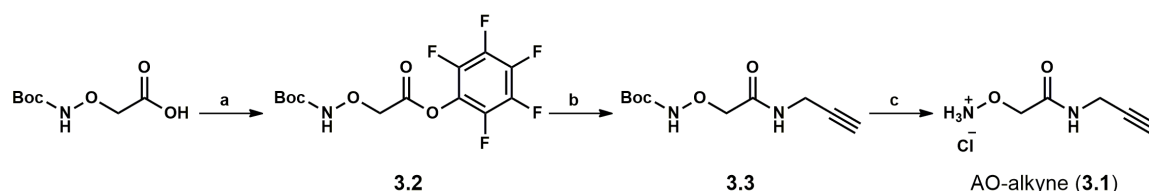
ADP-ribosylation (ADPr) has emerged as a major post-translational modification in cells. ADPr is catalyzed by a family of 17 enzymes in humans known as poly-ADP-ribose polymerases (PARPs), which transfer ADP-ribose from nicotinamide adenine dinucleotide (NAD^+) to amino acids on target proteins to form monomers (mono-ADPr) or polymers (poly-ADPr) of ADP-ribose.⁶ Despite their name, the majority of the PARP family members catalyze mono-ADPr; in fact, only four PARPs (PARP1, 2, 5a/b) have been shown to be *bona fide* poly-ADPr polymerases.²⁷ Methods for detecting ADPr in general, and mono-ADPr in particular, in cells are lacking. The use of radiolabelled NAD^+ and NAD^+ variants, such as biotin- NAD^+ ⁴⁴ or 6-alkyne- NAD^+ followed by click chemistry with an azide reporter^{45,84} has been useful for detecting mono-ADPr *in vitro* but cannot be used for detecting ADPr in cells. We therefore sought a strategy for detecting ADPr in cells.

Results and Discussion

Design of a clickable aminooxy probe for detection of ADP-ribosylated acidic residues

We focused our initial efforts on detecting proteins modified by ADP-ribose on the acidic amino acids glutamate (Glu) and aspartate (Asp) since recent proteomics studies demonstrate that these are major sites of ADPr in the cell.^{43,102} Seminal studies in the late 1970s demonstrated that the Glu- and Asp-ADP-ribose bond is cleaved rapidly by high concentrations of

hydroxylamine.^{103,104} The proposed mechanism for this cleavage involves transacylation from the ester between Glu or Asp and ADP-ribose to hydroxylamine, resulting in the formation of a hydroxamic acid derivative at the site of modification, with concomitant release of free ADP-ribose. This mechanism was exploited in a recent study that sought to characterize the Glu/Asp-ADP-ribosylated proteome.⁴³ Based on this mechanism, we designed an aminooxy alkyne probe (AO-alkyne, **3.1**) (**Figure 3-1a** and **Scheme 3-1**) for the detection of mono-ADPr of proteins on acidic amino acids. We envisioned that AO-alkyne would react with the ester of Glu/Asp-ADP-ribose forming an alkyne hydroxamic ester that could be subsequently detected after Cu-catalyzed conjugation (“click chemistry”) to an azide reporter.



Scheme 3-1. Synthesis of AO-alkyne (**3.1**). Reagents and conditions: a. TFA-OPfp, pyr, DCM (71% yield); b. propargylamine, DIPEA, DCM, (96% yield); c. 4N HCl, dioxane (63% yield).

AO-alkyne reacts with an aldehyde on Glu/Asp-ADP-ribose to form an oxime

We first determined if **3.1** could detect PARP10-mediated ADPr of SRSF protein kinase 2 (SRPK2) (**Figure 3-1b**). Previous studies demonstrated that SRPK2 is a substrate of PARP10,^{98,105} which transfers ADP-ribose onto acidic amino acids in target proteins.¹⁰⁶ We treated human PARP10 catalytic domain (hPARP10_{cat}) and SRPK2 with NAD⁺ (100 μ M) and then added **3.1** (100 μ M) at

various pH values followed by click conjugation to a biotin-azide reporter. Labeling of SRPK2 by **3.1** was NAD⁺-dependent and maximal at pH 5 (**Figure 3-1c**). In contrast, no labeling was detected at pH values greater than 7 (**Figure 3-1c**).

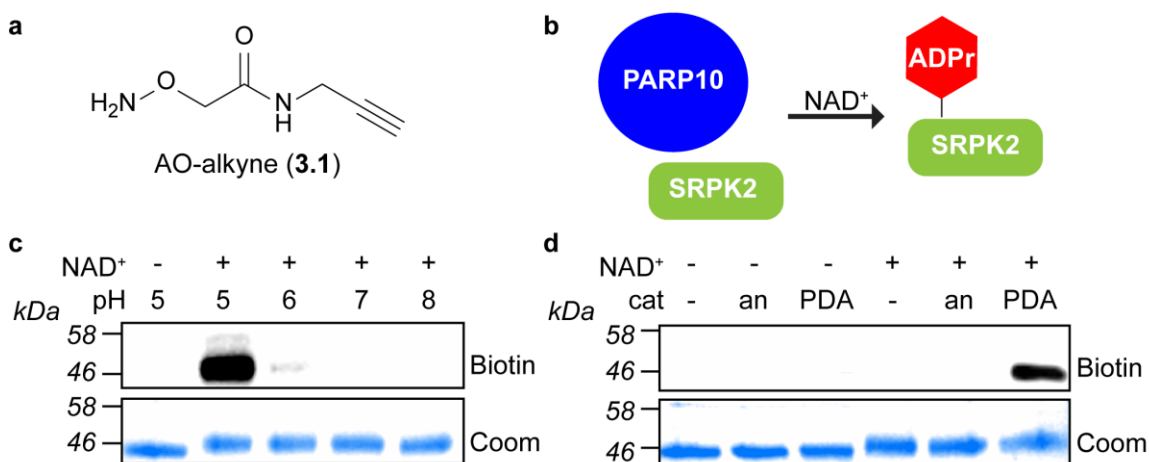


Figure 3-1. AO-alkyne, a clickable aminooxy probe that can detect ADPr of acidic amino acids. **(a)** Structure of bifunctional probe, AO-alkyne (**3.1**). The probe contains an aminooxy group for conjugation with the ADPr modification on acidic amino acids and an alkyne handle for subsequent click conjugation with an azido reporter. **(b)** Schematic showing PARP10 transferring the ADPr moiety of NAD⁺ onto its protein target SRPK2. **(c)** AO-alkyne-mediated labeling of ADPr-modified SRPK2 is pH dependent. SRPK2 was ADP-ribosylated by human PARP10 catalytic domain (hPARP10_{cat}) in the presence of NAD⁺ (100 μM). AO-alkyne selectively labels ADPr-modified SRPK2 in pH 5 acetate buffer as demonstrated by click conjugation with biotin-azide (100 μM). Proteins were resolved by SDS/PAGE and detected by Western blot with Streptavidin-HRP. **(d)** *p*-phenylenediamine (PDA, 10 mM) catalyzes the labeling of ADPr-modified SRPK2 by **3.1**. ADPr-modified SRPK2 in pH 7 phosphate buffer was treated with **3.1** (100 μM) followed by click conjugation with biotin-azide (100 μM). Proteins were resolved by SDS/PAGE and detected by Western blot with Streptavidin-HRP. In contrast to PDA, aniline (an) results in no labeling at pH 7. Coomassie (Coom) Brilliant Blue staining was used to demonstrate even loading.

These observations are inconsistent with a mechanism involving transacylation of the ester modification linking ADP-ribose to its protein target, which occurs at neutral and slightly basic pH values. Instead, we hypothesize that **3.1** forms an oxime bond with Glu/Asp-ADP-ribose on SRPK2, the formation of which is optimal at pH 4-5. Recently, it was shown that substituted anilines catalyze oxime

bond formation at neutral pH.¹⁰⁷ Indeed, when *p*-phenylenediamine (PDA) was added together with **3.1** at pH 7 we observed labeling of Glu/Asp-ADP-ribosylated SRPK2 (**Figure 3-1d**). The less effective oxime catalyst, aniline, did not result in labeling (**Figure 3-1d**). Using our optimized labeling conditions we were also able to detect ADPr of SRPK2 by another PARP, PARP15, which catalyzes mono-ADPr (**Figure 3-2**).²⁷

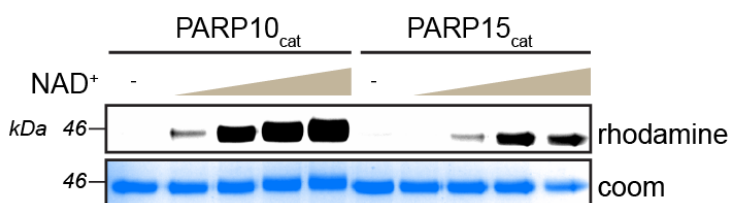


Figure 3-2. PARP10_{cat} and PARP15_{cat}-mediated ADP-ribosylation of SRPK2 *in vitro* is detected by **3.1** following click conjugation with rhodamine-azide. SRPK2 was ADP-ribosylated by PARP10_{cat} or PARP15_{cat} in the presence of NAD⁺ (0, 1, 10, 50, or 100 μM) at 30 °C for 1h, followed by labeling with **3.1** (100 μM) at pH 5 with PDA (10 mM) and subsequent click conjugation with rhodamine-azide (100 μM).

Taken together, these results suggest that **3.1** is reacting with an aldehyde that is present on Glu/Asp-ADP-ribose, leading to formation of a stable oxime.

An aldehyde exists at the C1'-position of Glu/Asp-ADP-ribose capable of reacting with aminooxy probes

The terminal ribose ring of free ADP-ribose tautomerizes between a ring-closed and a ring-opened form; the latter form contains an aldehyde at the C1'-position capable of reacting with an oxime at pH 4-5.¹⁰⁸ If PARP10-mediated ADPr of acidic amino acids involves the formation of a glycoside bond between Glu/Asp and the C1'-position of the terminal ribose ring – which is the currently

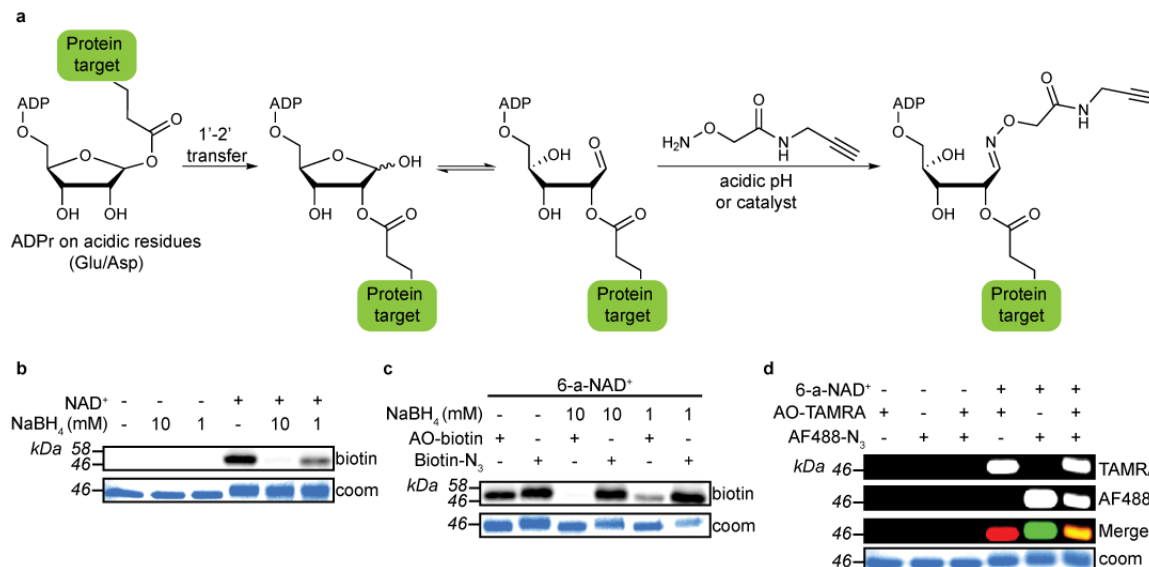


Figure 3-3. AO-alkyne reveals an unanticipated mechanism of ADPr on acidic residues. (a) Proposed mechanism of PARP catalyzed ADPr of acidic residues, glutamate (Glu) and aspartate (Asp). In this mechanism, the Glu/Asp side chain undergoes a 1'-2' transfer. The ribose ring is in equilibrium between its open and closed conformation. At acidic pH or in the presence of catalysis at neutral pH, **3.1** reacts with the free aldehyde at the C1' position, resulting in the formation of a stable oxime. (b) Borohydride reduction after ADPr blocks labeling of SRPK2 by 1. SRPK2 was ADP-ribosylated by hPARP10_{cat} in the presence of NAD⁺ (100 μM). ADP-ribose-modified SRPK2 was then treated with NaBH₄ for 15 min at room temperature prior to AO-biotin (100 μM) treatment at pH 5 with PDA catalysis. Click conjugation was then performed with biotin-azide (100 μM). Proteins were resolved by SDS/PAGE and detected by Western blot with Streptavidin-HRP. (c) Borohydride reduction does not result in loss of the ADP-ribose modification. SRPK2 was ADP-ribosylated by hPARP10_{cat} in the presence of the clickable NAD⁺ analogue, 6-a-NAD⁺ (100 μM). 6-a-ADP-ribose-modified SRPK2 was then treated with NaBH₄ for 15 min at room temperature prior to AO-biotin (100 μM) treatment at pH 5 with PDA catalysis. In some conditions, click conjugation was performed with biotin-azide (100 μM). Proteins were resolved by SDS/PAGE and detected by Western blot with Streptavidin-HRP. (d) Dual labeling of ADP-ribose at the C1' position and at the N6 position of ADP-ribose. SRPK2 was ADP-ribosylated by hPARP10_{cat} in the presence of 6-a-NAD⁺ (100 μM). AO-TAMRA (100 μM) was reacted with 6-a-ADP-ribose-SRPK2 at pH 5 with the PDA catalysis followed by click conjugation of AF488-azide (100 μM). Proteins were resolved by SDS/PAGE and detected by in-gel fluorescence scanning (Typhoon 9400).

We propose that a transfer of the Glu/Asp from the C1'-position to another site (i.e., C2') on the ribose ring is occurring (**Figure 3-3a**). This proposed C1'-C2' transfer frees up the C1' position, enabling **3.1** to react with the open-chain

aldehyde form at C1' at acidic pH or in the presence of PDA catalysis at neutral pH.

To test this proposed mechanism, we treated Glu/Asp-ADP-ribosylated SRPK2 with sodium borohydride (NaBH_4), which should reduce the C1' aldehyde, preventing oxime bond formation with an aminooxy probe. Indeed, we found that increasing concentrations of NaBH_4 blocked labeling of Glu/Asp-ADP-ribosylated SRPK2 by aminooxy-biotin (AO-biotin) (**Figure 3-3b**). While ester bonds are stable to NaBH_4 reduction,¹⁰⁹ we wanted to rule out hydrolysis of ADP-ribose at the ester linkage due to an increase in pH from NaBH_4 decomposition in aqueous media. We repeated the previous borohydride reduction experiment using an NAD^+ variant containing an alkyne modification at the N^6 -position of the adenosine ring (6-a- NAD^+)^{45,84} instead of native NAD^+ . The alkyne handle can be conjugated to an azide reporter and provides a secondary means to detect the ADP-ribose modification. Whereas NaBH_4 blocked AO-biotin-mediated labeling of 6-a-ADP-ribosylated SRPK2, it did not block click chemistry-mediated labeling of 6-a-ADP-ribosylated SRPK2 with biotin-azide (**Figure 3-3c**). Therefore, the Glu/Asp-ADP-ribose modification does not undergo hydrolysis at the ester linkage in reaction conditions that contain NaBH_4 , remaining attached to its protein target SRPK2. Together, these results support the presence of an aldehyde at the C1'-position of Glu/Asp-ADP-ribose that is capable of reacting with an aminooxy probe.

Our proposed mechanism suggests that a C1'-aldehyde and a C2'-Glu/Asp ester exist on the same ADP-ribose modification site. To examine this

idea, we determined if we could simultaneously label 6-a-Glu/Asp-ADP-ribosylated SRPK2 with an aminooxy TAMRA (AO-TAMRA) probe and an Alexa Fluor 488-azide (AF488-azide) probe using click chemistry. We found that 6-a-Glu/Asp-ADP-ribosylated SRPK2 is labeled with both fluorescent probes, as demonstrated by in-gel fluorescence scanning (**Figure 3d**). Taken together, our results support our proposed mechanism in which the Glu/Asp that is initially attached to the C1'-position of ADP-ribose is transferred to the C2' position, where transfer to the C3' position could also occur due to a C2'-C3' equilibrium.

Functional studies with aminooxy probes support a previously reported model of MacroD-mediated reversal of Glu/Asp-ADP-ribose

Recently, two independent studies demonstrated that a family of macrodomain-containing proteins (MacroD1 and D2) reverses mono-ADPr on acidic amino acids on proteins.^{110,111} The authors propose two divergent mechanisms of mono-ADPr reversal: in one study, the authors propose that the acidic amino acid is attached to the C1'-position and that MacroDs hydrolyze the glycosidic bond between Glu/Asp and ADP-ribose.¹¹¹ In the other study, the authors propose that the acidic amino acid is attached to the C2'-position and that MacroDs hydrolyze the ester bond between Glu/Asp and ADP-ribose.¹¹⁰ The latter model is based on the structural similarity between ADP-ribose and the sirtuin deacetylation product 2'-O-acetyl-ADP-ribose, which was the first characterized substrate of MacroDs.^{112,113} Our results support the second model of MacroD-mediated reversal of ADPr on acidic amino acids.

AO-alkyne detects PARP10 automodification in cells

Having examined the mechanism of PARP10-mediated ADPr of acidic amino acids, we next sought to determine if **3.1** could detect mono-ADPr of PARP10 in cells.

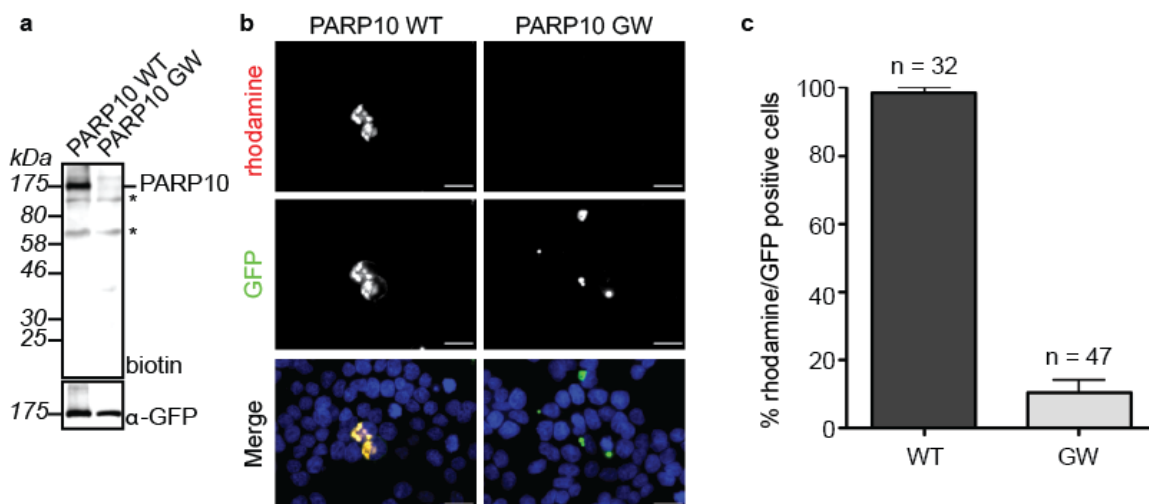


Figure 3-4. AO-alkyne detects auto-ADPr of PARP10 in cells. (a) HEK 293T cells expressing either GFP-PARP10 WT or GFP-PARP10 GW (catalytically dead) were treated with **3.1** (100 μM) and PDA (10 mM) for 1 h at 37 °C. Lysates were then subjected to click conjugation with biotin-azide (100 μM). Proteins were resolved by SDS/PAGE and detected by Western blot with either Streptavidin-HRP or an antibody against GFP. Bands marked with an asterisk represent endogenous biotinylated proteins. (b) HEK 293T cells overexpressing either GFP-PARP10 WT and GFP-PARP10 GW (catalytically dead) were treated similarly as in (a). After fixation, permeabilization, and blocking, the cells were subjected to click conjugation with rhodamine-azide (1 μM) for 30 min. Scale bar corresponds to 20 μm. (c) Quantitation of rhodamine-positive HEK293T cells expressing GFP-PARP10 WT or GFP-PARP10 GW. The number of rhodamine-positive cells was normalized to GFP-positive cells for both GFP-PARP10 WT ($n = 32$) and GFP-PARP10 GW ($n = 47$). Error bars represent S.E.M.

Human embryonic kidney (HEK) 293T cells expressing GFP-tagged PARP10 (GFP-PARP10 WT) were treated with **3.1** (100 μM) in the presence of the oxime catalyst PDA. Click conjugation of biotin-azide in lysates derived from GFP-PARP10 WT transfected HEK 293T cells resulted in labeling of a single band ~175 kDa, which is the size of GFP-PARP10 WT (**Figure 3-4a**). No labeling was

observed without the oxime catalysis or in the presence of aniline, consistent with our *in vitro* studies (**Figure 3-5**).

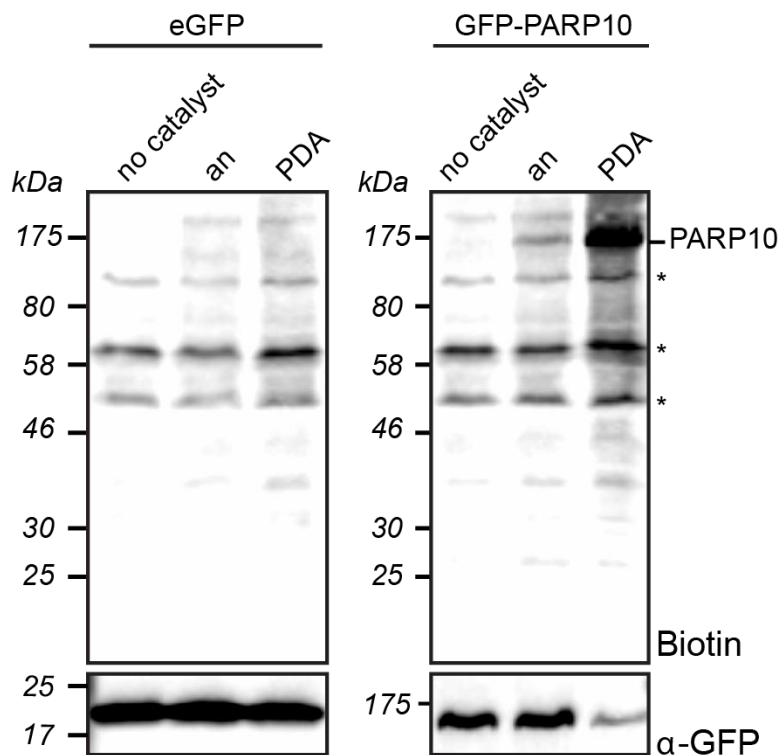


Figure 3-5. Labeling of ADP-ribosylated GFP-PARP10 by **3.1** is most efficient with PDA catalysis. HEK 293T cells overexpressing either GFP-PARP10 WT and eGFP (negative control) were treated with **3.1** (100 μ M) and PDA (10 mM) for 1 h at 37 $^{\circ}$ C. Lysates were subjected to click conjugation with biotin- N_3 (100 μ M) and analyzed via immunoblot. Detection with an α -GFP antibody serves as a loading control. Bands marked with an asterisk represent endogenous biotinylated proteins. PDA = *p*-phenylenediamine, an = aniline.

To determine if this labeling is due to PARP10 catalytic activity, we performed the same experiment with a catalytically inactive PARP10 mutant, PARP10 G888W (GFP-PARP10 GW).¹¹⁴ In contrast to results with GFP-PARP10 WT, no labeling was observed in GFP-PARP10 GW expressing cells (**Figure 3-4a**). These results are consistent with PARP10 undergoing auto-modification in cells, which has been demonstrated previously *in vitro*,^{27,106} but not in cells.

We next determined if we could use **3.1** to visualize ADP-ribosylated PARP10 in cells using fluorescence microscopy. In cells treated with **3.1** followed by click conjugation to rhodamine-azide after fixation we detected fluorescent labeling that co-localized with GFP-PARP10 WT (**Figure 3-4b,c**). The discrete localization of PARP10 protein and activity in large puncta in the cytoplasm is consistent with previous PARP10 localization studies.¹¹⁵ Importantly, we did not detect labeling in cells expressing GFP-PARP10 GW (**Figure 3-4b,c**). Together, these results demonstrate the utility of **3.1** for detecting PARP10 catalytic activity in cells.

AO-alkyne detects automodification of PARP11 on acidic residues

While these results demonstrate that **3.1** can efficiently detect the activity of PARP10 in cells, we wanted to determine if **3.1** could be used to detect the activity of others PARPs that catalyze ADPr on acidic amino acids on protein targets in cells. We first determined if we could detect the activity of PARP11, which catalyzes mono-ADPr, presumably on acidic amino acids.²⁷ Consistent with a recent study, we found that GFP-PARP11 localized in a distinct punctate pattern in the nucleus.¹⁰⁰ In cells treated with **3.1** followed by click conjugation to rhodamine-azide after fixation we detected fluorescent labeling that co-localized with GFP-PARP11 (**Figure 3-6**). This result not only demonstrates that we can detect the activity in cells of another PARP that catalyzes mono-ADPr, but also confirms that PARP11 catalyzes ADPr on acidic amino acids.

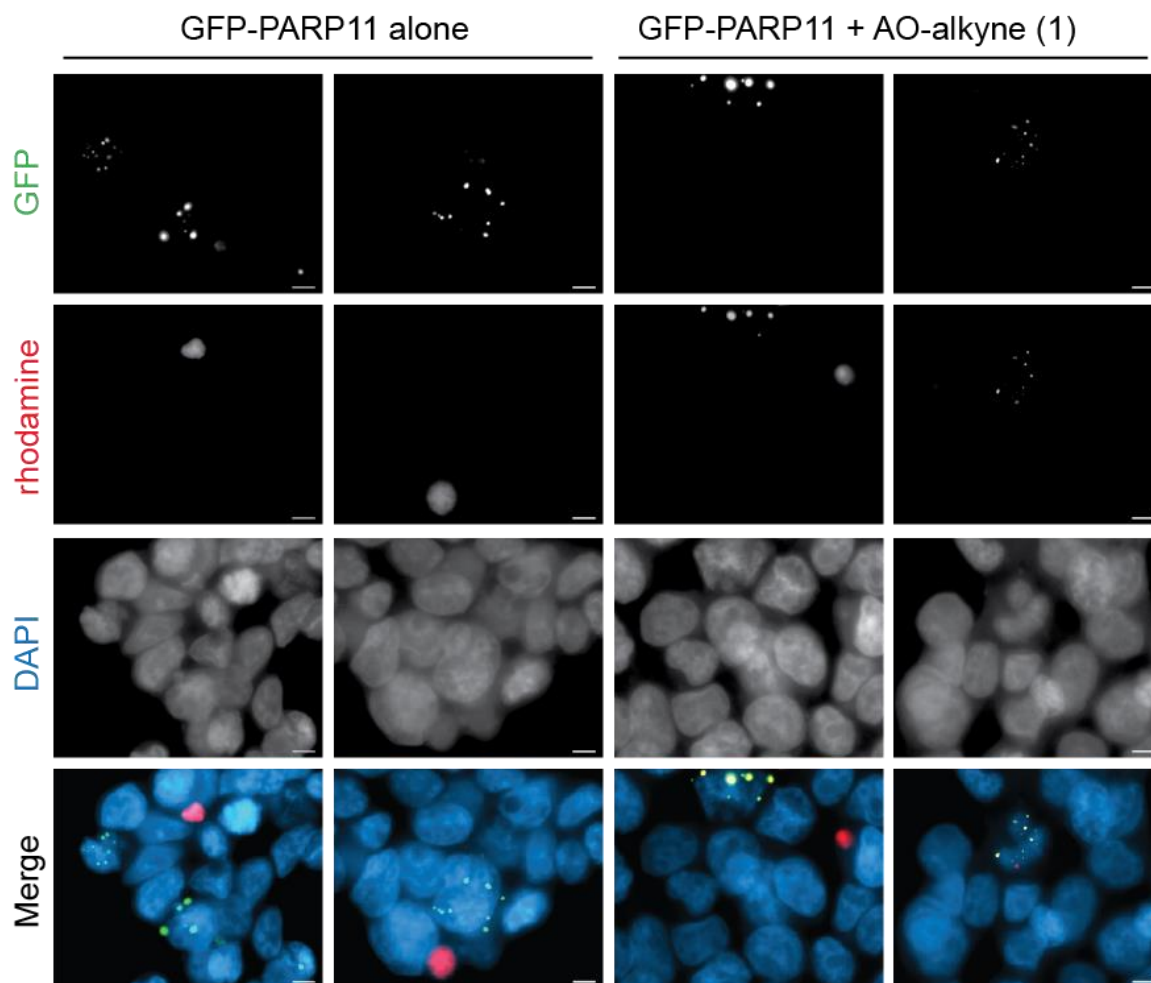


Figure 3-6. Detection of PARP11 activity in cells with **3.1**. HEK 293T cells expressing GFP-PARP11 WT were treated with or without **3.1** (100 μ M) and PDA (10 mM) for 1 h at 37 $^{\circ}$ C. After fixation, permeabilization, and blocking, the cells were subjected to click conjugation with rhodamine-azide (1 μ M) for 30 min. Scale bar corresponds to 5 μ m.

AO-alkyne detects stimulus-induced endogenous ADP-ribsoylation

We next focused on PARP1 and PARP2 since these PARPs are known to catalyze poly-ADPr on acidic amino acids in protein targets. To stimulate PARP1/2 activity, we used hydrogen peroxide (H_2O_2), which activates PARP1/2 by inducing oxidative DNA damage in the nucleus.^{24,116} We observed extensive biotin labeling in HEK 293T cells treated with H_2O_2 (500 μ M) followed by treatment with **3.1** and PDA and subsequent click conjugation with biotin-azide in

cell lysates (**Figure 3-7a**). This labeling was blocked by veliparib (3 μ M),⁷¹ a potent inhibitor of PARP1/2, demonstrating that labeling by **3.1** is dependent on PARP1/2 activity (**Figure 3-7a**). Using rhodamine-azide during the click conjugation step on fixed cells demonstrated that the H₂O₂-induced labeling was confined to the nucleus (**Figure 3-7b**), which is consistent with previous studies using an antibody specific for poly-ADPr.^{24,117}

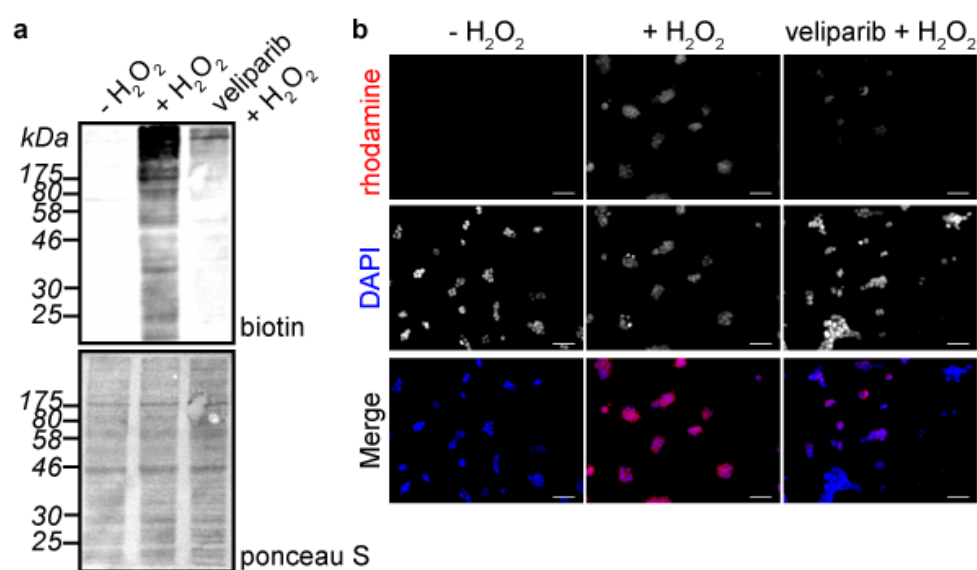


Figure 3-7. AO-alkyne detects ADP-ribose modification catalyzed by endogenous PARPs activated during oxidative stress. **(a)** HEK 293T cells were treated with H₂O₂ (500 μ M) for 15 min at 37 °C in the presence of the PARP1/2 inhibitor veliparib (3 μ M) or DMSO (control) followed by incubation with **3.1** (100 μ M) and PDA (10 mM) for 1 h at 37 °C. Lysates were subjected to click conjugation with biotin-azide (100 μ M) and analyzed via immunoblot. Staining of the membrane with Ponceau S serves as a loading control. **(b)** Cells were treated similarly as in **(a)**. After fixation, permeabilization, and blocking, the cells were subjected to click conjugation with rhodamine-azide (1 μ M) for 30 min. Scale bar corresponds to 50 μ m.

The nuclear specific labeling was also blocked by veliparib (**Figure 3-4b**). Together, these results demonstrate that **3.1** can be used to detect stimulus-induced, endogenous ADPr.

An improved 2,4-dimethoxyaniline catalyst for detecting protein ADPr using AO-alkyne

We have optimized labeling conditions for PARP10 using **3.1** and an improved aniline catalyst, 2,4-dimethoxyaniline (DMA), which avoids potential cellular toxicity concerns of PDA.¹¹⁸ In this protocol, HEK293T cells are transiently transfected with GFP-PARP10. Cells are then treated with **3.1** and DMA for 1 hour. Following lysis, click conjugation is performed with a biotin-azide reporter to detect ADP-ribose-modified GFP-PARP10 via immunoblot with streptavidin-conjugated horseradish peroxidase (strep-HRP) (see **Appendix A**).¹⁰¹

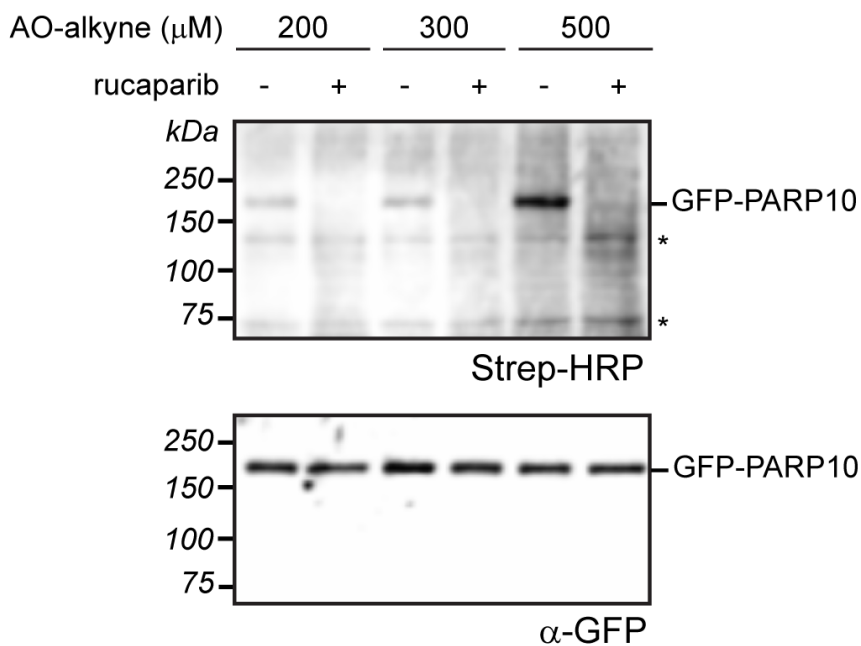


Figure 3-8. Optimized labeling conditions for detection of auto-ADPr of GFP-PARP10 in HEK293T cells using AO-alkyne and DMA. Cells are treated with **3.1** (at 200, 300, or 500 μ M) in the presence of DMA catalyst (5 mM) for 1 h at 37 °C. In some conditions, cells were preincubated with rucaparib (30 μ M) overnight prior to treatment with **3.1**. Upon lysis and click conjugation with biotin azide (100 μ M), Strep-HRP was used to detect auto-ADPr of GFP-PARP10. An antibody against GFP (α -GFP) was used as a loading control. Bands marked with an asterisk represent endogenous biotinylated proteins.

We show that optimal labeling conditions can be achieved with **3.1** (500 μ M) using a lower concentration of DMA catalyst (5 mM) compared to the previous labeling conditions using PDA catalyst (10 mM). The signal due to auto-ADPr of PARP10 can be blocked by pre-incubating with the pan-PARP inhibitor rucaparib, which has been shown previously to inhibit PARP10^{64,65} (**Figure 3-8**).

Conclusions and Future Directions

In summary, AO-alkyne not only provided new insights into the mechanism of ADPr on acidic amino acids, but also demonstrated utility as a probe to detect both mono- and poly-ADPr in cells. Given that acidic amino acids are major targets of ADPr in cells, AO-alkyne will be a useful probe for examining this modification in cells under various stimulation paradigms, and for detecting changes in ADPr in diseased cells (e.g. cancer cells). Moreover, AO-alkyne can be used to examine ADPr of acidic amino acids on a subcellular level, which will provide important insight into the spatial regulation of ADPr in cells.

A limitation of AO-alkyne, however, is that it is most efficient labeling highly expressed targets (e.g., overexpressed PARPs, **Figures 3-4, 3-6**) or due to stimulation of PARP activity (e.g., oxidative DNA damage from exogenous peroxide treatment, **Figure 3-7**), which could potentially limit the identification of low abundance protein targets. Future directions to improve the labeling efficiency of AO-alkyne could focus on: 1) the design of optimized aminooxy probes and 2) the investigation of cellular conditions that increase overall ADPr levels.

Second generation aminooxy probes could be based on more nucleophilic aminooxy groups, improved catalysts, or a combination of both, to increase the overall efficiency of the oxime ligation at physiological pH. Studies have shown that addition of a dimethylaminoethyl (DMAE) group to hydroxylamine increases the rate of oxime formation 3-fold at neutral pH,¹¹⁹ suggesting that aminooxy probes containing a DMAE group could potentially have increased labeling efficiency in the cell. Recent studies have identified improved bifunctional catalysts that contain proton donors (e.g., carboxyl, tetrazole, or phosphonate) *ortho* to the nucleophilic amine group of aniline that provide acid/base catalysis during the reaction and greatly improve reaction rates.^{120,121} Another approach to improve oxime formation efficiency in the cell is to create a dual functional probe containing both an aminooxy group and a catalyst. This probe could minimize the amount of catalyst required due to an effective increase in concentration, and thereby reduce the amount needed and suppress potential cellular toxicity concerns.

The investigation of cellular conditions that increase overall ADPr levels could also improve labeling efficiency of aminooxy probes. Modulating the activity of the enzymes that remove the ADP-ribose modification in cells could provide a global increase in the levels of ADP-ribosylated protein targets, allowing the conjugation of AO-alkyne or second generation probes to low abundance protein targets. In cells with genetic knockout (KO) of glycohydrolases known to remove mono-ADP-ribosylation on proteins (a gift from Gyula Timiniszky, LMU Munich), we have found that cellular ADPr levels differ. When PARP10 is overexpressed

in U-2 OS cells with knockout of terminal ADP-ribose protein glycohydrolase (TARG1/C6orf130)¹²² a dramatic increase in the overall labeling of PARP10 can be observed in comparison to WT. Knockout of glycohydrolase MACRO domain-containing protein 2 (MacroD2)^{110,111} does not exhibit the same effect as TARG1 (**Figure 3-9**).

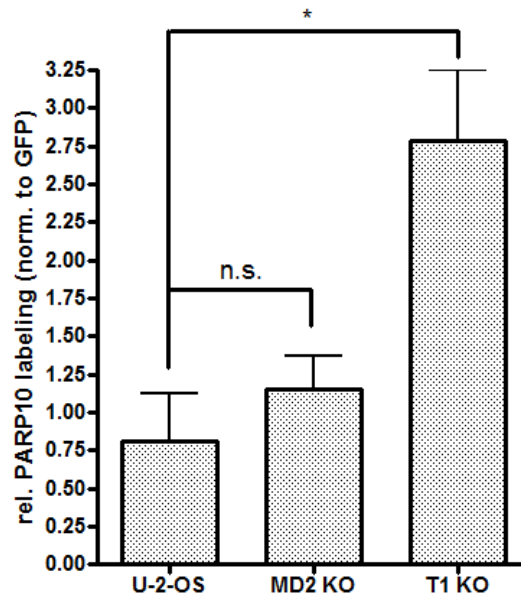


Figure 3-9. Quantification of PARP10 labeling under glycohydrolase knockout U-2 OS cell lines. Lysates were prepared from U-2 OS WT, MacroD2 (MD2) KO, or TARG1 (T1 KO) lines expressing GFP-PARP10 and automodification of PARP10 was measured using a pan-ADP-ribose binding reagent. Levels were normalized to GFP measured using an α -GFP antibody. * $p < 0.05$ by one-way ANOVA, $n = 3$.

Expression of PARP10 in a TARG1 KO background increases auto-ADPr of PARP10 compared to WT, suggesting that overall ADPr levels are increased when TARG1 is knocked out. Investigation of AO-alkyne labeling in cells expressing PARP10 and other PARPs under these knockout conditions could increase labeling of low abundance targets and inform future biological studies.

Experimental

Chemical Synthesis

General. ^1H NMR spectra were recorded on a Bruker DPX spectrometer at 400 MHz. Chemical shifts are reported as parts per million (ppm) downfield from an internal tetramethylsilane standard or solvent references. Dichloromethane (DCM), pyridine (pyr), and *N,N*-diisopropylethylamine (DIPEA) were dried using a solvent purification system manufactured by Glass Contour, Inc. (Laguna Beach, CA). All other solvents were of ACS chemical grade (Fisher Scientific) and used without further purification unless otherwise indicated. Commercially available starting reagents were used without further purification. (Boc-aminooxy)acetic acid (98%, Acros Organics), trifluoroacetic acid pentafluorophenyl ester (TFA-OPfp, 98%, Sigma-Aldrich), and mono-propargylamine (99%, Acros Organics) were used as received.

Synthesis of 2-Aminoxy-N-(propargyl)acetamide (AO-alkyne, 3.1):

Pentafluorophenyl (Boc-aminooxy)acetate (3.2): To a solution of (Boc-aminooxy)acetic acid (100 mg, 0.523 mmol) in DCM (3 mL) was added pyridine (46 μL , 0.570 mmol, 1.1 equiv.) and TFA-OPfp (176 mg, 0.628 mmol, 1.2 equiv.) and the reaction was stirred at rt for 1h. The reaction was concentrated *in vacuo*. The crude residue was redissolved in EtOAc (5 mL), washed with 5% aq. NaHCO_3 (3 x 5 mL) and brine (1 x 5 mL), dried over Na_2SO_4 , filtered, and concentrated *in vacuo* to yield **3.2** as a white solid (133 mg, 71%) that was used

in subsequent reactions without further purification. ^1H NMR (400 MHz, DMSO- d_6): δ 10.41 (s, 1H), 4.89 (s, 2H), 1.42 (s, 9H).

2-(Boc-aminooxy)-N-propargylacetamide (3.3): To a solution of **3.2** (80 mg, 0.224 mmol) in DCM (3 mL) was added DIPEA (43 μL , 0.246 mmol, 1.1 equiv.) and propargylamine (16 μL , 0.250 mmol, 1.1 equiv.). The reaction was stirred at rt for 1h, after which the DCM was removed *in vacuo*. The crude residue was redissolved in EtOAc (5 mL), washed with 5% aq. NaHCO_3 (3 x 5 mL) and brine (1 x 5 mL), dried over Na_2SO_4 , filtered, and concentrated *in vacuo* to yield **3.3** as a light yellow oil (49 mg, 96%) that was used in the following deprotection step without further protection. ^1H NMR (400 MHz, DMSO- d_6): δ 10.28 (s, 1H), 8.39 (t, 1H), 4.18 (s, 2H), 3.91 (dd, 2H), 3.13 (t, 1H), 1.41 (s, 9H).

2-Aminoxy-N-(propargyl)acetamide (AO-alkyne, 3.1): **3.3** (22 mg, 0.096 mmol) was dissolved in 4N HCl in dioxane (1.9 mL), and the reaction was stirred at rt for 1 h, in which a yellow color gradually developed. The reaction was concentrated *in vacuo*. The crude yellow residue was taken up in a minimal amount of MeOH (1 mL) and precipitated into anhydrous Et_2O (20 mL) to form a cloudy suspension. After storage at $-20\text{ }^\circ\text{C}$ overnight, a ppt formed, which was collected via centrifugation. The solid was rinsed with Et_2O (10 mL) and dried *in vacuo* to yield the HCl salt of the product as a light orange solid (10 mg, 63%). ^1H NMR (400 MHz, DMSO- d_6): δ 10.74 (bs, 3H), 8.70 (t, 1H), 4.49 (s, 2H), 3.91 (dd, 2H), 3.18 (t, 1H).

Other Methods

Cloning and mutagenesis. cDNA encoding human PARP10 was obtained from a HeLa cell cDNA library. cDNA encoding mouse PARP11 was obtained from a mouse embryonic day 16 cDNA library. Full-length PARP11 was cloned into pEGFP-C1 (Clontech). The catalytic domain (residues 809-1017) of PARP10 was PCR-amplified from the cDNA library using primers with non-complementary restriction enzyme sites located at the 5' and 3' ends. The catalytic domain (residues 481-661) of PARP15 was PCR-amplified from a synthetic PARP15 (human) gene fragment (GeneArt® Strings™ DNA Fragments, Life Technologies) using primers with non-complementary restriction enzyme sites located at the 5' and 3' ends. Amplified products for both PARP10_{cat} and PARP15_{cat} were cloned into pET-28b+ (Novagen) for expression. The construct for His-tagged SRPK2 (human) was obtained from Addgene (Plasmid #39047) in pNIC28-Bsa4 and contains a deletion of internal segment 268-518. The construct for full length GFP-tagged PARP10 for mammalian expression was obtained from Paul Chang at Massachusetts Institute of Technology (Cambridge, MA). The PARP10 G888W (GW) mutant was generated using the QuickChange II XL site-directed mutagenesis kit (Agilent). Plasmids were sequenced from both the 5' and 3' direction to confirm the coding sequence.

Expression and purification of PARP10_{cat}, PARP15_{cat}, and SRPK2. PARP10_{cat}, PARP15_{cat}, and SRPK2 were expressed in the *Escherichia coli* BL21 pRARE2 strain (EMD Millipore). Cells were first cultured in LB media overnight at

225 rpm and 37°C in an Excella® E24 Incubator (New Brunswick Scientific). One liter of TB media (12 g Bacto Tryptone (BD Biosciences), 24 g Bacto Yeast Extract (BD Biosciences), 0.4% glycerol, 17 mM KH₂PO₄, 72 mM KHPO₄, 50 µg/ml kanamycin, 34 µg/ml chloramphenicol) was inoculated with the starting culture and grown to OD₆₀₀ = 0.8 – 1.0 at 225 rpm and 37°C. The temperature was reduced to 16°C and expression was induced by adding isopropyl β-d-thiogalactoside (IPTG) to 0.4 mM. After incubation at 16°C for 18 – 24 h, cells were harvested by centrifugation at 6,000 g for 10 min. The cell pellet was resuspended in lysis buffer (100 mM HEPES, pH 7.5, 0.5 mM tris(2-carboxyethyl)phosphine hydrochloride (TCEP•HCl, Thermo Scientific Pierce), 500 mM NaCl, 10 mM imidazole, 10% glycerol, 1 mM benzamidine, 1 mM phenylmethylsulfonyl fluoride (PMSF), 8.3 mg/L DNase I (Roche)) at 4°C, subjected to cell lysis using a Sonifier 450 (Branson) at 4°C, and the resulting lysate was clarified by centrifugation at 12,000 g for 30 min at 4°C. Lysates were incubated with pre-washed Ni-NTA agarose resin (50% slurry, Qiagen) with end-over-end rotation at 4°C for 1 h. Following extensive washing with buffer B1+25 (20 mM HEPES, pH 7.5, 0.5 mM TCEP•HCl, 1 mM PMSF, 1 mM benzamidine, 500 mM NaCl, 25 mM imidazole) protein was eluted in buffer B1+200 (20 mM HEPES, pH 7.5, 0.5 mM TCEP•HCl, 500 mM NaCl, 200 mM imidazole) for PARP10_{cat} and PARP15_{cat}, and B1+100 (20 mM HEPES, pH 7.5, 0.5 mM TCEP•HCl, 500 mM NaCl, 100 mM imidazole) for SRPK2. Fractions containing desired protein were collected and dialyzed to 50 mM Tris-HCl, pH 7.5, 0.1 mM EDTA, 1 mM β-Me, 0.4 M NaCl at 4°C. Protein concentrations were determined

by Bradford assay with BSA standards and purity was assessed by PageBlue staining (Pierce) after SDS-polyacrylamide gel electrophoresis (SDS-PAGE). $\geq 90\%$ purity was achieved for PARP10_{cat} and PARP15_{cat}. $\geq 50\%$ purity was achieved for SRPK2.

ADP-ribosylation assay for PARP10 with AO-alkyne labeling and immunoblot detection. 810 ng of PARP10_{cat} and 2.8 μ g of SPRK2 were incubated with 100 μ M NAD⁺ in reaction buffer (50 mM Tris-HCl pH 8.0, 100 mM NaCl, 4 mM MgCl₂, 0.5 mM TCEP•HCl) at 30 °C for 1 h. The reaction was quenched by the addition of 10% SDS to a final concentration of 2%. A 3.5X stock of AO-alkyne at pH 5 (525 mM acetate, 787.5 mM NaCl), pH 6, pH 7, pH 8 (all 525 mM phosphate, 787.5 mM NaCl) with or without catalyst (at 35 mM) was added to the reaction mixture (final [AO-alkyne] = 100 μ M) and incubated at rt for 1 h. A 4X stock of CB (400 μ M of tris[(1-benzyl-1*H*-1,2,3-triazol-4-yl)methyl]amine (TBTA), 4 mM CuSO₄, 400 μ M biotin-azide (Biotin-PEG3-Azide, Click Chemistry Tools), 4 mM TCEP•HCl in 1X phosphate buffered saline (PBS) with 1% SDS) was added to the reaction mixture (final [biotin-azide] = 100 μ M) and incubated at rt for 30 min. 4X sample buffer with 5% β -mercaptoethanol (BME) was added. The reaction was diluted 1:40 with 1X sample buffer prior to fractionation by SDS-PAGE, and subsequent immunoblot detection was performed using a ChemiDoc™ MP Imaging System (Bio-Rad). Coomassie staining was performed on undiluted reaction mixtures after fractionation by SDS-PAGE. Each experiment was repeated at least twice, shown are representative images.

ADP-ribosylation assay for PARP10 and PARP15 with AO-alkyne labeling and fluorescence detection. 405 ng of either PARP10_{cat} or PARP15_{cat} and 1.4 µg of SRPK2 were incubated with NAD⁺ (0, 1, 10, 50, 100 µM) in reaction buffer (50 mM Tris-HCl pH 8.0, 100 mM NaCl, 4 mM MgCl₂, 0.5 mM TCEP•HCl) at 30 °C for 1 h. The reaction was quenched by the addition of 10% SDS to a final concentration of 2%. A 3.5X stock of AO-alkyne at pH 5 (525 mM acetate, 787.5 mM NaCl, 35 mM PDA) was added to the reaction mixture (final [AO-alkyne] = 100 µM) and incubated at rt for 1 h. A 4.5X stock of CB (450 µM of TBTA, 4.5 mM CuSO₄, 450 µM rhodamine-azide (Sulforhodamine B Azide, Click Chemistry Tools), 4.5 mM TCEP•HCl in 1X PBS with 1% SDS was added to the reaction mixture (final [rhodamine-azide] = 100 µM) and incubated at rt for 30 min. 4X sample buffer (with 5% BME) was added prior to fractionation by SDS-PAGE, and subsequent fluorescence detection was performed using a ChemiDoc™ MP Imaging System (Bio-Rad). Coomassie staining of the same gel was performed after fluorophore visualization.

Borohydride reduction. ADP-ribosylation of SRPK2 by PARP10_{cat} was performed as outlined above except using 911 ng PARP10_{cat} and 3.15 µg of SRPK2 with either NAD⁺ or 6-a-NAD⁺ at 100 µM. The reaction was quenched by the addition of 10% SDS to a final concentration of 2%. The reaction mixture was aliquoted, and 3X NaBH₄ solutions in 1X PBS were added for final concentrations of 10 mM NaBH₄, 1 mM NaBH₄ and PBS only (no NaBH₄). The reaction was incubated at rt for 15 min. A 4.5X stock of AO-biotin (Aldehyde

Reactive Probe, ARP, Cayman Chemical) in pH 5 buffer (675 mM acetate, 1M NaCl, 45 mM PDA) or a 4.5X stock of biotin-azide in pH 5 CB (675 mM acetate, 1M NaCl, 450 μ M of TBTA, 4.5 mM CuSO₄, 450 μ M biotin-azide, 4.5 mM TCEP•HCl) was added for a final concentration of 100 μ M for both AO-biotin and biotin-azide. The reaction was incubated at rt for 1 h prior to dilution with 4X sample buffer (with 5% BME). The reaction was diluted 1:20 with 1X sample buffer prior to fractionation by SDS-PAGE, and subsequent immunoblot detection was performed using a ChemiDoc™ MP Imaging System. Coomassie staining was performed after fractionation by SDS-PAGE on undiluted reaction mixtures of a replicate experiment performed with twice the amounts of both PARP10_{cat} and SRPK2. Each experiment was repeated at least twice, shown are representative images.

Dual fluorophore labeling. ADP-ribosylation of SRPK2 by PARP10_{cat} was performed as outlined above using 810 ng PARP10_{cat} and 2.8 μ g of SRPK2 with 6-a-NAD⁺ at 100 μ M. The reaction was quenched by the addition of 10% SDS to a final concentration of 2%. A 3.5X stock of AO-TAMRA (Aminooxy-5(6)-TAMRA, Cayman Chemical) in pH 5 buffer (525 mM acetate, 787.5 mM NaCl, 35 mM PDA) or a 3.5X mock solution (containing all components except substitution of DMSO for AO-TAMRA) was added to the reaction mixture (final [AO-TAMRA] = 100 μ M). The reaction was incubated at rt for 1 h. A 4.5X stock of CB (450 μ M of TBTA, 4.5 mM CuSO₄, 450 μ M AF488-azide (Alexa Fluor® 488 Azide, Life Technologies), 4.5 mM TCEP•HCl in 1X PBS with 1% SDS) or a 4.5X mock

solution (containing all components except substitution of DMSO for AF488-azide) was added to the reaction mixture (final [AF488-azide] = 100 μ M) and incubated at rt for 30 min. 4X sample buffer (with 5% BME) was added prior to fractionation by SDS-PAGE. Imaging was performed on a Typhoon 9400 (GE Healthcare Life Sciences) using recommended laser settings and filter sets for AF488 (Ex: 488 nm, PMT: 400V; Em: 526 nm SP) and TAMRA (Ex: 532 nm, PMT: 400V; Em: 580 nm BP 30 nm). Coomassie staining of the same gel was performed after fluorophore visualization. Each experiment was repeated at least twice, shown are representative images.

Cell culture and reagents. HEK 293T cells were grown at 37 °C and 5% CO₂. Cells were passaged in DMEM + 10% FBS (Gibco) + penicillin/streptomycin (Invitrogen). Antibodies used for immunoblot detection were α -GFP (ab13970, Abcam) and goat α -chicken IgY-HRP (sc-2428, Santa Cruz Biotechnology). Primary antibodies (stored at 1 mg ml⁻¹) were used at 1:5,000 and secondary antibodies at 1:5,000 for immunoblot assays. Streptavidin-HRP (Jackson ImmunoResearch) was stored at -20°C in a 50% glycerol mix (0.5 mg ml⁻¹) and was used at 1:1,000 for immunoblot assays.

Transfection of HEK 293T cells. HEK 293T cells were grown in 6-well plates to a confluency of 80-90%. Cells were transfected with 2 μ g plasmid DNA using standard CalPhos™ (Clontech) transfection techniques. After incubation for 7 h, cells were washed with media (1 mL) and fed fresh media (2 mL) and allowed to

grow overnight. Transfection efficiency was verified via microscopy and ranged from 50-60%.

H₂O₂ treatment of HEK 293T cells. HEK 293T cells were grown in 6-well plates to a confluency of 50-60%. Cells were pretreated with media containing veliparib (3 μ M) or DMSO for 10 min. Half of the media was removed and 2X H₂O₂ was added. This media was added back to cells (final [H₂O₂] = 500 μ M) and incubated for 15 min.

AO-alkyne cellular labeling and click conjugation of lysates. Cells were treated with **1** (100 - 500 μ M) and PDA (10 mM) or DMA (5 mM) and incubated for 1 h. Media was removed and cells were washed with cold (4 °C) PBS and lysed by freezing in N₂ (l) and thawing in either cold PBS or buffer containing 25 mM HEPES pH 7.5, 50 mM NaCl, 10% glycerol, 1% Nonidet P-40 (NP-40), and 1X cOmplete EDTA-free protease inhibitor cocktail (Roche) and subjected to centrifugation at 5,000 g for 5 min for PBS samples at 4°C and 14,000 g for 5 min at 4 °C for all other samples. Total protein concentration in the lysate was determined by Bradford assay with a BSA standard curve. Lysates containing normalized protein levels were subjected to click conjugation with 9X CB (900 μ M of TBTA, 9 mM CuSO₄, 900 μ M biotin-azide, 9 mM TCEP•HCl in 1X PBS with 1% SDS) and incubated at rt for 30 min. 4X sample buffer (with 5% BME) was added prior to fractionation by SDS-PAGE.

Click conjugation of AO-alkyne labeled cells and microscopy. Cells were labeled with **1** as above. Media was removed and replaced with fresh media for 5 min. Cells were washed with 1X PBS and fixed with 4% PFA in 1X PBS for 15 min at rt. The cells were washed 3 x 5 min with 1X PBS. Cells were permeabilized with 0.2% Triton X-100 in 1X PBS for 5 min at rt followed by washing with 1X PBS for 5 min. The cells were blocked in 3% BSA in 1X PBS at 4 °C for 2 h. The Click-iT® Cell Reaction Buffer Kit (Life Technologies) was used for in-cell click conjugation of rhodamine-azide (1 μ M, Sulforhodamine B Azide, Click Chemistry Tools). Cells were washed 2X with 3% BSA and ddH₂O. Coverslips were mounted with ProLong® Gold Antifade Mountant with DAPI (Life Technologies). Images were taken on a Zeiss ApoTome wide-field microscope with the following channel parameters: blue, Ex: 380/40, Em: 445/50; green, Ex: 470/40, Em: 525/50; red: Ex: 545/25, Em: 605/70; and objectives: 20x0.8 PlanApo, 60x1.4 PlanApo. Images were processed in Zen 2012 (Zeiss) and levels were linearly adjusted in Adobe Photoshop CS5.

Chapter 4: Development of a Chemical Genetics Strategy for Selective Inhibition of PARP10

Rory K. Morgan, Ian Carter-O'Connell, and Michael S. Cohen

Portions of this chapter were originally published in *Bioorg. Med. Chem. Lett.* on November 1, 2015 in volume 25, issue 21, pages 4770–4773 (Copyright © 2015 Elsevier Ltd.).¹²³ It has been adapted for this dissertation and reprinted with permission. This work was in collaboration with Ian Carter-O'Connell who cloned, expressed, and purified the PARP10_{cat} mutants.

Abstract

The lack of inhibitors that are selective for individual poly-ADP-ribose polymerase (PARP) family members has limited our understanding of their roles in cells. Here, we describe a chemical genetics approach for generating selective inhibitors of an engineered variant of PARP10. We synthesized a series of C-7 substituted 3,4-dihydroisoquinolin-1(2H)-one (dq) analogues designed to selectively inhibit a mutant of PARP10 (LG-PARP10) that contains a unique pocket in its active site. A dq analogue containing a bromo at the C-7 position demonstrated a 10-fold selectivity for LG-PARP10 compared to its WT counterpart. The bromo modification was translated to two additional scaffolds to increase potency (2-3-fold) and selectivity (2-fold) for LG-PARP10 over WT-PARP10 compared to the bromo-modified dq analogue. Analysis of bromo-modified inhibitors in cells revealed a lack of selectivity for LG-PARP10 over WT-PARP10, demonstrating that a chemical genetics strategy with LG-PARP10 is most likely not feasible and additional mutations within PARP10 will need to be explored to obtain selective inhibition of PARP10.

Introduction

Poly-ADP-ribose polymerases (PARPs) are a family of 17 ubiquitously expressed enzymes in humans that catalyze the transfer of the ADP-ribose moiety from nicotinamide adenine dinucleotide (NAD⁺) to their target proteins, a process known as ADP-ribosylation (ADPr). Only four PARPs catalyze poly-ADPr (PARPs 1, 2, 5a, and 5b), whereas the majority of the PARPs catalyze mono-ADPr.²⁷ PARPs are found throughout the cell and play roles in diverse cellular processes, including transcriptional⁶ and post-transcriptional regulation,¹²⁴ protein degradation,¹²⁵ cell signaling^{34,126} and the unfolded protein response.³³ However, the cellular functions and targets of most PARPs—especially those that catalyze mono-ADPr—remain unknown and current strategies to study PARP function are insufficient to provide a comprehensive view of their role in cellular processes. This is due, in large part, to the dearth of inhibitors that selectively inhibit an individual PARP family member.

A major hurdle for developing selective PARP inhibitors is the high structural conservation of the catalytic domain among PARPs. While the primary sequences are semi-divergent (displaying ~50% similarity),²¹ their structures are highly conserved in the nicotinamide-binding site, which is the major binding site for the majority of PARP inhibitors.⁷⁰ To address this challenge, we implemented a chemical genetics strategy, commonly referred to as the “bump-hole” method, for the development of selective PARP inhibitors. This strategy has been successfully used for identifying highly selective inhibitors of individual enzymes within a highly conserved family,⁴⁷ most notably protein kinases.⁵¹ In this chapter,

we describe a bump-hole approach for identifying selective inhibitors of individual PARPs.

We previously described a bump-hole method for identifying the direct protein targets of PARPs that catalyze poly-ADPr.⁸⁴ This method involved mutating a lysine residue (Lys903 in human PARP1, which we refer to as the “ceiling” position) in the nicotinamide-binding site to an alanine to create a unique pocket for accommodating a C-5 ethyl group on the nicotinamide ring of the NAD⁺ analogue. We sought to adopt this chemical genetics strategy to generate selective inhibitors of PARP10. We focused our initial efforts on PARP10 since its mono-ADPr activity has been well characterized in vitro.¹⁰⁶ While inhibitors of PARP10 have been previously reported, they are not selective among the PARP family.⁷⁷

Results and Discussion

Structural data guides the design of a chemical genetics strategy

We first examined the crystal structure of PARP10 bound to the nicotinamide bioisostere 3-aminobenzamide (3-AB) (PDB ID: 3HKV) to identify potential inhibitor-sensitizing positions within the nicotinamide binding site (PDB ID: 3HKV) (**Figure 4-1a**). We focused on Leu926 (human PARP10 numbering) because it occupies the same space in the nicotinamide-binding pocket as the ceiling lysine of PARP1. We reasoned that mutation of Leu926 to either an alanine or glycine would create a unique pocket for orthogonal inhibitors. We first determined if mutation of Leu926 to an alanine or glycine (LA-PARP10 or LG-

PARP10, respectively) affects the activity of the catalytic domain of PARP10 (PARP10_{cat}).

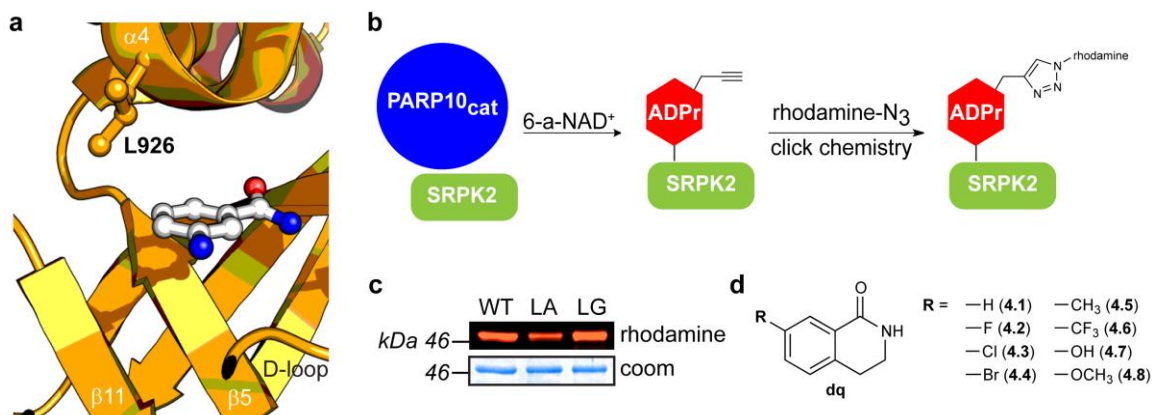


Figure 4-1. A chemical genetics strategy for generating selective inhibitors of PARP10. **(a)** Structure of PARP10 with nicotinamide isostere 3-aminobenzamide (3-AB) (PDB ID: 3HKV) with mutated residue (L926) indicated. **(b)** Schematic showing the PARP10-mediated transfer of alkyne-tagged ADP-ribose onto SRPK2 from 6-a-NAD⁺, followed by click conjugation with a fluorescent azide reporter (rhodamine-N₃). **(c)** Activity comparison of engineered PARP10_{cat} mutants L926A (LA) and L926G (LG) to WT-PARP10_{cat}. **(d)** Structure of C-7 substituted dq analogues **4.1** – **4.8** designed to selectively inhibit engineered PARP10 mutants.

To test the activity of LA-, LG-, and WT-PARP10_{cat} we monitored ADP-ribosylation of SRSF protein kinase 2 (SRPK2), a previously characterized PARP10 substrate,^{98,105} using *N*⁶-alkyne-NAD⁺ (6-a-NAD⁺)^{45,84} and click conjugation to a fluorescent azide reporter (**Figure 4-1b**). Using this assay, we found that both engineered PARP10_{cat} mutants exhibited similar activity to the WT-PARP10_{cat} (**Figure 4-1c**). A more detailed analysis using a range of 6-a-NAD⁺ concentrations revealed that LG-PARP10_{cat} exhibited ~60% activity of WT-PARP10_{cat} (**Figure 4-2**).

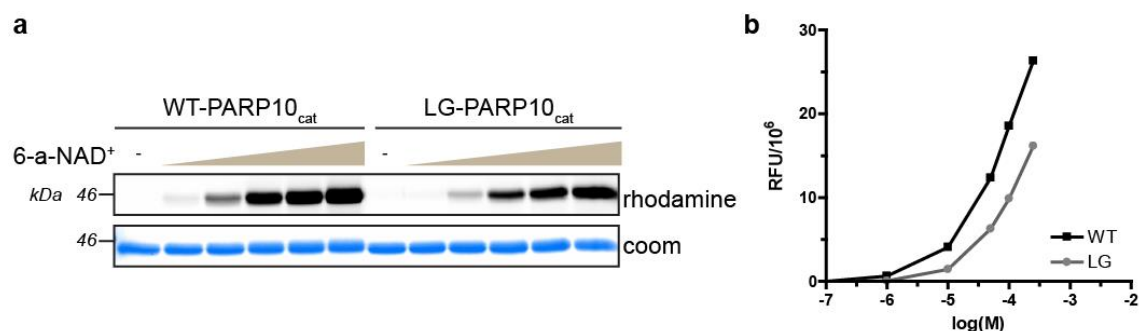
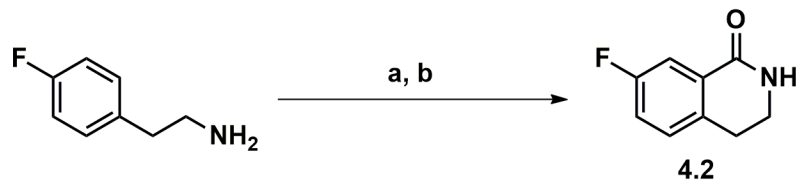


Figure 4-2. LG-PAPR10_{cat} exhibits similar activity to WT-PARP10_{cat}. **(a)** 6-a-NAD⁺ dose-response curves for WT-PARP10_{cat} and LG-PARP10_{cat}. SRPK2 was ADP-ribosylated by PARP10_{cat} with 6-a-NAD⁺ (0, 1, 10, 50, 100, 250 μ M) at 30 °C for 1h. Reactions were conducted in the presence of [DMSO] = 0.125% to mimic conditions used to assay dq compounds. The reactions were subjected to click conjugation with rhodamine-azide (100 μ M) prior to separation by SDS-PAGE. In-gel fluorescence detection (rhodamine) was used to quantify the relative amount of ADP-ribose transferred to SRPK2 (46.7 kDa) as a readout of PARP10_{cat} activity. Coomassie (coom) Brilliant Blue staining was used as a loading control. **(b)** Quantitation of results shown in **(a)**.

Synthesis of C-7 substituted dihydroisoquinolin-1(2H)-ones

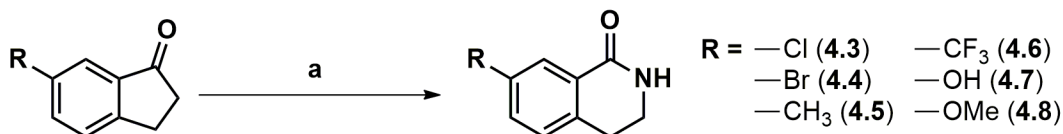
We next sought to identify compounds that could selectively inhibit our engineered PARP10 mutants. As a starting point for our inhibitor design, we selected 3,4-dihydroisoquinolin-1(2H)-one (dq, **4.1**), a pan-PARP inhibitor scaffold that binds in the same orientation as 3-AB in the nicotinamide binding site.⁶⁴ We designed a series of dq analogues containing various substituents at the C-7 position to probe the size and shape of the unique pocket in our engineered PARP10 mutants (**Figure 4-1d**). We used two different strategies to synthesize C-7 dq analogues. The fluoro-substituted dq derivative **4.2** was synthesized via a previously described route that involves the formation of the methylcarbamate species from p-fluorophenethylamine followed by intramolecular cyclization in triflic acid (**Scheme 4-1**).¹²⁷



Scheme 4-1. Synthesis of analogue **4.2** via intramolecular aromatic substitution reaction. Reagents and conditions: a. methylchloroformate, DIPEA, DMF; b) TfOH (61% over two steps).

Analogues **4.3** – **4.8** were synthesized using the Schmidt reaction (**Scheme 4-2**).

The reaction resulted in a mixture of both N-alkyl and N-aryl regioisomers, which were easily resolved with standard normal phase chromatography. The percentage of the desired N-alkyl isomer obtained from the Schmidt reaction ranged from 26 – 63%. The yield of the N-alkyl isomer was highest for 1-indanones where the 6-position substituent was highly electron donating (e.g., -OH, -OCH₃), whereas N-alkyl regioselectivity decreased with electron withdrawing substituents (e.g., -Cl, -Br, -CF₃).



Scheme 4-2. Syntheses of analogues **4.3** – **4.8** via Schmidt reaction. Reagents and conditions: a. NaN₃, DCM/methanesulfonic acid (2:1) (31 – 80% yield overall, N-alkyl isomer: 26 – 63%).

C-7 substituted dq analogues are selective for LG-PARP10

We first tested our panel of C-7 substituted dq analogues against our engineered PARP10_{cat} mutants. In a preliminary screen, we found that none of the compounds inhibited the LA-PARP10_{cat} mutant (data not shown); therefore, we focused on LG-PARP10_{cat}. We found that most of the C-7 substituted dq

analogues inhibited LG-PARP10_{cat} more potently than the parent dq scaffold **4.1** (Figure 4-3a,b, Table 4-1).

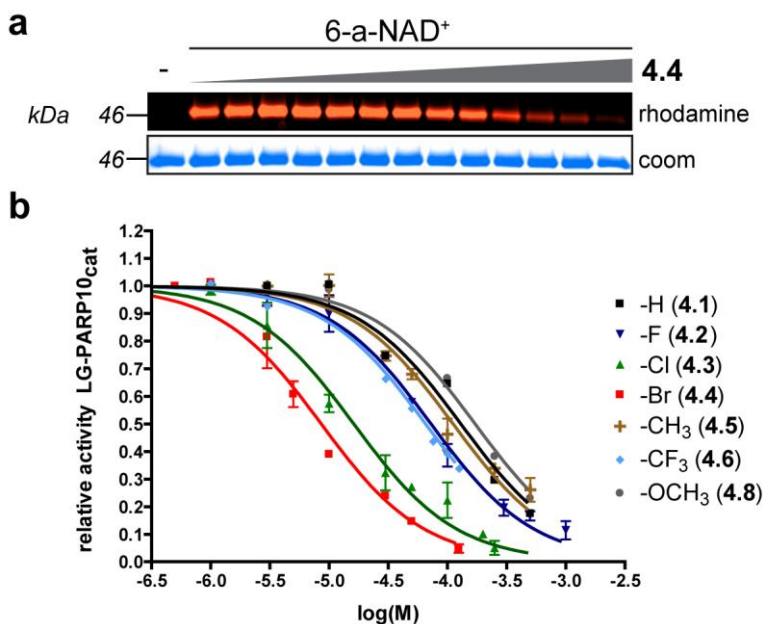


Figure 4-3. C-7 substituted dq analogues selectively inhibit LG-PARP10_{cat}. (a) Representative fluorescent gel image showing a dose-dependent inhibition of LG-PARP10_{cat}-mediated ADPr of SRPK2 by 7-Br-dq (**4.4**). SRPK2 (3 μ M) was ADP-ribosylated by LG-PARP10_{cat} (500 nM) with 6-a-NAD⁺ (100 μ M) in the presence of analogue **4.4** (0 – 125 μ M) at 30 °C for 1h. Following click conjugation to rhodamine-azide (100 μ M), proteins were resolved by SDS-PAGE and detected via in-gel fluorescence. Coomassie (Coom) Brilliant Blue staining was used to demonstrate even loading. (b) IC₅₀ curves for C7-substituted dq analogues against LG-PARP10_{cat}. Activity was determined as described in (a). Error bars represent S.E.M., n = 2.

A clear structure-activity relationship was observed for the halogen series: increasing the size of the halogen group resulted in increased potency against LG-PARP10_{cat}, with the bromo-substituted dq analogue **4.4** exhibiting the greatest potency (IC₅₀ = 8.6 μ M; Figure 4-3a,b, Table 4-1). Unlike the halogen-substituted analogues, the methyl (**4.5**), methoxy (**4.8**), and hydroxyl (**4.7**) dq analogues did not exhibit increased potency compared to **4.1** (Figure 4-3b, Table 4-1). The trifluoromethyl dq analogue **4.6** exhibited a modest, 2-fold increase in potency compared to **4.1** (Figure 4-3b, Table 4-1).

Table 4-1. C-7 substituted dq analogues selectively inhibit the engineered PARP10 mutant, LG-PARP10_{cat}.

	-R	LG-PARP10 _{cat}		WT-PARP10 _{cat}	WT-PARP1
		IC ₅₀ (μM)	pIC ₅₀ ± S.E.M. ^a	IC ₅₀ (μM)	IC ₅₀ (μM)
4.1	H	130	3.89 ± 0.06	~30	~100
4.2	F	72.7	4.14 ± 0.04	~100	~100
4.3	Cl	16.2	4.79 ± 0.04	>100	~100
4.4	Br	8.6	5.07 ± 0.05	>100	>100
4.5	CH ₃	112	3.95 ± 0.04	>100	>100
4.6	CF ₃	65.5	4.18 ± 0.04	>100	>100
4.7	OH	>30	n.d.	n.d.	n.d.
4.8	OCH ₃	172	3.77 ± 0.03	>100	>100

^aS.E.M. from two representative dose-response experiments

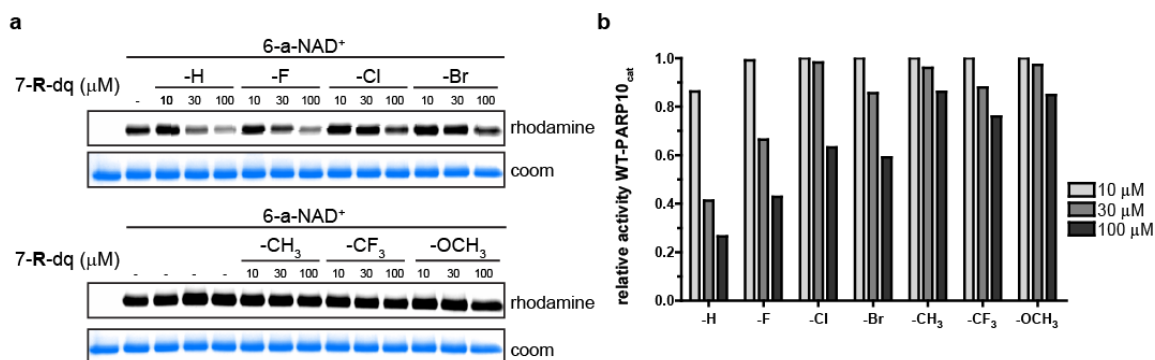


Figure 4-4. Screening of C7-substituted dq analogues against WT-PARP10_{cat}. (a) SRPK2 was ADP-ribosylated by WT-PARP10_{cat} with 100 μM 6-a-NAD⁺ in the presence of indicated 7-R-dq analogues (0, 10, 30, and 100 μM) at 30 °C for 1h. No inhibitor control contains [DMSO] = 0.125%. The reactions were subjected to click conjugation with rhodamine-azide (100 μM) prior to separation by SDS-PAGE. In-gel fluorescence detection (rhodamine) was used to quantify the relative amount of ADP-ribose transferred to SRPK2 (46.7 kDa) as a readout of WT-PARP10_{cat} activity. Coomassie (coom) Brilliant Blue staining was used as a loading control. (b) Quantitation of results shown in (a).

Importantly, none of the C-7 substituted dq analogues appreciably inhibited WT-PARP10_{cat} at concentrations up to 100 μM (**Figure 4-4**, **Table 4-1**). Moreover, dq analogues with C-7 substituents larger than chlorine exhibited IC₅₀ values greater than 100 μM against WT-PARP1 (**Figure 4-5**, **Table 4-1**), which is consistent with a pharmacophore analysis of PARP1 inhibitors.⁷⁰ Taken together, these

results demonstrate that PARP10 can be engineered to generate unique inhibitor sensitivity for C-7 substituted dq analogues.

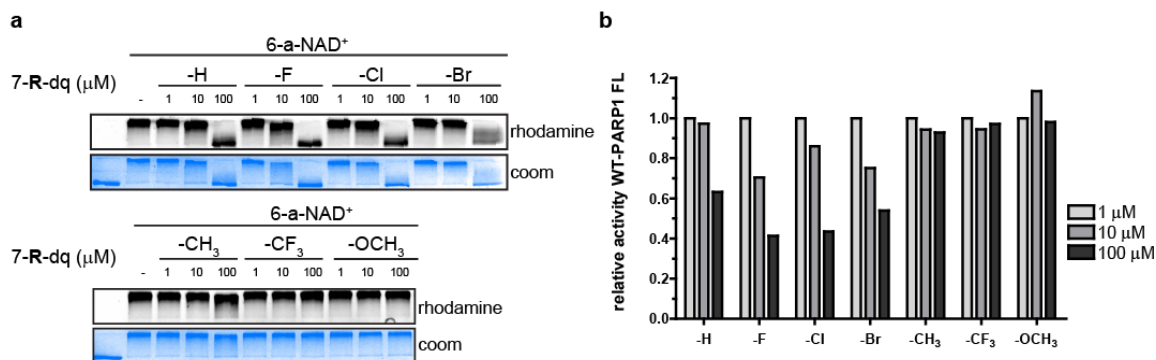


Figure 4-5. Screening of C7-substituted dq analogues against WT-PARP1. **(a)** WT-PARP1 was automodified with 100 μM 6-a-NAD⁺ in the presence of indicated 7-R-dq analogues (0, 1, 10, and 100 μM) at 30 °C for 1h. No inhibitor control contains [DMSO] = 0.125%. The reactions were subjected to click conjugation of rhodamine-azide (100 μM) prior to separation by SDS-PAGE. In-gel fluorescence detection (rhodamine) was used to quantify the relative amount of poly-ADP-ribose (PAR) of automodified WT-PARP1 (113 kDa) as a readout of WT-PARP1 activity. Coomassie (coom) Brilliant Blue staining was used as a loading control. **(b)** quantitation of results shown in **(a)**.

A 7-Br substituted dq compound selectively inhibits full-length PARP10

Several PARPs exhibit auto-ADPr activity, including PARP10.¹ Auto-ADPr of PARP10 is most robust using the full-length protein expressed in mammalian cells (data not shown). We next sought to determine if **4.4** could selectively inhibit the auto-ADPr of full-length GFP-tagged LG-PARP10 (GFP-LG-PARP10) expressed in human embryonic kidney (HEK) 293T cells. For these experiments, we developed a modified GFP-immunoprecipitation (IP)-auto-ADPr assay¹ using 6-alkyne-NAD⁺ as a substrate. We found that **4.4** inhibited the auto-ADPr of GFP-LG-PARP10 in a dose-dependent manner (**Figure 4-6**). By contrast, auto-ADPr of GFP-WT-PARP10 was unaffected by up to 100 μM of **4.4** (**Figure 4-6**).

These results demonstrate that **4.4** can selectively inhibit the auto-ADPr activity of the full-length, engineered PARP10 mutant, GFP-LG-PARP10.

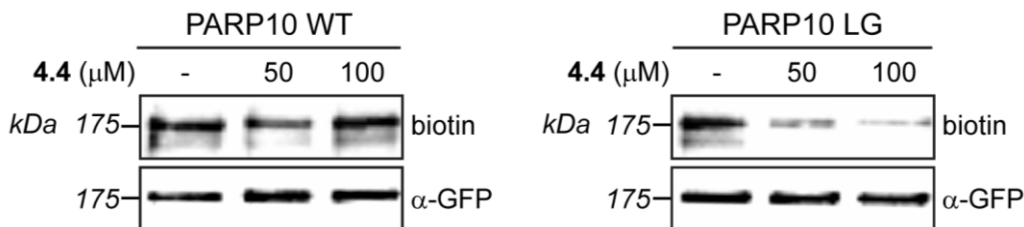


Figure 4-6. 7-Br-dq (**4.4**) selectively inhibits the auto-ADPr activity of full-length LG-PARP10. HEK 293T cells overexpressing GFP-WT-PARP10, GFP-LG-PARP10, or GFP-GW-PARP10 were harvested 24 h after transfection, and GFP-tagged PARP10 proteins were immunoprecipitated using an anti-GFP antibody. Auto-ADPr assays were performed on immunoprecipitates using 6-a-NAD⁺. After click conjugation with biotin-azide proteins were resolved by SDS/PAGE and detected by Western blot with either Streptavidin-HRP or an antibody against GFP.

PARP10 L926G mutation does not perturb activity in cells

The long-term goal is to use the described chemical genetic strategy to selectively inhibit PARP10 in cells. An important criterion for this strategy is that LG-PARP10 can functionally replace WT-PARP10. We therefore determined if GFP-LG-PARP10 exhibited the same auto-ADPr activity as GFP-WT-PARP10 in cells. For this experiment, we used an aminooxy-alkyne (AO-alkyne) clickable probe that can detect ADPr in cells (Chapter 3).⁹⁹ AO-alkyne reacts with ADP-ribosylated proteins forming an oxime bond, which can be detected by click chemistry using an azide reporter.⁹⁹ HEK 293T cells overexpressing either GFP-WT-PARP10, GFP-LG-PARP10, or the catalytically inactive mutant GFP-G888W (GW)-PARP10 were treated with AO-alkyne (100 μM) in the presence of the oxime catalyst *p*-phenylenediamine (10 mM) followed by click conjugation with biotin-azide. We found that GFP-WT-PARP10 and GFP-LG-PARP10 exhibited

similar auto-ADPr activity in cells, whereas GFP-GW-PARP10 was inactive (**Figure 4-7**). These results demonstrate that the Leu926 to glycine mutation does not significantly perturb the cellular activity of PARP10.

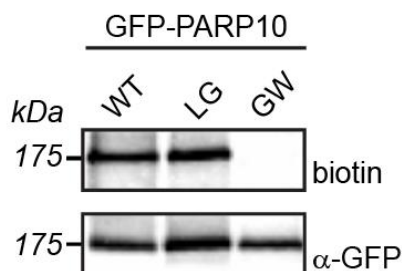
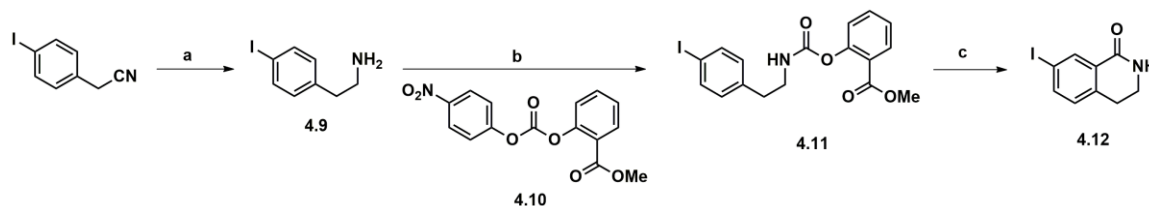


Figure 4-7. Cellular auto-ADPr activity of GFP-tagged full-length LG-PARP10 is similar to WT-PARP10, as measured in cells using AO-alkyne. HEK 293T cells overexpressing either GFP-WT-PARP10, GFP-LG-PARP10, or catalytically dead GFP-G888W (GW)-PARP10 were treated with AO-alkyne (100 μ M) and *p*-phenylenediamine (PDA, 10 mM) for 1 h at 37 $^{\circ}$ C as described previously.⁹⁹ Lysates were subjected to click conjugation with biotin-azide (100 μ M). Proteins were resolved by SDS/PAGE and detected by Western blot with either Streptavidin-HRP or an antibody against GFP.

A 7-iodo substituted dq compound exhibits similar selectivity

The next goal for the chemical genetics strategy was to further increase selectivity for the LG-PARP10 mutant versus WT. The clear halogen preference for the pocket formed by mutation of the leucine to a glycine prompted us to investigate the next element in the halogen series: iodine. The synthesis of 7-iodo modified dq analogue **4.12** is outlined in **Scheme 4-3**.

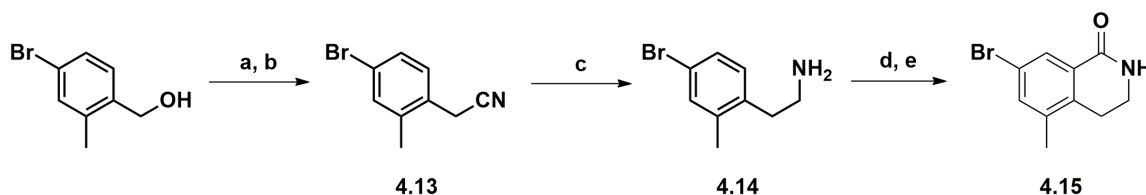


Scheme 4-3. Synthesis of 7-I-dq analogue **4.12**. Reagents and conditions: a. BH_3 , THF (65% yield); b) **10**, THF (86% yield); c. TfOH , DCM (48% yield).

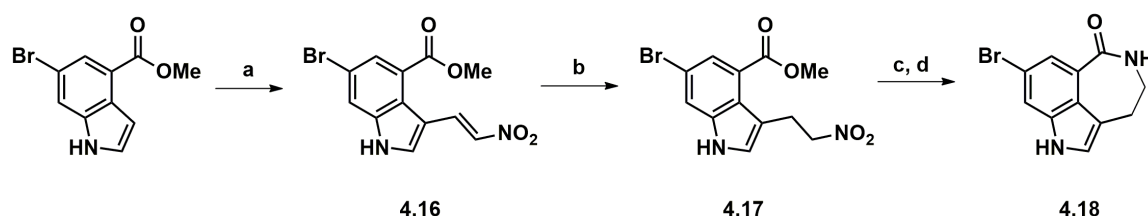
Analogue **4.12** was assayed against both LG-PARP10_{cat} and WT-PARP10_{cat} and only exhibited a slight increase in potency for the PARP10 mutant (IC_{50} = 6.1 μ M) compared to the bromo-modified analogue **4.4** (8.6 μ M). Considering that the iodo group only afforded a modest increase in potency, the bromo-substituent was selected as the preferred modification going forward.

Transfer of bromo group to different inhibitor scaffolds maintains selectivity

In order to move into cellular studies with a chemical genetics strategy, a more potent inhibitor (e.g., $IC_{50} \leq 1$ μ M) was desired. We proposed that transferring the bromo group to different inhibitor scaffolds could increase potency while still maintaining selectivity for the LG-PARP10 mutant over WT. We chose the a) 5-methyl-3,4-dihydroisoquinolin-1(2*H*)-one and b) 4,5-dihydro-1*H*-azepino[5,4,3-*cd*]indol-6(3*H*)-one or [5,6,7] tricyclic indole lactam (TIL) inhibitor scaffolds⁷⁰ and appended a bromo group in the analogous position as **4.4** to yield 7-Br-5-Me-dq **4.15** (**Scheme 4-4**) and 8-Br-TIL **4.18** (**Scheme 4-5**), respectively.



Scheme 4-4. Synthesis of 7-Br-5-Me-dq (**4.15**). Reagents and conditions: a. MsCl, Et₃N; b. KCN, DMF (66% yield over two steps); c. ZrCl₄, NaBH₄, THF (27%); d. **10**, THF; e. TfOH, DCM (29% yield over two steps).



Scheme 4-5. Synthesis of 8-Br-TIL (**4.18**). Reagents and conditions: a. 1-(dimethylamino)-2-nitroethylene (DMANE), TFA/DCM (4:3) (67% yield); b. NaBH₄/H₃BO₃, IPA/THF (1:3) (53% yield); c. Zn, HCl, MeOH/H₂O; d. aq. NaOH (82% yield over two steps).

The potency and selectivity of **4.15** and **4.18** were determined for LG-PARP10_{cat} and WT-PARP10_{cat}. Both **4.15** and **4.18** were 2-3-fold more potent than **4.4**, and their selectivity was also >20-fold selective for LG-PARP10_{cat} versus WT-PARP10_{cat} (**Table 4-2**), a two-fold improvement over **4.4**. Therefore, by transferring the bromo substituent to different inhibitor scaffolds, potency and selectivity could be improved.

Table 4-2. Bromo-substituted analogues selectively inhibit the engineered PARP10 mutant, LG-PARP10_{cat}.

		LG-PARP10 _{cat} IC ₅₀ (μM)	WT-PARP10 _{cat} IC ₅₀ (μM)	WT-PARP10/ LG-PARP10
4.4	7-Br-dq	8.6	>100	>10
4.15	7-Br-5-Me-dq	2.5	53	>20
4.18	8-Br-TIL	5.1	>100	~20

Selectivity of compounds observed *in vitro* does not translate in cells

All selectivity studies so far were performed *in vitro*, either with catalytic domains of PARP10 (**Table 4-1** and **Table 4-2**) or immunoprecipitated full-length PARP10 from mammalian expression (**Figure 4-6**). We wanted to determine if the selectivity of compounds **4.15** and **4.18** observed *in vitro* translated to a cellular system. Our aim was to validate this chemical genetics strategy as a

means to achieve selective inhibition of PARP10 for future cellular studies of PARP10-mediated ADPr. We incubated HEK293T cells expressing either GFP-LG-PARP10 or GFP-WT-PARP10 with increasing concentrations of both **4.15** and **4.18** and measured the auto-ADPr of PARP10 using a pan-ADP-ribose binding reagent.¹²⁸ A dose-dependent decrease in the auto-ADPr was observed for LG-PARP10, as expected; however, a decrease in the auto-ADPr of WT-PARP10 was also observed (**Figure 4-8**).

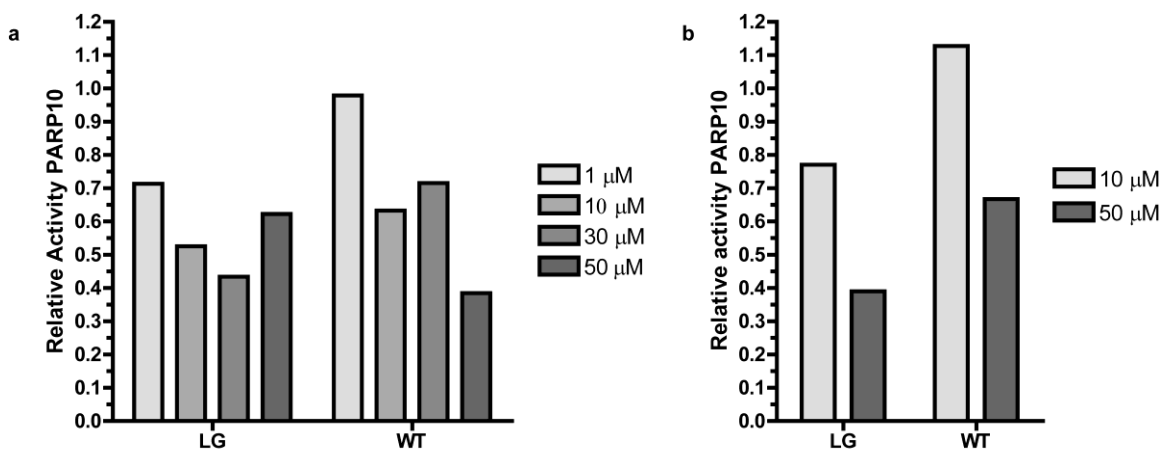


Figure 4-8. Compounds **4.15** and **4.18** do not maintain selectivity for full-length LG-PARP10 versus WT-PARP10 in cells. HEK293T cells expressing GFP-LG-PARP10 or GP-WT-PARP10 were incubated with increasing concentrations of (a) **4.15** or (b) **4.18** in serum free media for 1 h. Lysates were prepared and auto-ADPr of PARP10 was analyzed with a pan-ADP-ribose binding reagent (α -APDr).¹²⁸ Relative activity is compared to no inhibitor control.

The selectivity of compounds **4.15** and **4.18** observed *in vitro* unfortunately did not translate to full-length LG-PARP10 in cells. The conformation of full-length LG-PARP10 in the cell could be different from its conformation *in vitro*. This could be due to the binding of specific proteins in the cell that cause a conformational change in full-length LG-PARP10 that is not recapitulated during immunoprecipitation where washings could potentially destabilize binding

interactions. Additionally, cellular compartmentalization is lost upon lysis, which could potentially change binding interactions that are favored in specific locations throughout the cell. While the leucine to glycine mutant of PARP10 can be selectively inhibited by bromo-modified inhibitors *in vitro*, additional mutations within the active site of PARP10 and the corresponding orthogonal inhibitors will need to be explored to impart selective inhibition over wild-type PARP10 in cells.

Conclusions and Future Directions

In this study, we used a bump-hole strategy to successfully identify a series of C-7 substituted dq analogues that selectively inhibit the engineered PARP10 mutant, LG-PARP10_{cat}. The most potent C-7 substituted dq analogue is the bromo-substituted analogue **4.4**, which exhibited a greater than 10-fold selectivity for LG- versus WT-PARP10_{cat}. To our knowledge this is the first study that demonstrates the use of halogen-substitution to generate selective inhibitors using the bump-hole approach. Two additional scaffolds were adorned with a bromo-substituent to increase potency while maintaining selectivity for LG-PARP10_{cat}. When these inhibitors (**4.15** or **4.18**) were assayed against full-length LG-PARP10 versus WT-PARP10, the selectivity observed *in vitro* did not translate in cells. The LG-PARP10 mutant behaves differently *in vitro* than in a cellular system, prompting the need to explore other possible PARP10 mutants for a chemical genetics strategy to achieve selective inhibition.

A possible strategy could involve the mutation of an isoleucine residue (I978 in PARP10, see Chapter 2) to a cysteine residue. This would allow for

potential inhibition with covalent inhibitors containing previously identified electrophiles (e.g, halomethyl ketones, acrylamides, vinylsulfonylamides, etc.).⁸³ This may offer advantages over a traditional “bump-hole” competitive inhibitor strategy, in that inhibition of the mutant would be irreversible, potentially enabling far greater selectivity differences. The I978 residue is also highly conserved among the mono-ADPr subclass of PARPs,⁸⁰ suggesting that this strategy may be more translatable to this entire subclass of PARPs to achieve selective inhibition.

Experimental

Chemical Synthesis

General. ^1H NMR were recorded on a Bruker DPX spectrometer at 400 MHz. Chemical shifts were reported as parts per million (ppm) downfield from an internal tetramethylsilane standard or from solvent references. Dichloromethane (DCM), *N,N*-dimethylformamide (DMF), and *N,N*-diisopropylethylamine (DIPEA) were dried using a solvent purification system manufactured by Glass Contour, Inc. (Laguna Beach, CA). All other solvents were of ACS chemical grade (Fisher Scientific) and used without further purification unless otherwise indicated. Commercially available 1-indanones from Fisher Scientific or Sigma Aldrich were >95% pure and used without further purification. 4-fluorophenethylamine (98%) and 3,4-dihydro-2*H*-isoquinolin-1-one (dq, **4.1**) (95%) were purchased from CombiBlocks (San Diego, CA) and used as received. *N*⁶-alkyne-NAD⁺ (6-a-NAD⁺) was synthesized as previously described (Chapter 2).⁸⁴

Synthesis of 7-fluoro-3,4-dihydroisoquinolin-1(2H)-one (7-F-dq, 4.2): The procedure of Kurouchi et al. was followed as previously described,¹²⁷ with minor modifications. To a solution of 4-fluorophenethylamine (208.8 mg, 1.5 mmol) and DIPEA (0.29 mL, 1.65 mmol) in DMF (5.6 mL), methyl chloroformate (0.13 mL, 1.65 mmol) was slowly added at 0 °C, and the reaction mixture was stirred at rt for 1h. The reaction was quenched with water (19 mL) and extracted with EtOAc (2 x 20 mL). The combined organic phases were washed with brine, dried over Na₂SO₄, filtered, and concentrated *in vacuo* to yield methyl 4-

fluorophenethylcarbamate as a colorless oil (246.4 mg, 83%) which was used in the next step without further purification. Methyl 4-fluorophenethylcarbamate (crude): ^1H NMR (400 MHz, $\text{DMSO}-d_6$) δ 7.28 – 7.16 (m, 2H), 7.15 – 7.03 (m, 2H), 3.49 (s, 3H), 3.23 – 3.10 (m, 2H), 2.68 (t, J = 7.3 Hz, 2H). To the methyl carbamate intermediate (147.9 mg, 0.75 mmol) was slowly added trifluoromethanesulfonic acid (3.26 mL, 37.1 mmol) at 0 °C. The resulting mixture was heated at 70 °C for 24 h with stirring. The reaction was quenched by pouring over ice-water (37 mL) and extracted with DCM (2 x 20 mL). The combined organic phases were washed with brine, dried over Na_2SO_4 , filtered, and concentrated *in vacuo*. The crude residue was purified via ISCO Combiflash chromatography (silica, 4g; 20-100% EtOAc in hexanes) to yield the product as a white solid (90 mg, 73%). ^1H NMR (400 MHz, $\text{DMSO}-d_6$) δ 8.11 (s, 1H), 7.53 (dd, J = 9.4, 2.8 Hz, 1H), 7.43 – 7.25 (m, 2H), 3.44 – 3.35 (m, 2H), 2.88 (t, J = 6.6 Hz, 2H).

General procedure for synthesis of 3,4-dihydroisoquinolin-1(2H)-ones from 1-indanones via Schmidt reaction: To a solution of an appropriate 1-indanone (0.5 mmol) in 2:1 DCM:methanesulfonic acid (4.6 mL) at 0 °C was added NaN_3 (48.8 mg, 0.75 mmol) portionwise over 30 min. The resulting mixture was allowed to warm to rt and stirred overnight. The reaction mixture was quenched with 1 N NaOH (3 mL) at 0 °C, and the DCM layer was removed. The aqueous layer was extracted with DCM or EtOAc (for –OH derivative). The combined organic layers were washed with H_2O and brine, dried over Na_2SO_4 , and concentrated *in vacuo*.

The *N*-alkyl and *N*-aryl amide regioisomers were separated via ISCO CombiFlash chromatography (silica, 4g; 20-100% EtOAc in hexanes).

Synthesis of 7-chloro-3,4-dihydroisoquinolin-1(2H)-one (7-Cl-dq, 4.3): from 6-chloro-1-indanone; yield: 73.2 mg (0.40 mmol, 80%); isomer ratio: *N*-alkyl 26%, *N*-aryl 74%. ¹H NMR (400 MHz, DMSO-*d*₆) δ 8.12 (s, 1H), 7.77 (d, *J* = 2.4 Hz, 1H), 7.54 (dd, *J* = 8.1, 2.4 Hz, 1H), 7.42 – 7.28 (m, 1H), 3.46 – 3.35 (m, 2H), 2.89 (t, *J* = 6.6 Hz, 2H).

Synthesis of 7-bromo-3,4-dihydroisoquinolin-1(2H)-one (7-Br-dq, 4.4): from 6-bromo-1-indanone; yield: 87.5 mg (0.39 mmol, 78%); isomer ratio: *N*-alkyl 27%, *N*-aryl 73%. ¹H NMR (400 MHz, DMSO-*d*₆) δ 8.12 (s, 1H), 7.91 (d, *J* = 2.2 Hz, 1H), 7.72 – 7.61 (m, 1H), 7.30 (d, *J* = 8.1 Hz, 1H), 3.43 – 3.35 (m, 2H), 2.87 (t, *J* = 6.6 Hz, 2H).

Synthesis of 7-methyl-3,4-dihydroisoquinolin-1(2H)-one (7-Me-dq, 4.5): from 6-methyl-1-indanone; yield: 60.9 mg (0.38 mmol, 76%); isomer ratio: *N*-alkyl 44%, *N*-aryl 56%. ¹H NMR (400 MHz, DMSO-*d*₆) δ 7.88 (s, 1H), 7.65 (d, *J* = 1.9 Hz, 1H), 7.27 (ddd, *J* = 7.7, 2.0, 0.8 Hz, 1H), 7.18 (d, *J* = 7.7 Hz, 1H), 3.43 – 3.25 (m, 2H), 2.84 (t, *J* = 6.6 Hz, 2H).

Synthesis of 7-(trifluoromethyl)-3,4-dihydroisoquinolin-1(2H)-one (7-CF₃-dq, 4.6): from 6-(trifluoromethyl)-1-indanone; yield: 72.9 mg (0.34, 68%); isomer ratio: *N*-

alkyl 28%, *N*-aryl 72%. ^1H NMR (400 MHz, DMSO- d_6) δ 8.22 (s, 1H), 8.13 – 8.02 (m, 1H), 7.94 – 7.75 (m, 1H), 7.58 (d, J = 8.0 Hz, 1H), 3.41 (td, J = 6.6, 2.9 Hz, 2H), 3.01 (t, J = 6.6 Hz, 2H).

Synthesis of 7-hydroxy-3,4-dihydroisoquinolin-1(2H)-one (7-OH-dq, 4.7): from 6-hydroxy-1-indanone; yield: 25.5 mg (0.16 mmol, 31%); isomer ratio: *N*-alkyl 52%, *N*-aryl 48%. ^1H NMR (400 MHz, DMSO- d_6) δ 9.49 (s, 1H), 7.85 (s, 1H), 7.24 (d, J = 2.7 Hz, 1H), 7.09 (d, J = 8.2 Hz, 1H), 6.84 (dd, J = 8.2, 2.7 Hz, 1H), 3.30 (td, J = 6.6, 2.8 Hz, 2H), 2.76 (t, J = 6.6 Hz, 2H).

Synthesis of 7-methoxy-3,4-dihydroisoquinolin-1(2H)-one (7-OMe-dq, 4.8): from 6-methoxy-1-indanone; yield: 67.5 mg (0.38 mmol, 76%); isomer ratio: *N*-alkyl 63%, *N*-aryl 37%. ^1H NMR (400 MHz, DMSO- d_6) δ 7.96 (s, 1H), 7.35 (d, J = 2.8 Hz, 1H), 7.22 (d, J = 8.4 Hz, 1H), 7.04 (dd, J = 8.3, 2.8 Hz, 1H), 3.77 (s, 3H), 3.34 – 3.23 (m, 2H), 2.81 (t, J = 6.6 Hz, 2H).

Synthesis of 7-iodo-3,4-dihydroisoquinolin-1(2H)-one (7-I-dq, 4.12):

4-iodophenethylamine (**4.9**): To a solution of 4-iodophenylacetonitrile (0.5 g, 2.1 mmol) in THF (6 mL) in a pressure vessel was slowly added BH_3 -THF complex (10.3 mL, 1M, 10.3 mmol) at 0 °C via syringe dropwise over 10 min. The vessel was purged with Ar, sealed, and heated at 72 °C for 3 h. The mixture was cooled to 0 °C and quenched with 6 M HCl (1 mL), immediately forming a ppt. The reaction was left stirring overnight, and the ppt was filtered off and rinsed with

Et₂O. The ppt was redissolved in 1M NaOH (50 mL) and extracted with DCM (2 x 50 mL). The combined organic layers were dried over Na₂SO₄, filtered, and concentrated *in vacuo* to yield **4.9** as a pale yellow oil (330 mg, 1.34 mmol, 65% yield). ¹H NMR (400 MHz, DMSO-*d*₆) δ 7.77 – 7.46 (m, 2H), 7.18 – 6.74 (m, 2H), 2.72 (dd, *J* = 7.8, 6.4 Hz, 2H), 2.57 (t, *J* = 7.1 Hz, 2H), 1.29 (d, *J* = 48.0 Hz, 2H).

methyl 2-(((4-nitrophenoxy)carbonyl)oxy)benzoate (**4.10**): To 4-nitrophenyl chloroformate (2.02 g, 10 mmol) in DCM (40 mL) was added Et₃N (4.18 mL, 30 mmol) at 0 °C followed by methyl salicylate (2.03 mL, 16 mmol). The reaction was stirred overnight, gradually warming to rt. The reaction was concentrated *in vacuo* to yield a yellowish residue, which was taken up in EtOAc (100 mL). The Et₃N•HCl salts were filtered, and the filtrate was concentrated *in vacuo*. The resulting residue was triturated with hexanes/Et₂O (1:1) and filtered to yield **4.10** as an off-white solid (1.99 g, 80% yield). ¹H NMR (400 MHz, DMSO-*d*₆) δ 8.47 – 8.27 (m, 2H), 8.03 (dd, *J* = 7.8, 1.8 Hz, 1H), 7.79 (ddd, *J* = 8.2, 7.4, 1.7 Hz, 1H), 7.70 – 7.60 (m, 2H), 7.60 – 7.44 (m, 2H), 3.89 (s, 3H).

methyl 2-(((4-iodophenethyl)carbamoyl)oxy)benzoate (**4.11**): To a solution of **4.9** (67 mg, 0.27 mmol) in THF (2 mL) was added **4.10** (78 mg, 0.25 mmol). The resulting solution was allowed to stir at rt until TLC analysis (1:1 hexanes:Et₂O) revealed consumption of starting amine (2 h). The THF was removed *in vacuo* and the crude residue was purified via ISCO CombiFlash chromatography (silica, 4g; 0-100% Et₂O in hexanes) to yield the carbamoyl salicylate product **4.11** (90

mg, 0.21 mmol, 86% yield). ^1H NMR (400 MHz, CDCl_3) δ 8.28 – 7.92 (m, 1H), 7.73 – 7.61 (m, 2H), 7.54 (td, $J = 7.7, 1.7$ Hz, 1H), 7.30 (d, $J = 7.7$ Hz, 1H), 7.14 (d, $J = 8.1$ Hz, 1H), 7.08 – 6.95 (m, 2H), 3.51 (q, $J = 6.8$ Hz, 2H), 2.86 (t, $J = 7.0$ Hz, 2H).

7-iodo-3,4-dihydroisoquinolin-1(2H)-one (7-I-dq, **4.12**): The procedure was followed as described previously.¹²⁹ To a solution of **4.11** (87 mg, 0.21 mmol) in DCM (1 mL) at 0 °C was added triflic acid (0.18 mL, 2.1 mmol) dropwise. The resulting mixture was allowed to warm to rt over 1.5 h. The reaction was quenched with ice-cold water (20 mL) and extracted with DCM (2 x 50 mL). The combined organic layers were dried over Na_2SO_4 , filtered, and concentrated *in vacuo*. The resulting crude mixture was purified via ISCO CombiFlash chromatography (silica, 4g; 0-100% EtOAc in DCM; product elutes at ~ 80% EtOAc) to yield **4.11** as a white solid (27 mg, 0.099 mmol, 48% yield). ^1H NMR (400 MHz, $\text{DMSO}-d_6$) δ 8.09 (d, $J = 2.0$ Hz, 1H), 8.06 (s, 1H), 7.81 (dd, $J = 7.9, 2.0$ Hz, 1H), 7.14 (d, $J = 8.0$ Hz, 1H), 3.42 – 3.35 (m, 2H)*, 2.85 (t, $J = 6.6$ Hz, 2H), *obscured by HOD peak.

*Synthesis of 7-bromo-5-methyl-3,4-dihydroisoquinolin-1(2H)-one (7-Br-5-Me-dq, **4.15**):*

4-bromo-2-methylphenylacetonitrile (**4.13**): To a solution of 4-bromo-2-methylbenzyl alcohol (0.3 g, 1.5 mmol) in DCM (3 mL) and Et_3N (0.275 mL, 1.97 mmol) at 0 °C was added mesyl chloride (0.13 mL, 1.72 mmol) via syringe

dropwise. The reaction was gradually warmed to rt and stirred for 23 h before quenching with sat. NaHCO_3 (10 mL). The DCM layer was collected. The aqueous layer was extracted with DCM (3 x 10 mL). The combined organic layers were washed with brine, dried over Na_2SO_4 , filtered, and concentrated *in vacuo* to yield the crude mesylate. The mesylate was taken up in DMF (4 mL), and KCN (0.11 g, 1.75 mmol) and H_2O (1 mL) was added. The reaction was stirred at 60 °C for 2.5 h and diluted with EtOAc (10 mL) and water (10 mL). The EtOAc layer was washed with brine (3 x 10 mL), dried over Na_2SO_4 , filtered, and concentrated *in vacuo*. The crude residue was purified via ISCO CombiFlash chromatography (silica, 12 g; 0-50% EtOAc in hexanes; product elutes at ~15% EtOAc) to yield **4.13** as an off-white solid (0.21 g, 1.0 mmol, 66% yield). ^1H NMR (400 MHz, $\text{DMSO}-d_6$) δ 7.52 – 7.46 (m, 1H), 7.44 (dd, J = 8.2, 2.2 Hz, 1H), 7.29 (d, J = 8.2 Hz, 1H), 3.98 (s, 2H), 2.29 (s, 3H).

4-bromo-2-methylphenethylamine (**4.14**): To a solution of ZrCl_4 (0.51 g, 2.2 mmol) in THF (8.6 mL) was added NaBH_4 (0.33 g, 8.7 mmol) in three portions and stirred for 1h under Ar. To the reaction was added **4.13** (0.19 g, 0.90 mmol) followed by additional NaBH_4 (0.12 g, 3.2 mmol) and ZrCl_4 (0.12 g, 0.51 mmol). The reaction was allowed to stir for 18 h and quenched with dilute aq. NH_3 at 0 °C. The mixture was extracted with DCM (3 x 25 mL), and the combined organic layers were dried over Na_2SO_4 , filtered, and concentrated *in vacuo*. The crude residue was purified via ISCO CombiFlash chromatography (silica, 4 g; 0-100% MeOH in DCM; product elutes at ~20% MeOH) to yield **4.14** as an oil (53 mg,

0.25 mmol, 27% yield). ^1H NMR (400 MHz, $\text{DMSO}-d_6$) δ 7.34 (d, J = 2.1 Hz, 1H), 7.28 (dd, J = 8.1, 2.2 Hz, 1H), 7.08 (d, J = 8.1 Hz, 1H), 2.69 (dd, J = 8.9, 6.4 Hz, 2H), 2.60 (dd, J = 8.2, 5.8 Hz, 2H), 2.26 (s, 3H).

7-bromo-5-methyl-3,4-dihydroisoquinolin-1(2H)-one (7-Br-5-Me-dq, **4.15**): To a solution of **4.14** (50 mg, 0.23 mmol) in DCM (1.2 mL) was added **4.10** (67 mg, 0.21 mmol). The resulting solution was allowed to stir at rt until TLC analysis (1:1 hexanes: Et_2O) revealed consumption of starting amine. Triflic acid (0.18 mL, 2.1 mmol) was added dropwise at 0 °C, and the reaction was stirred, gradually warming to rt over 1.5 h. The reaction was quenched with ice-cold water (20 mL) and extracted with DCM (2 x 50 mL). The combined organic layers were dried over Na_2SO_4 , filtered, and concentrated *in vacuo*. The resulting crude mixture was purified via ISCO CombiFlash chromatography (silica, 4g; 10-100% EtOAc in hexanes; product elutes at ~ 80% EtOAc) to yield **4.15** as a white solid (15 mg, 0.062 mmol, 29% yield). ^1H NMR (400 MHz, $\text{DMSO}-d_6$) δ 8.07 (s, 1H), 7.79 (d, J = 2.2 Hz, 1H), 7.58 (dd, J = 2.2, 0.8 Hz, 1H), 3.30 (2H)*, 2.78 (t, J = 6.7 Hz, 2H), 2.27 (s, 3H), * obscured by HOD peak.

*Synthesis of 8-bromo-4,5-dihydro-1H-azepino[5,4,3-cd]indol-6(3H)-one (8-Br-TIL, **4.18**):*

(*E*)-methyl 6-bromo-3-(2-nitrovinyl)-1H-indole-4-carboxylate (**4.16**): To a solution of 1-(dimethylamino)-2-nitroethylene (DMANE) (0.31 g, 3.2 mmol) in TFA (4.8 mL) was added methyl 6-bromo-1-indole-4-carboxylate (1.0 g, 4.0 mmol) in DCM

(3.6 mL) dropwise with stirring. The reaction was allowed to stir at rt for 1.25 h and quenched with H₂O (50 mL). The DCM layer was collected, and the aqueous layer was extracted with DCM (3 x 20 mL). The combined organic layers were dried over Na₂SO₄, filtered, and concentrated *in vacuo*. The crude residue was purified via ISCO CombiFlash chromatography (silica, 12 g; 0-100% EtOAc in hexanes) to yield **4.16** as a bright orange solid (0.70 g, 2.2 mmol, 67% yield). ¹H NMR (400 MHz, DMSO-*d*₆) δ 12.68 (s, 1H), 9.05 (d, *J* = 13.4 Hz, 1H), 8.57 (d, *J* = 3.1 Hz, 1H), 8.03 (dd, *J* = 13.3, 1.0 Hz, 1H), 7.96 (t, *J* = 1.4 Hz, 1H), 7.86 (d, *J* = 1.7 Hz, 1H), 3.94 (d, *J* = 1.0 Hz, 3H).

methyl 6-bromo-3-(2-nitroethyl)-1H-indole-4-carboxylate (**4.17**): To a solution of **4.16** (0.65 g, 2.0 mmol) in THF/IPA (1:3, 160 mL) was added H₃BO₃ (0.74 g, 12 mmol) followed by NaBH₄ (0.45 g, 12 mmol) in two portions over 15 min. The resulting solution was allowed to stir overnight at rt (18 h). The reaction was concentrated to *ca.* one-quarter volume, and the reaction was quenched with 2 M HCl (10 mL). The mixture was concentrated *in vacuo*, and the resulting residue was taken up in EtOAc (15 mL) and H₂O (10 mL). The EtOAc layer was removed, and the aqueous layer was extracted with EtOAc (2 x 15 mL). The combined organic layers were washed with water (10 mL), dried over Na₂SO₄, filtered, and concentrated *in vacuo*. The crude residue was purified via ISCO CombiFlash chromatography (silica, 12 g; 0-50% EtOAc in hexanes) to yield **4.17** as a pale purple solid (0.35 g, 1.1 mmol, 53% yield). ¹H NMR (400 MHz, DMSO-

d_6) δ 11.57 (s, 1H), 7.82 (d, J = 1.8 Hz, 1H), 7.65 (d, J = 1.9 Hz, 1H), 7.43 (d, J = 2.6 Hz, 1H), 4.74 (t, J = 6.9 Hz, 2H), 3.89 (s, 3H), 3.46 (t, J = 6.9 Hz, 2H).

8-bromo-4,5-dihydro-1*H*-azepino[5,4,3-*cd*]indol-6(3*H*)-one (8-Br-TIL, **4.18**): To a vigorously stirring solution of **4.17** (0.23 g, 0.69 mmol) in MeOH/2 N HCl (aq) (1:1, 21 mL) in a pressure vessel was added Zn metal (1.1 g, 16.5 mmol) portionwise. The reaction was capped and heated at 105 °C with stirring for 1.5 h. The hot reaction mixture was filtered with a Büchner funnel to remove excess Zn. The filtrate was treated with 2 N NaOH (12.9 mL) to form a thick, white ppt. The ppt was filtered off and rinsed with MeOH. The filtrate was concentrated *in vacuo* to remove most of the MeOH, and the remaining aq. portion was extracted with EtOAc (3 x 20 mL). The combined organic layers were dried over Na₂SO₄, filtered, and concentrated *in vacuo*. The crude residue was purified via ISCO CombiFlash chromatography (silica, 4 g; 0-10% MeOH in DCM; product elutes at ~4% B) to yield **4.18** (150 mg, 0.57 mmol, 82% yield). ¹H NMR (400 MHz, DMSO- d_6) δ 11.28 (s, 1H), 8.19 (t, J = 5.7 Hz, 1H), 7.70 (s, 2H), 7.31 (dd, J = 2.4, 1.1 Hz, 1H), 3.56 – 3.37 (m, 2H)*, 2.91 (s, 2H), *obscured by HOD peak.

Other Methods

Cloning and mutagenesis. cDNA encoding full length human PARP1, human PARP10 catalytic domain, and SRPK2 were obtained as previously described (Chapters 2 and 3).^{84,99} The PARP10 catalytic domain L926A (LA-PARP10_{cat}) and L926G (LG-PARP10_{cat}) mutants were generated using the QuickChange® II

XL site-directed mutagenesis kit (Agilent). Plasmids were sequenced from both the 5' and 3' direction to confirm the coding sequence.

Recombinant protein production and purification. PARP10_{cat} and SRPK2 were expressed and purified as described previously (Chapter 3).⁹⁹ PARP1 FL was prepared as previously described (Chapter 2).⁸⁴

PARP activity assay with 6-a-NAD⁺ and fluorescence detection. For PARP10 activity assays, 0.01 nmol of PARP10_{cat} enzyme was used to ADP-ribosylate 0.06 nmol of SRPK2 with 100 μ M 6-a-NAD⁺ in 20 μ L of reaction buffer (50 mM Tris-HCl pH 8.0, 100 mM NaCl, 4 mM MgCl₂, 0.5 mM TCEP•HCl) at 30 °C for 1 h. For PARP1 activity assays, 0.01 nmol of PARP1 FL was automodified in the presence of 100 μ M 6-a-NAD⁺ in 20 μ L of reaction buffer above (+ 10 ng/mL activated DNA) at 30 °C for 1 h. Compounds were screened in the presence of DMSO at 0.125% for all reactions. The reaction was quenched by the addition of a 3X stock of freshly prepared CB (300 μ M of tris[(1-benzyl-1*H*-1,2,3-triazol-4-yl)methyl]amine (TBTA), 3 mM CuSO₄, 300 μ M sulforhodamine-azide (Click Chemistry Tools), 3 mM TCEP•HCl in 1X phosphate buffered saline (PBS) with 3% SDS; final [rhodamine-azide] = 100 μ M) and incubated at rt for 30 min. 4X sample buffer with 5% β -mercaptoethanol (BME) was added. The reactions were fractionation by SDS-PAGE, and in-gel fluorescence detection was performed using a ChemiDoc™ MP Imaging System (Bio-Rad). Coomassie staining was performed as a loading control. Inhibitor dose-response curves were fitted using

nonlinear regression analysis (sigmoidal dose-response) in Prism 4 (GraphPad Software). For curves where 100% inhibition could not be achieved due to solubility of analogues, the curves were constrained to a minimum value of zero. Each experiment was repeated at least twice, shown are representative images.

PARP10 auto-ADP-ribosylation activity assay in cells using AO-alkyne.

Auto-ADPr levels for PARP10 in HEK293T cells were determined as previously described (Chapter 3).⁹⁹ HEK293T cells expressing GFP-tagged PARP10 WT or PARP10 L926G and G888W variants were treated with medium containing AO-alkyne (100 μ M) and *p*-phenylenediamine (PDA, 10 mM) and incubated for 1 h. The medium was removed and cells were washed with cold (4 °C) PBS and lysed by freezing in N₂ (l) and thawing in buffer containing 25 mM HEPES at pH 7.5, 50 mM NaCl, 10% glycerol, 1% Nonidet P-40 (NP-40), and 1X complete EDTA-free protease inhibitor cocktail (Roche) and subjected to centrifugation at 14,000g for 5 min at 4 °C. Total protein concentration in the lysate was determined by Bradford assay with a BSA standard curve. Lysates containing normalized protein levels were subjected to click conjugation with 9X CB (900 μ M of TBTA, 9 mM CuSO₄, 900 μ M biotin-azide (Biotin-PEG₃-Azide, Click Chemistry Tools), 9 mM TCEP-HCl in 1X PBS with 1% SDS) and incubated at room temperature for 30 min. A 4X sample buffer (with 5% BME) was added prior to fractionation by SDS-PAGE. Immunblot detection with Streptavidin-HRP was used to quantify levels of biotinylated GFP-PARP10. An antibody against GFP was used to quantify total GFP-PARP10 levels.

PARP10 immunoprecipitation (IP) auto-ADP-ribosylation activity assay. IP- auto-ADP-ribosylation assays were performed as described previously²⁷ with the exception that 6-alkyne-NAD⁺ (6-a-NAD⁺),⁸⁴ a NAD⁺ analogue that can be coupled to biotin-azide via the copper(I) catalyzed [3+2] cycloaddition reaction, was used instead of ³²P-NAD⁺. HEK 293T cells were transfected with GFP-WT-, LG-, or GW-PARP10 expression plasmids using the CalPhosTM mammalian transfection kit. Cells were collected 24 h post-transfection and lysed in 250 μ L/well cytosolic lysis buffer (CLB: 50 mM HEPES [pH 7.4], 150 mM NaCl, 1 mM MgCl₂, 1 mM TCEP, 1% Triton X-100) with cOmpleteTM protease inhibitors. Lysates were clarified by centrifugation at 14,000x rpm for 10 min at 4°C. Protein-G magnetic beads (PureProteomeTM, Millipore; 50 μ L suspended bead slurry) were incubated with anti-GFP antibody (mouse monoclonal, LifeTechnologies clone 3E6; 0.5 μ g per mg lysate protein) for 15 min at 25°C, 650 rpm. Sample lysates were added to anti-GFP (mouse monoclonal, LifeTechnologies clone 3E6; 0.5 μ g per mg lysate protein) conjugated protein-G magnetic beads for 2 h at 4°C with rotation to immunoprecipitate GFP-tagged proteins. Following removal of supernatant, beads were washed once with CLB, three times with CLB + 1 mM NaCl, and once with PARP reaction buffer (PRB: 50 mM Tris-HCl [pH 7.5], 50 mM NaCl, 0.5 mM TCEP, 0.1% Triton X-100) with cOmpleteTM protease inhibitors for 5 min per wash. 200 μ M 6-a-NAD⁺ in PRB was added to beads and incubated for 60 min at 25°C/650 rpm. Following removal of 6-a-NAD⁺, beads were washed twice with PRB containing 500 mM NaCl for 5 min per wash. Click reaction mixture (1 mM CuSO₄, 1 mM TCEP, 100

μ M TBTA, 100 μ M biotin-azide; 25 μ L volume) was added to beads and incubated for 1 h at 25°C/650 rpm. Following removal of click reaction mixture, Laemmli sample buffer with 5% β -mercaptoethanol (25 μ L volume) was added to beads. Samples were heated at 95°C for 5 min and then loaded on 10% SDS-PAGE gels and transferred onto 0.45 μ m nitrocellulose membranes (Protran®, Amersham). Membrane blots were blocked with 5% milk-TBST for 1 h at room temperature. Blots were probed with either an anti-GFP antibody or streptavidin-HRP. Blots were imaged for chemiluminescent signal on a ChemiDoc MP system (Bio-Rad).

GFP-PARP10 cellular ADP-ribosylation assay. HEK 293T cells were transfected with GFP-PARP10 (2 μ g) using the calcium phosphate method (Clontech). 24 h post transfection, cells were treated with increasing concentrations of **4.15** or **4.18** in serum-free media at 37 °C. Cells were washed with PBS, frozen at -80 °C, and lysed (25 mM HEPES adjusted to pH 7.5 with HCl or NaOH, 50 mM NaCl, 10% (v/v) glycerol, 1% Nonidet P-40 (NP-40) with cOmplete™ protease inhibitors (Roche). Lysates were centrifuged at 14,000g for 5 min at 4 °C and supernatants were transferred to a new tube with 2x Laemmli sample buffer with 5% β -mercaptoethanol. Samples were resolved by SDS-PAGE and transferred onto nitrocellulose membranes. Membrane blots were blocked with 5% milk-TBST for 1 h at RT, followed by incubation with a pan-ADP-ribose binding reagent¹²⁸ or a chicken GFP antibody (ab13970, Abcam) for 1 h at

RT, followed by incubation with HRP-conjugated secondary antibodies. Proteins were detected by chemiluminescence.

Chapter 5: Rational Design Strategies for Selective Inhibition of PARP10

Rory K. Morgan, Ilsa T. Kirby, Anke Vermehren-Schmaedick, Michael S. Cohen

Portions of this chapter detail work of a manuscript in preparation. This work was done in collaboration with Ilsa Kirby who expressed and purified many of the PARP constructs used in this chapter. Dr. Anke Vermehren-Schmaedick performed the IP-auto-ADPr assays to determine compound inhibition.

Abstract

There is a lack of small-molecule probes that are selective for individual poly(ADP-ribose) polymerase (PARP) family members that catalyze ADP-ribosylation (ADPr). In particular, very few probes exist that selectively inhibit the mono-ADPr subclass of PARPs. Here, we describe two strategies to selectively inhibit PARP10, a member of the mono-ADPr subclass of PARPs. Both strategies rely on targeting a portion of the D-loop, a structural element within the PARP family active site that displays sequence variability. In the first strategy, we synthesized 3,4-dihydroisoquinolin-1(2*H*)-one (dq) probes to target a hydrophobic pocket within the nicotinamide-binding site formed by the N-terminal region of the D-loop of PARP10. We found that a 5- and 6-substituted dq probe demonstrated selectivity for PARP10 over other PARP family members. In the second strategy, we developed electrophilic probes to target a unique cysteine residue within the C-terminal region of the D-loop of PARP10. We found that an acrylamide-modified 8-methylquinazolin-4(3*H*)-one (mq) probe potently inhibited PARP10. SAR studies with additional mq probes of varying linker length suggest a covalent mode of inhibition. These two strategies will serve as a platform for future small-molecule probe development for PARP10 and other mono-ADPr PARPs.

Introduction

The poly(ADP-ribose) polymerase (PARP) family of enzymes (17 in humans; also known as ADP-ribosyltransferases or ARTDs) catalyze the transfer of ADP-ribose onto amino acids of protein substrates from donor nicotinamide adenine dinucleotide (NAD⁺) in a process known as ADP-ribosylation (ADPr). In recent years, PARPs have emerged as major regulators of cellular processes ranging from chromatin regulation, transcription, RNA biology, DNA repair, stress responses, and metabolism.¹³⁰ PARPs can be divided into two subfamilies based on their differences in catalytic activity: those that catalyze poly-ADPr (PARPs 1, 2, 5a, 5b) and those that catalyze mono-ADPr (PARPs 3, 4, 6-8, 10-12, 14-16).²⁷ Much progress has been made in understanding the functions of PARPs with poly-ADPr activity such as PARP1, PARP2, and the tankyrases (PARPs 5a, b) due to the development of selective inhibitors for these PARPs. However, a comprehensive understanding of the functions of the remaining PARPs that catalyze mono-ADPr has been hindered due to a lack of selective inhibitors. To date, there have been only a few reports of inhibitor development directed toward PARPs with mono-ADPr activity, but many of these reported inhibitors are not selective or have only been profiled against a select number of PARP family members.^{75–78,131}

PARP10 (ARTD10) is a member of the subclass of PARPs that catalyze mono-ADPr and has been implicated in various biological pathways involving DNA repair¹³² and inflammation,³⁴ yet a clear connection of PARP catalytic activity to the regulation of these pathways is still not clear. A selective small

molecule probe of PARP10 could enable detailed mechanistic studies of PARP10-mediated biology and help to validate PARP10 as a therapeutic target for diseases such as cancer.²⁶

The development of selective inhibitors of individual PARP family members has been hindered due to the highly conserved catalytic domain of the PARP family. The D-loop, however, is one of the regions of high sequence variability among the PARP family.⁸⁰ We proposed that targeting this structural element for inhibitor development could impart selectivity for PARP10 over other family members. We devised two strategies for obtaining selective inhibition of PARP10 with small-molecule probes: 1) targeting a hydrophobic subpocket within the nicotinamide-binding site of PARP10 formed by C-terminal D-loop residues; and 2) targeting a noncatalytic, nonconserved cysteine residue on the N-terminal region of the D-loop of PARP10. These strategies will guide the development of small-molecule probes with selectivity for PARP10 and could serve as a general platform for obtaining selective inhibition of other PARP family members.

Results and Discussion

Strategy 1: Targeting a hydrophobic subpocket within the nicotinamide-binding site of PARP10

A recent study described a small-molecule chemical probe known as OUL35 (**Figure 5-1**) as a potent and selective inhibitor of PARP10, exhibiting >12-fold selectivity over other PARP family members examined.⁷⁸ Of the PARPs

tested in the study, OUL35 was not assayed against PARP11. We profiled OUL35 against a panel of PARPs for its ability to inhibit the ADPr of the promiscuous PARP substrate SRSF protein kinase 2 (SRPK2)^{98,99} using NAD⁺ (100 μ M).

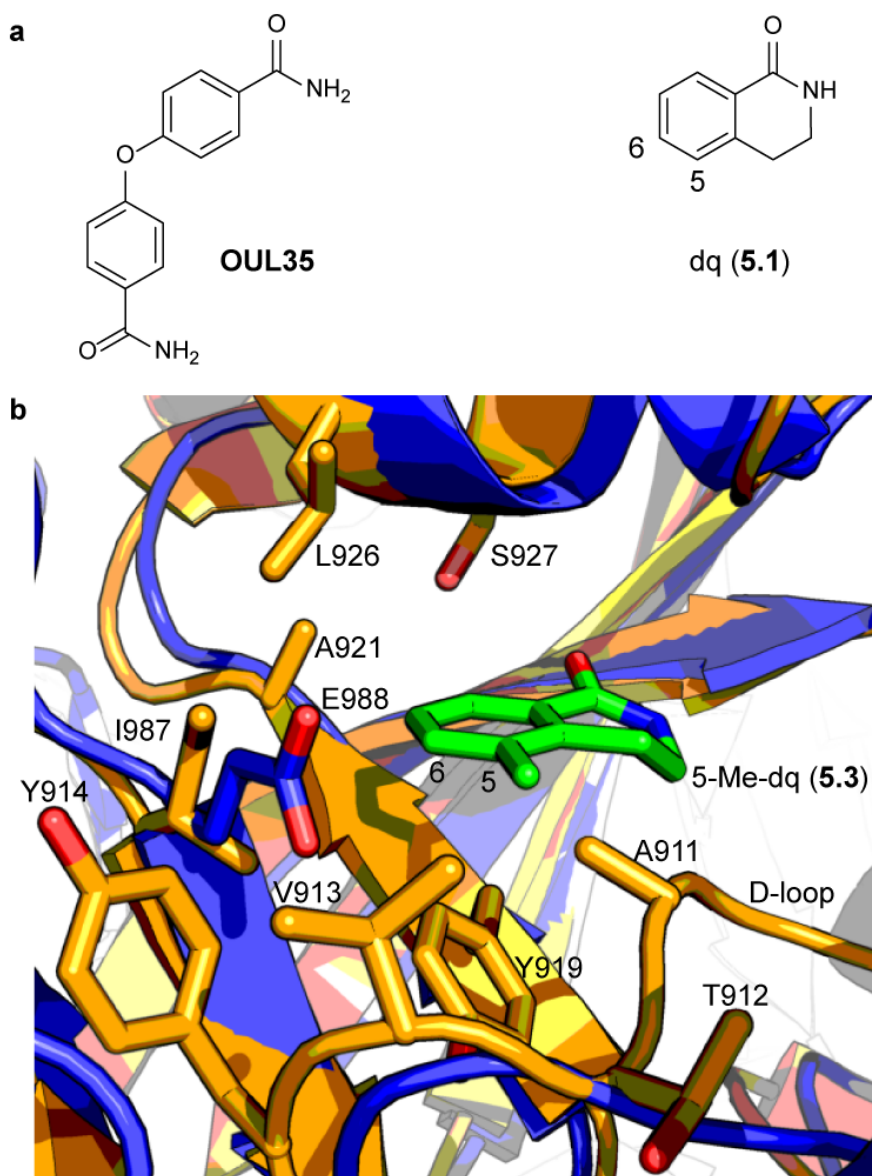


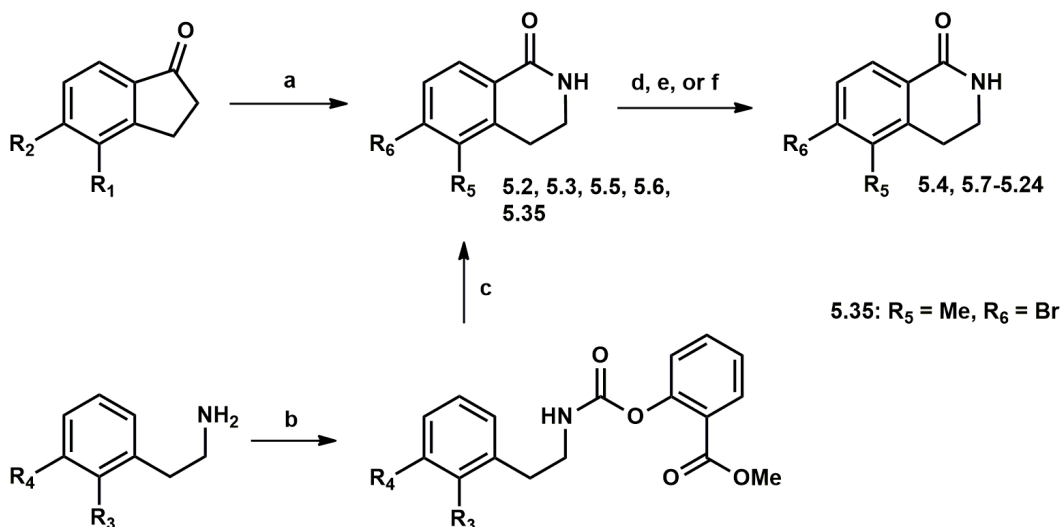
Figure 5-1. Rational design of a selective inhibitor of PARP10 based on a 3,4-dihydroisoquinolin-1(2*H*)-one scaffold. **(a)** Structure of previously reported PARP10-selective inhibitor **OUL35**⁷⁸ and 3,4-dihydroisoquinolin-1(2*H*)-one (dq, **5.1**) scaffold with 5- and 6-positions indicated. **(b)** Structure of PARP10 (orange, PDB ID: 3HKV) overlaid with cocrystal structure of PARP1 and 5-methyl-dq (**5.3**) (blue, PDB ID: 1PAX).¹³³

In our hands, OUL35 exhibited only 2-fold greater potency for PARP10 in comparison to PARP11 (**Table 5-1**). This prompted us to develop a small-molecule chemical probe with greater selectivity for PARP10. Our best inhibitors will aid future studies of PARP10 biology without confounding results due to inhibition of closely-related PARP family members (e.g., PARP11).

The 3,4-dihydroisoquinolin-1(2*H*)-one (dq, **5.1**; **Figure 5-1a**) scaffold has been utilized in the development of inhibitors for PARP1.^{70,134} We showed previously that **5.1** can be modified to inhibit PARP10 using a chemical genetics strategy (Chapter 4)¹²³ and reasoned that **5.1** would be a good starting point for optimizing an inhibitor with increased selectivity for PARP10 over PARP11. We analyzed the structure of PARP10 overlaid with the cocrystal structure of PARP1 and 5-methyl-dq (**5.3**) and hypothesized that modifications on the 5- and 6-position of the dq scaffold would interact with a hydrophobic pocket in PARP10, created by I987 and D-loop residues Y914, V913, and A911 (**Figure 5-1b**). The 5- and 6-positions of the dq scaffold could potentially orient themselves in a similar manner to the phenoxy group in the 4-position of the benzamide core scaffold of OUL35. The 4-phenoxy of OUL35 was proposed to interact with this hydrophobic subpocket within the nicotinamide binding site of PARP10 based on molecular modeling simulations and mutagenesis studies.⁷⁸

In order to determine selectivity for PARP10 over PARP11, a structure-activity relationship (SAR) study was performed with dq compounds substituted at both the 5- and 6-position. The synthesis of the dq scaffold involved either a Schmidt reaction of substituted 1-indanones or an acid-catalyzed cyclization of

carbamoyl salicylates of substituted phenethylamines.¹²⁹ To introduce aryl modifications on the dq scaffold, a Suzuki reaction on bromo-modified dq compounds **5.2**, **5.5**, or **5.35** was performed using the corresponding aryltrifluoroborate or arylboronic acid species (**Scheme 5-1**).

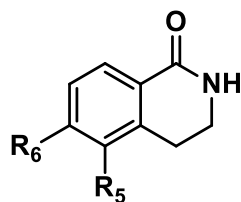


Scheme 5-1. Synthesis of 3,4-dihydroisoquinolin-1(2H)-ones with modifications at the 5- and 6-position. Reagents and conditions: a. NaN₃ (1.5 equiv), DCM/methanesulfonic acid (2:1) (26-60% yield); b. **4.10** (Chapter 4) (1.05 equiv), THF (74% yield); c. TfOH (10 equiv), DCM (65-84% yield); d. R-BF₃K (1.5 equiv), Pd(OAc)₂ (5 mol%), RuPhos (10 mol%), Cs₂CO₃ (3 equiv), toluene/H₂O (3:1) (45% yield); e. R-B(OH)₂, Pd(OAc)₂ (1 mol%), TBAB (1 equiv), K₂CO₃ (10 equiv), H₂O (42-93% yield); f. R-B(OH)₂, Pd(dppf)Cl₂ • CH₂Cl₂ (5 mol%), aq. K₂CO₃ (6 equiv), toluene/EtOH (3:1), (50-92% yield).

A 6-phenyl substituted dq compound is selective for PARP10 over PARP11

The compounds were screened for inhibition against PARP10- and PARP11-mediated ADP-ribosylation of SPRK2 (**Table 5-1**) using NAD⁺ (100 μM). Unsubstituted **5.1** was 9-fold more selective for PARP11 than PARP10 (IC₅₀ = 8 μM versus 70 μM). Substitutions at the 5-position of **5.1** increased potency for both PARP10 and PARP11, yet selectivity for PARP11 was still retained. Compound **5.4** with a phenyl group at the 5-position was the most potent (1.2 μM) and selective (30-fold) for PARP11 among the set of compounds tested.

Table 5-1. *In vitro* IC₅₀ values for selected 5- and 6-substituted dq compounds against PARP10_{cat} and PARP11.



ID	-R ₅	-R ₆	PARP10 _{cat}		PARP11		PARP10 S.R. ^b
			IC ₅₀ (μM)	pIC ₅₀ ± S.E.M. ^a	IC ₅₀ (μM)	pIC ₅₀ ± S.E.M. ^a	
OUL35	-	-	1.3	5.88 ± 0.02	2.1	5.68 ± 0.03	1.6
5.1	H	H	70.3	4.15 ± 0.03	8.0	5.10 ± 0.04	0.11
5.2	Br	H	10.1	4.99 ± 0.04	2.9	5.54 ± 0.04	0.29
5.3	Me	H	8.6	5.01 ± 0.03	2.1	5.67 ± 0.05	0.24
5.4	Ph	H	35.0	4.46 ± 0.04	1.2	5.93 ± 0.04	0.03
5.5	H	Br	17.1	4.77 ± 0.03	13.5	4.87 ± 0.03	0.79
5.6	H	Me	33.1	4.48 ± 0.04	34.1	4.47 ± 0.06	1.0
5.7	H	Bn	>50	-	16.7	4.78 ± 0.03	<0.33
5.8	H	Ph	2.5	5.61 ± 0.03	8.7	5.06 ± 0.03	3.5
5.9	H	3-F-Ph	1.4	5.85 ± 0.03	6.1	5.22 ± 0.04	4.4
5.10	H	3-Cl-Ph	1.1	5.95 ± 0.02	5.8	5.24 ± 0.03	5.3
5.11	H	3-Me-Ph	2.1	5.67 ± 0.02	4.6	5.34 ± 0.03	2.2
5.12	H	3-CF ₃ -Ph	2.3	5.65 ± 0.03	17.4	4.76 ± 0.04	7.6
5.13	H	3-Ac-Ph	1.6	5.81 ± 0.04	4.9	5.31 ± 0.05	3.1
5.14	Me	Ph	1.6	5.80 ± 0.03	26.4	4.58 ± 0.07	17
5.15	Me		2.5	5.60 ± 0.04	30.4	4.52 ± 0.06	12
5.16	Me		1.4	5.84 ± 0.03	21.2	4.67 ± 0.04	15
5.17	Me		1.1	5.96 ± 0.03	4.2	5.38 ± 0.04	3.8
5.18	Me		0.71	6.15 ± 0.03	12.0	4.92 ± 0.05	17
5.19	Me		1.8	5.75 ± 0.02	14.0	4.86 ± 0.04	7.8

^aS.E.M. from three representative dose-response experiments

^bselectivity ratio = IC₅₀ PARP11/IC₅₀ PARP10

When compared to unsubstituted **5.1**, 6-position modifications increased potency for PARP10 but had no effect or decreased potency for PARP11. In particular, with the addition of a phenyl group at the 6-position (compound **5.8**), potency for PARP10 was increased 28-fold from **5.1**. Compound **5.8** was also 4-fold more selective for PARP10 over PARP11, highlighting **5.8** as a starting point to further increase selectivity for PARP10.

Meta-position modifications at the 6-position phenyl group of dq increase selectivity for PARP10 over PARP11

We proposed that modifications on the phenyl ring of compound **5.8** might further increase the selectivity for PARP10 over PARP11. We began by introducing small substituents at the *ortho*-, *meta*-, or *para*-position. Substituents at the *para*-position had little effect on the potency of the compounds for both PARP10 and PARP11, while substituents at the *ortho*-position greatly reduced potency compared to **5.8** (see **Appendix B**). However, modifications at the *meta*-position of the phenyl ring had modest increases in potency for both PARP10 and PARP11 compared to **5.8** (**Table 5-1**). There was an exception with the trifluoromethyl-modified **5.12**, which showed a 2-fold decrease in potency for PARP11 compared to **5.8**. Compound **5.12**, in turn, exhibited the greatest selectivity for PARP10 over PARP11 (8-fold), a 2-fold improvement from parent **5.8**. We sought to further increase this observed selectivity for PARP10 over PARP11.

Combined 5- and 6-position modifications on dq further increase selectivity for PARP10 over PARP11

We hypothesized that combining the most promising modifications at both the 5- and 6-position of the dq scaffold could have a synergistic effect of both increasing potency as well as selectivity for PARP10. Compound **5.3**, with a methyl group at the 5-position, resulted in an 8-fold increase in potency for PARP10 compared to unsubstituted **5.1** (8.6 μ M versus 70 μ M) (**Table 5-1**). Compound **5.14**, with a methyl and phenyl group at the 5- and 6-position, respectively, resulted in a further 5-fold increase in potency for PARP10 compared to **5.3** (1.6 μ M versus 8.6 μ M) (**Table 5-1**). To our surprise, the selectivity of **5.14** for PARP10 over PARP11 (17-fold) compared to the selectivity of **5.3** for PARP10 over PARP11 (0.24-fold) was improved 70-fold by the combination of both the 5-methyl and 6-phenyl modifications in **5.14**. Compound **5.14** both increased potency and selectivity for PARP10 over PARP11 compared to **5.3**.

Substitution of 6-position phenyl group for a pyridinyl group on dq increases solubility while still maintaining PARP10 selectivity

We encountered aqueous solubility issues, however, at higher concentrations when assaying **5.14**. We therefor sought modifications at the 6-position that could maintain the increased selectivity observed with **5.14** while mitigating any solubility issues. We turned to the synthesis of compounds with heterocyclic modifications at the 6-position with the potential to increase aqueous

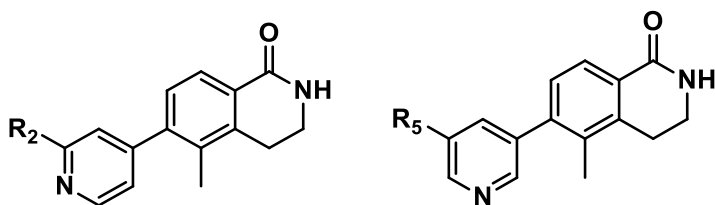
solubility. These would be combined with the corresponding methyl group at the 5-position of the dq scaffold (**Table 5-1**). We found that pyridin-3-yl (**5.15**), pyridin-4-yl (**5.16**), and 1*H*-pyrrolo[2,3-*b*]pyridin-5-yl (**5.18**) modifications at the 6-position in combination with the 5-methyl modification maintained a similar PARP11/PARP10 selectivity ratio as **5.14** (12-, 15-, and 17-fold, respectively, versus 17-fold). Both 1*H*-indol-5-yl (**5.17**) and quinolin-3-yl (**5.19**) modifications at the 6-position resulted in decreased selectivity compared to **5.14** (4- and 8-fold versus 17-fold). Compounds **5.15** and **5.16**, with pyridinyl modifications at the 6-position, exhibited increased solubility compared to **5.14** and were taken forward for further optimization.

A 6-position trifluoromethyl-modified pyridinyl group on dq is the most selective modification for PARP10

We first focused our attention on generating a set of compounds based on **5.16** with halogen modifications at the *meta*-position of the pyridinyl ring given our results from **Table 5-1**. We introduced fluoro, chloro, or trifluoromethyl groups at the 2-position of the pyridin-4-yl group (**Table 5-2**). Overall, the introduction of a fluoro group (**5.20**) or a trifluoromethyl group (**5.22**) increased selectivity almost 2-fold further for PARP10 over PARP11 compared to **5.16** (24- or 29-fold versus 15-fold). A chloro group (**5.21**) retained similar selectivity for PARP10 over PARP11. Similar selectivity trends were observed for **5.23** (-F) and **5.24** (-CF₃) containing a pyridin-3-yl group, increasing selectivity >2-fold for PARP10 over PARP11 compared to **5.15** (25- or 34-fold versus 12-fold). Compound **5.24**

exhibited the greatest selectivity overall for PARP10 over PARP11 (35-fold); however, **5.22** (29-fold selectivity) was slightly more potent for PARP10 overall (1.8 μ M versus 2.7 μ M).

Table 5-2. *In vitro* IC₅₀ values for **5.20** – **5.24** against PARP10_{cat} and PARP11.



ID	-R ₂	-R ₅	PARP10 _{cat}		PARP11		PARP10 S.R. ^b
			IC ₅₀ (μ M)	pIC ₅₀ \pm S.E.M. ^a	IC ₅₀ (μ M)	pIC ₅₀ \pm S.E.M. ^a	
5.16	H		1.4	5.84 \pm 0.03	21.2	4.67 \pm 0.04	15
5.20	F		1.9	5.71 \pm 0.03	44.7	4.35 \pm 0.05	24
5.21	Cl		1.8	5.76 \pm 0.03	27.0	4.57 \pm 0.02	15
5.22	CF ₃		1.8	5.74 \pm 0.02	51.7	4.29 \pm 0.04	29
5.15		H	2.5	5.60 \pm 0.04	30.4	4.52 \pm 0.06	12
5.23		F	2.2	5.66 \pm 0.02	54.7	4.23 \pm 0.03	25
5.24		CF ₃	2.7	5.57 \pm 0.03	92.1	4.04 \pm 0.03	34

^aS.E.M. from three representative dose-response experiments

^bselectivity ratio = IC₅₀ PARP11/IC₅₀ PARP10

We have shown that **5.22** is 29-fold more selective for PARP10_{cat} over PARP11 (**Table 5-2**). We next wanted to determine the selectivity profile for **5.22** against a panel of PARP family members. We screened **5.22** against PARP family members in a plate assay that measures ADPr of SRPK2 using an *N*⁶-alkyne tagged NAD⁺ (6-a-NAD⁺), a clickable NAD⁺ analogue.^{45,84} Compound **5.22** did not inhibit H-Y-E PARPs (PARPs 1-4 and PARP5b) up to 100 μ M and exhibited greater than 37-fold selectivity for PARP10 (**Table 5-3**). The observed selectivity is most likely due to differences in the last position of the H-Y-E catalytic triad of these enzymes versus the H-Y-I triad found in PARP10.²²

Table 5-3. Selectivity profile of **5.22** against PARP family members.

Enzyme	IC ₅₀ (μM)	pIC ₅₀ ± S.E.M. ^a	PARP10 S.R. ^d
PARP1	>>100	-	>>37
PARP2	>100	-	>37
PARP3	>>100	-	>>37
PARP4 _{brct-cat}	>100	-	>37
PARP5b _{cat}	>>100	-	>>37
PARP6 _S	>30 ^b	-	>10
PARP6 _L	>30 ^b	-	>10
PARP7 _{cat}	19.1	4.72	7.1
PARP8	>30 ^b	-	>10
PARP10 _{cat}	2.7	5.56 ± 0.06	1
PARP11	62.9	4.20 ± 0.06	23
PARP12	>30 ^b	-	>10
PARP14 _{cat-wwc}	60.5	4.22 ± 0.04	22
PARP15 _{cat}	62.9	4.20 ± 0.05	23
PARP16	6.7 ^c	5.17 ± 0.08	2.5

^aS.E.M. from two representative dose-response experiments^bmeasured using IP-auto-ADPr assay^cautomodification using NAD⁺ (400 μM)^dselectivity ratio = IC₅₀ PARPX/IC₅₀ PARP10

The glutamate (E988 in PARP1) in PARPs 1-4 and PARP 5b most likely clashes with the pyridiny-4-yl group at the 6-position of **5.22**. PARP10 contains an isoleucine (I978) at this position that could potentially accommodate this group (**Figure 5-1b**).

Compound **5.22** is >20-fold selective for H-Y-Φ PARPs PARP11, PARP14, and PARP15 (**Table 5-3**). For PARPs 6, 8, and 12 of the H-Y-Φ subclass, a PARP immunoprecipitation (IP)-auto-ADPr activity assay in the presence of **5.22** was performed as previously described.¹²³ In this assay, PARP enzymes are immunoprecipitated from lysates prepared from HEK293T cells expressing a GFP-tagged PARP using a GFP-antibody immobilized on beads. Incubation of PARP-bound beads with 6-a-NAD⁺ as a substrate in the presence of **5.22** did not inhibit PARP6 (short and long isoforms), PARP8, and PARP12 up

to 30 μM , exhibiting >10-fold selectivity for PARP10 (**Table 5-3**). Compound **5.22** exhibits a 7-fold selectivity for PARP10 over PARP7 ($\text{IC}_{50} = 19.1 \mu\text{M}$ versus 2.7 μM) (**Table 5-3**). Compound **5.22** is 2.5-fold more potent for PARP16 ($\text{IC}_{50} = 6.7 \mu\text{M}$ versus 2.7 μM) (**Table 5-3**). Taken together, these experiments demonstrate that **5.22** is >37-fold selective for PARP10 against the H-Y-E subclass of PARPs, and >10-fold selective for PARP10 against the H-Y- Φ subclass of PARPs with the exception of PARP7 (7-fold selective) and PARP16 (2.5-fold selective).

Compound 5.22 inhibits PARP10 auto-ADP-ribosylation in cells

We next determined if **5.22** could inhibit PARP10-dependent ADPr in cells. PARP10 is one of the most well-characterized mono-ADPr/H-Y- Φ PARPs and is known to exhibit robust auto-ADPr activity in cells.⁹⁹ Human embryonic kidney (HEK) 293T cells expressing full-length PARP10 were treated with increasing concentrations of **5.22** (1 – 100 μM). Auto-ADPr of PARP10 was monitored by Western blot using an ADP-ribose binding reagent.¹²⁸ We found that **5.22** inhibited auto-ADPr of PARP10 as well as PARP10-mediated ADPr of high molecular weight (HMW) targets in a dose-dependent manner (**Figure 5-2a**). The EC_{50} for inhibition of PARP10-mediated ADPr of HMW targets by **22** was lower compared to inhibition of auto-ADPr of PARP10 itself (2.3 μM versus 11 μM) (**Figure 5-2b**), which could be due to the relative stoichiometry differences between the levels of endogenous PARP10 targets and overexpressed PARP10. Both EC_{50} values were in agreement with the *in vitro* calculated IC_{50} value for **5.22** against PARP10_{cat} (1.8 μM) (**Table 5-1**). These results demonstrate that

5.22 is membrane permeable and inhibits auto-ADPr of full-length PARP10 and ADPr of PARP10 targets in cells.

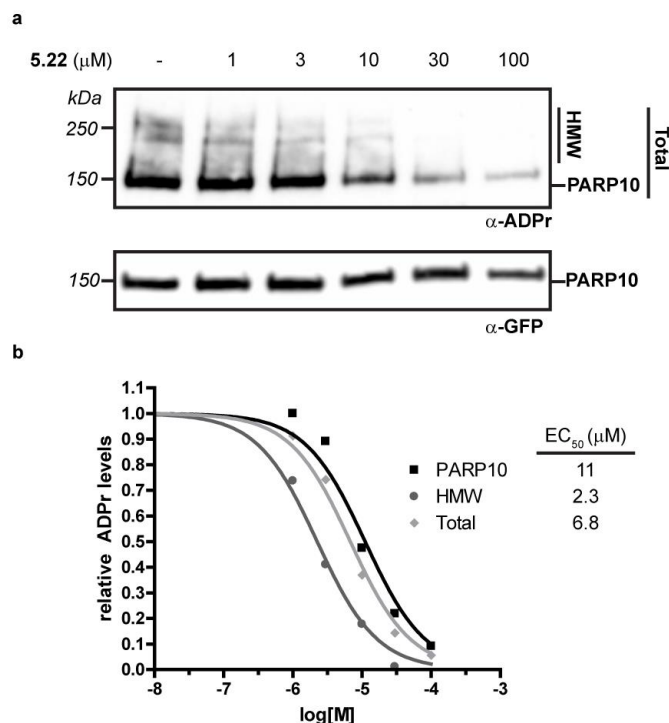


Figure 5-2. Compound **5.22** inhibits PARP10-dependent ADPr in cells. **(a)** Dose-dependent inhibition of PARP10 by **5.22** in cells. HEK293T cells were transfected with GFP-PARP10 and incubated with increasing concentrations of **5.22** (1 – 100 μM) for 3 h. Lysates were prepared and auto-ADPr of PARP10 and its high molecular weight (HMW) targets were analyzed with an ADP-ribose binding reagent (α -APDr) **(b)** Quantification of data shown in **(a)**.

Compound 5.22 is >10-fold selective for PARP10 with activity in cells

In summary, **5.22** exhibited a >10-fold selectivity for PARP10 over a panel of PARPs with the exception of PARP7 and PARP16 (<10-fold). Compared to the previously reported PARP10 selective inhibitor **OUL35**, **5.22** demonstrates an improved selectivity profile over PARP11. **OUL35** is only 2-fold selective for PARP10 over PARP11, while the selectivity of **5.22** for PARP10 over PARP11 is 29-fold, a 15-fold improvement in selectivity over **OUL35**. Compound **5.22** is also cell-permeable and inhibits auto-ADPr of PARP10 in cells.

Strategy 2: Targeting a noncatalytic, nonconserved cysteine residue on the D-loop of PARP10

The N-terminal region of the D-loop within the active site of PARP family members displays a high degree of structural variability,²⁵ suggesting that this region could be targeted with small-molecule probes to achieve selective inhibition. In particular, a number of PARPs of the mono-ADPr subclass contain a cysteine residue within the N-terminal region of the D-loop,⁸⁰ which could be targeted with electrophilic probes for irreversible inhibition.

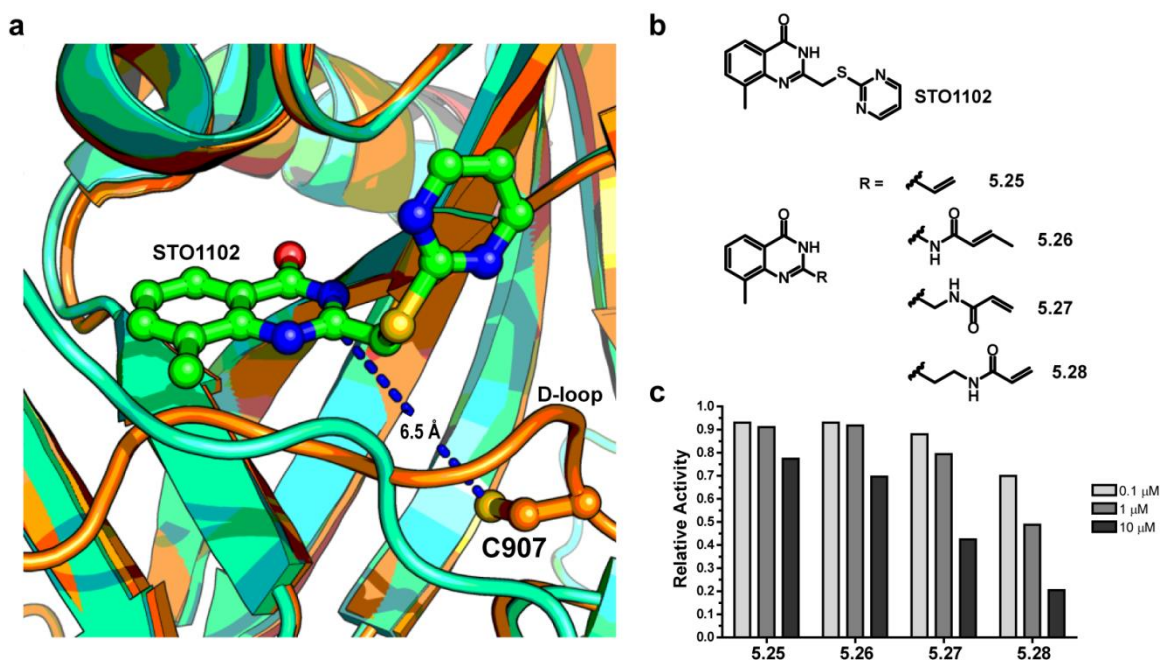


Figure 5-3. Development of electrophilic probes targeting C907 of PARP10. **(a)** Overlay of PARP10 (orange) and cocrystal structure of PARP15 (cyan) with quinazolin-4(3H)-one inhibitor STO1102 (green). D-loop residue C907 of PARP10 and distance from 2-position of quinazolin-4(3H)-one core scaffold of STO1102 is indicated. **(b)** Structure of STO1102 and electrophilic inhibitors **5.25** – **5.28** with varying linker lengths from core scaffold to electrophilic group. **(c)** Quantification of PARP10_{cat}-mediated ADPr of SRPK2 in the presence of **5.25** – **5.28** (1 h pre-incubation) and NAD⁺ (100 μM). ADP-ribosylated SRPK2 was detected using AO-alkyne and TAMRA-N₃ and quantified using in-gel fluorescence (See Chapter 3). Signal is relative to no inhibitor control.

Targeted covalent inhibitors have been successfully used to obtain selective inhibition within highly conserved enzymes families like the kinases.⁸³ We proposed that PARP10, which contains a noncatalytic and nonconserved cysteine residue (C907) within the N-terminal region of the D-loop, could be targeted with electrophilic probes to achieve selective inhibition over other PARP family members.

We began by analyzing the crystal structure of the catalytic domain of PARP10 overlaid with the cocrystal structure of PARP15 and an 8-methylquinazolin-4(3*H*)-one (mq)-based inhibitor known as STO1102 (**Figure 5-3a**). We hypothesized that attaching various electrophiles with different linker lengths at the 2-position of the mq scaffold could probe the reactivity and distance of C907 on the D-loop of PARP10 (**Figure 5-3b**). Due to the flexible nature of the D-loop of PARP10, we envisioned that flexible alkyl linkers would increase the overall probability of reacting with the D-loop cysteine. We synthesized a series of electrophilic probes containing vinyl or acryloyl groups appended to the 2-position of the mq scaffold (**Scheme 5-2**). The synthesis of **5.25** – **5.28** began with 2-amino-3-methylbenzoic acid (or benzamide) starting material, which was converted to the corresponding mq scaffold with the appropriate group at the 2-position for subsequent addition of the electrophilic group.

The electrophilic probes **5.25** – **5.28** were then screened to determine inhibition of PARP10_{cat}-mediated ADPr of SPRK2 in the presence of NAD⁺ (100 μM) (**Figure 5-2c**). Electrophiles **5.25** (2-vinyl) and **5.26** (2-*trans*-crotonamide)

An N-(2-ethyl)acrylamide-substituted mq probe is potent toward PARP10

In summary, electrophilic probe **5.28**, containing an acrylamide group and a two carbon linker to the core mq scaffold, was potent toward PARP10 among the electrophilic probes examined in this study. A trend was also observed with the linker length, as electrophilic probe **5.27** has one less carbon between the acrylamide group and the mq scaffold and exhibited ~10-fold reduction in potency. Future studies will examine the potency through: (1) the synthesis of longer linkers to determine optimal linker length and (2) the synthesis of rigid linkers (e.g., aryl or constrained rings) to determine the effect of linker flexibility on potency, and (3) the evaluation of different electrophiles for increased potency. Preliminary studies suggest a covalent inhibition mechanism based on observed differences in potency with different linker lengths. The mode of inhibition, however, will need further validation through: (1) mutagenesis of the cysteine residue, (2) washout experiments to evaluate the kinetics of inhibition, and (3) structural data to confirm covalent bond formation between the cysteine residue and electrophile.

Conclusions and Future Directions

In this study, we used two rational design strategies to obtain selective inhibition of PARP10 with small-molecule probes. In the first strategy, a hydrophobic pocket formed by C-terminal D-loop residues of PARP10 was targeted with 5- and 6-position modifications on a dq scaffold. SAR studies with PARP10 and PARP11 revealed that 6-position aryl modifications combined with

a 5-position methyl group on the dq scaffold exhibited greater selectivity for PARP10 over PARP11. In particular, **5.22**, containing a trifluoromethyl-modified pyridinyl group and a methyl group at the 5- and 6-positions of dq, respectively, was 29-fold more selective for PARP10 over PARP11. Compound **5.22** also exhibited >10-fold selectivity for PARP10 over twelve active PARP family members including PARPs that catalyze both poly- and mono-ADPr, suggesting that the combined 5- and 6-position modifications discriminate between both enzyme subclasses. Future studies will focus on the effect of different modifications at the 5 and 6-position of dq on potency and selectivity for PARP10. We have shown that additional modifications on dq are potent for PARP10 (see **Appendix B**). In particular, a 5-benzyl group was 10-fold more potent than a 5-methyl group against PARP10. In addition, a 6-phenethyl group exhibited similar potency to a 6-phenyl group against PARP10 but may impart differences in selectivity versus other PARP enzymes. The different combinations of 5- and 6-position modifications on dq could have interesting selectivity outcomes for different PARPs and potentially serve as a filter for obtaining selective inhibition among the PARP family.

In the second strategy, a cysteine residue located within the N-terminal region of the D-loop of PARP10 was targeted with electrophilic probes. Preliminary results suggest that electrophilic probe **5.28**, containing a two-carbon linker between an acrylamide group and the core mq scaffold, was potent toward PARP10. Once a covalent mode of inhibition is confirmed, the design of second generation inhibitors could include translating the promising 5- and 6-position

modifications from the dq scaffold in the first strategy to the mq scaffold (**Figure 5-4**). The combination of the two strategies could further increase potency and selectivity for PARP10. The strategies covered in this study could also provide a platform for future probe development for other PARP family members.

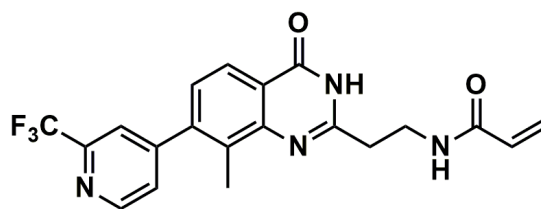


Figure 5-4. Potential second generation electrophilic probe for selective inhibition of PARP10. The probe combines a trifluoromethyl-modified pyridinyl modification (strategy 1) on an mq scaffold containing an acrylamide group (strategy 2).

Experimental

Chemistry Methods

General. ^1H NMR were recorded on a Bruker DPX spectrometer at 400 MHz. Chemical shifts are reported as parts per million (ppm) downfield from an internal tetramethylsilane standard or solvent references. Dichloromethane (DCM) and tetrahydrofuran (THF) were dried using a solvent purification system manufactured by Glass Contour, Inc. (Laguna Beach, CA). Triethylamine (Et_3N) was stored over NaOH. All other solvents were of ACS chemical grade (Fisher Scientific) and used without further purification unless otherwise indicated. Commercially available 1-indanones, phenethylamines, boronic acids, trifluoroborates, and 3,4-dihydro-2*H*-isoquinolin-1-one (dq, **5.1**) were purchased from CombiBlocks (San Diego, CA) and were >95% pure and used without further purification. All other reagents were of ACS chemical grade (Fisher Scientific) and used as received. *N*-6 alkyne- NAD^+ (6-a- NAD^+) was synthesized as previously described (Chapter 2).⁸⁴

Synthesis of 4-(4-carbamoylphenoxy)benzamide (OUL35): To a solution of 4,4'-dicarboxydiphenylether (0.26 g, 1.0 mmol) in THF (10 mL) was added 1,1'-carbonyldiimidazole (0.36 g, 2.2 mmol) at 0 °C. The mixture was allowed to stir for 0.5 h, gradually warming to rt. NH_3 (0.36 mL, 7 N in MeOH, 2.5 mmol) was added at 0 °C, and the reaction mixture was allowed to stir overnight, gradually warming to rt. The reaction was concentrated, and the crude residue was purified via ISCO CombiFlash chromatography (silica, 4g; 0-10% MeOH in DCM) to yield

a white solid (15 mg, 6% yield). ^1H NMR (400 MHz, $\text{DMSO}-d_6$) δ 7.97 (s, 1H), 7.95 – 7.88 (m, 2H), 7.35 (s, 1H), 7.19 – 6.99 (m, 2H).

Synthesis of 3,4-dihydroisoquinolin-1(2H)-ones:

General Method A: To a solution of an appropriate 1-indanone (0.5 mmol) in 2:1 DCM:methanesulfonic acid (4.6 mL) at 0 °C was added NaN_3 (48.8 mg, 0.75 mmol) portionwise over 30 min. The resulting mixture was allowed to warm to rt and stirred overnight. The reaction mixture was quenched with 1 N NaOH (3 mL) at 0 °C, and the DCM layer was removed. The aqueous layer was extracted with DCM or EtOAc (for –OH derivative). The combined organic layers were washed with H_2O and brine, dried over Na_2SO_4 , filtered, and concentrated *in vacuo*. The *N*-alkyl and *N*-aryl amide regioisomers were separated via ISCO CombiFlash chromatography (silica, 4g; 20-100% EtOAc in hexanes).

General Method B: The procedure was followed as described previously.¹²⁹ To a solution of an appropriate carbamoyl salicylate (0.5 mmol) in DCM (2.5 mL) at 0 °C was added triflic acid (0.44 mL, 5 mmol) dropwise. The resulting mixture was allowed to warm to rt over 3h. The reaction was quenched with ice-cold water (50 mL) and extracted with DCM (2 x 50 mL). The combined organic layers were dried over Na_2SO_4 , filtered, and concentrated *in vacuo*. The resulting crude mixture was purified via ISCO CombiFlash chromatography (silica, 4g; 20-100% EtOAc in hexanes).

5-bromo-3,4-dihydroisoquinolin-1(2H)-one (5.2): Using General Method A from 4-bromo-1-indanone (50 mg, 0.24 mmol); yield: 14.1 mg *N*-alkyl isomer (0.06 mmol, 26%). ¹H NMR (400 MHz, DMSO-*d*₆) δ 8.11 (s, 1H), 7.88 (dd, *J* = 7.7, 1.2 Hz, 1H), 7.78 (dd, *J* = 7.9, 1.3 Hz, 1H), 7.31 (t, *J* = 7.8 Hz, 1H), 3.39 (td, *J* = 6.7, 2.9 Hz, 2H), 2.96 (t, *J* = 6.6 Hz, 2H); HRMS (ESI+) for C₉H₈BrNO [M+H] expected: *m/z* = 225.98620, found: *m/z* = 225.98675.

5-methyl-3,4-dihydroisoquinolin-1(2H)-one (5.3): Using General Method B from crude carbamoyl salicylate of 2-methylphenethylamine (81.1 mg, 0.6 mmol); yield: 52 mg (0.32 mmol, 65%). ¹H NMR (400 MHz, DMSO-*d*₆) δ 7.90 (s, 1H), 7.80 – 7.51 (m, 1H), 7.42 – 7.29 (m, 1H), 7.22 (t, *J* = 7.6 Hz, 1H), 3.36 (2H)*, 2.82 (t, *J* = 6.7 Hz, 2H), 2.27 (s, 3H), *obscured by HOD peak; HRMS (ESI+) for C₁₀H₁₁NO [M+H] expected: *m/z* = 162.09134, found: *m/z* = 162.09137.

6-bromo-3,4-dihydroisoquinolin-1(2H)-one (5.5): Using General Method A from 5-bromo-1-indanone (1.0 g, 4.74 mmol); yield: 639 mg *N*-alkyl isomer (2.83 mmol, 60%). ¹H NMR (400 MHz, DMSO-*d*₆) δ 8.03 (s, 1H), 7.75 (d, *J* = 8.2 Hz, 1H), 7.64 – 7.42 (m, 2H), 3.36 (td, *J* = 6.6, 2.8 Hz, 2H), 2.91 (t, *J* = 6.6 Hz, 2H); HRMS (ESI+) for C₉H₈BrNO [M+H] expected: *m/z* = 225.98620, found: *m/z* = 225.98671.

6-methyl-3,4-dihydroisoquinolin-1(2H)-one (5.6): Using General Method A from 5-methyl-1-indanone (200 mg, 1.37 mmol); yield: 88 mg *N*-alkyl isomer (0.55 mmol, 40%). NMR (400 MHz, DMSO-*d*₆) δ 7.83 (s, 1H), 7.71 (d, *J* = 7.8 Hz, 1H),

7.27 – 6.93 (m, 2H), 3.34 (td, $J = 6.6, 2.7$ Hz, 2H), 2.84 (t, $J = 6.6$ Hz, 2H), 2.32 (s, 3H); HRMS (ESI+) for $C_{10}H_{11}NO$ $[M+H]$ expected: $m/z = 162.09134$, found: $m/z = 162.09065$.

6-bromo-5-methyl-3,4-dihydroisoquinolin-1(2H)-one (**5.35**): Using General Method B from purified carbamoyl salicylate (**5.36**) of 3-bromo-2-methylphenethylamine (**5.37**) (1.25 g, 3.19 mmol) except a different purification protocol was followed. The crude residue was taken up in hexanes/ Et_2O (1:1, 100 mL) and additional hexanes (100 mL) were added to ppt product. The solid was filtered and washed with hexanes to yield the product as a white solid (645 mg, 84%). 1H NMR (400 MHz, $DMSO-d_6$) δ 8.02 (s, 1H), 7.77 – 7.38 (m, 2H), 3.37 (dt, $J = 6.8, 3.4$ Hz, 2H), 2.91 (t, $J = 6.7$ Hz, 2H), 2.36 (s, 3H).

Synthesis of carbamoyl salicylates: To a solution of an appropriate phenethylamine (0.5 mmol) in THF (12 mL) was added **4.10** (See Chapter 4) (167 mg, 0.525 mmol). The resulting solution was allowed to stir at rt until TLC analysis (1:1 hexanes: Et_2O) revealed consumption of starting amine. The THF was removed *in vacuo* and the crude residue was purified via ISCO CombiFlash chromatography (silica, 4g; 0-100% Et_2O in hexanes) to yield the carbamoyl salicylate product.

methyl 2-(((3-bromo-2-methylphenethyl)carbamoyl)oxy)benzoate (**5.36**): from 3-bromo-2-methylphenethylamine (**5.37**) (1.0 g, 4.67 mmol); yield: 1.36 g (3.47

mmol, 74%) as a viscous clear oil. ^1H NMR (400 MHz, $\text{DMSO-}d_6$) δ 7.98 (t, J = 5.8 Hz, 1H), 7.84 (dd, J = 7.7, 1.8 Hz, 1H), 7.62 (ddd, J = 8.2, 7.4, 1.8 Hz, 1H), 7.47 (dt, J = 8.0, 2.2 Hz, 1H), 7.35 (td, J = 7.6, 1.1 Hz, 1H), 7.27 – 7.20 (m, 1H), 7.17 (dd, J = 8.1, 1.1 Hz, 1H), 7.08 (t, J = 7.7 Hz, 1H), 3.76 (s, 3H), 3.21 (dt, J = 8.1, 6.1 Hz, 2H), 2.87 (dd, J = 8.9, 6.3 Hz, 2H), 2.38 (s, 3H).

Synthesis of 3-bromo-2-methylphenethylamine (5.37):

3-bromo-2-methylbenzyl alcohol (5.38): To a solution of 3-bromo-2-methylbenzoic acid (2.15 g, 10.0 mmol) in THF (20 mL) at 0 °C was slowly added BH_3 -THF complex (30 mL, 1 M, 30 mmol) via syringe. The reaction mixture was gradually warmed to rt and allowed to stir for 2h. The mixture was cooled to 0 °C with an ice bath and quenched with MeOH until no bubbling occurred. The rxn mixture was concentrated *in vacuo* to remove solvent. The residue was redissolved in EtOAc and washed with water, sat. NaHCO_3 , and brine. The organic layer was dried over Na_2SO_4 , filtered, and concentrated *in vacuo* to yield the product as an off-white solid (1.91 g, 95%). ^1H NMR (400 MHz, $\text{DMSO-}d_6$) δ 7.48 (d, J = 8.1 Hz, 1H), 7.38 (d, J = 7.6 Hz, 1H), 7.11 (t, J = 7.8 Hz, 1H), 5.25 (td, J = 5.4, 1.0 Hz, 1H), 4.52 (d, J = 5.4 Hz, 2H), 2.30 (s, 3H).

2-(3-bromo-2-methylphenyl)acetonitrile (5.39): To a solution of **5.38** (1.81 g, 9.0 mmol) in DCM (18 mL) and Et_3N (2.5 mL, 18 mmol) at 0 °C was added mesyl chloride (0.84 mL, 10.8 mmol) via syringe dropwise. The rxn was gradually warmed to rt and stirred for 2h before quenching with sat. NaHCO_3 (50 mL). The

DCM layer was collected. The aqueous layer was extracted with DCM (3 x 50 mL). The combined organic layers were washed with brine, dried over Na₂SO₄, filtered, and concentrated *in vacuo* to yield the crude mesylate. The mesylate was taken up in DMSO (20 mL) and KCN (2.34 g, 36 mmol) was added. The reaction was stirred at 35 °C for 3h and quenched with water (50 mL) to form a ppt. The ppt was filtered, washed with water to remove traces of DMSO, and dried *in vacuo* to yield the product as an off-white solid (1.29 g, 68%). ¹H NMR (400 MHz, DMSO-*d*₆) δ 7.60 (dd, *J* = 8.1, 1.2 Hz, 1H), 7.39 (d, *J* = 7.5 Hz, 1H), 7.18 (t, *J* = 7.8 Hz, 1H), 4.11 (s, 2H), 2.37 (s, 3H).

3-bromo-2-methylphenethylamine (5.37): To a solution of **5.39** (1.2 g, 5.71 mmol) in THF (11.5 mL) in a pressure vessel was slowly added BH₃-THF complex (57 mL, 1M, 57 mmol) at 0 °C via syringe dropwise over 10 min. The vessel was purged with Ar, sealed, and heated at 60 °C for 2.5h. The rxn was quenched with water (5 mL) followed by 4N HCl in dioxane (15 mL). The rxn was allowed to stir overnight at rt. The rxn was concentrated *in vacuo* to yield a white residue, which was triturated with Et₂O (100 mL). The solids were collected and rinsed with additional Et₂O (25 mL), dried *in vacuo*, and taken up in a minimal amount of MeOH (10 mL). The pH of the solution was brought to 10 with 10% aq. NaOH. The mixture was extracted with DCM (3 x 15 mL), dried over Na₂SO₄, filtered, and concentrated *in vacuo* to yield the product (as free base) as an amorphous off-white solid (1.04 g, 85%). ¹H NMR (400 MHz, DMSO-*d*₆) δ 7.43 (dd, *J* = 7.9,

1.3 Hz, 1H), 7.28 – 7.10 (m, 1H), 7.04 (t, $J = 7.8$ Hz, 1H), 2.71 (q, $J = 3.5$ Hz, 3H), 2.34 (s, 3H).

Synthesis of aryl-substituted 3,4-dihydroisoquinolin-1(2H)-ones via Suzuki-Miyaura cross-coupling:

General Method A: A mixture of an appropriate bromo-modified dq (0.25 mmol), potassium alkyltrifluoroborate (0.375 mmol), Pd(OAc)₂ (2.8 mg, 0.0125 mmol), RuPhos (11.7 mg, 0.025 mmol), and Cs₂CO₃ (244 mg, 0.75 mmol) was suspended in toluene/H₂O (3:1, 3 mL) and the mixture was bubbled with Ar for 10 min. The reaction was sealed and heated at 95 °C for 3h. The rxn was concentrated *in vacuo* and portioned between DCM/H₂O (1:1, 10 mL). The DCM layer was removed. The aqueous layer was further extracted with DCM (2 x 10 mL). The combined organic layers were dried over Na₂SO₄, filtered, and concentrated *in vacuo*. The crude residue was taken up in MeOH/0.1% aqueous formic acid (3:1, 4 mL) and purified via preparatory HPLC. Fractions containing product were pooled and concentrated *in vacuo* to yield the product.

General Method B: A mixture of an appropriate bromo-modified dq (0.25 mmol), arylboronic acid (0.275 mmol), K₂CO₃ (346 mg, 2.50 mmol), tetrabutylammonium bromide (81 mg, 0.25 mmol) was suspended in ddH₂O (0.5 mL) under Ar atmosphere. Pd(OAc)₂ (0.56 mg, 0.0025 mmol) was added, and the reaction was sealed and warmed to 95 °C for 3h. After cooling to rt, the reaction mixture was diluted with EtOAc (10 mL), dried over Na₂SO₄, filtered, and concentrated *in*

vacuo. The crude residue was purified over a short plug of silica, eluting first with DCM, followed by 20% EtOAc/Hex, and finally with EtOAc to elute product.

General Method C: A mixture of an appropriate bromo-modified dq (0.125 mmol), arylboronic acid (0.25 mmol), Pd(dppf)Cl₂ • CH₂Cl₂ (5 mol%), aq. K₂CO₃ (0.038 mL, 2M, 0.75 mmol) was suspended in toluene/EtOH (3:1, 2.3 mL) and the mixture was bubbled with Ar for 10 min. The reaction was refluxed at 110 °C under Ar for 3h. The rxn was concentrated *in vacuo* and portioned between DCM/H₂O (1:1, 10 mL). The DCM layer was removed. The aqueous layer was further extracted with DCM (2 x 10 mL). The combined organic layers were dried over Na₂SO₄, filtered, and concentrated *in vacuo*. The crude residue was taken up in MeOH/0.1% aqueous formic acid (3:1, 4 mL) and purified via preparatory HPLC. Fractions containing product were pooled and concentrated *in vacuo* to yield the product.

5-phenyl-3,4-dihydroisoquinolin-1(2H)-one (5.4): Using General Method B from **5.2** (35 mg, 0.15 mmol) and phenylboronic acid (20.8 mg, 0.17mmol); yield: 29 mg (0.13 mmol, 84%). ¹H NMR (400 MHz, DMSO-*d*₆) δ 8.01 (s, 1H), 7.90 (dd, *J* = 6.6, 2.5 Hz, 1H), 7.57 – 7.18 (m, 7H), 3.26 (td, *J* = 6.5, 2.8 Hz, 2H), 2.82 (t, *J* = 6.5 Hz, 2H); HRMS (ESI+) for C₁₅H₁₃NO [M+H] expected: *m/z* = 224.10699, found: *m/z* = 224.10747; HRMS (ESI+) for C₁₅H₁₃NO [M+H] expected: *m/z* = 224.10699, found: *m/z* = 224.10747.

6-benzyl-3,4-dihydroisoquinolin-1(2H)-one (5.7): Using General Method A from **5.5** (50 mg, 0.22 mmol) and potassium benzyltrifluoroborate (65.3 mg, 0.33 mmol); yield: 23.5 mg (0.10 mmol, 45%). ¹H NMR (400 MHz, DMSO-*d*₆) δ 7.84 (s, 1H), 7.75 (d, *J* = 7.9 Hz, 1H), 7.40 – 7.01 (m, 7H), 3.32 (2H)*, 2.84 (t, *J* = 6.6 Hz, 2H), *obscured by HOD peak; HRMS (ESI+) for C₁₆H₁₅NO [M+H] expected: *m/z* = 238.12264, found: *m/z* = 238.12322.

6-phenyl-3,4-dihydroisoquinolin-1(2H)-one (5.8): Using General Method B from **5.5** (50 mg, 0.22 mmol) and phenylboronic acid (29.7 mg, 0.24mmol); yield: 39 mg (0.18 mmol, 80%). ¹H NMR (400 MHz, DMSO-*d*₆) δ 7.96 (s, 1H), 7.91 (d, *J* = 7.9 Hz, 1H), 7.79 – 7.69 (m, 2H), 7.68 – 7.59 (m, 2H), 7.49 (t, *J* = 7.6 Hz, 2H), 7.42 (dd, *J* = 7.0, 1.8 Hz, 1H), 3.41 (td, *J* = 6.5, 2.8 Hz, 2H), 2.98 (t, *J* = 6.6 Hz, 2H); HRMS (ESI+) for C₁₅H₁₃NO [M+H] expected: *m/z* = 224.10699, found: *m/z* = 224.10770.

6-(3-fluorophenyl)-3,4-dihydroisoquinolin-1(2H)-one (5.9): Using General Method B from **5.5** (30 mg, 0.13 mmol) and 3-fluorophenylboronic acid (20.4 mg, 0.15 mmol); yield: 26.9 mg (0.11 mmol, 84%). ¹H NMR (400 MHz, DMSO-*d*₆) δ 7.99 (s, 1H), 7.91 (d, *J* = 8.6 Hz, 1H), 7.68 (dd, *J* = 5.9, 2.2 Hz, 2H), 7.64 – 7.44 (m, 3H), 7.34 – 7.15 (m, 1H), 3.41 (td, *J* = 6.6, 2.7 Hz, 2H), 2.98 (t, *J* = 6.5 Hz, 2H); HRMS (ESI+) for C₁₅H₁₂FNO [M+H] expected: *m/z* = 242.09757; found: *m/z* = 242.09821.

6-(3-chlorophenyl)-3,4-dihydroisoquinolin-1(2H)-one (**5.10**): Using General Method B from **5.5** (25 mg, 0.11 mmol) and 3-chlorophenylboronic acid (19 mg, 0.12 mmol); yield: 12 mg (0.047 mmol, 42%). ¹H NMR (400 MHz, DMSO-*d*₆) δ 8.00 (s, 1H), 7.91 (d, *J* = 8.5 Hz, 1H), 7.79 (t, *J* = 1.7 Hz, 1H), 7.74 – 7.64 (m, 3H), 7.57 – 7.42 (m, 2H), 3.40 (td, *J* = 6.6, 2.7 Hz, 2H), 2.98 (t, *J* = 6.6 Hz, 2H); HRMS (ESI+) for C₁₅H₁₂ClNO [M+H] expected: *m/z* = 258.06802; found: *m/z* = 258.06876.

6-(3-methylphenyl)-3,4-dihydroisoquinolin-1(2H)-one (**5.11**): Using General Method B from **5.5** (25 mg, 0.11 mmol) and 3-methylphenylboronic acid (16.5 mg, 0.12 mmol); yield: 20 mg (0.084 mmol, 76%). ¹H NMR (400 MHz, DMSO-*d*₆) δ 7.95 (s, 1H), 7.90 (d, *J* = 7.9 Hz, 1H), 7.66 – 7.58 (m, 2H), 7.57 – 7.46 (m, 2H), 7.37 (t, *J* = 7.6 Hz, 1H), 7.22 (d, *J* = 7.4 Hz, 1H), 3.40 (td, *J* = 6.5, 2.8 Hz, 2H), 2.97 (t, *J* = 6.6 Hz, 2H), 2.38 (s, 3H); HRMS (ESI+) for C₁₆H₁₅NO [M+H] expected: *m/z* = 238.12264, found: *m/z* = 238.12317.

6-(3-trifluoromethylphenyl)-3,4-dihydroisoquinolin-1(2H)-one (**5.12**): Using General Method B from **5.5** (25 mg, 0.11 mmol) and 3-trifluoromethylphenylboronic acid (23.1 mg, 0.12 mmol); yield: 22 mg (0.076 mmol, 68%). ¹H NMR (400 MHz, DMSO-*d*₆) δ 8.11 – 7.98 (m, 3H), 7.93 (d, 1H), 7.84 – 7.68 (m, 4H), 3.41 (td, *J* = 6.6, 2.7 Hz, 2H), 2.99 (t, *J* = 6.6 Hz, 2H); HRMS (ESI+) for C₁₆H₁₂F₃NO [M+H] expected: *m/z* = 292.09438; found: *m/z* = 292.09497.

6-(3-acetylphenyl)-3,4-dihydroisoquinolin-1(2H)-one (**5.13**): Using General Method B from **5.5** (30 mg, 0.13 mmol) and 3-acetylphenylboronic acid (23.9 mg, 0.15 mmol); yield: 32.4 mg (0.12 mmol, 93%). ¹H NMR (400 MHz, DMSO-*d*₆) δ 8.24 (t, *J* = 1.8 Hz, 1H), 8.05 – 7.97 (m, 3H), 7.94 (d, *J* = 8.6 Hz, 1H), 7.76 – 7.69 (m, 2H), 7.65 (t, *J* = 7.7 Hz, 1H), 3.42 (td, *J* = 6.6, 2.8 Hz, 2H), 3.00 (t, *J* = 6.5 Hz, 2H), 2.67 (s, 3H); HRMS (ESI+) for C₁₇H₁₅NO₂ [M+H] expected: *m/z* = 266.11756, found: *m/z* = 266.11819.

5-methyl-6-phenyl-3,4-dihydroisoquinolin-1(2H)-one (**5.14**): Using General Method B from **5.35** (17 mg, 0.071 mmol) and phenylboronic acid (17 mg, 0.139 mmol), additional purification using preparatory HPLC; yield: 9.6 mg (0.040 mmol, 57%). ¹H NMR (400 MHz, DMSO-*d*₆) δ 7.95 (s, 1H), 7.78 (d, *J* = 7.9 Hz, 1H), 7.54 – 7.43 (m, 2H), 7.42 – 7.37 (m, 1H), 7.35 – 7.26 (m, 2H), 7.18 (d, *J* = 7.9 Hz, 1H), 3.41 (td, *J* = 6.6, 2.7 Hz, 2H), 2.89 (t, *J* = 6.6 Hz, 2H), 2.15 (s, 3H); HRMS (ESI+) for C₁₆H₁₅NO [M+H] expected: *m/z* = 238.12264, found: *m/z* = 238.12318.

5-methyl-6-(pyridiny-3-yl)-3,4-dihydroisoquinolin-1(2H)-one (**5.15**): Using General Method C from **5.35** (30 mg, 0.125 mmol) and 3-pyridinylboronic acid (30.7 mg, 0.250 mmol); yield: 19.7 mg (0.083 mmol, 66%). ¹H NMR (400 MHz, DMSO-*d*₆) δ 8.61 (d, *J* = 4.8 Hz, 1H), 8.55 (s, 1H), 8.00 (s, 1H), 7.87 – 7.73 (m, 2H), 7.50 (dd, *J* = 7.8, 4.8 Hz, 1H), 7.23 (d, *J* = 7.9 Hz, 1H), 3.42 (td, *J* = 6.6, 2.7 Hz, 2H), 2.91

(t, $J = 6.6$ Hz, 2H), 2.16 (s, 3H); HRMS (ESI+) for $C_{15}H_{14}N_2O$ [M+H] expected: $m/z = 239.11789$, found: $m/z = 239.11837$.

5-methyl-6-(pyridin-4-yl)-3,4-dihydroisoquinolin-1(2H)-one (**5.16**): Using General Method C from **5.35** (30 mg, 0.125 mmol) and 4-pyridinylboronic acid (30.7 mg, 0.250 mmol); yield: 19.1 mg (0.080 mmol, 64%). 1H NMR (400 MHz, DMSO- d_6) δ 8.76 – 8.53 (m, 2H), 8.01 (s, 1H), 7.82 (d, $J = 7.9$ Hz, 1H), 7.46 – 7.31 (m, 2H), 7.22 (d, $J = 8.0$ Hz, 1H), 3.41 (td, $J = 6.7, 2.8$ Hz, 2H), 2.91 (t, $J = 6.6$ Hz, 2H), 2.16 (s, 3H); HRMS (ESI+) for $C_{15}H_{14}N_2O$ [M+H] expected: $m/z = 239.11789$, found: $m/z = 239.11819$.

6-(1H-indol-5-yl)-5-methyl-3,4-dihydroisoquinolin-1(2H)-one (**5.17**): Using General Method C from **5.35** (30 mg, 0.125 mmol) and 5-indolylboronic acid (40.3 mg, 0.250 mmol); yield: 23.7 mg (0.086 mmol, 69%). 1H NMR (400 MHz, DMSO- d_6) δ 11.19 (s, 1H), 7.91 (s, 1H), 7.76 (d, $J = 7.9$ Hz, 1H), 7.45 (td, $J = 4.1, 2.0$ Hz, 2H), 7.40 (t, $J = 2.8$ Hz, 1H), 7.21 (d, $J = 7.9$ Hz, 1H), 7.11 – 6.91 (m, 1H), 6.58 – 6.37 (m, 1H), 3.42 (td, $J = 6.6, 2.6$ Hz, 2H), 2.90 (t, $J = 6.6$ Hz, 2H), 2.18 (s, 3H); HRMS (ESI+) for $C_{18}H_{16}N_2O$ [M+H] expected: $m/z = 277.13354$, found: $m/z = 277.13422$.

*5-methyl-6-(1H-pyrrolo[2,3-*b*]pyridin-5-yl)-3,4-dihydroisoquinolin-1(2H)-one* (**5.18**): Using General Method C from **5.35** (30 mg, 0.125 mmol) and 1H-pyrrolo[2,3-*b*]pyridin-5-ylboronic acid (40.5 mg, 0.250 mmol); yield: 23.4 mg

(0.084 mmol, 67%). ^1H NMR (400 MHz, DMSO- d_6) δ 11.77 (s, 1H), 8.15 (d, J = 2.1 Hz, 1H), 7.96 (s, 1H), 7.90 (d, J = 2.1 Hz, 1H), 7.80 (d, J = 7.9 Hz, 1H), 7.54 (dd, J = 3.4, 2.5 Hz, 1H), 7.25 (d, J = 7.9 Hz, 1H), 6.49 (dd, J = 3.4, 1.8 Hz, 1H), 3.42 (td, J = 6.6, 2.7 Hz, 2H), 2.92 (t, J = 6.6 Hz, 2H), 2.19 (s, 3H); HRMS (ESI+) for $\text{C}_{17}\text{H}_{15}\text{N}_3\text{O}$ $[\text{M}+\text{H}]$ expected: m/z = 278.12879, found: m/z = 278.12951.

5-methyl-6-(quinolin-3-yl)-3,4-dihydroisoquinolin-1(2H)-one (5.19): Using General Method C from **5.35** (30 mg, 0.125 mmol) and quinolone-3-boronic acid (43.3 mg, 0.250 mmol); yield: 30.9 mg (0.107 mmol, 86%). ^1H NMR (400 MHz, DMSO- d_6) δ 8.89 (d, J = 2.3 Hz, 1H), 8.37 (d, J = 2.3 Hz, 1H), 8.15 – 7.97 (m, 3H), 7.87 (d, J = 7.9 Hz, 1H), 7.82 (ddd, J = 8.4, 6.7, 1.4 Hz, 1H), 7.72 – 7.62 (m, 1H), 7.36 (d, J = 7.9 Hz, 1H), 3.44 (td, J = 6.6, 2.7 Hz, 2H), 2.95 (t, J = 6.6 Hz, 2H), 2.22 (s, 3H); HRMS (ESI+) for $\text{C}_{19}\text{H}_{16}\text{N}_2\text{O}$ $[\text{M}+\text{H}]$ expected: m/z = 289.13354, found: m/z = 289.13444.

6-(2-fluoropyridin-4-yl)-5-methyl-3,4-dihydroisoquinolin-1(2H)-one (5.20): Using General Method C from **5.35** (30 mg, 0.125 mmol) and 2-fluoropyridine-4-boronic acid (35.2 mg, 0.250 mmol); yield: 24.5 mg (0.096 mmol, 77%). ^1H NMR (400 MHz, DMSO- d_6) δ 8.32 (d, J = 5.1 Hz, 1H), 8.04 (s, 1H), 7.83 (d, J = 8.0 Hz, 1H), 7.35 (ddd, J = 5.2, 2.2, 1.3 Hz, 1H), 7.25 (d, J = 8.0 Hz, 1H), 7.21 (d, J = 1.6 Hz, 1H), 3.41 (td, J = 6.7, 2.7 Hz, 2H), 2.91 (t, J = 6.6 Hz, 2H), 2.17 (s, 3H); HRMS (ESI+) for $\text{C}_{15}\text{H}_{13}\text{FN}_2\text{O}$ $[\text{M}+\text{H}]$ expected: m/z = 257.10847, found: m/z = 257.10901.

6-(2-chloropyridin-4-yl)-5-methyl-3,4-dihydroisoquinolin-1(2H)-one (**5.21**): Using General Method C from **5.35** (30 mg, 0.125 mmol) and 2-chloropyridine-4-boronic acid (39.3 mg, 0.250 mmol); yield: 17.0 mg (0.062 mmol, 50%). ¹H NMR (400 MHz, DMSO-*d*₆) δ 8.49 (dd, *J* = 5.1, 0.7 Hz, 1H), 8.04 (s, 1H), 7.82 (d, *J* = 7.9 Hz, 1H), 7.53 (dd, *J* = 1.5, 0.7 Hz, 1H), 7.42 (dd, *J* = 5.1, 1.5 Hz, 1H), 7.25 (d, *J* = 7.9 Hz, 1H), 3.41 (td, *J* = 6.7, 6.2, 2.4 Hz, 2H), 2.91 (t, *J* = 6.6 Hz, 2H), 2.16 (s, 3H); HRMS (ESI+) for C₁₅H₁₃ClN₂O [M+H] expected: *m/z* = 273.07892, found: *m/z* = 273.07935.

5-methyl-6-(2-(trifluoromethyl)pyridin-4-yl)-3,4-dihydroisoquinolin-1(2H)-one (**5.22**): Using General Method C from **5.35** (30 mg, 0.125 mmol) and 2-trifluoromethylpyridine-4-boronic acid (47.7 mg, 0.250 mmol); yield: 35.1 mg (0.115 mmol, 92%). ¹H NMR (400 MHz, DMSO-*d*₆) δ 8.86 (d, *J* = 5.0 Hz, 1H), 8.06 (s, 1H), 7.89 (s, 1H), 7.85 (d, *J* = 8.0 Hz, 1H), 7.74 (dd, *J* = 5.0, 1.5 Hz, 1H), 7.30 (d, *J* = 7.9 Hz, 1H), 3.42 (td, *J* = 6.6, 2.7 Hz, 2H), 2.92 (t, *J* = 6.6 Hz, 2H), 2.17 (s, 3H); HRMS (ESI+) for C₁₆H₁₃F₃N₂O [M+H] expected: *m/z* = 307.10527, found: *m/z* = 307.10590.

6-(5-fluoropyridin-3-yl)-5-methyl-3,4-dihydroisoquinolin-1(2H)-one (**5.23**): Using General Method C from **5.35** (30 mg, 0.125 mmol) and 5-fluoropyridine-3-boronic acid (35.2 mg, 0.250 mmol); yield: 28.5 mg (0.111 mmol, 89%). ¹H NMR (400 MHz, DMSO-*d*₆) δ 8.63 (d, *J* = 2.7 Hz, 1H), 8.44 (s, 1H), 8.03 (s, 1H), 7.90 – 7.64 (m, 2H), 7.27 (d, *J* = 7.9 Hz, 1H), 3.41 (td, *J* = 6.7, 2.6 Hz, 2H), 2.91 (t, *J* = 6.6

Hz, 2H), 2.17 (s, 3H); HRMS (ESI+) for $C_{15}H_{13}FN_2O$ [M+H] expected: $m/z = 257.10847$, found: $m/z = 257.10758$.

5-methyl-6-(5-(trifluoromethyl)pyridin-3-yl)-3,4-dihydroisoquinolin-1(2H)-on (5.24):

Using General Method C from **5.35** (30 mg, 0.125 mmol) and 3-trifluoromethylpyridine-5-boronic acid (47.7 mg, 0.250 mmol); yield: 33.5 mg (0.109 mmol, 87%). 1H NMR (400 MHz, DMSO- d_6) δ 9.03 (d, $J = 2.2$ Hz, 1H), 8.88 (d, $J = 1.5$ Hz, 1H), 8.23 (t, $J = 1.6$ Hz, 1H), 8.04 (s, 1H), 7.84 (d, $J = 8.0$ Hz, 1H), 7.31 (d, $J = 8.0$ Hz, 1H), 3.42 (td, $J = 6.4, 2.4$ Hz, 2H), 2.92 (t, $J = 6.6$ Hz, 2H), 2.16 (s, 3H); HRMS (ESI+) for $C_{16}H_{13}F_3N_2O$ [M+H] expected: $m/z = 307.10527$, found: $m/z = 307.10605$.

Synthesis of 8-methyl-2-vinylquinazolin-4(3H)-one (5.25):

2-amino-3-methylbenzamide (5.29): To a solution of 2-amino-3-methylbenzoic acid (1.1 g, 7.6 mmol) in THF (40 mL) was added carbonyldiimidazole (1.3 g, 9.5 mmol) and the reaction was stirred at rt for 2 h under Ar. To the reaction was added NH_3 in MeOH (7N, 80 mL, 560 mmol). The reaction was stirred at rt for 18 h, concentrated *in vacuo*, and purified via ISCO CombiFlash chromatography to separate the methyl benzoate and benzamide products. Yield of benzamide product **5.25**: 0.50 g, 3.3 mmol, 44% yield. 1H NMR (400 MHz, DMSO- d_6) δ 7.73 (s, 1H), 7.41 (dd, $J = 8.0, 1.5$ Hz, 1H), 7.06 (d, $J = 6.9$ Hz, 1H), 6.44 (dd, $J = 8.0, 7.2$ Hz, 1H), 6.40 (s, 2H), 2.06 (s, 3H).

2-(3-chloropropanamido)-3-methylbenzamide (5.30): To a solution of **5.29** (100 mg, 0.67 mmol) in THF (3 mL) at 0 °C was added 3-chloropropionyl chloride (0.032 mL, 0.33 mmol) dropwise, instantly forming a ppt. The reaction was stirred at 0 °C for 1 h, gradually warming to rt. To the reaction mixture was added H₂O to ppt the product. The ppt was collected via centrifugation and washed with water. The filtrate was concentrated *in vacuo* and redissolved in a minimal amount of MeOH and ppt with H₂O to collect more product. Yield of **5.30**: 51 mg, 0.21 mmol, 64% yield. ¹H NMR (400 MHz, DMSO-*d*₆) δ 9.62 (s, 1H), 7.54 (s, 1H), 7.33 (d, *J* = 7.7 Hz, 3H), 7.21 (t, *J* = 7.6 Hz, 1H), 3.85 (t, *J* = 6.3 Hz, 2H), 2.78 (t, *J* = 6.3 Hz, 2H), 2.17 (s, 3H).

8-methyl-2-vinylquinazolin-4(3H)-one (5.25): To a mixture of 5% NaOH (aq)/EtOH (2:1, 1.8 mL) was added **5.30** (0.11 g, 0.46 mmol). The reaction was stirred at reflux for 5 min and cooled to rt over 15 min. Acetic acid (0.12 mL, 2 mmol) was added to acidify the reaction, immediately forming a ppt. The ppt was collected via filtration, washed with water, and concentrated *in vacuo*. Yield of **5.25**: 72 mg, 0.39 mmol, 78% yield. ¹H NMR (400 MHz, DMSO-*d*₆) δ 12.30 (s, 1H), 8.07 – 7.81 (m, 1H), 7.66 (ddd, *J* = 7.3, 1.7, 0.9 Hz, 1H), 7.37 (t, *J* = 7.6 Hz, 1H), 6.77 – 6.37 (m, 2H), 5.82 (dd, *J* = 8.6, 3.4 Hz, 1H), 2.55 (s, 3H).

Synthesis of *(E)*-*N*-(8-methyl-4-oxo-3,4-dihydroquinazolin-2-yl)but-2-enamide (**5.26**):

2-amino-8-methylquinazolin-4(3H)-one (**5.32**): A mixture of methyl 2-amino-3-methyl benzoate (0.21 g, 1.25 mmol), chloroformamidine chloride (0.22 g, 1.87 mmol), and dimethyl sulfone (5.88 g) were heated at 150 °C with stirring for 2.25 h. The reaction was removed from heat and allowed to cool to rt. Concentrated NH₄OH (10 mL) and H₂O (10 mL) were added, and the reaction was stirred overnight. The ppt was collected via filtration, washed with water, MeOH, acetone, and CHCl₃, and concentrated *in vacuo*. Yield of **5.32**: 0.14 g, 0.79 mmol, 63% yield. ¹H NMR (400 MHz, DMSO-*d*₆) δ 10.92 (s, 1H), 7.86 – 7.55 (m, 1H), 7.42 (d, *J* = 7.0 Hz, 1H), 6.97 (t, *J* = 7.5 Hz, 1H), 6.34 (s, 2H), 2.35 (s, 3H).

(E)-*N*-(8-methyl-4-oxo-3,4-dihydroquinazolin-2-yl)but-2-enamide (**5.26**): A mixture of **5.32** (30 mg, 0.17 mmol) in dimethylacetamide (1 mL) was heated briefly at 50 °C to promote dissolution. Upon clearing, DIPEA (0.15 mL, 0.86 mmol) was added and the reaction was cooled to 0 °C. To the mixture was added *trans*-crotonyl chloride (0.025 mL, 0.26 mmol) dropwise, and the reaction was gradually warmed to rt and stirred for 18 h. The reaction was quenched with saturated NaHCO₃ (aq) and diluted with H₂O and DCM. The DCM layer was removed and dried over Na₂SO₄, filtered, and concentrated *in vacuo*. The crude residue was purified via ISCO CombiFlash chromatography. Yield of **5.26**: 11 mg, 0.045 mmol, 26% yield. ¹H NMR (400 MHz, DMSO-*d*₆) δ 12.23 (s, 1H), 11.51 (s, 1H), 7.90 (d, *J* = 7.8 Hz, 1H), 7.63 (d, *J* = 7.3 Hz, 1H), 7.28 (t, *J* = 7.6 Hz, 1H),

7.14 – 6.92 (m, 1H), 6.34 (dd, $J = 15.3, 1.9$ Hz, 1H), 2.50 (3H)*, 1.91 (dd, $J = 6.9, 1.7$ Hz, 3H), *obscured by residual DMSO solvent peak.

Synthesis of N-((8-methyl-4-oxo-3,4-dihydroquinazolin-2-yl)methyl)acrylamide (5.27):

2-(chloromethyl)-8-methylquinazolin-4(3H)-one (5.33): To a solution of NaOMe (54 mg, 1.0 mmol) in MeOH was added chloroacetonitrile (0.95 mL, 15.0 mmol), and the reaction was stirred at rt for 30 min. To the mixture was added a solution of 2-amino-3-methylbenzoic acid (0.73 g, 4.85 mmol) in MeOH (15 mL), and the reaction was stirred at rt for 18, gradually forming a ppt. The reaction was heated at 80 °C for 2h to further drive the reaction to completion and then cooled to 0 °C. The ppt was filtered, washed with MeOH, water, and additional MeOH. Yield of **5.27**: 0.70 g, 3.37 mmol, 69% yield. ^1H NMR (400 MHz, DMSO- d_6) δ 12.61 (s, 1H), 8.00 (dd, $J = 8.1, 1.5$ Hz, 1H), 7.83 – 7.63 (m, 1H), 7.47 (t, $J = 7.6$ Hz, 1H), 2.57 (s, 3H).

2-(aminomethyl)-8-methylquinazolin-4(3H)-one (5.34): A mixture of **5.27** (0.20 g, 0.96 mmol) in NH_3 in MeOH (7 N, 10 mL, 70 mmol) in a pressure vessel was heated at 60 °C for 20 h. The reaction was cooled to rt, and the formed ppt was filtered. The filtrate was concentrated *in vacuo*, and the residue was triturated with MeOH (3 x 5 mL). The remaining solid was concentrated *in vacuo* to remove residual MeOH. Yield of **5.34**: 0.11 g, 0.57 mmol, 59% yield). ^1H NMR (400 MHz,

DMSO- d_6) δ 7.96 (dt, J = 7.8, 1.3 Hz, 1H), 7.71 (dt, J = 7.3, 1.2 Hz, 1H), 7.43 (t, J = 7.6 Hz, 1H), 4.07 (s, 2H), 2.60 (s, 3H).

N-((8-methyl-4-oxo-3,4-dihydroquinazolin-2-yl)methyl)acrylamide (**5.27**): To a solution of **5.34** (20 mg, 0.11 mmol) in DMF (1 mL) was added DIPEA (0.09 mL, 0.53 mmol), and the mixture was heated briefly at 50 °C to promote dissolution. After clearing, the reaction was cooled to 0 °C and acryloyl chloride (0.013 mL, 0.16 mmol) was added dropwise. The reaction was stirred at 0 °C for 0.5 h and quenched with H₂O. The reaction was extracted with DCM. The DCM layer was washed with sat. NaHCO₃ (aq) and brine, dried over Na₂SO₄, filtered, and concentrated *in vacuo*. The crude residue was purified via ISCO CombiFlash chromatography (silica, 4g; 0-100% EtOAc in hexanes). Yield of **5.27**: 5.3 mg, 0.022 mmol, 20% yield). ¹H NMR (400 MHz, DMSO- d_6) δ 12.19 (s, 1H), 8.59 (t, J = 5.6 Hz, 1H), 7.93 (dd, J = 7.6, 1.4 Hz, 1H), 7.65 (d, J = 7.2 Hz, 1H), 7.36 (t, J = 7.6 Hz, 1H), 6.37 (dd, J = 17.1, 10.3 Hz, 1H), 6.13 (dd, J = 17.1, 2.1 Hz, 1H), 5.66 (dd, J = 10.2, 2.1 Hz, 1H), 4.32 (d, J = 5.7 Hz, 2H), 2.50 (3H)*, *obscured by residual DMSO solvent peak.

Synthesis of N-(2-(8-methyl-4-oxo-3,4-dihydroquinazolin-2-yl)ethyl)acrylamide (**5.28**):

2-(2-aminoethyl)-8-methylquinazolin-4(3H)-one (**5.31**): A mixture of **5.30** (30 mg, 0.125 mmol) in NH₃ in MeOH (7 N, 2 mL, 14 mmol) in a pressure vessel was heated at 60 °C for 20 h. The reaction was allowed to cool to rt, and H₂O (10 mL)

and concentrated NH_4OH (1 mL) were added. The ppt was collected via centrifugation and concentrated *in vacuo*. Yield of **5.28**: 24 mg, 0.108 mmol, 86% yield. ^1H NMR (400 MHz, $\text{DMSO}-d_6$) δ 7.88 (dd, $J = 7.9, 1.3$ Hz, 1H), 7.63 – 7.50 (m, 1H), 7.30 (t, $J = 7.6$ Hz, 1H), 3.04 (t, $J = 6.6$ Hz, 2H), 2.79 (t, $J = 6.6$ Hz, 2H), 2.41 (s, 3H).

N-(2-(8-methyl-4-oxo-3,4-dihydroquinazolin-2-yl)ethyl)acrylamide (**5.28**):

Followed same procedure as **5.27** except **5.31** (20 mg, 0.098 mmol) was used in place of **5.34**. Yield of **5.28**: 8.0 mg, 0.031 mmol, 32% yield. ^1H NMR (400 MHz, $\text{DMSO}-d_6$) δ 12.20 (s, 1H), 8.20 (d, $J = 5.9$ Hz, 1H), 8.02 – 7.80 (m, 1H), 7.73 – 7.54 (m, 1H), 7.34 (t, $J = 7.6$ Hz, 1H), 6.19 (dd, $J = 17.1, 10.1$ Hz, 1H), 6.06 (dd, $J = 17.1, 2.3$ Hz, 1H), 5.56 (dd, $J = 10.0, 2.3$ Hz, 1H), 3.61 (q, $J = 6.7$ Hz, 2H), 2.80 (t, $J = 6.8$ Hz, 2H), 2.51 (s, 3H)*, *obscured by residual DMSO solvent peak.

Other Methods

Cloning. cDNA encoding full length human PARP1, full length human PARP2, human PARP10 catalytic domain, human PARP15 catalytic domain, and SRPK2 were obtained as previously described (Chapters 2 and 3).^{84,99} cDNA encoding full length human PARP11 and cDNA encoding the human PARP4 catalytic and BRCT domains (aa1-572, PARP4_{brct-cat}) were obtained using gBlock gene fragments containing the PARP11 gene as template (IDT) and the following primers (IDT) for subsequent Gibson assembly cloning.

PARP11:

Forward

ATCGAGGAAAACCTGTACTTCCAATCCAATTTTCACAAAGCAGAAGAATTATT
TTCT

Reverse

CTCGAATTCGGATCCGTTATCCACTTCCAATTCAATGAAAGTCTATCAAGTA
CTCAGGAT

PARP4_{brct-cat}:

Forward

TACTTCCAATCCAATGCAGTGATGGGAATCTTTGCAAATTG

Reverse

TTATCCACTTCCAATGTTATTAGTCCTTTATCTGATCTCCAGGCAT

The amplified fragments were gel purified and cloned into a pET-His-SUMO-TEV LIC cloning vector (1B), a gift from Scott Gradia (Addgene plasmid # 29653) by an isothermal assembly protocol using the Gibson assembly mix (NEB). cDNA encoding the human PARP14 catalytic and WWE domains (aa1459-1801, PARP14_{cat-wwe}) was cloned into the pNIC-Bsa4 vector using standard procedures.

Expression and Purification of human PARP1, PARP2, PARP10_{cat}, PARP15_{cat}, and SRPK2. Human PARP1, PARP2, PARP10_{cat}, PARP15_{cat}, and SRPK2 were expressed as previously described (Chapters 2 and 3).^{84,99} Greater than or equal to 90% purity was achieved for human PARP1, PARP2,

PARP10_{cat}, and PARP15_{cat}. Greater than or equal to 70% purity was achieved for SRPK2.

Expression and Purification of human full length PARP11. pET-His-SUMO-TEV-PARP11 plasmid was transformed into *E.coli* BL21 pRARE2 strain (Novagen) cells for SUMO-PARP11 expression, and grown on LB agar plates (with Kanamycin and Chloramphenicol) overnight at 37 °C. A swath of cells was inoculated into a 10 ml starter culture of LB media (with 50 µg/ml Kanamycin, 34 µg/ml chloramphenicol) at 225 rpm, 37 °C overnight. One or more liters of terrific broth (TB) media (12 g bacto tryptone, 24 g yeast extract, 0.4% glycerol, 17mM KH₂PO₄, 72mM K₂HPO₄, 1% glucose, 50 µg/ml Kanamycin, 34 µg/ml chloramphenicol) was inoculated with the starter culture and grown to an OD = 0.4-0.5 at 37 °C, 225 rpm. Isopropyl-β-thiogalactoside, IPTG (Sigma-Aldrich) was added to 0.4mM to induce protein expression for 2.5-3 hours at 37 °C, 225 rpm. Cells were harvested by centrifuging, resuspended in lysis buffer containing PMSF and lysed by sonication at 0 °C (Branson sonifier 450). The lysate containing the soluble protein was clarified by centrifugation (12,000g, 30 min at 4 °C). PARP11 was purified in a single step using immobilized metal affinity chromatography (Ni-NTA resin, Qiagen). ~70% purity was achieved.

Expression and Purification of human PARP14_{cat-wwe}. PARP14_{cat-wwe} was expressed in the *Escherichia coli* BL21 pRARE2 strain (EMD Millipore). Cells were first cultured in LB media overnight at 225 rpm and 37 °C in an Excella®

E24 Incubator (New Brunswick Scientific). Two liters of TB media (12 g Bacto Tryptone (BD Biosciences), 24 g Bacto Yeast Extract (BD Biosciences), 0.4% glycerol, 17 mM KH_2PO_4 , 72 mM K_2HPO_4 , 1% glucose, 50 $\mu\text{g/ml}$ kanamycin, 34 $\mu\text{g/ml}$ chloramphenicol) was inoculated with the starting culture and grown to $\text{OD}_{600} = 1.0$ at 225 rpm and 37 °C. The temperature was reduced to 16 °C and expression was induced by adding isopropyl β -D-thiogalactoside (IPTG) to 0.4 mM. After incubation at 16 °C for 24 h, cells were harvested by centrifugation, resuspended in lysis buffer [20 mM HEPES, pH 7.5, 1 mM β -mercaptoethanol (β -Me), 1 mM benzamidine, 0.2% NP-40, 0.2% TWEEN-20, 500 mM NaCl, 1 mM phenylmethylsulfonyl fluoride (PMSF), 8.3 mg/L DNase I (Roche)] at 4 °C, and lysed by sonication at 0 °C, and the resulting lysate was clarified by centrifugation at 12,000 G for 30 minutes at 4 °C. PARP14_{cat-wwe} was purified in a single step using immobilized metal affinity chromatography (Ni-NTA resin, Qiagen). Greater than or equal to 90% purity was achieved.

SRPK2 Plate Assays for inhibitor profiling with PARP10_{cat} and PARP11 using NAD⁺. 96-well nickel coated plate (Pierce) was incubated with His₆-tagged SRPK2 in hB (50 mM HEPES pH 7.5, 300 mM NaCl, 4 mM MgCl_2 , 0.2 mM TCEP) for 1 h at rt. After extensively washing the plate, PARPs in hB were added to individual wells of the 96-well plate. Varying concentrations of 2X inhibitor were pre-incubated with 200 μM NAD⁺ in hB at room temperature, then added to the plate. Final reaction concentrations: PARP10_{cat}: 3 nM, PARP11_{FL}: 3 nM, both in hB, 100 μM NAD⁺. This reaction proceeded for 60 minutes at 30 °C. The plate

was then washed three times with 1X PBST and blocked with 5% milk (Carnation) in 1X PBST for 30 minutes at rt. The plate was then washed three times with 1X PBST and incubated with a pan-ADP-ribose binding reagent¹²⁸ (10 ng/mL in 1X PBST, 2% BSA, 1 mg/mL NaN₃) for 30 minutes at rt. The plate was then washed three times with 1X PBST and incubated with Peroxidase AffiniPure Goat Anti-Rabbit IgG (H+L) (Jackson ImmunoResearch) at 1:25,000 (in 5% milk in 1X PBST). The plate was then washed three times with 1X PBST, once with 1X PBS, and then developed with QuantaRed™ Enhanced Chemifluorescent HRP Substrate (Thermo) for 60 seconds before quenching with Quanta Red Stop Solution. Fluorescence for each sample and control was read at excitation 570 nM and emission 600 nM with a Spectra Max i3 (Molecular Devices) within five minutes of development. Inhibitor dose response curves were fit using linear regression in Prism 4 (GraphPad™ Software). The mean pIC₅₀ for each compound was calculated from at least three independent assays.

SRPK2 Plate Assay for inhibitor profiling of PARPs using 6-a-NAD⁺. The assay was performed as above except with the following modifications. NAD⁺ was replaced with 6-a-NAD⁺ at the same concentration. Final reaction concentrations: PARP1_{FL} and PARP2_{FL}: 25 nM in hB with 0.1 mg/mL activated DNA (Sigma D4522); PARP3_{FL}: 300 nM in hB with 2.5 μM dNick 5'P;¹³⁵ PARP5b_{cat}: 100 nM, PARP10_{cat}: 2 nM, PARP11_{FL}: 2 nM, PARP14_{wwe-cat}: 2 nM, PARP15_{cat}: 2 nM all in hB, 100 μM 6-a-NAD⁺. After the ADP-ribosylation reaction, the plate was then washed three times with 1X PBST (1X PBS, 0.01% Tween-

20), once with 1X PBS, then click conjugation was performed in CB (100 μ M biotin-PEG3-azide, 100 μ M Tris[(1-benzyl-1H-1,2,3-triazol-4-yl)methyl]amine (TBTA, Sigma), 1 mM CuSO₄, 1 mM TCEP, 1X PBS) for 30 minutes at RT. The plate was then washed three times with 1X PBST, once with 1X PBS, and then blocked with 1% milk (Carnation) in 1X PBST for 30 minutes at rt. The plate was then washed three times with 1X PBST, once with 1X PBS, and then incubated with Strep-HRP (300 ng/ μ L BSA, 0.05 ng/ μ L Strep-HRP, 1X PBS) for 30 minutes at RT. The plate was then washed three times with 1X PBST, once with 1X PBS, and then developed, measured, and quantified as above.

GFP-PARP10 cellular ADP-ribosylation assay. A similar procedure was followed as outlined in Chapter 4.

PARP immunoprecipitation (IP) auto-ADP-ribosylation activity assay. IP-auto-ADPr assays were performed as described previously (Chapter 4).¹²³

Chapter 6: Concluding Remarks

The poly(ADP-ribose) polymerase (PARP) family catalyzes the post-translational modification ADP-ribosylation (ADPr) from nicotinamide adenine dinucleotide (NAD⁺). ADPr is one a few cellular reactions that consumes the essential NAD⁺ cofactor, a strikingly different role than NAD⁺ as a redox carrier in oxidoreductase metabolic reactions.² This feature connects NAD⁺ to the regulation of protein function and cellular signaling. It is not surprising that many PARP family enzymes are involved in stress signaling pathways,^{26,136} as the consumption of NAD⁺ can have destructive effects on metabolic pathways and activate stress responses.^{137,138} The role of PARP1 in DNA damage repair highlights this energy-survival connection, as high levels of DNA damage can lead to PARP1 overactivation and eventually result in apoptosis. This forms the foundation for PARP1 inhibitors as treatments for certain types of cancers.³⁰ While the connection of PARP1 to DNA damage is well-established and validated as a therapeutic strategy, the remaining family members, especially those that catalyze mono-ADPr, still need to be investigated. As many mono-ADPr PARPs have already been linked to certain signaling pathways with aberrant activity during disease (e.g., PARP16 in the unfolded protein response),³³ understanding their roles on a mechanistic level will provide insight into possible therapeutic strategies.

One of the major limitations in the study of mono-ADPr PARP biology is the lack of methods to decipher their functional roles. In particular, many of the targets of mono-ADPr PARPs are unknown or not fully characterized. This is due in part to the lack of methods to discriminate protein targets of a single PARP

among the entire PARP family, as all PARPs share the same common NAD⁺ substrate. Additionally, the ability to detect the mono-ADPr modification in cells has been limited. Most techniques are suited to use in lysates, which can misrepresent the concentrations and compartmentalization of protein targets in the cell. Many inhibitors also exhibit polypharmacology among the PARP family and do not allow the connection of a given phenotype to a single PARP family member due to confounding inhibition of multiple PARP family members.

In Chapter 2, I developed modified NAD⁺ analogues that are selectively used by a single engineered PARP family member. This strategy was applied to both the poly- and mono-ADPr subclasses of PARPs. The orthogonal NAD⁺ analogue-engineered PARP pairs were used to identify direct protein targets of an individual PARP family member in cell lysate, where multiple PARP family members are present. This novel approach overcame the problems associated with previous methods that only capture targets of ADPr on a global level. Now the specific targets of an individual PARP can be identified to further understand their roles and biological pathways in which they elicit their function.

In Chapter 3, I developed a clickable probe that detects cellular ADPr. The probe can be dosed directly to cells for labeling over a given time period, prior to or after a specific stimulus, providing a snapshot of ADPr levels. The probe also revealed an unanticipated mechanism for ADPr at acidic residues. A mechanism in which the ADPr shifts positions on the ribose ring was revealed through functional studies with the probe. This mechanism has important implications for how we think about the modification, and more importantly, how the modification

is recognized and reversed in the cell. It also reveals an important evolutionary link between NAD⁺-consuming enzymes and the regulation of ADP-ribose, which may be a tactic for maintaining energy homeostasis in the cell.

In Chapters 4 and 5, I developed strategies to obtain selective inhibition of the mono-ADPr PARP, PARP10. In Chapter 4, I focused on a chemical genetics strategy to obtain selective inhibition. I developed chemical probes to inhibit a mutant of PARP10 with >20-fold selectivity *in vitro* over other PARP family members. When this strategy was adapted for a cellular system, the selectivity unfortunately did not translate. The strategy that I developed, however, can serve as a platform for future chemical genetic strategies pursuing different mutants and corresponding orthogonal probes.

In Chapter 5, I turned my attention to developing chemical probes that can selectively inhibit wild-type PARP10. After SAR studies of a series of dq compounds against both PARP10 and PARP11, modifications were discovered that imparted selectivity for PARP10 over PARP11 (29-fold), as well as selectivity over a large majority of PARP family members (ranging from >10-37-fold). I also synthesized a series of electrophilic probes to target a nonconserved cysteine residue in the active site of PARP10. Preliminary studies suggest a covalent mode of inhibition between the Cys electrophile and the core scaffold. These strategies to achieve selective inhibition of a PARP family member will be valuable for future studies aimed at probe optimization for increased selectivity among the PARPs.

Overall, I anticipate that these chemical tools developed during my dissertation will serve to further our understanding of ADP-ribosylation and the PARP family. They will provide a toolbox for future investigation into identifying the direct protein targets of a PARP, monitoring cellular ADP-ribosylation, and dynamically modulating the activity of a single PARP. The PARP field will advance as these new chemical tools are utilized to provide a clearer picture of PARP family-member-specific function.

References

1. Gupte, R., Liu, Z. & Kraus, W. L. PARPs and ADP-ribosylation: recent advances linking molecular functions to biological outcomes. *Genes Dev* **31**, 101–126 (2017).
2. Belenky, P., Bogan, K. L. & Brenner, C. NAD⁺ metabolism in health and disease. *Trends Biochem Sci* **32**, 12–19 (2007).
3. Landry, J. *et al.* The silencing protein SIR2 and its homologs are NAD-dependent protein deacetylases. *Proc Natl Acad Sci U S A* **97**, 5807–5811 (2000).
4. Denu, J. M. The Sir2 family of protein deacetylases. *Curr Opin Chem Biol* **9**, 431 (2005).
5. Gusea, A. H. Cyclic ADP-ribose. *Cell Signal* **11**, 309–316 (1999).
6. Gibson, B. A. & Kraus, W. L. New insights into the molecular and cellular functions of poly(ADP-ribose) and PARPs. *Nat Rev Mol Cell Biol* **13**, 411–424 (2012).
7. Daniels, C. M., Ong, S.-E. & Leung, A. K. L. The Promise of Proteomics for the Study of ADP-Ribosylation. *Mol Cell* **58**, 911–924 (2015).
8. Eaton, M. D. The Purification and Concentration of Diphtheria Toxin: I. Evaluation of Previous Methods; Description of a New Procedure. *J Bacteriol* **31**, 347–366 (1936).
9. Freeman, V. J. Studies on the virulence of bacteriophage-infected strains of *Corynebacterium diphtheriae*. *The Lancet* **251**, 97 (1951).

10. Simon, N. C., Aktories, K. & Barbieri, J. T. Novel bacterial ADP-ribosylating toxins: structure and function. *Nat Rev Microbiol* **12**, 599–611 (2014).
11. Naglich, J. G., Metherall, J. E., Russell, D. W. & Eidels, L. Expression cloning of a diphtheria toxin receptor: identity with a heparin-binding EGF-like growth factor precursor. *Cell* **69**, 1051–1061 (1992).
12. Honjo, T., Nishizuka, Y. & Hayaishi, O. Diphtheria toxin-dependent adenosine diphosphate ribosylation of aminoacyl transferase II and inhibition of protein synthesis. *Journal of Biological Chemistry* **243**, 3553–3555 (1968).
13. Strauss, N. THE EFFECT OF DIPHTHERIA TOXIN ON THE METABOLISM OF HELA CELLS. *Journal of Experimental Medicine* **109**, 145 (1959).
14. Howard-Jones, N. Robert Koch and the cholera vibrio: a centenary. *BMJ* **288**, 379–381 (1984).
15. De, S. N. & Chatterje, D. N. Enterotoxicity of Bacteria-free Culture-filtrate of *Vibrio cholerae*. *Nature* **183**, 1533 (1959).
16. Lencer, W. I., Hirst, T. R. & Holmes, R. K. Membrane traffic and the cellular uptake of cholera toxin. *Biochimica et Biophysica Acta (BBA) - Molecular Cell Research* **1450**, 177 (1999).
17. Bobak, D. A. *et al.* Mechanism of activation of cholera toxin by ADP-ribosylation factor (ARF): both low- and high-affinity interactions of ARF with guanine nucleotides promote toxin activation. *Biochemistry* **29**, 855–861 (1990).

18. Gill, D. M. & Meren, R. ADP-ribosylation of membrane proteins catalyzed by cholera toxin: basis of the activation of adenylate cyclase. *Proc Natl Acad Sci U S A* **75**, 3050–3054 (1978).
19. Cassel, D. & Pfeuffer, T. Mechanism of cholera toxin action: covalent modification of the guanyl nucleotide-binding protein of the adenylate cyclase system. *Proc Natl Acad Sci U S A* **75**, 2669–2673 (1978).
20. Zolkiewska, A. Ecto-ADP-ribose transferases: cell-surface response to local tissue injury. *Physiology (Bethesda)* **20**, 374–381 (2005).
21. Amé, J.-C., Spenlehauer, C. & de Murcia, G. The PARP superfamily. *Bioessays* **26**, 882–893 (2004).
22. Hottiger, M. O., Hassa, P. O., Lüscher, B., Schüler, H. & Koch-Nolte, F. Toward a unified nomenclature for mammalian ADP-ribosyltransferases. *Trends Biochem Sci* **35**, 208–219 (2010).
23. Chambon, P., Weill, J. D. & Mandel, P. Nicotinamide mononucleotide activation of a new DNA-dependent polyadenylic acid synthesizing nuclear enzyme. *Biochem Biophys Res Commun* **11**, 39 (1963).
24. Amé, J. C. *et al.* PARP-2, A novel mammalian DNA damage-dependent poly(ADP-ribose) polymerase. *J Biol Chem* **274**, 17860–17868 (1999).
25. Otto, H. *et al.* In silico characterization of the family of PARP-like poly(ADP-ribosyl)transferases (pARTs). *BMC Genomics* **6**, 139 (2005).
26. Vyas, S. & Chang, P. New PARP targets for cancer therapy. *Nat Rev Cancer* **14**, 502–509 (2014).

27. Vyas, S. *et al.* Family-wide analysis of poly(ADP-ribose) polymerase activity. *Nat Commun* **5**, 4426 (2014).
28. Yang, C.-S. *et al.* Ubiquitin Modification by the E3 Ligase/ADP-Ribosyltransferase Dtx3L/Parp9. *Mol Cell* **66**, 503–516.e5 (2017).
29. Kutuzov, M. M., Khodyreva, S. N., Schreiber, V. & Lavrik, O. I. Role of PARP2 in DNA repair. *Molecular Biology* **48**, 485 (2014).
30. Krishnakumar, R. & Kraus, W. L. The PARP side of the nucleus: molecular actions, physiological outcomes, and clinical targets. *Mol Cell* **39**, 8–24 (2010).
31. Riffell, J. L., Lord, C. J. & Ashworth, A. Tankyrase-targeted therapeutics: expanding opportunities in the PARP family. *Nat Rev Drug Discov* **11**, 923–936 (2012).
32. Vyas, S., Chesarone-Cataldo, M., Todorova, T., Huang, Y.-H. & Chang, P. A systematic analysis of the PARP protein family identifies new functions critical for cell physiology. *Nat Commun* **4**, 2240 (2013).
33. Jwa, M. & Chang, P. PARP16 is a tail-anchored endoplasmic reticulum protein required for the PERK- and IRE1 α -mediated unfolded protein response. *Nat Cell Biol* **14**, 1223–1230 (2012).
34. Verheugd, P. *et al.* Regulation of NF- κ B signalling by the mono-ADP-ribosyltransferase ARTD10. *Nat Commun* **4**, 1683 (2013).
35. Huang, J. Y., Wang, K., Vermehren-Schmaedick, A., Adelman, J. P. & Cohen, M. S. PARP6 is a regulator of hippocampal dendritic morphogenesis. *Sci Rep* **6**, 18512 (2016).

36. Daugherty, M. D., Young, J. M., Kerns, J. A. & Malik, H. S. Rapid evolution of PARP genes suggests a broad role for ADP-ribosylation in host-virus conflicts. *PLoS Genet* **10**, e1004403 (2014).
37. Czapski, G. A., Adamczyk, A., Strosznajder, R. P. & Strosznajder, J. B. Expression and activity of PARP family members in the hippocampus during systemic inflammation: their role in the regulation of prooxidative genes. *Neurochem Int* **62**, 664–673 (2013).
38. Ménissier de Murcia, J. *et al.* Functional interaction between PARP-1 and PARP-2 in chromosome stability and embryonic development in mouse. *EMBO J* **22**, 2255–2263 (2003).
39. Kawamitsu, H. *et al.* Monoclonal antibodies to poly(adenosine diphosphate ribose) recognize different structures. *Biochemistry* **23**, 3771–3777 (1984).
40. Bartolomei, G., Leutert, M., Manzo, M., Baubec, T. & Hottiger, M. O. Analysis of Chromatin ADP-Ribosylation at the Genome-wide Level and at Specific Loci by ADPr-ChAP. *Mol Cell* **61**, 474–485 (2016).
41. Jungmichel, S. *et al.* Proteome-wide identification of poly(ADP-Ribosylation) targets in different genotoxic stress responses. *Mol Cell* **52**, 272–285 (2013).
42. Martello, R. *et al.* Proteome-wide identification of the endogenous ADP-ribosylome of mammalian cells and tissue. *Nat Commun* **7**, 12917 (2016).
43. Zhang, Y., Wang, J., Ding, M. & Yu, Y. Site-specific characterization of the Asp- and Glu-ADP-ribosylated proteome. *Nat Methods* **10**, 981–984 (2013).

44. Zhang, J. Use of biotinylated NAD to label and purify ADP-ribosylated proteins. *Meth Enzymol* **280**, 255–265 (1997).
45. Jiang, H., Kim, J. H., Frizzell, K. M., Kraus, W. L. & Lin, H. Clickable NAD analogues for labeling substrate proteins of poly(ADP-ribose) polymerases. *J Am Chem Soc* **132**, 9363–9372 (2010).
46. Koh, J. T. Engineering selectivity and discrimination into ligand-receptor interfaces. *Chem Biol* **9**, 17–23 (2002).
47. Islam, K. Allele-Specific Chemical Genetics: Concept, Strategies, and Applications. *ACS Chem. Biol.* **10**, 343–363 (2015).
48. Belshaw, P. J., Schoepfer, J. G., Liu, K.-Q., Morrison, K. L. & Schreiber, S. L. Rational Design of Orthogonal Receptor–Ligand Combinations. *Angewandte Chemie International Edition in English* **34**, 2129 (1995).
49. Shah, K., Liu, Y., Deirmengian, C. & Shokat, K. M. Engineering unnatural nucleotide specificity for Rous sarcoma virus tyrosine kinase to uniquely label its direct substrates. *Proc Natl Acad Sci U S A* **94**, 3565–3570 (1997).
50. Liu, Y., Shah, K., Yang, F., Witucki, L. & Shokat, K. M. Engineering Src family protein kinases with unnatural nucleotide specificity. *Chem Biol* **5**, 91–101 (1998).
51. Bishop, A. C. *et al.* A chemical switch for inhibitor-sensitive alleles of any protein kinase. *Nature* **407**, 395–401 (2000).
52. Shah, K. & Shokat, K. M. A chemical genetic screen for direct v-Src substrates reveals ordered assembly of a retrograde signaling pathway. *Chem Biol* **9**, 35–47 (2002).

53. Blethrow, J. D., Glavy, J. S., Morgan, D. O. & Shokat, K. M. Covalent capture of kinase-specific phosphopeptides reveals Cdk1-cyclin B substrates. *Proc Natl Acad Sci U S A* **105**, 1442–1447 (2008).
54. Islam, K., Zheng, W., Yu, H., Deng, H. & Luo, M. Expanding cofactor repertoire of protein lysine methyltransferase for substrate labeling. *ACS Chem. Biol.* **6**, 679–684 (2011).
55. Islam, K. *et al.* Defining efficient enzyme-cofactor pairs for bioorthogonal profiling of protein methylation. *Proc Natl Acad Sci U S A* **110**, 16778–16783 (2013).
56. Yang, C. *et al.* Labeling lysine acetyltransferase substrates with engineered enzymes and functionalized cofactor surrogates. *J Am Chem Soc* **135**, 7791–7794 (2013).
57. Yang, Y.-Y., Ascano, J. M. & Hang, H. C. Bioorthogonal chemical reporters for monitoring protein acetylation. *J Am Chem Soc* **132**, 3640–3641 (2010).
58. Wallrodt, S., Buntz, A., Wang, Y., Zumbusch, A. & Marx, A. Bioorthogonally Functionalized NAD(+) Analogues for In-Cell Visualization of Poly(ADP-Ribose) Formation. *Angew Chem Int Ed Engl* **55**, 7660–7664 (2016).
59. Westcott, N. P., Fernandez, J. P., Molina, H. & Hang, H. C. Chemical proteomics reveals ADP-ribosylation of small GTPases during oxidative stress. *Nat Chem Biol* **13**, 302–308 (2017).
60. Miwa, M. & Masutani, M. PolyADP-ribosylation and cancer. *Cancer Sci* **98**, 1528–1535 (2007).

61. Farmer, H. *et al.* Targeting the DNA repair defect in BRCA mutant cells as a therapeutic strategy. *Nature* **434**, 917–921 (2005).
62. Bryant, H. E. *et al.* Specific killing of BRCA2-deficient tumours with inhibitors of poly(ADP-ribose) polymerase. *Nature* **434**, 913–917 (2005).
63. Kaelin, W. G. The concept of synthetic lethality in the context of anticancer therapy. *Nat Rev Cancer* **5**, 689–698 (2005).
64. Wahlberg, E. *et al.* Family-wide chemical profiling and structural analysis of PARP and tankyrase inhibitors. *Nat Biotechnol* **30**, 283–288 (2012).
65. Thorsell, A.-G. *et al.* Structural Basis for Potency and Promiscuity in Poly(ADP-ribose) Polymerase (PARP) and Tankyrase Inhibitors. *J Med Chem* **60**, 1262–1271 (2017).
66. Steffen, J. D., Brody, J. R., Armen, R. S. & Pascal, J. M. Structural implications for selective targeting of parps. *Front Oncol* **3**, 301 (2013).
67. Lopez, M. S. *et al.* Staurosporine-derived inhibitors broaden the scope of analog-sensitive kinase technology. *J Am Chem Soc* **135**, 18153–18159 (2013).
68. Wang, H. *et al.* Inducible protein knockout reveals temporal requirement of CaMKII reactivation for memory consolidation in the brain. *Proc Natl Acad Sci U S A* **100**, 4287–4292 (2003).
69. Carroll, A. S., Bishop, A. C., DeRisi, J. L., Shokat, K. M. & O'Shea, E. K. Chemical inhibition of the Pho85 cyclin-dependent kinase reveals a role in the environmental stress response. *Proc Natl Acad Sci U S A* **98**, 12578–12583 (2001).

70. Ferraris, D. V. Evolution of poly(ADP-ribose) polymerase-1 (PARP-1) inhibitors. From concept to clinic. *J Med Chem* **53**, 4561–4584 (2010).
71. Donawho, C. K. *et al.* ABT-888, an orally active poly(ADP-ribose) polymerase inhibitor that potentiates DNA-damaging agents in preclinical tumor models. *Clin Cancer Res* **13**, 2728–2737 (2007).
72. Chen, B. *et al.* Small molecule-mediated disruption of Wnt-dependent signaling in tissue regeneration and cancer. *Nat Chem Biol* **5**, 100–107 (2009).
73. Lau, T. *et al.* A novel tankyrase small-molecule inhibitor suppresses APC mutation-driven colorectal tumor growth. *Cancer Res* **73**, 3132–3144 (2013).
74. Johannes, J. W. *et al.* Pyrimidinone nicotinamide mimetics as selective tankyrase and wnt pathway inhibitors suitable for in vivo pharmacology. *ACS Med Chem Lett* **6**, 254–259 (2015).
75. Peng, B., Thorsell, A.-G., Karlberg, T., Schöler, H. & Yao, S. Q. Small molecule microarray based discovery of PARP14 inhibitors. *Angew Chem Int Ed Engl* **56**, 248–253 (2017).
76. Yoneyama-Hirozane, M. *et al.* Identification of PARP14 inhibitors using novel methods for detecting auto-ribosylation. *Biochem Biophys Res Commun* **486**, 626–631 (2017).
77. Ekblad, T. *et al.* Towards small molecule inhibitors of mono-ADP-ribosyltransferases. *Eur J Med Chem* **95**, 546–551 (2015).

78. Venkannagari, H. *et al.* Small-Molecule Chemical Probe Rescues Cells from Mono-ADP-Ribosyltransferase ARTD10/PARP10-Induced Apoptosis and Sensitizes Cancer Cells to DNA Damage. *Cell Chem Biol* **23**, 1251–1260 (2016).
79. Upton, K. *et al.* Design and synthesis of potent inhibitors of the mono(ADP-ribosyl)transferase, PARP14. *Bioorg Med Chem Lett* **27**, 2907–2911 (2017).
80. Pinto, A. F. & Schüler, H. Comparative structural analysis of the putative mono-ADP-ribosyltransferases of the ARTD/PARP family. *Curr Top Microbiol Immunol* **384**, 153–166 (2015).
81. Andersson, C. D. *et al.* Discovery of ligands for ADP-ribosyltransferases via docking-based virtual screening. *J Med Chem* **55**, 7706–7718 (2012).
82. Ekblad, T., Camaioni, E., Schüler, H. & Macchiarulo, A. PARP inhibitors: polypharmacology versus selective inhibition. *FEBS J* **280**, 3563–3575 (2013).
83. Singh, J., Petter, R. C., Baillie, T. A. & Whitty, A. The resurgence of covalent drugs. *Nat Rev Drug Discov* **10**, 307–317 (2011).
84. Carter-O’Connell, I., Jin, H., Morgan, R. K., David, L. L. & Cohen, M. S. Engineering the substrate specificity of ADP-ribosyltransferases for identifying direct protein targets. *J Am Chem Soc* **136**, 5201–5204 (2014).
85. Carter-O’Connell, I. *et al.* Identifying Family-Member-Specific Targets of Mono-ARTDs by Using a Chemical Genetics Approach. *Cell Rep* **14**, 621–631 (2016).

86. Bürkle, A. Poly(ADP-ribose). The most elaborate metabolite of NAD⁺. *FEBS J* **272**, 4576–4589 (2005).
87. Hertz, N. T. *et al.* Chemical genetic approach for kinase-substrate mapping by covalent capture of thiophosphopeptides and analysis by mass spectrometry. *Curr Protoc Chem Biol* **2**, 15–36 (2010).
88. Islam, K. *et al.* Bioorthogonal profiling of protein methylation using azido derivative of S-adenosyl-L-methionine. *J Am Chem Soc* **134**, 5909–5915 (2012).
89. Wang, L., Brock, A., Herberich, B. & Schultz, P. G. Expanding the genetic code of *Escherichia coli*. *Science* **292**, 498–500 (2001).
90. Hest, J. v, Kiick, K. L. & Tirrell, D. A. Efficient incorporation of unsaturated methionine analogues into proteins in vivo. *Journal of the American ...* (2000). at <<http://pubs.acs.org/doi/abs/10.1021/ja992749j>>
91. Ruf, A., de Murcia, G. & Schulz, G. E. Inhibitor and NAD⁺ binding to poly(ADP-ribose) polymerase as derived from crystal structures and homology modeling. *Biochemistry* **37**, 3893–3900 (1998).
92. Karlberg, T., Hammarström, M., Schütz, P., Svensson, L. & Schüler, H. Crystal structure of the catalytic domain of human PARP2 in complex with PARP inhibitor ABT-888. *Biochemistry* **49**, 1056–1058 (2010).
93. Narwal, M., Venkannagari, H. & Lehtiö, L. Structural basis of selective inhibition of human tankyrases. *J Med Chem* **55**, 1360–1367 (2012).

94. Beneke, S., Alvarez-Gonzalez, R. & Bürkle, A. Comparative characterisation of poly(ADP-ribose) polymerase-1 from two mammalian species with different life span. *Exp Gerontol* **35**, 989–1002 (2000).
95. Nottbohm, A. C., Dothager, R. S., Putt, K. S., Hoyt, M. T. & Hergenrother, P. J. A Colorimetric Substrate for Poly(ADP-Ribose) Polymerase-1, VPARP, and Tankyrase-1. *Angew. Chem. Int. Ed.* **46**, 2066 (2007).
96. Mandal, P. K. & McMurray, J. S. Pd-C-induced catalytic transfer hydrogenation with triethylsilane. *J Org Chem* **72**, 6599–6601 (2007).
97. Lindgren, A. E. G. *et al.* PARP inhibitor with selectivity toward ADP-ribosyltransferase ARTD3/PARP3. *ACS Chem Biol* **8**, 1698–1703 (2013).
98. Venkannagari, H., Fallarero, A., Feijs, K. L. H., Lüscher, B. & Lehtiö, L. Activity-based assay for human mono-ADP-ribosyltransferases ARTD7/PARP15 and ARTD10/PARP10 aimed at screening and profiling inhibitors. *Eur J Pharm Sci* **49**, 148–156 (2013).
99. Morgan, R. K. & Cohen, M. S. A Clickable Aminooxy Probe for Monitoring Cellular ADP-Ribosylation. *ACS Chem Biol* **10**, 1778–1784 (2015).
100. Meyer-Ficca, M. L. *et al.* Spermatid head elongation with normal nuclear shaping requires ADP-ribosyltransferase PARP11 (ARTD11) in mice. *Biol Reprod* **92**, 80 (2015).
101. Morgan, R. K. & Cohen, M. S. Detecting Protein ADP-Ribosylation Using a Clickable Aminooxy Probe. *Methods Mol Biol* **1608**, 71–77 (2017).

102. Daniels, C. M., Ong, S.-E. & Leung, A. K. L. Phosphoproteomic Approach to Characterize Protein Mono- and Poly(ADP-ribosyl)ation Sites from Cells. *Journal of proteome research* **13**, 3510 (2014).
103. Bredehorst, R. *et al.* Two different types of bonds linking single ADP-ribose residues covalently to proteins. Quantification in eukaryotic cells. *Eur J Biochem* **92**, 129–135 (1978).
104. Riquelme, P. T., Burzio, L. O. & Koide, S. S. ADP ribosylation of rat liver lysine-rich histone in vitro. *J Biol Chem* **254**, 3018–3028 (1979).
105. Feijs, K. L. *et al.* ARTD10 substrate identification on protein microarrays: regulation of GSK3 β by mono-ADP-ribosylation. *Cell Commun Signal* **11**, 5 (2013).
106. Kleine, H. *et al.* Substrate-assisted catalysis by PARP10 limits its activity to mono-ADP-ribosylation. *Mol Cell* **32**, 57–69 (2008).
107. Wendeler, M., Grinberg, L., Wang, X., Dawson, P. E. & Baca, M. Enhanced catalysis of oxime-based bioconjugations by substituted anilines. *Bioconjug Chem* **25**, 93–101 (2014).
108. Moyle, P. M. & Muir, T. W. Method for the synthesis of mono-ADP-ribose conjugated peptides. *J Am Chem Soc* **132**, 15878–15880 (2010).
109. Chaikin, S. W. & Brown, W. G. Reduction of Aldehydes, Ketones and Acid Chlorides by Sodium Borohydride. *J Am Chem Soc* **71**, 122 (1949).
110. Rosenthal, F. *et al.* Macrod domain-containing proteins are new mono-ADP-ribosylhydrolases. *Nat Struct Mol Biol* **20**, 502–507 (2013).

111. Jankevicius, G. *et al.* A family of macrodomain proteins reverses cellular mono-ADP-ribosylation. *Nat Struct Mol Biol* **20**, 508–514 (2013).
112. Peterson, F. C. *et al.* Orphan macrodomain protein (human C6orf130) is an O-acyl-ADP-ribose deacylase: solution structure and catalytic properties. *J Biol Chem* **286**, 35955–35965 (2011).
113. Chen, D. *et al.* Identification of macrodomain proteins as novel O-acetyl-ADP-ribose deacetylases. *J Biol Chem* **286**, 13261–13271 (2011).
114. Yu, M. *et al.* PARP-10, a novel Myc-interacting protein with poly(ADP-ribose) polymerase activity, inhibits transformation. *Oncogene* **24**, 1982–1993 (2005).
115. Kleine, H. *et al.* Dynamic subcellular localization of the mono-ADP-ribosyltransferase ARTD10 and interaction with the ubiquitin receptor p62. *Cell Commun Signal* **10**, 28 (2012).
116. Schraufstatter, I. U., Hinshaw, D. B., Hyslop, P. A., Spragg, R. G. & Cochrane, C. G. Oxidant injury of cells. DNA strand-breaks activate polyadenosine diphosphate-ribose polymerase and lead to depletion of nicotinamide adenine dinucleotide. *J Clin Invest* **77**, 1312–1320 (1986).
117. Bürkle, A., Chen, G., Küpper, J. H., Grube, K. & Zeller, W. J. Increased poly(ADP-ribosyl)ation in intact cells by cisplatin treatment. *Carcinogenesis* **14**, 559–561 (1993).
118. Yuen, L. H., Saxena, N. S., Park, H. S., Weinberg, K. & Kool, E. T. Dark hydrazone fluorescence labeling agents enable imaging of cellular aldehydic load. *ACS Chem Biol* **11**, 2312–2319 (2016).

119. Kool, E. T., Crisalli, P. & Chan, K. M. Fast alpha nucleophiles: structures that undergo rapid hydrazone/oxime formation at neutral pH. *Org Lett* **16**, 1454–1457 (2014).
120. Crisalli, P. & Kool, E. T. Water-soluble organocatalysts for hydrazone and oxime formation. *J Org Chem* **78**, 1184–1189 (2013).
121. Crisalli, P. & Kool, E. T. Importance of ortho proton donors in catalysis of hydrazone formation. *Org Lett* **15**, 1646–1649 (2013).
122. Sharifi, R. *et al.* Deficiency of terminal ADP-ribose protein glycohydrolase TARG1/C6orf130 in neurodegenerative disease. *EMBO J* **32**, 1225–1237 (2013).
123. Morgan, R. K., Carter-O'Connell, I. & Cohen, M. S. Selective inhibition of PARP10 using a chemical genetics strategy. *Bioorg Med Chem Lett* **25**, 4770–4773 (2015).
124. Leung, A. K. L. *et al.* Poly(ADP-ribose) regulates stress responses and microRNA activity in the cytoplasm. *Mol Cell* **42**, 489–499 (2011).
125. Cho-Park, P. F. & Steller, H. Proteasome regulation by ADP-ribosylation. *Cell* **153**, 614–627 (2013).
126. Huang, S.-M. A. *et al.* Tankyrase inhibition stabilizes axin and antagonizes Wnt signalling. *Nature* **461**, 614–620 (2009).
127. Kurouchi, H. *et al.* Activation of electrophilicity of stable Y-delocalized carbamate cations in intramolecular aromatic substitution reaction: evidence for formation of diprotonated carbamates leading to generation of isocyanates. *J Org Chem* **77**, 9313–9328 (2012).

128. Gibson, B. A. *et al.* Chemical genetic discovery of PARP targets reveals a role for PARP-1 in transcription elongation. *Science* **353**, 45–50 (2016).
129. Kurouchi, H., Sumita, A., Otani, Y. & Ohwada, T. Protonation switching to the least-basic heteroatom of carbamate through cationic hydrogen bonding promotes the formation of isocyanate cations. *Chemistry (Easton)* **20**, 8682–8690 (2014).
130. Gupte, R., Liu, Z. & Kraus, W. L. PARPs and ADP-ribosylation: recent advances linking molecular functions to biological outcomes. *Genes Dev* **31**, 101–126 (2017).
131. Upton, K. *et al.* Design and synthesis of potent inhibitors of the mono(ADP-ribosyl)transferase, PARP14. *Bioorg Med Chem Lett* **27**, 2907–2911 (2017).
132. Nicolae, C. M. *et al.* The ADP-ribosyltransferase PARP10/ARTD10 interacts with proliferating cell nuclear antigen (PCNA) and is required for DNA damage tolerance. *J Biol Chem* **289**, 13627–13637 (2014).
133. Ruf, A., Mennissier de Murcia, J., de Murcia, G. & Schulz, G. E. Structure of the catalytic fragment of poly(AD-ribose) polymerase from chicken. *Proc Natl Acad Sci U S A* **93**, 7481–7485 (1996).
134. Suto, M. J., Turner, W. R., Arundel-Suto, C. M., Werbel, L. M. & Sebolt-Leopold, J. S. Dihydroisoquinolinones: the design and synthesis of a new series of potent inhibitors of poly(ADP-ribose) polymerase. *Anticancer Drug Des* **6**, 107–117 (1991).
135. Langelier, M.-F., Riccio, A. A. & Pascal, J. M. PARP-2 and PARP-3 are selectively activated by 5' phosphorylated DNA breaks through an allosteric

- regulatory mechanism shared with PARP-1. *Nucleic Acids Res* **42**, 7762–7775 (2014).
136. Luo, X. & Kraus, W. L. On PAR with PARP: cellular stress signaling through poly(ADP-ribose) and PARP-1. *Genes Dev* **26**, 417–432 (2012).
137. Ying, W., Alano, C. C., Garnier, P. & Swanson, R. A. NAD⁺ as a metabolic link between DNA damage and cell death. *J Neurosci Res* **79**, 216–223 (2005).
138. Ha, H. C. & Snyder, S. H. Poly(ADP-ribose) polymerase is a mediator of necrotic cell death by ATP depletion. *Proc Natl Acad Sci U S A* **96**, 13978–13982 (1999).
139. Carter-O’Connell, I. & Cohen, M. S. Identifying Direct Protein Targets of Poly-ADP-Ribose Polymerases (PARPs) Using Engineered PARP Variants-Orthogonal Nicotinamide Adenine Dinucleotide (NAD⁺) Analog Pairs. *Curr Protoc Chem Biol* **7**, 121–139 (2015).

Appendix A: Protocol for Detecting Protein ADP-ribosylation Using a Clickable Aminoxy Probe

Rory K. Morgan and Michael S. Cohen

This protocol originally appeared in *Methods Mol. Bio* published online on July 11, 2017 as part of Alexei V. Tulin (ed.), Poly(ADP-Ribose) Polymerase: Methods and Protocols (Copyright © Springer Science+Business Media LLC 2017).¹⁰¹

1. Materials

1.1 Cell Culture and Transfection

1. HEK 293T cells
2. Cell media: Dulbecco's Modified Eagle Medium (DMEM), high glucose, with 10% fetal bovine serum (FBS), 1% GlutaMAX™ supplement, 1% penicillin/streptomycin (Pen-Strep). Filter sterilize and store at 4 °C.
3. GFP-PARP10 plasmid DNA²⁷ in diethylpyrocarbonate (DEPC)-treated water (>1 µg/µL) (see **Note 1**).
4. Sterile water
5. Calcium chloride (CaCl₂): 2M solution in water
6. 2x HEPES-buffered saline (HBS): 50 mM 4-(2-hydroxyethyl)-1-piperazineethanesulfonic acid (HEPES), 280 mM NaCl, 1.5 mM

Na₂HPO₄ adjusted to pH 7.05-7.12 with NaOH. Filter sterilize, aliquot, and store at -20 °C.

1.2 *In cellulo* labeling of protein ADP-ribosylation on acidic amino acids using AO-alkyne

1. Cell media
2. Aminoxy-alkyne-HCl (AO-alkyne) [6]: 200 mM stock solution in DMSO (400x). Store at -20 °C.
3. 2,4-Dimethoxyaniline (DMA) catalyst: 1 M stock solution in DMSO (200x). Make solution fresh for each use.
4. PBS (1x): Store at 4 °C.

1.3 Generation of lysates and click chemistry

1. Lysis buffer (see **Note 2**): 25 mM HEPES adjusted to pH 7.5 with HCl or NaOH, 50 mM NaCl, 10% (v/v) glycerol, 1% Nonidet P-40 (NP-40), and 1x protease inhibitor cocktail (see **Note 3**). Store at 4 °C.
2. Microcentrifuge (Eppendorf 5418) with rotor (Eppendorf FA-45-18-11)
3. Bradford reagent
4. Bovine serum albumin (BSA): 1.0 mg/mL to 0.2 mg/mL standards in water
5. Click buffer (9x):
 - a. PBS (1x) with 1% (w/v) SDS

Add the following components to the buffer in the following order (see **Note 4**):

- b. Tris[(1-benzyl-1*H*-1,2,3-triazol-4-yl)methyl]amine (TBTA): 18 mM stock solution in DMSO (20x). Store at -20 °C.
 - c. Copper(II) sulfate (CuSO₄): 45 mM stock solution in water (5x). Store at room temperature.
 - d. Biotin-PEG3-Azide (Click Chemistry Tools): 9 mM stock solution in DMSO (10x). Store at -20 °C.
 - e. Tris(2-carboxyethyl)phosphine hydrochloride (TCEP): 90 mM stock solution in water (10x) (see **Note 5**).
6. Sample buffer (4x): 200 mM tris(hydroxymethyl)aminomethane-HCl (Tris-Cl) adjusted to pH 6.8 with HCl, 8% (w/v) SDS, 40% (v/v) glycerol, 50 mM ethylenediaminetetraacetic acid (EDTA), 0.08% (w/v) bromophenol blue. Store indefinitely at room temperature. For a working solution, add 50 µL of 14.7 M β-mercaptoethanol (BME) to 950 µL of 4x sample buffer. Store up to 6 weeks at -20 °C after addition of BME.

7. Protein ladder: 10 - 250 kD

1.4 SDS-PAGE and immunoblotting

- 1. SDS-PAGE electrophoretic system
- 2. 4% stack/10% resolving Tris-Cl SDS-PAGE gel
- 3. SDS-PAGE running buffer: 0.025M Tris, 0.192M glycine, 0.1% (w/v) SDS
- 4. Nitrocellulose
- 5. Immunoblot transfer system

6. Transfer buffer: 0.025M Tris, 0.192M glycine, 20% MeOH. Store at 4 °C.
7. Tris-buffered saline (TBS; 10x): 500 mM Tris-Cl adjusted to pH 7.6 with HCl, 1.5 M NaCl
8. TBS (1x) containing 0.1% Tween-20 (TBST)
9. Blocking solution: 5% (w/v) milk in TBST
10. Streptavidin-HRP buffer: 1:3333 dilution in TBST. Dissolve 3 µL 0.5 mg/mL stock streptavidin-HRP (Jackson ImmunoResearch) in 10 mL TBST.
11. Anti-GFP antibody: 1:1000 dilution in antibody dilution (AbDil) buffer. Dissolve 2 µL 1.0 mg/mL stock (Abcam) in 10 mL AbDil (see **Note 6**).

2. Methods

Carry out all procedures at room temperature unless specified otherwise. Cells are grown in a 6-well plate at 37 °C in the presence of 5% CO₂.

2.1 Transfection

1. Seed HEK293T cells the day before transfection so that ~70% confluency is reached at time of transfection (see **Note 7**).
2. Prepare transfection solution by diluting GFP-PARP10 plasmid DNA in sterile water containing 248 mM CaCl₂ (see **Note 8**).
3. While gently vortexing, add 2x HBS solution dropwise to solution in Step 2. Allow to incubate at room temperature for 5-15 minutes.

4. Add 200 λ transfection solution from Step 3 to each well of a 6-well plate. Gently rock plate back and forth to mix (see **Note 9**). Incubate cells for 6-8h.
5. Remove media containing transfection mixture and wash once with media and replace with fresh media. Incubate overnight (see **Note 10**).

2.2 *In cellulo* labeling of protein ADP-ribosylation on acidic amino acids using AO-alkyne

1. Prepare labeling media (see **Note 11**). To pre-warmed cell media add 400x stock of AO-alkyne and 200x stock of DMA catalyst and mix by pipetting mixture up and down (see **Note 12**).
2. Remove media from cells and replace with 2 mL labeling media from Step 1. Incubate for 1h.
3. Remove media and wash cells 1x with cold PBS. Cells can be frozen at -80 °C until ready for next step.

2.3 Generation of lysates and click chemistry

1. Lyse cells in 150 λ cold lysis buffer per well of a 6-well plate. Allow plate to sit on ice while cells thaw in lysis buffer. Pipet lysates up and down gently to mix (5-10X). Centrifuge samples at 14,000g for 5 minutes at 4 °C.
2. Quantify total protein levels using Bradford reagent (see **Note 13**).

3. Normalize protein levels using lysis buffer as a diluent. A total protein concentration of 2-5 mg/mL is suggested for efficient click chemistry in next step.
4. Add 5 λ 9x click buffer to 40 λ normalized lysates from Step 3. Incubate for 30 minutes (see **Note 14**).
5. Add 15 λ 4x sample buffer to each sample. Boil samples at 95 °C for 5 minutes.

2.4 SDS-PAGE and immunoblotting

1. Load the samples (20 – 50 μ g total protein) and protein ladder to a 4%/10% Tris-Cl gel and fractionate via SDS-PAGE (see **Note 15**).
2. Move the gel to an immunoblot system and transfer the proteins from the gel to a nitrocellulose membrane (see **Note 16**).
3. Block membrane for 1h and probe with streptavidin-HRP or GFP for 1h to quantify labeling of PARP10 and protein levels of PARP10, respectively.

3. Notes

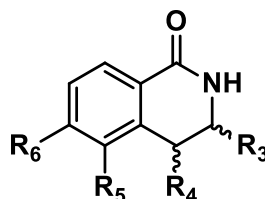
1. Plasmid DNA obtained from midi-preparation should be sufficiently pure and at a concentration suitable for transfection.
2. Do not use lysis buffers containing Tris buffer or disulfide reducing agents (e.g., DTT, BME) as they can inhibit the click reaction.
3. EDTA-free inhibitor cocktail should be used to prevent inhibition of click reaction via chelation of copper by EDTA.

4. A noticeable color change from light blue to darker yellow-green should occur upon addition of TCEP.
5. Prepare fresh for best results.
6. Antibody dilution (AbDil) buffer: TBST with 2% BSA and 0.1% sodium azide (NaN_3).
7. A 1:6 split of fully confluent HEK293T cells is usually sufficient to achieve ~70% confluency 18-24h post-seeding.
8. 2 μg of GFP-PARP10 plasmid DNA per well of a 6-well plate is sufficient for ~50-75% transfection efficiency of HEK293T cells.
9. Avoid mixing in a circular fashion as this concentrates the transfection mixture in the center of the well.
10. Transfection can be verified by fluorescence microscopy. About 50-75% transfection efficiency can be observed with GFP-PARP10 18h post-transfection.
11. Pre-warming media to 37 °C prior to addition of DMA catalyst stock solution aids in solubility.
12. This results in final concentrations of 500 μM AO-alkyne and 5 mM DMA catalyst and 0.75% DMSO.
13. Samples in lysis buffer will need to be diluted 1:10 with water to avoid interference of detergent with Bradford reagent.
14. To increase signal, biotinylated proteins can be enriched via immunoprecipitation using NeutrAvidin agarose resin as outlined previously.^{84,85,139}

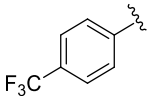
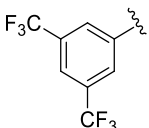
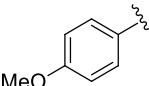
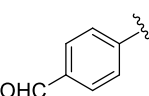
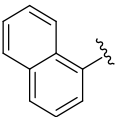
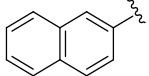
15. 150V for 60 minutes is sufficient to resolve GFP-PARP10 (137 kD).
16. Overnight transfer (16h) at 30V at 4 °C results in complete transfer of proteins to nitrocellulose membrane.

Appendix B: Table of IC₅₀ Values for Additional dq Compounds

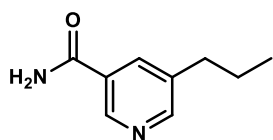
Table B-1. Approximate IC₅₀ values for additional dq compounds not appearing in Chapter 5



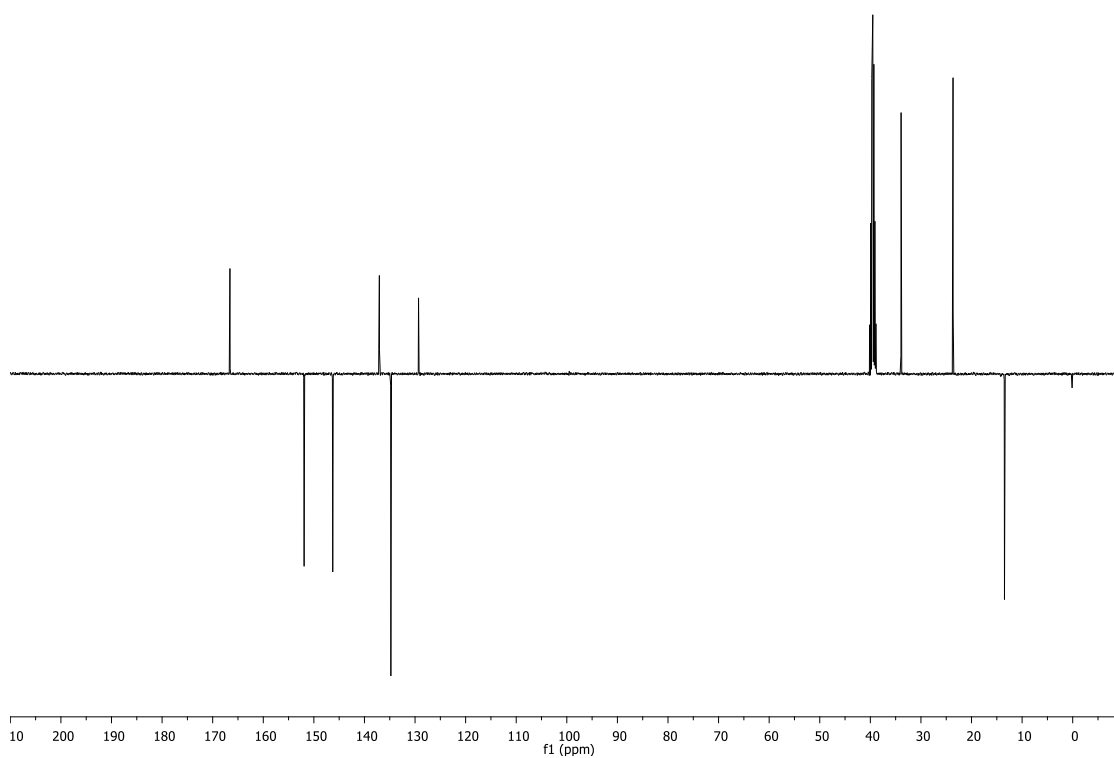
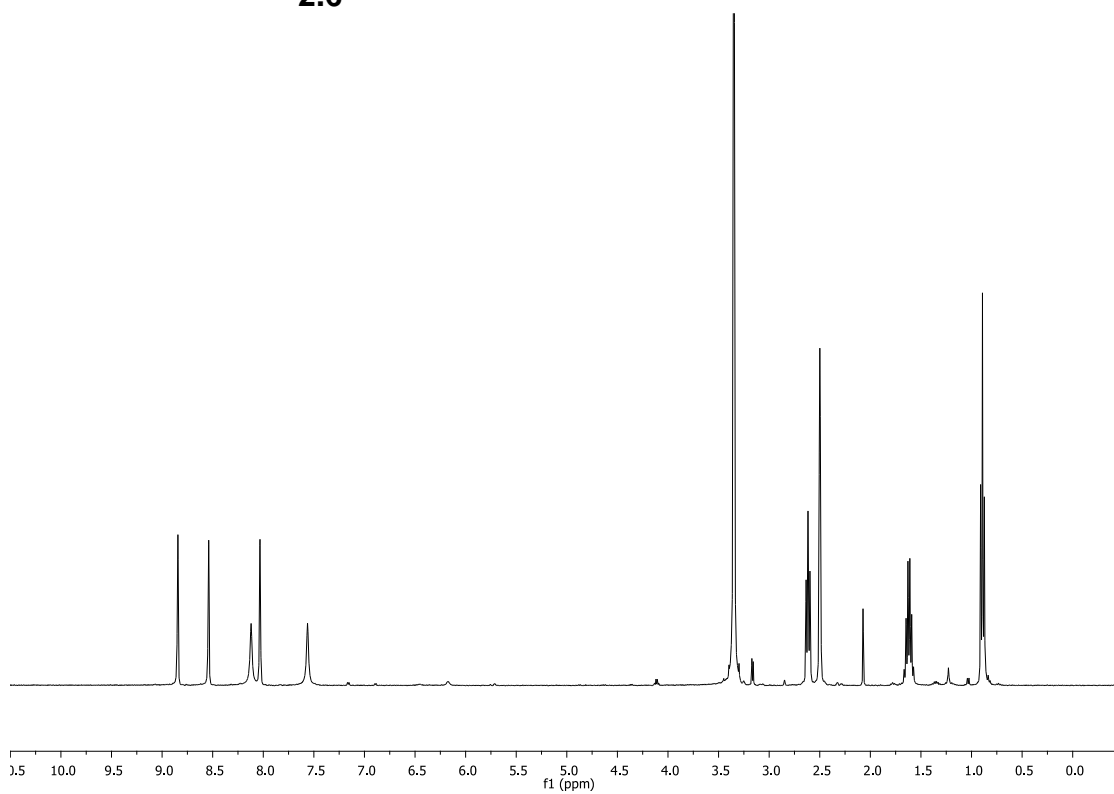
ID	-R ₃	-R ₄	-R ₅	-R ₆	IC ₅₀ (μM)			
					PARP10	PARP11	PARP14	PARP15
5.1	H	H	H	H	70.3	8.0	>30	>30
5.40	COOMe	H	H	H	>30			
5.41	COOH	H	H	H	>30			
5.42	H	Me	H	H	~30	~30		>30
5.43	H	Ph	H	H	>30			
5.44	H	H	Cl	H	~5			
5.45	H	H	Et	H	~5	~1	>30	~30
5.46	H	H	OMe	H	~5			
5.47	H	H	NH ₂	H	>30			
5.48	H	H	NHAc	H	>30			
5.49	H	H	NHBz	H	~30			
5.50	H	H	Bn	H	~1	<1	>30	~30
5.51	H	H	OBn	H	~5			
5.52	H	H	H	Et	~30	~30	>30	>30
5.53	H	H	H	PhenEt	~5			
5.54	H	H	H		7.5	~30		
5.55	H	H	H		2.5	4.9		
5.56	H	H	H		~30	>30		
5.57	H	H	H		2.8	8.8		
5.58	H	H	H		28	>30		

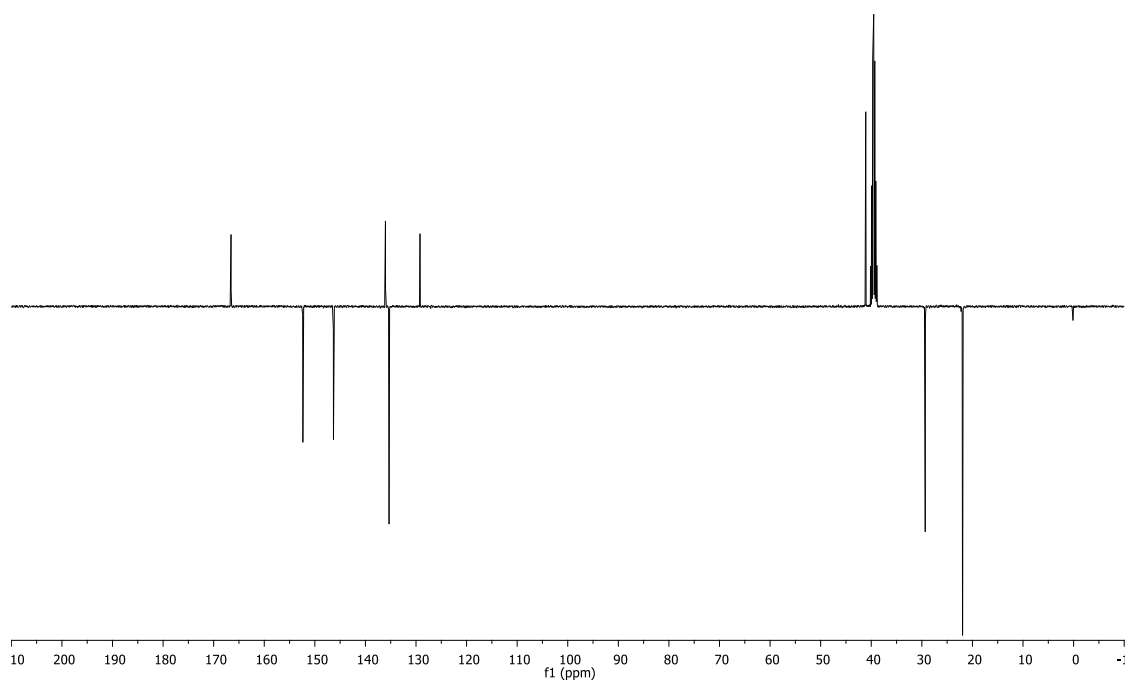
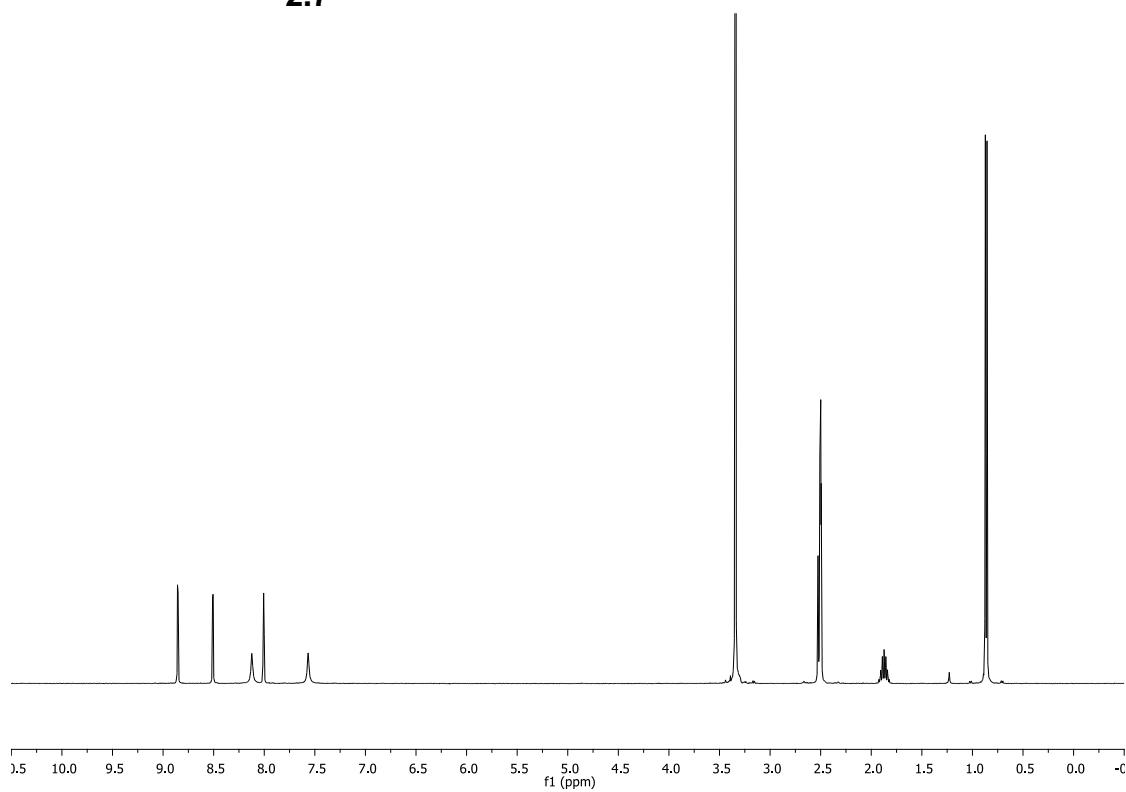
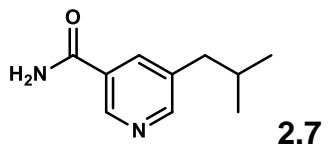
5.59	H	H	H		5.5	32
5.60	H	H	H		>30	>30
5.61	H	H	H		5.0	8.3
5.62	H	H	H		5.5	11
5.63	H	H	H		17.4	10.6
5.64	H	H	H		2.2	12.4

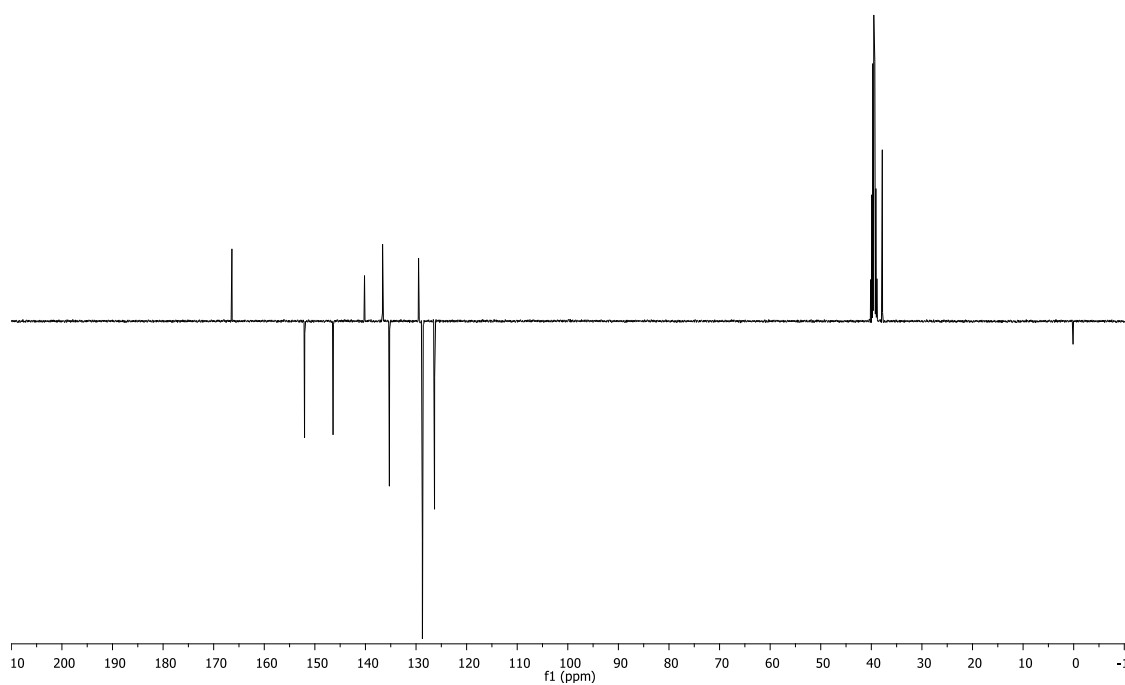
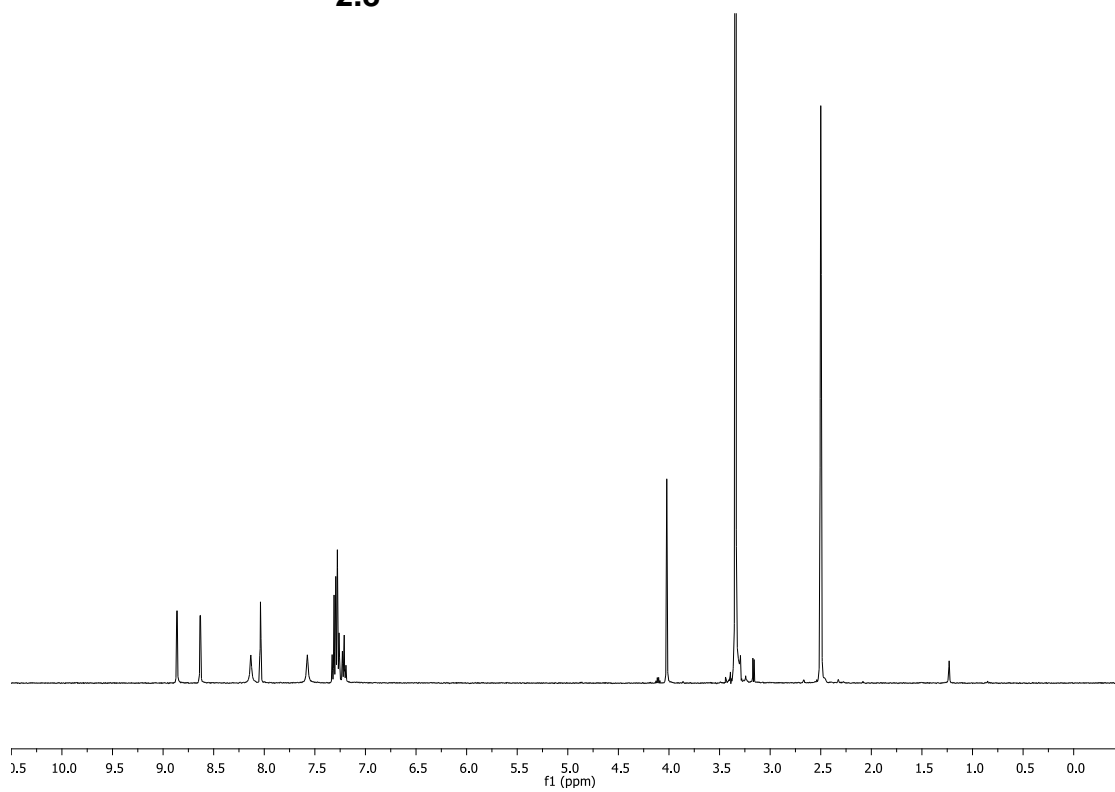
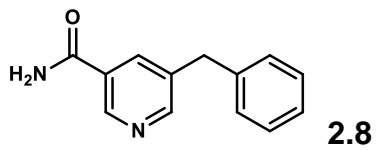
Appendix C: ^1H and ^{13}C NMR Spectra

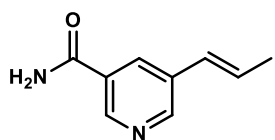


2.6

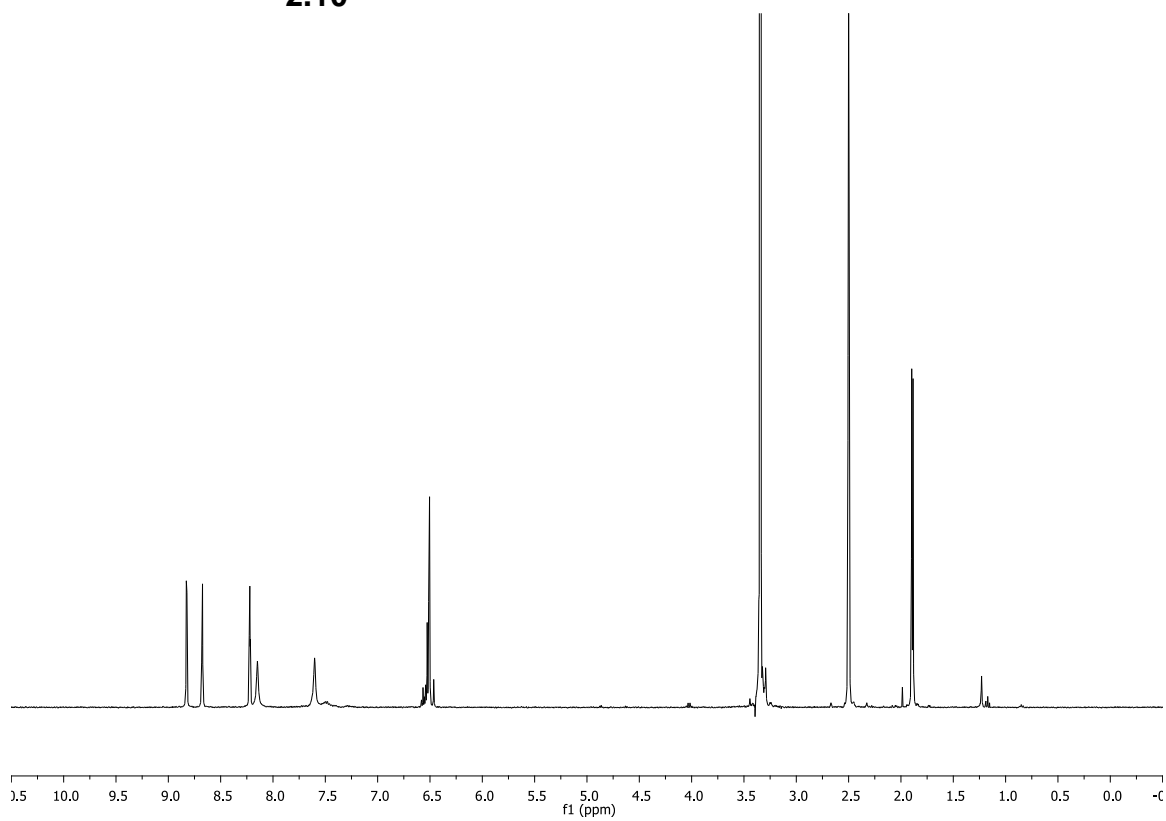


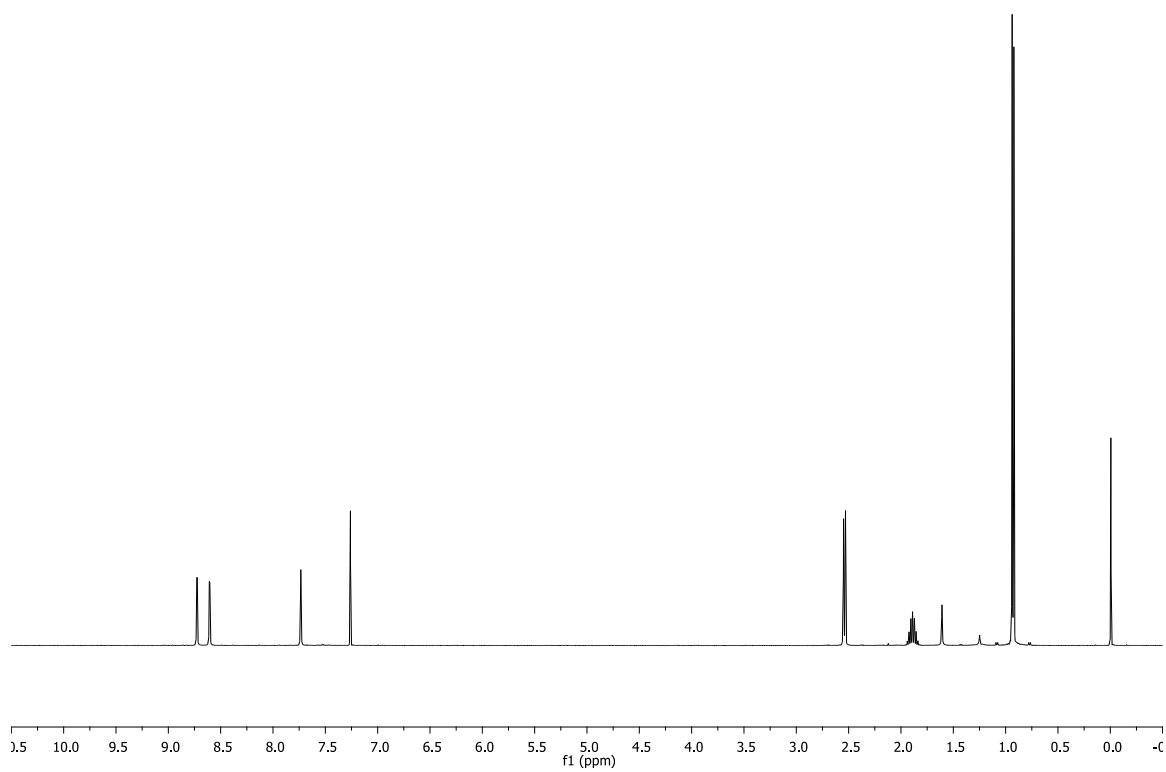
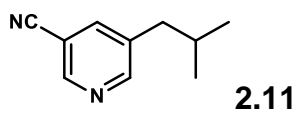


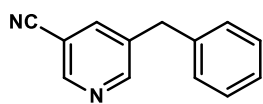




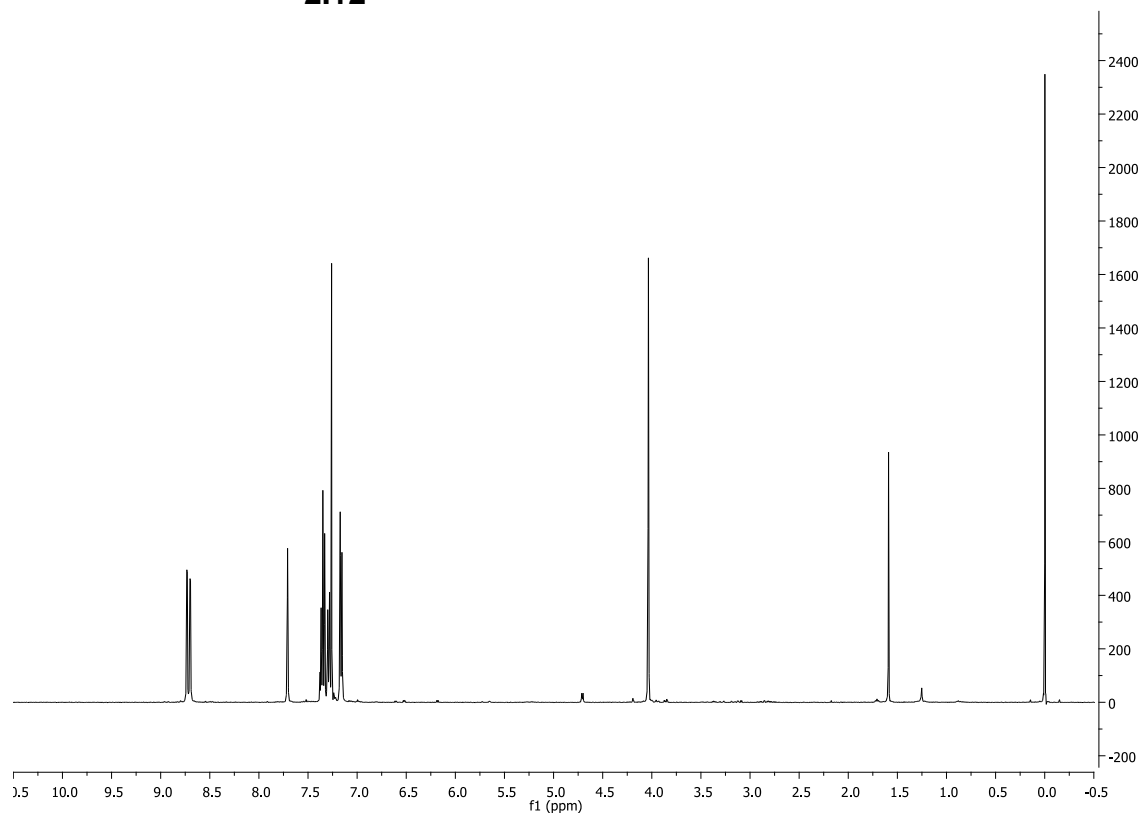
2.10

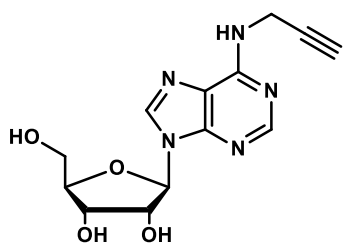




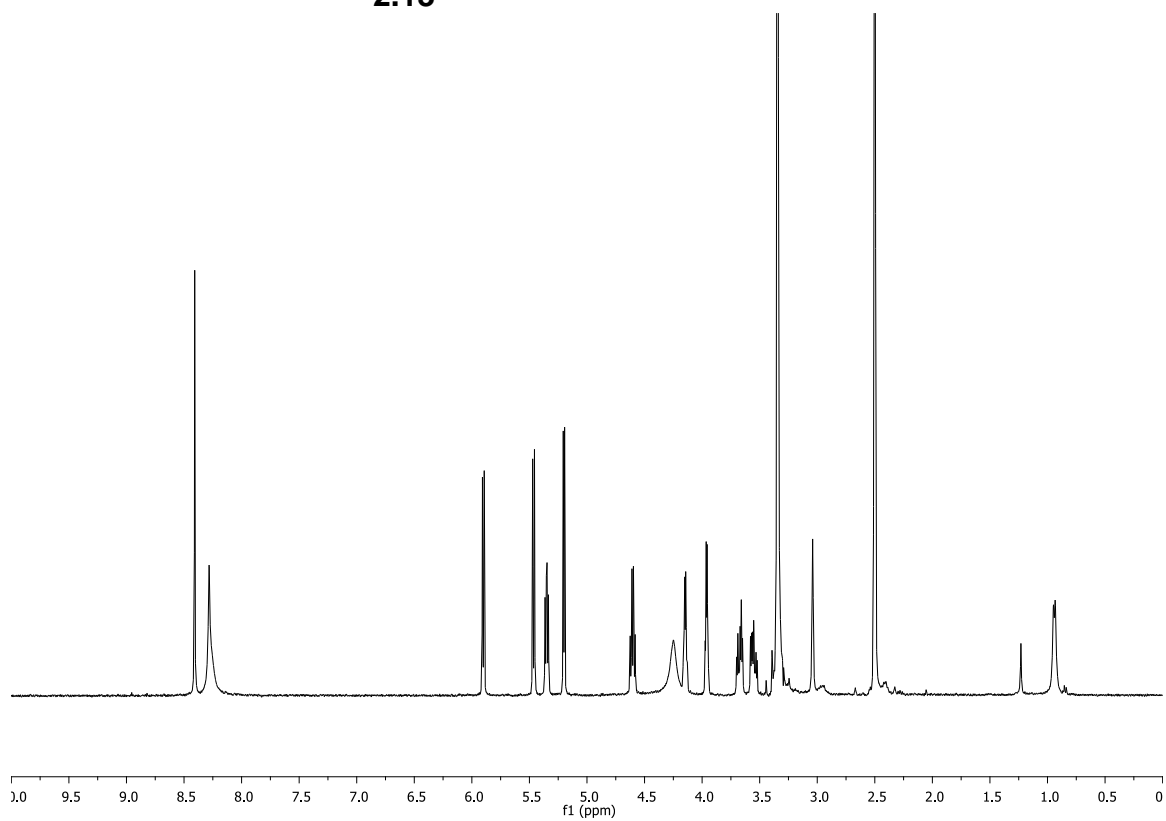


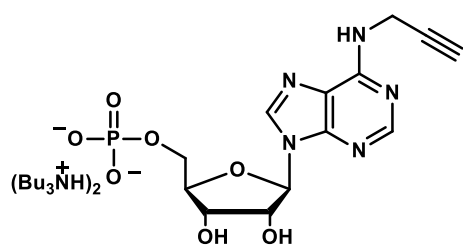
2.12



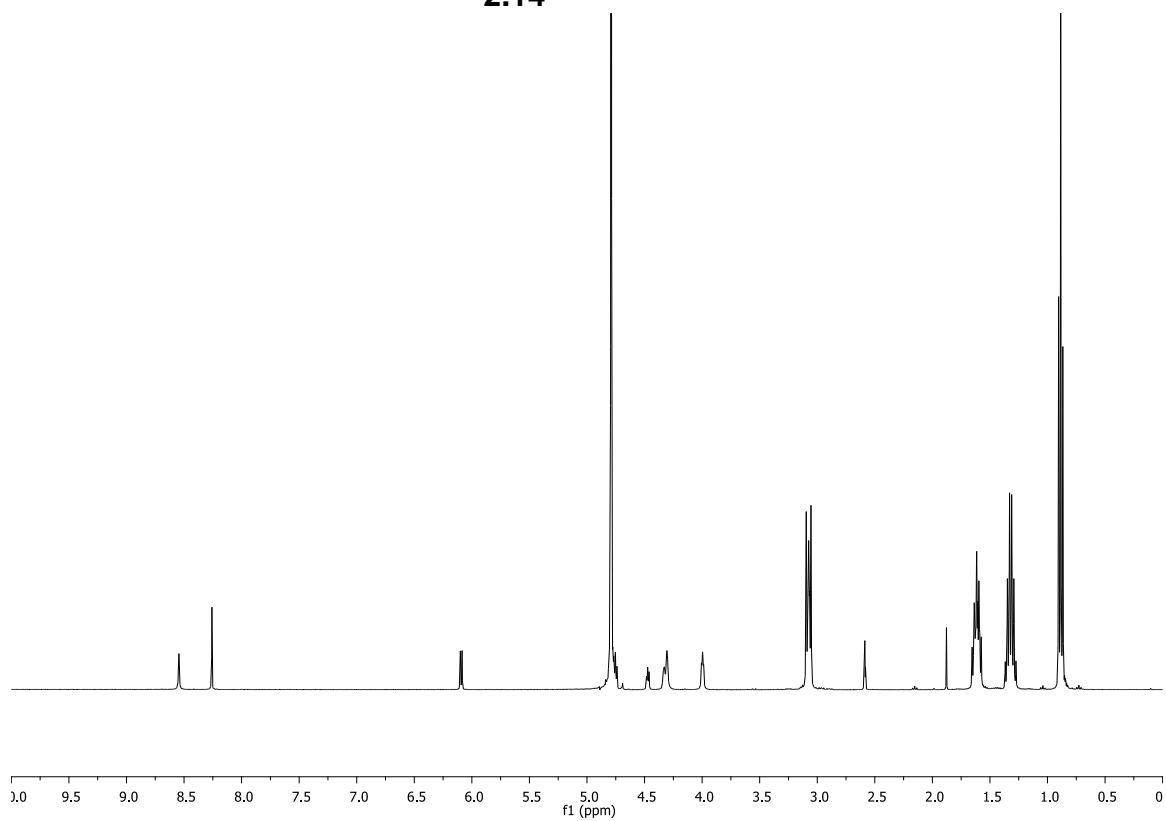


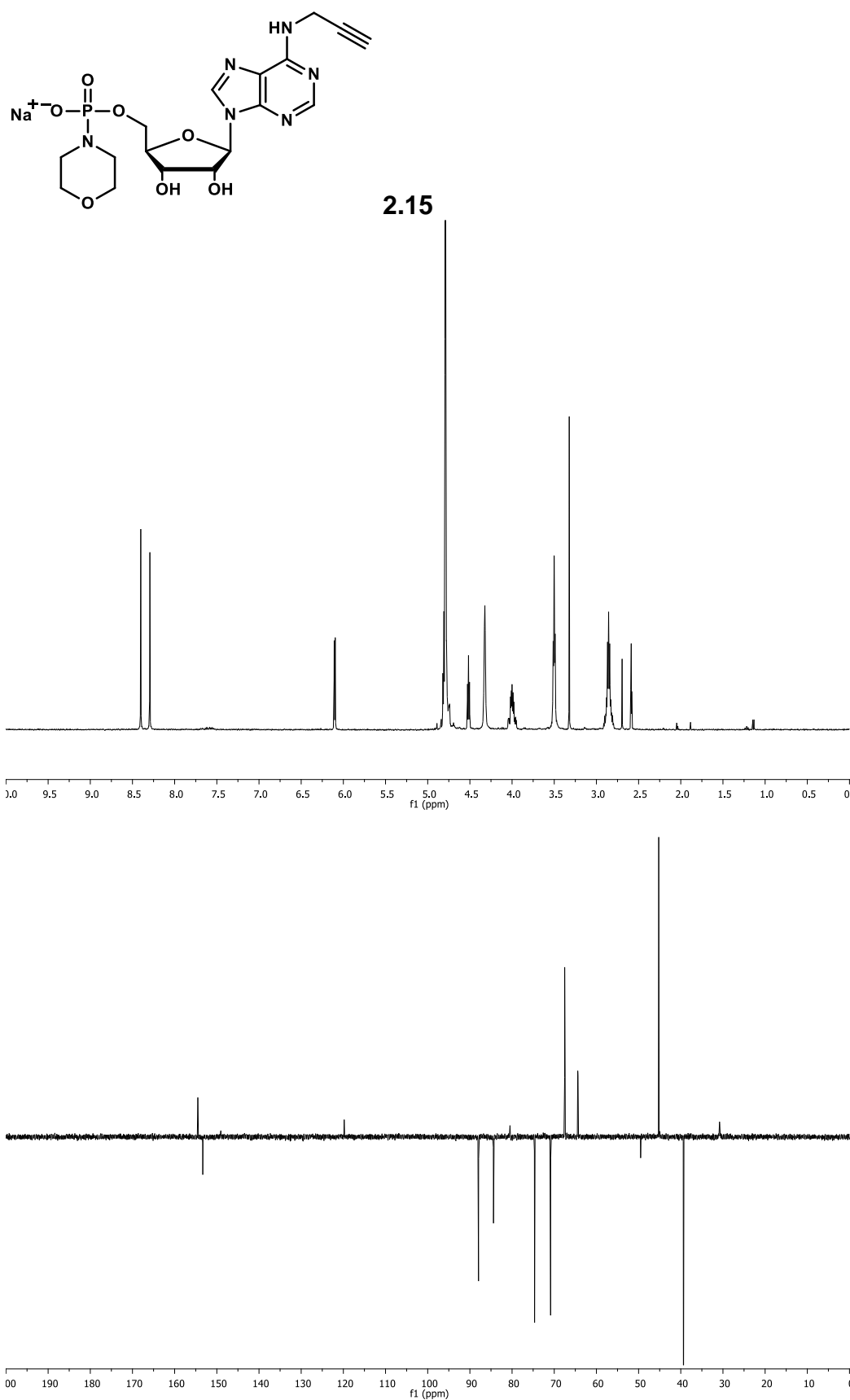
2.13

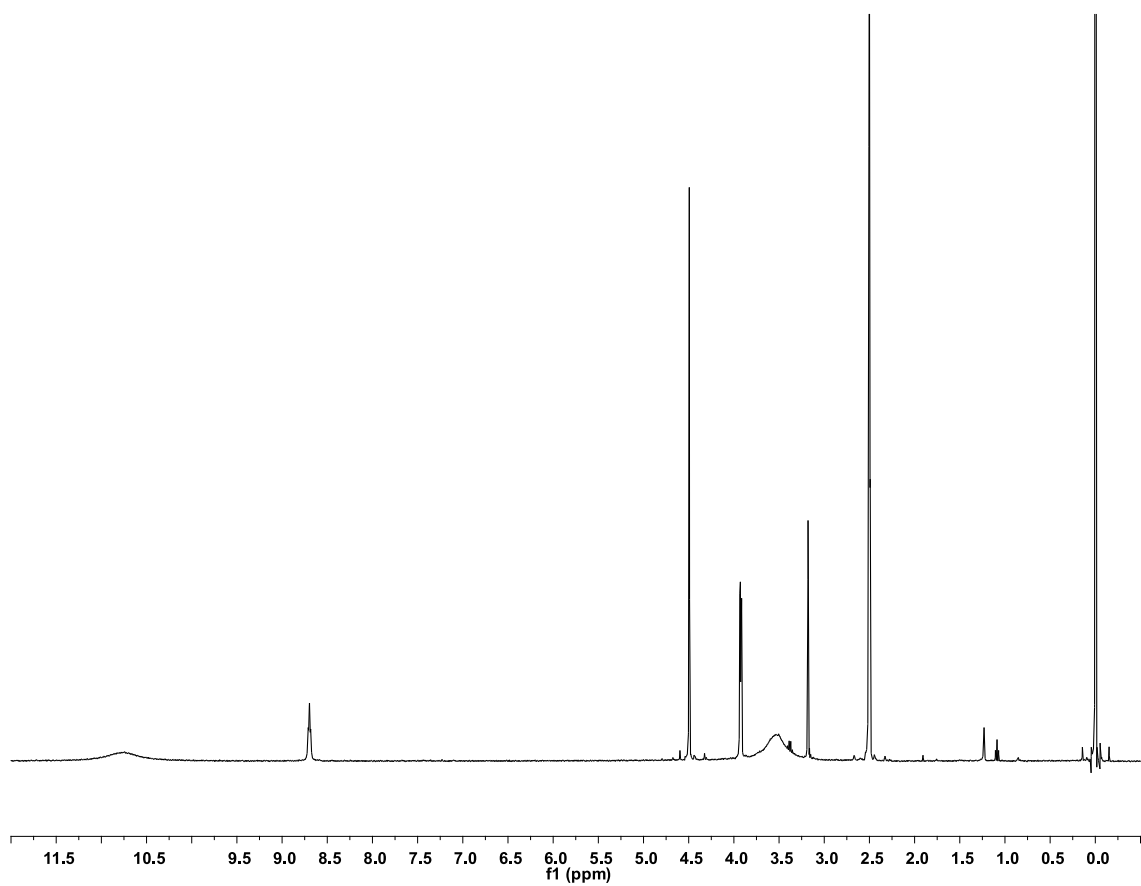
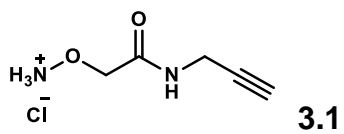


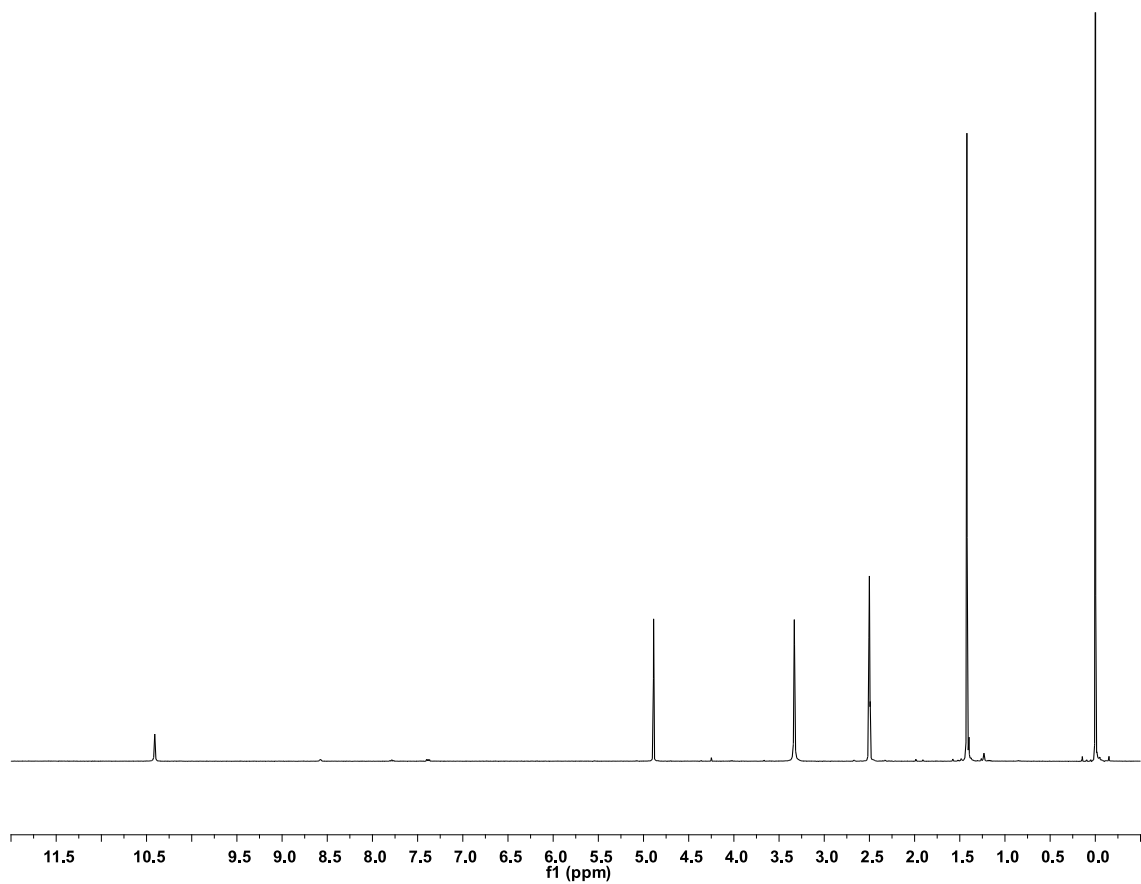
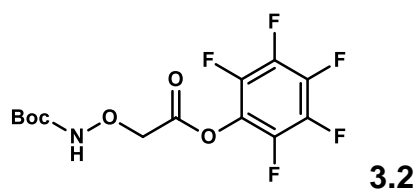


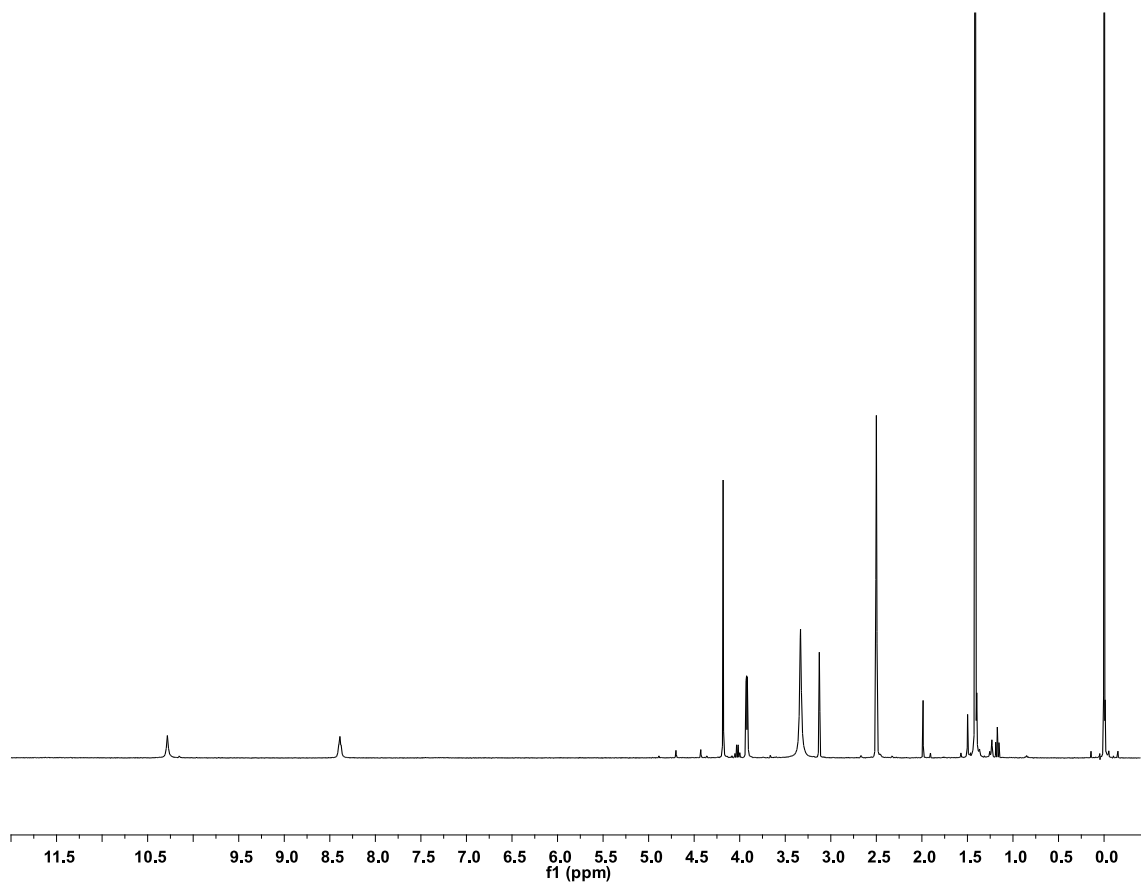
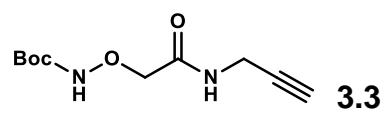
2.14

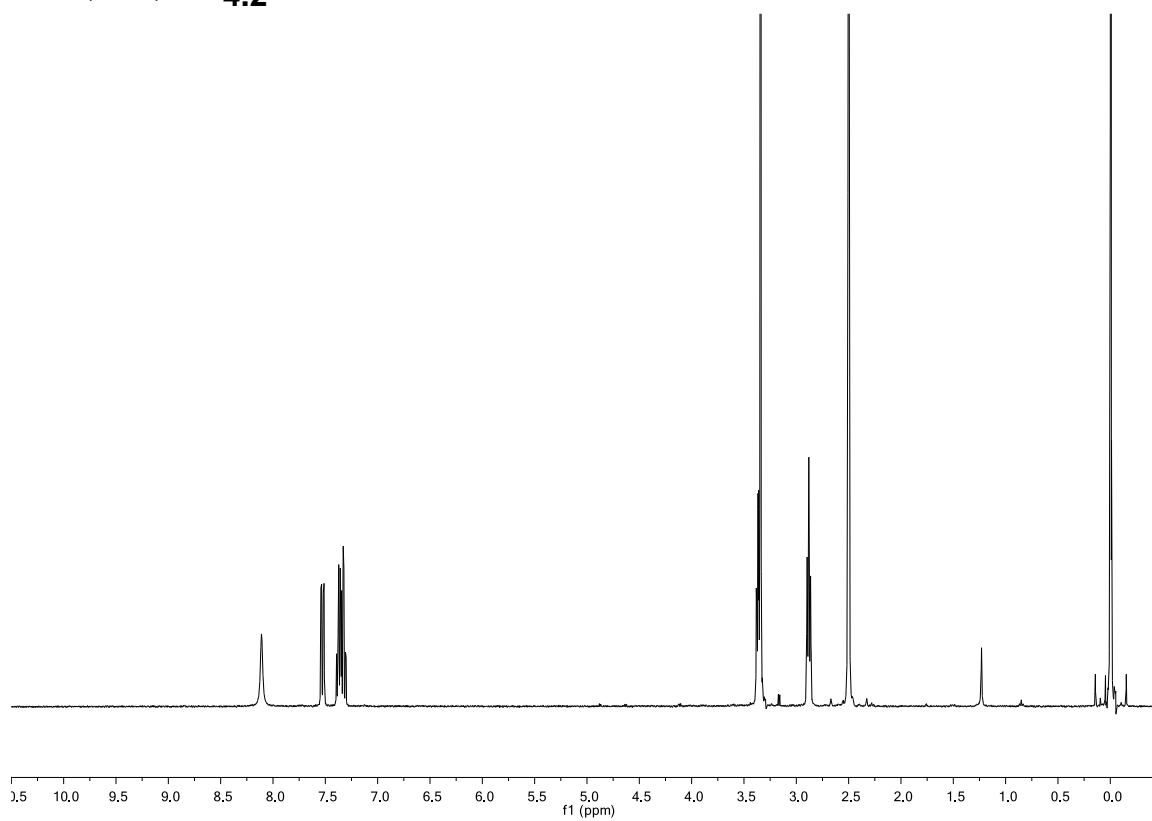
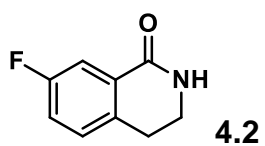


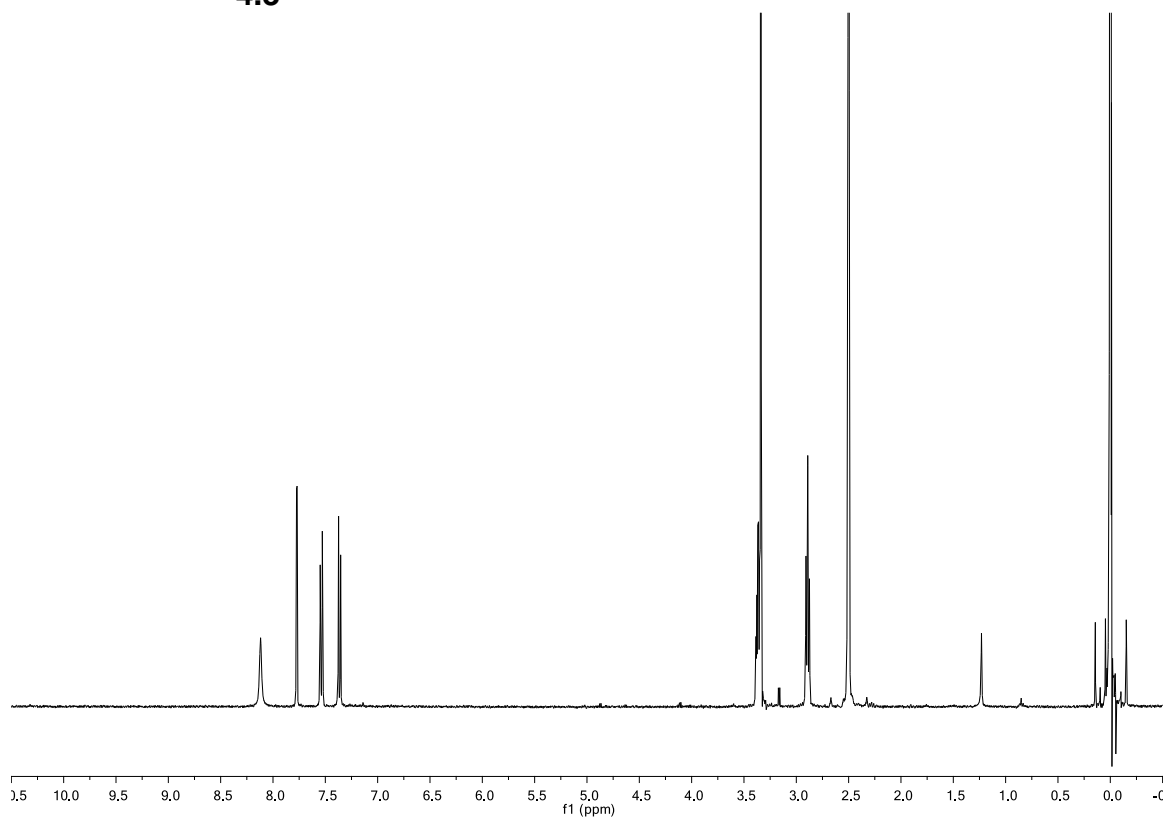
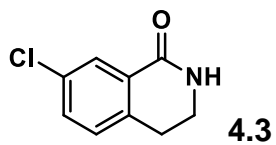


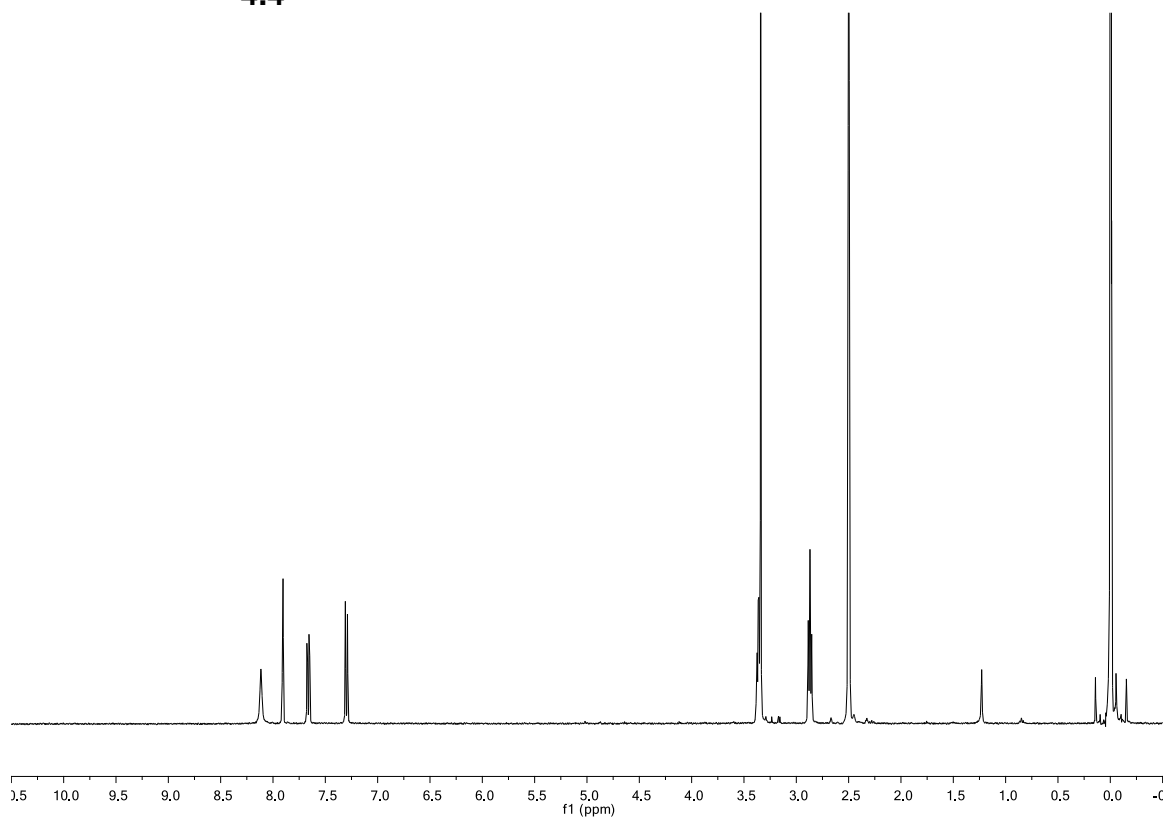


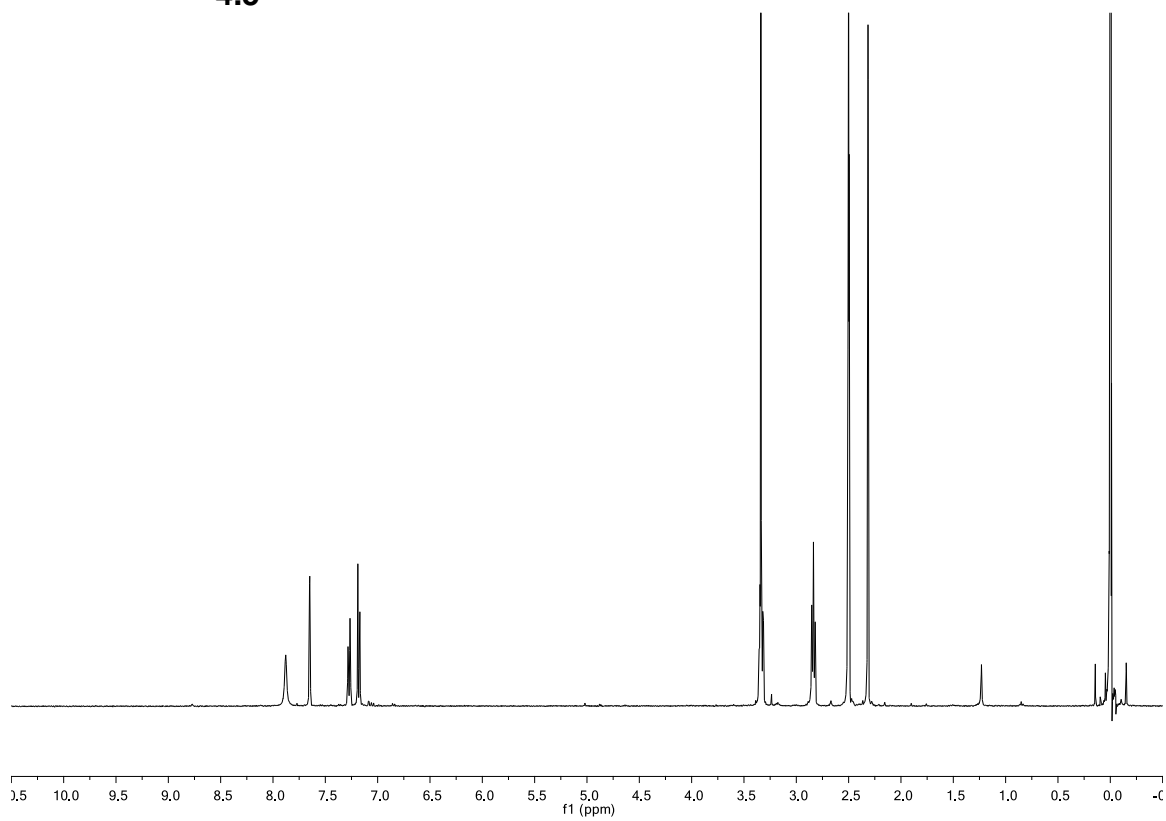
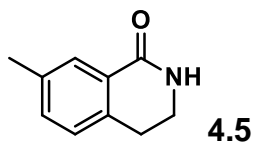


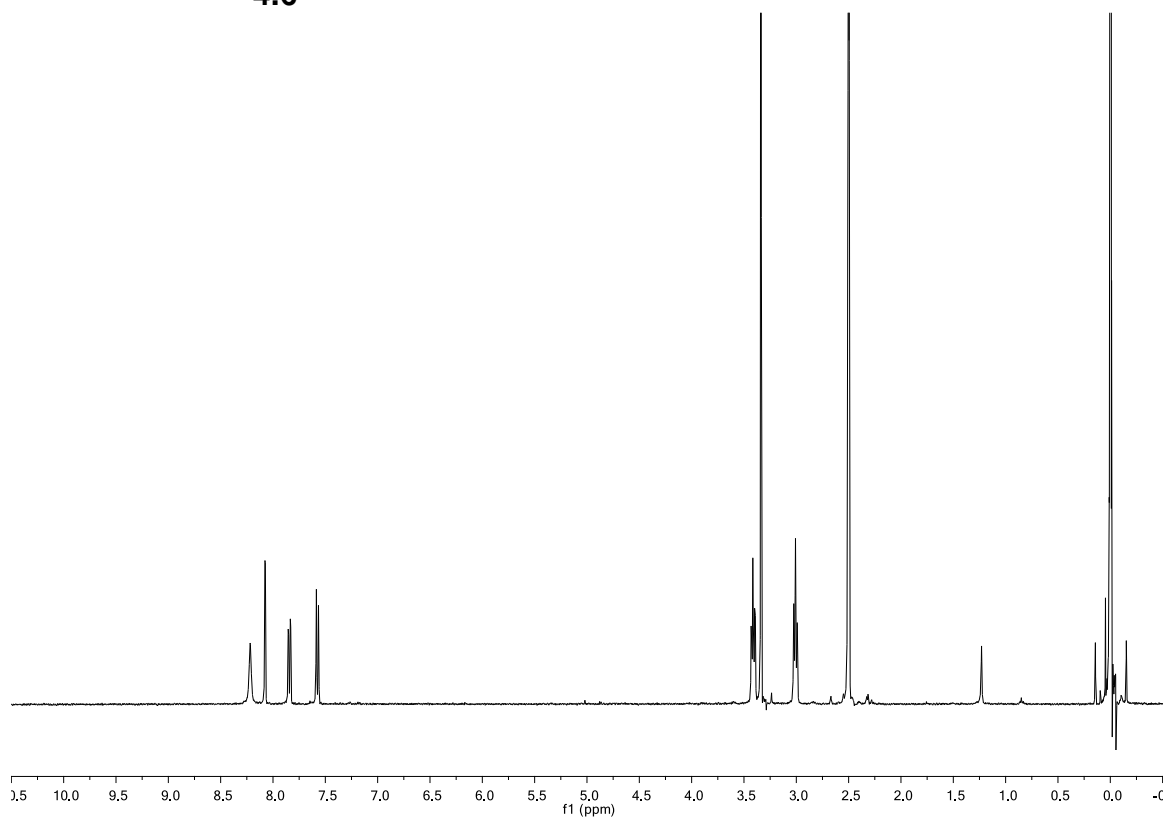
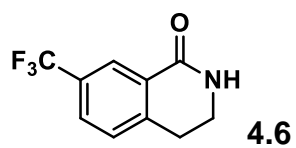


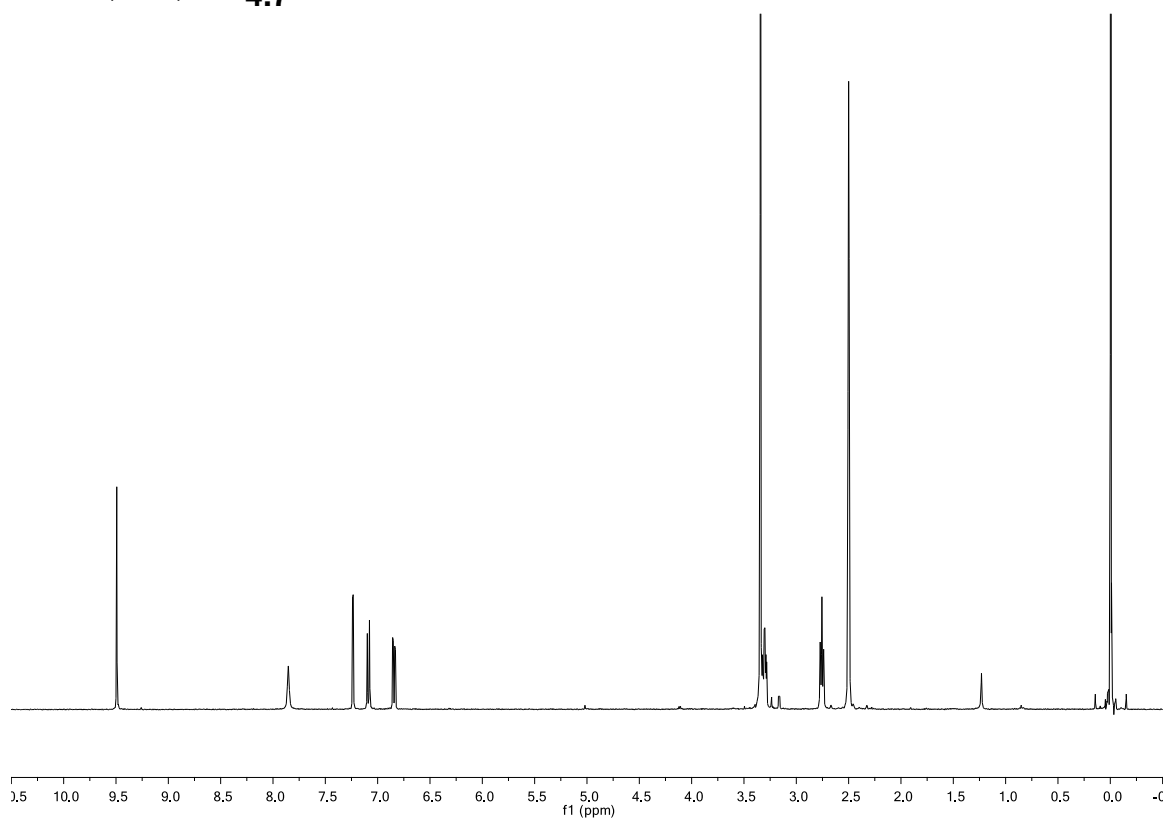
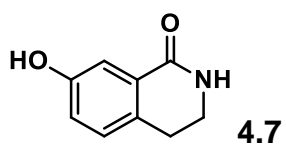


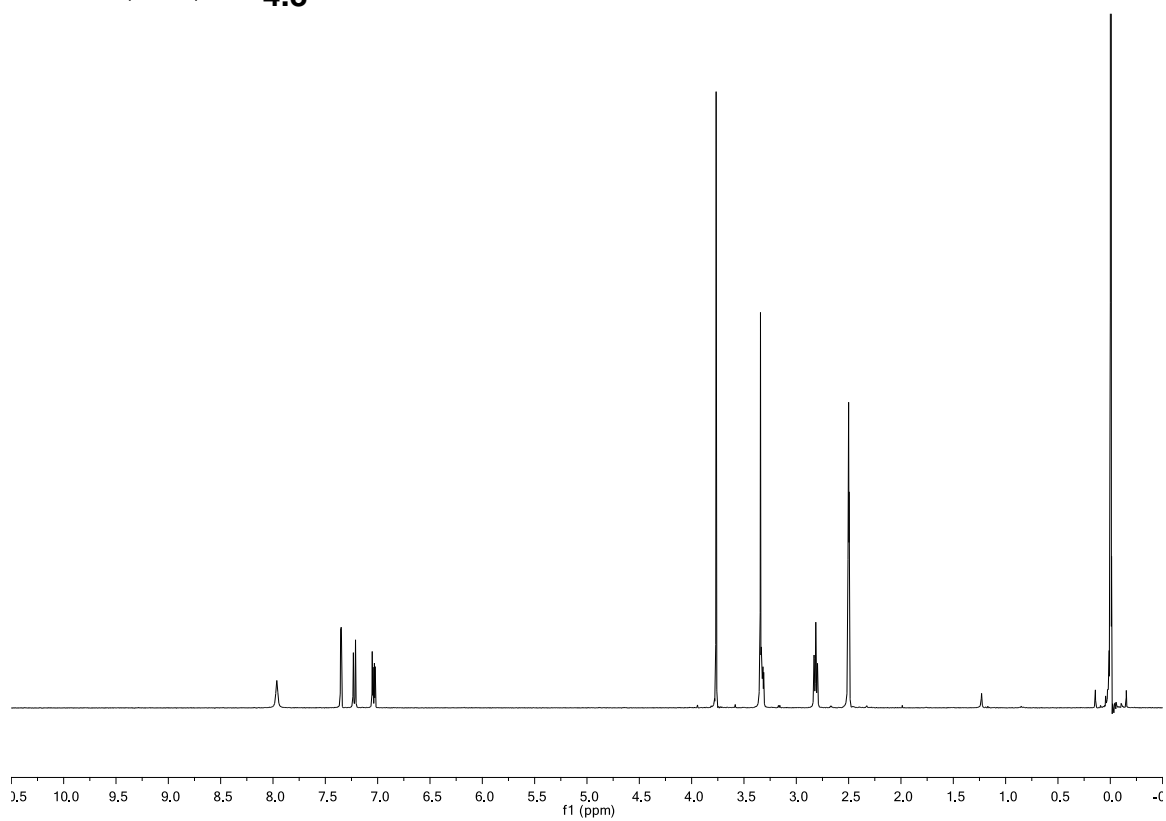
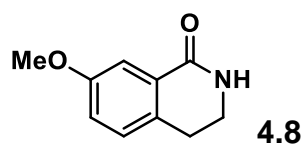


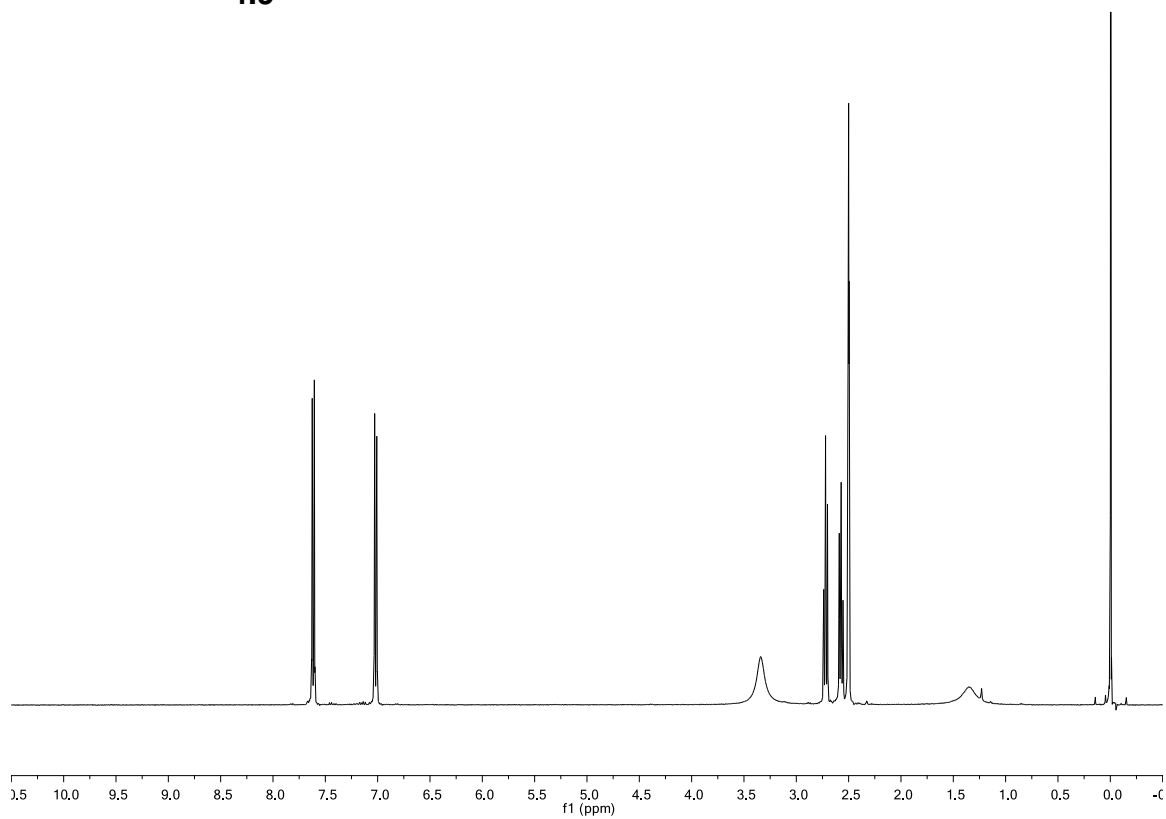
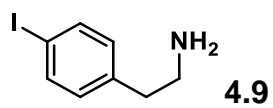


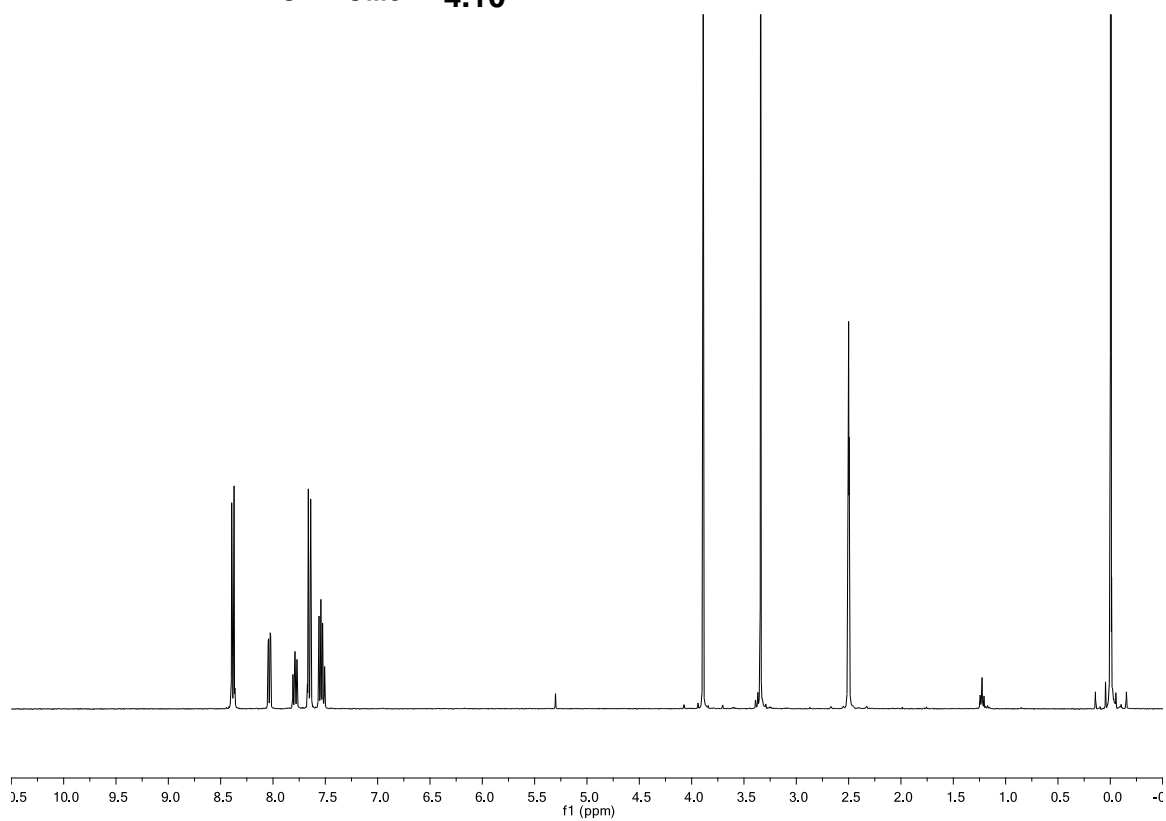
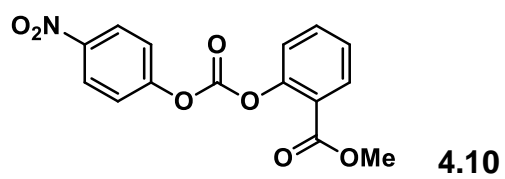


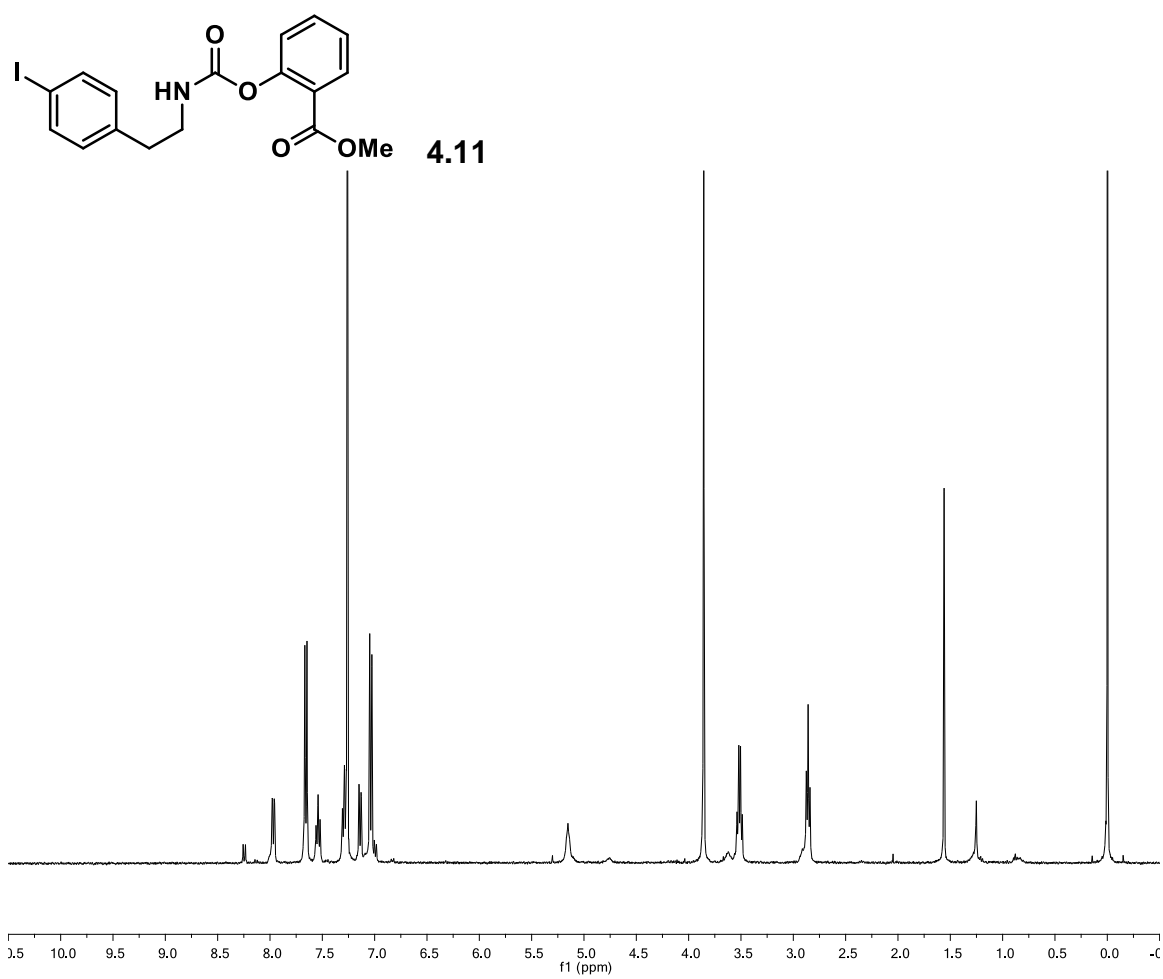


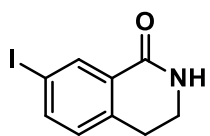




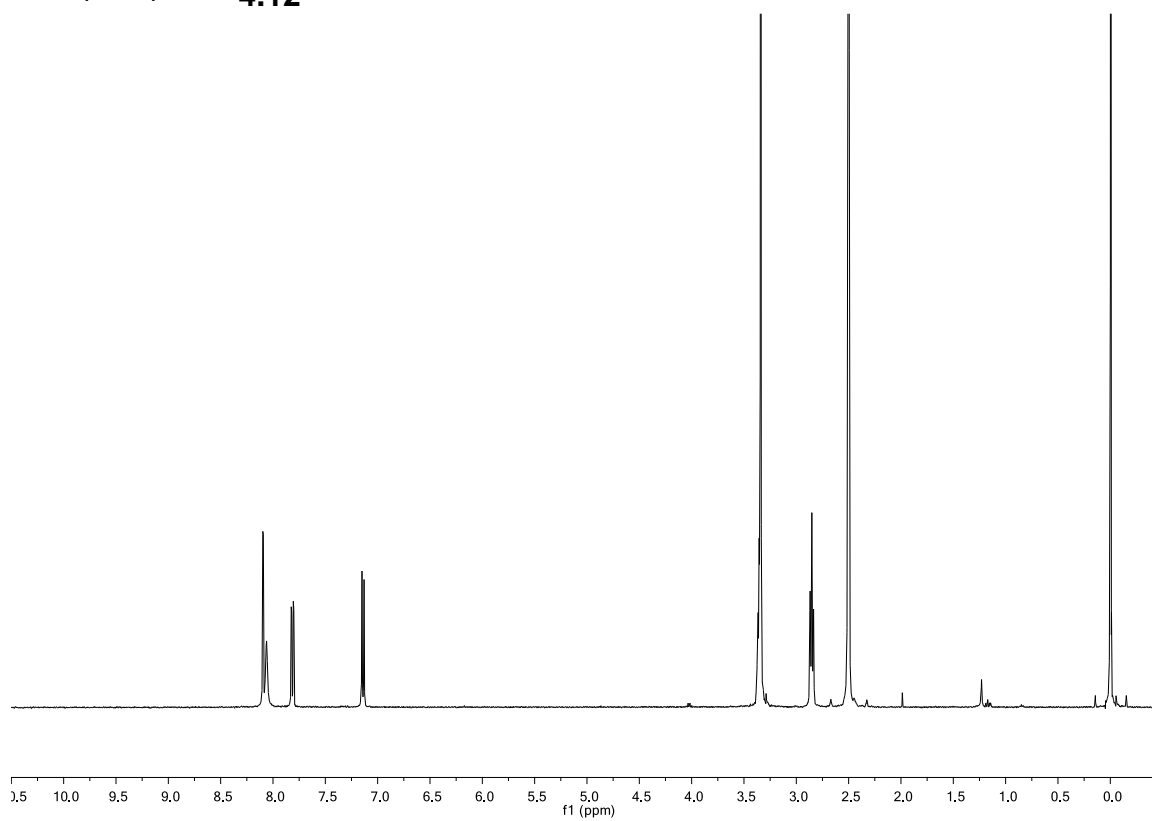


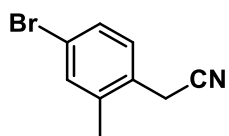




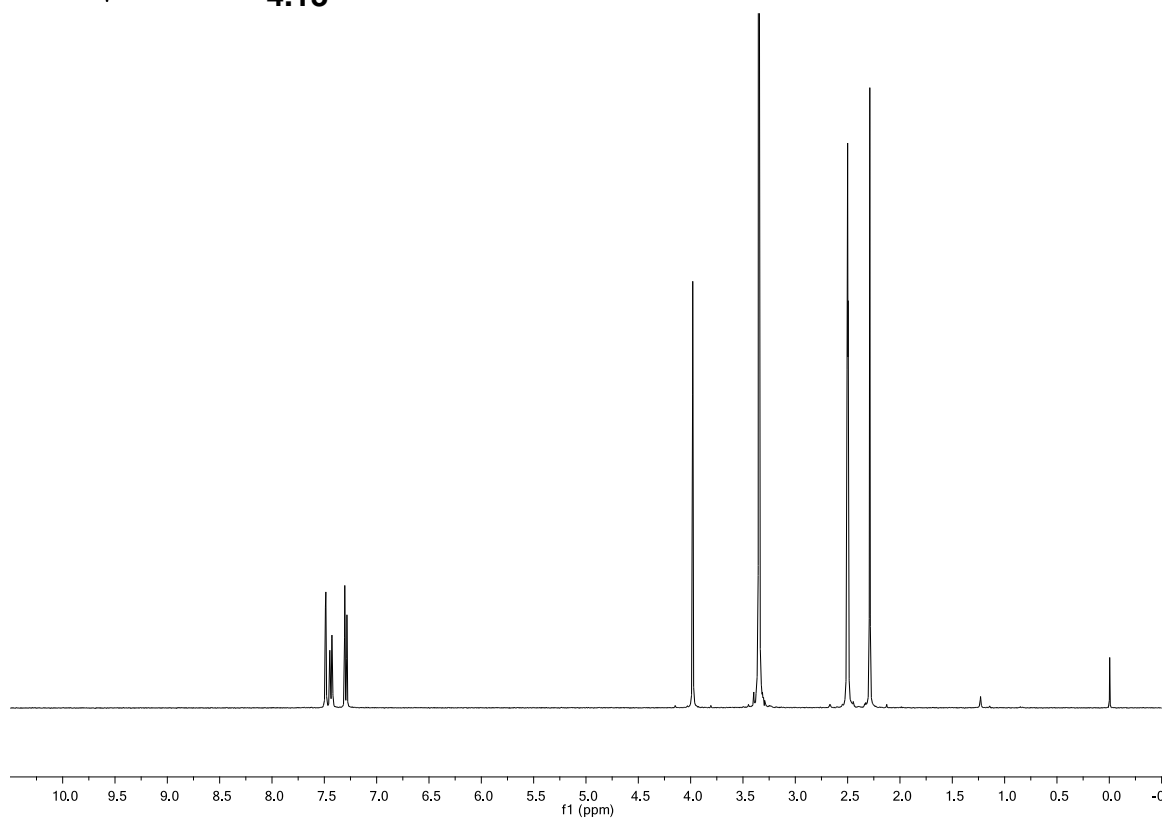


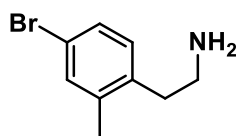
4.12



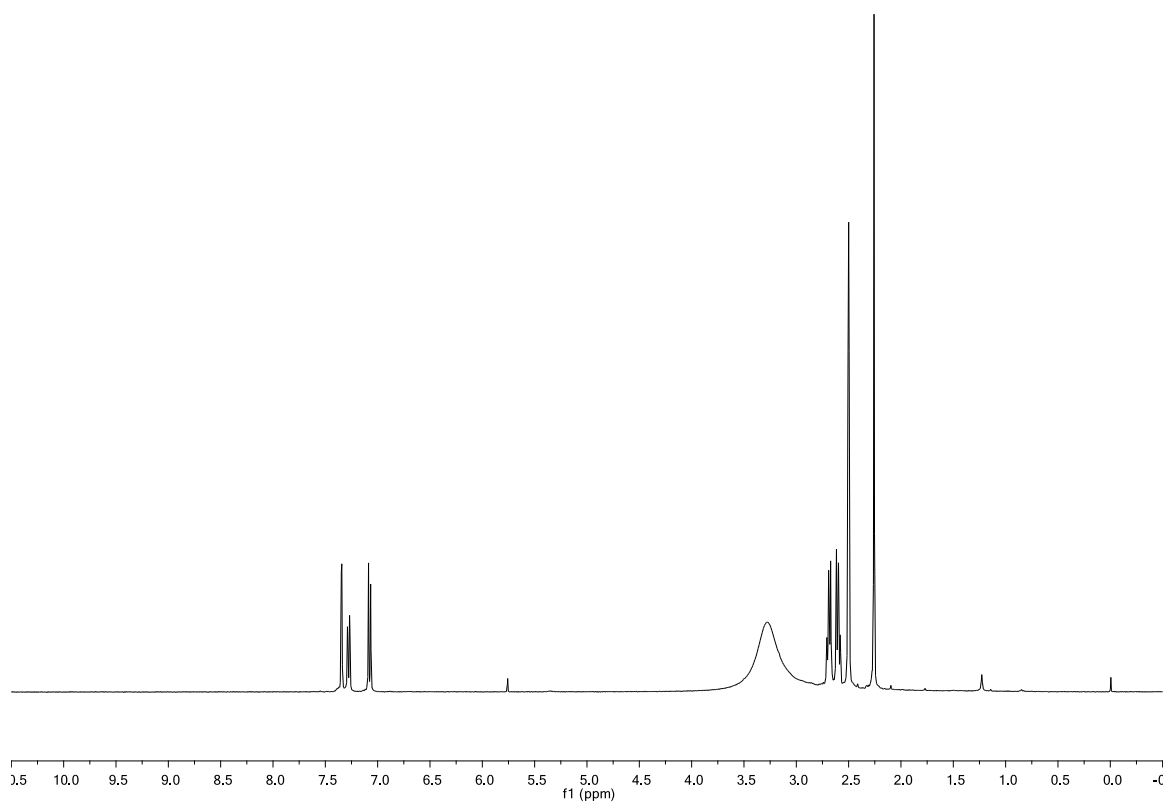


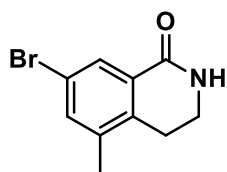
4.13



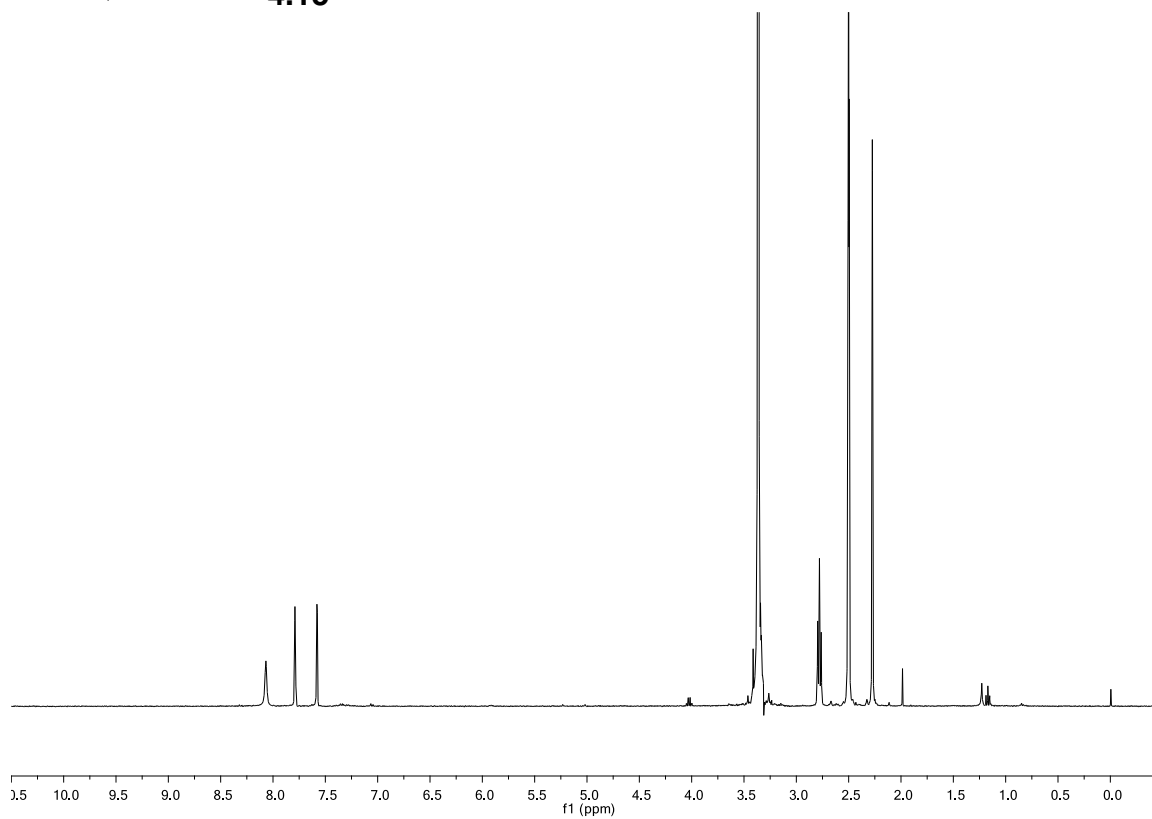


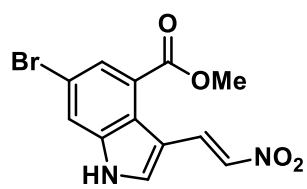
4.14



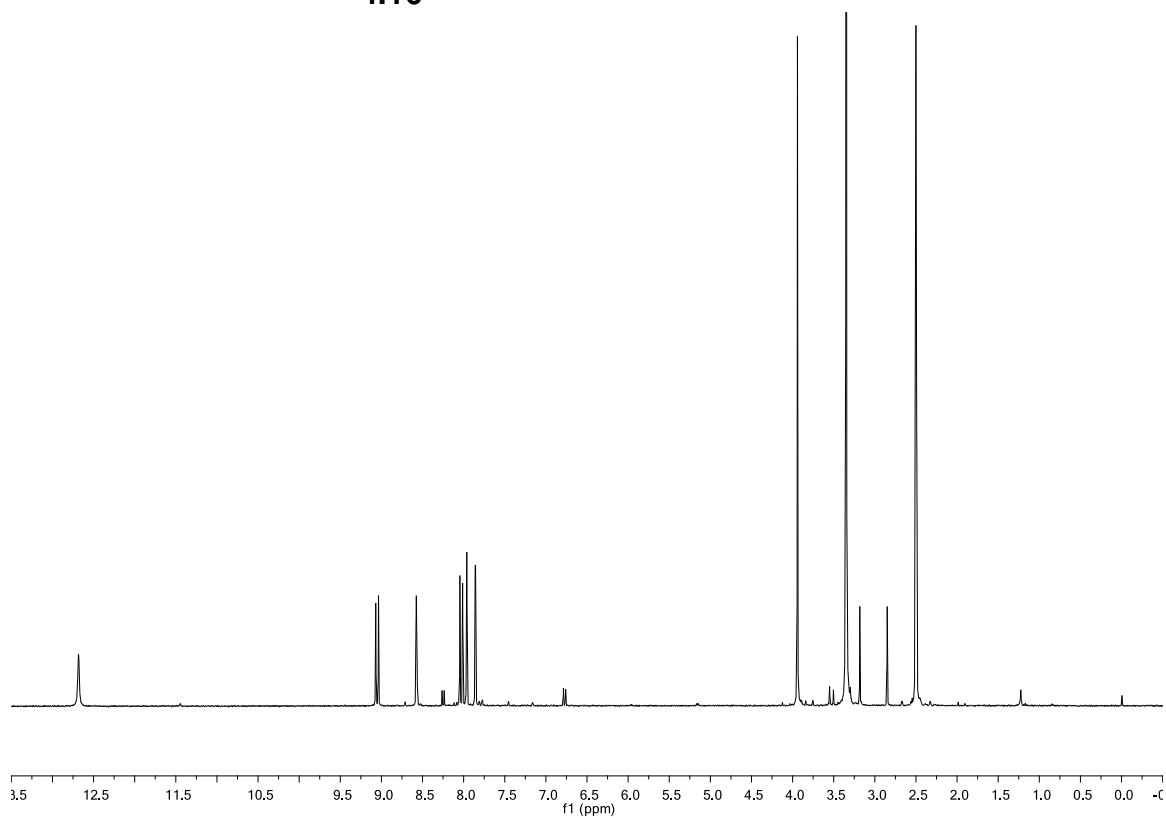


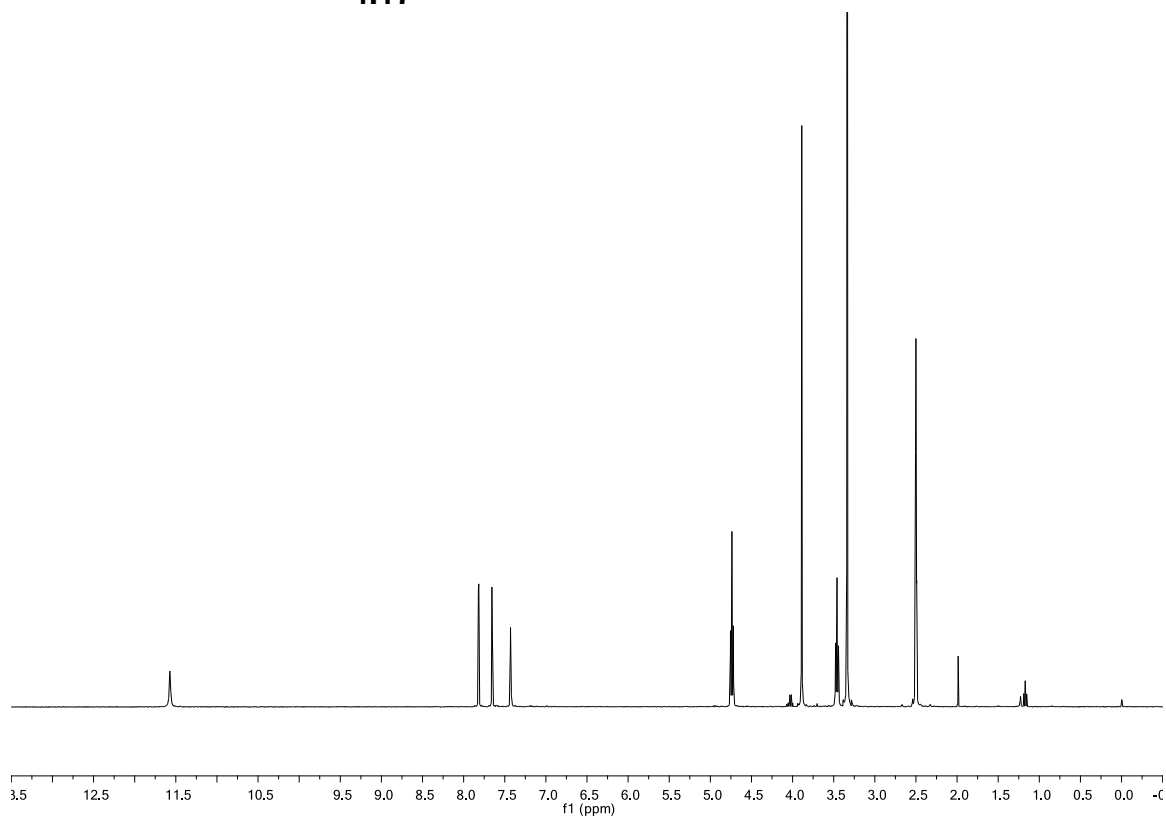
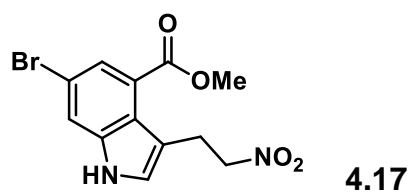
4.15

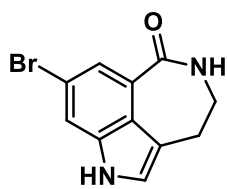




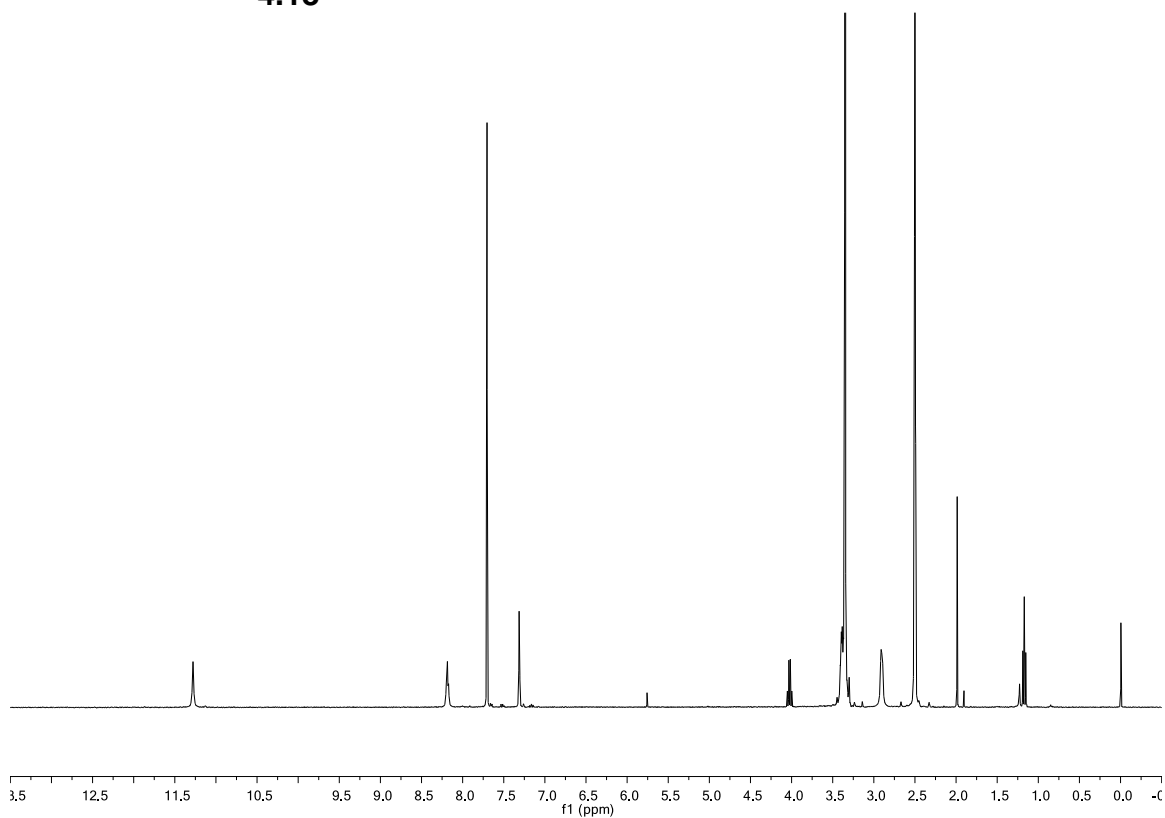
4.16

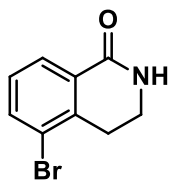




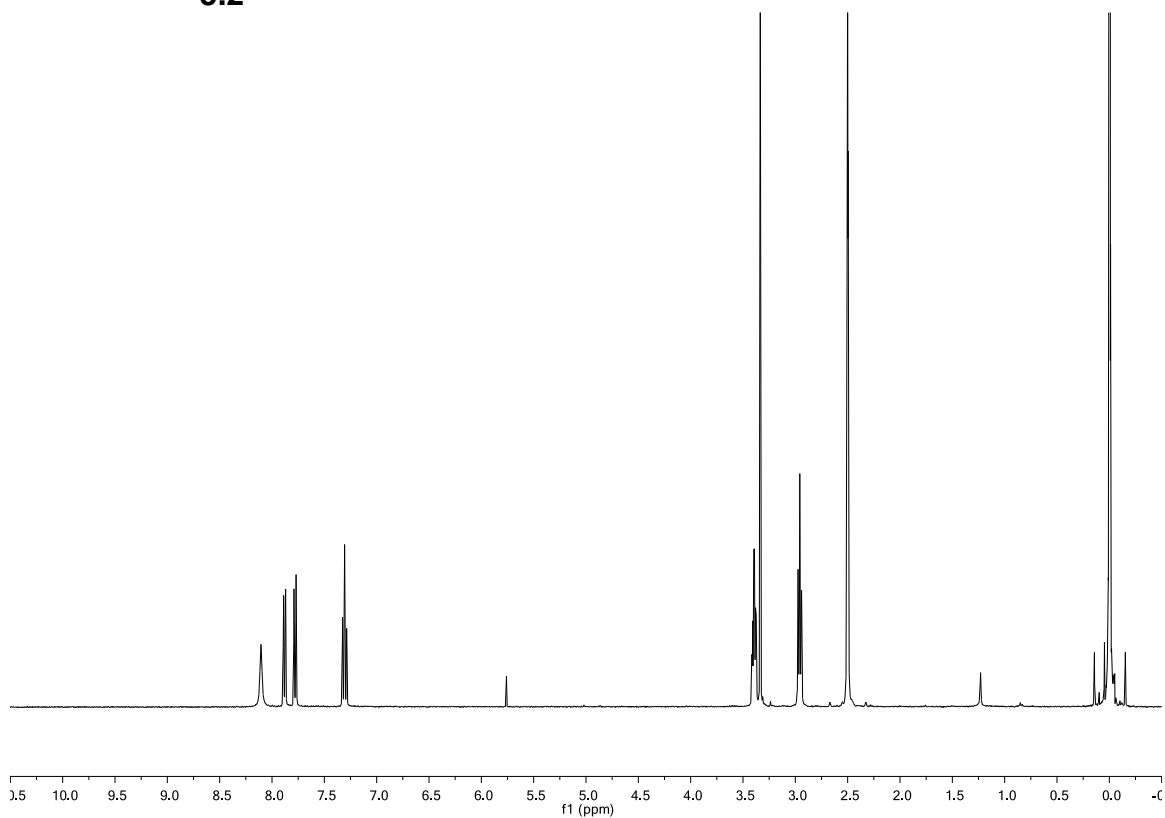


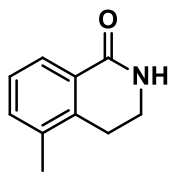
4.18



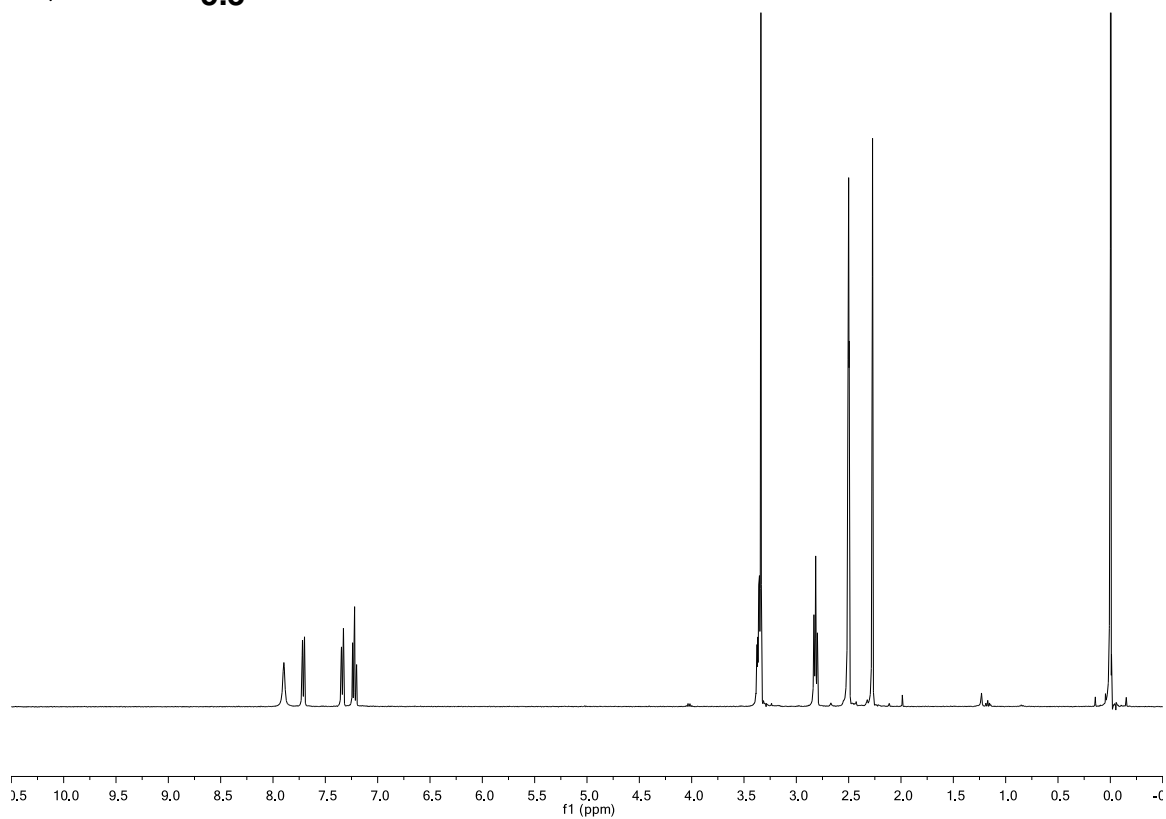


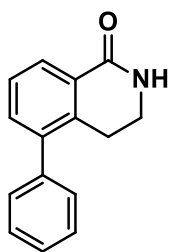
5.2



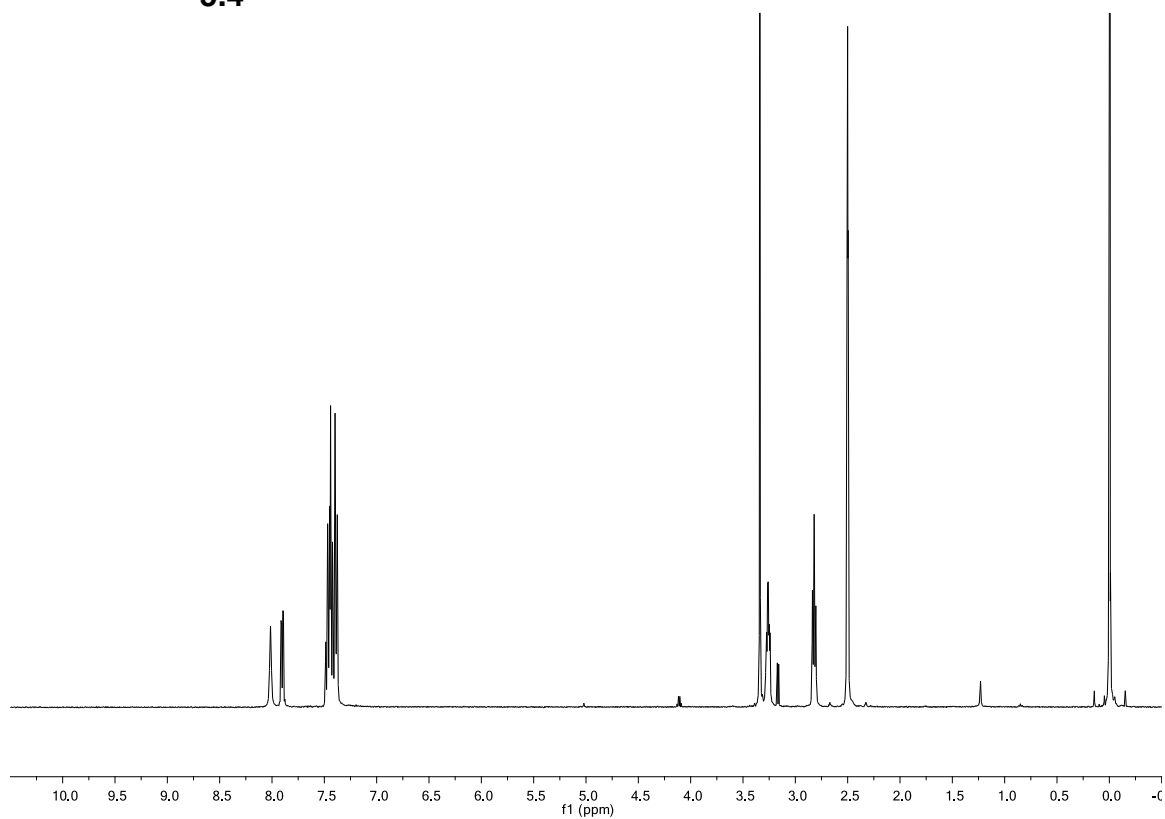


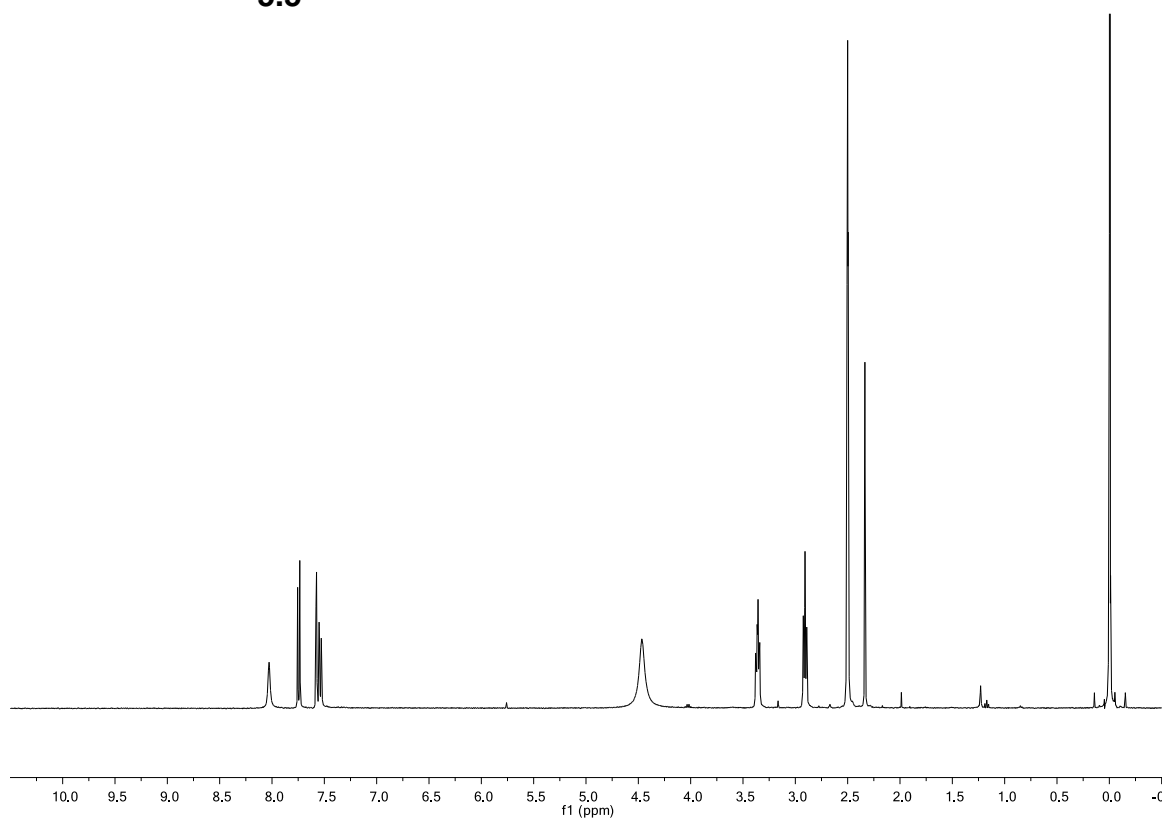
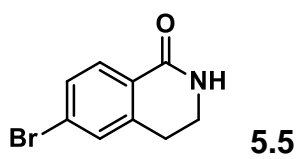
5.3

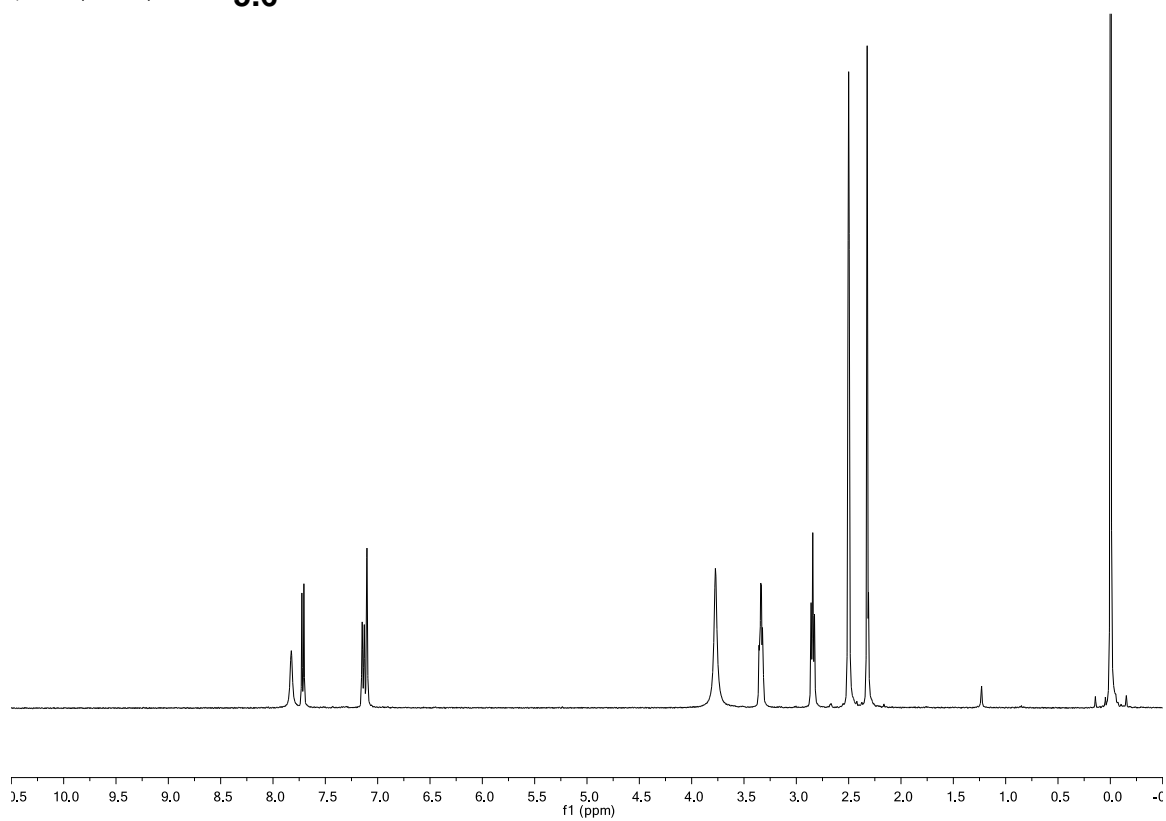
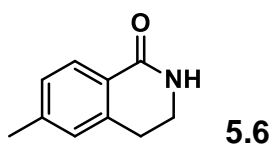


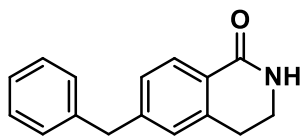


5.4

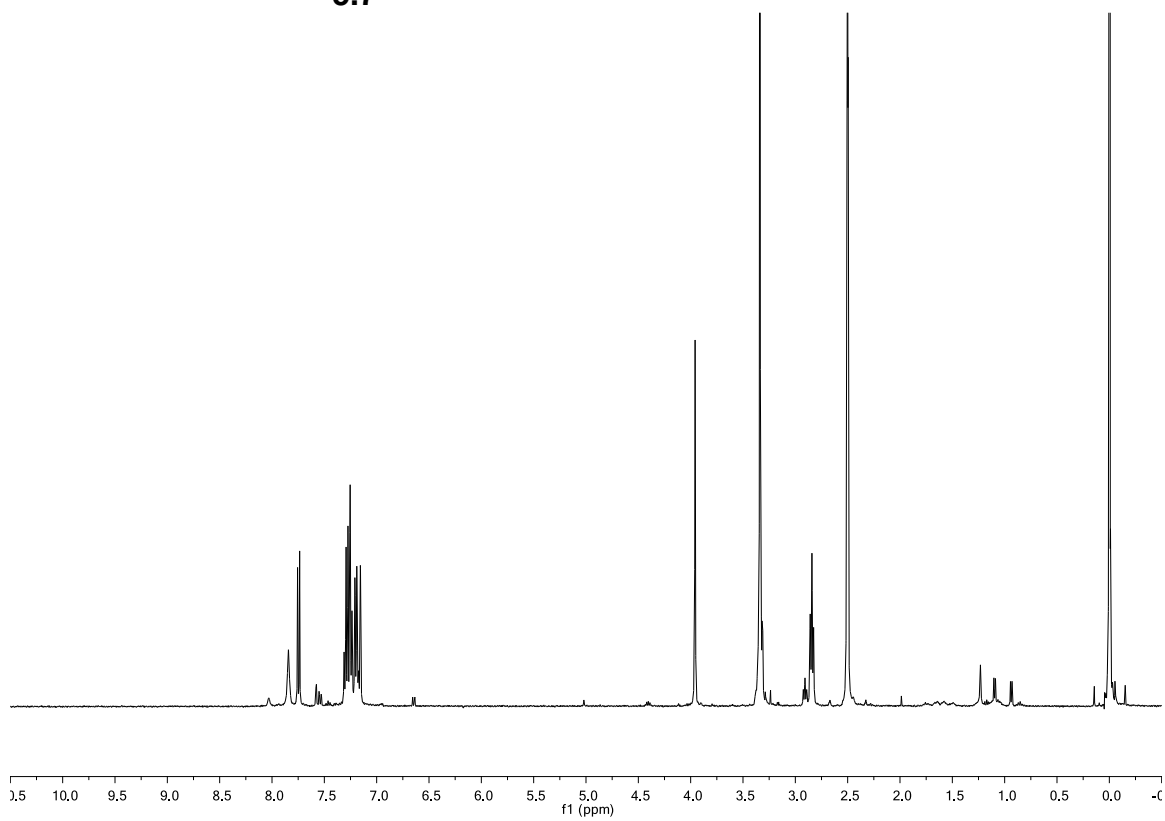


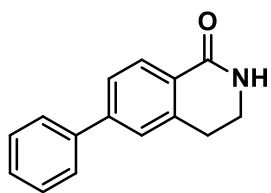




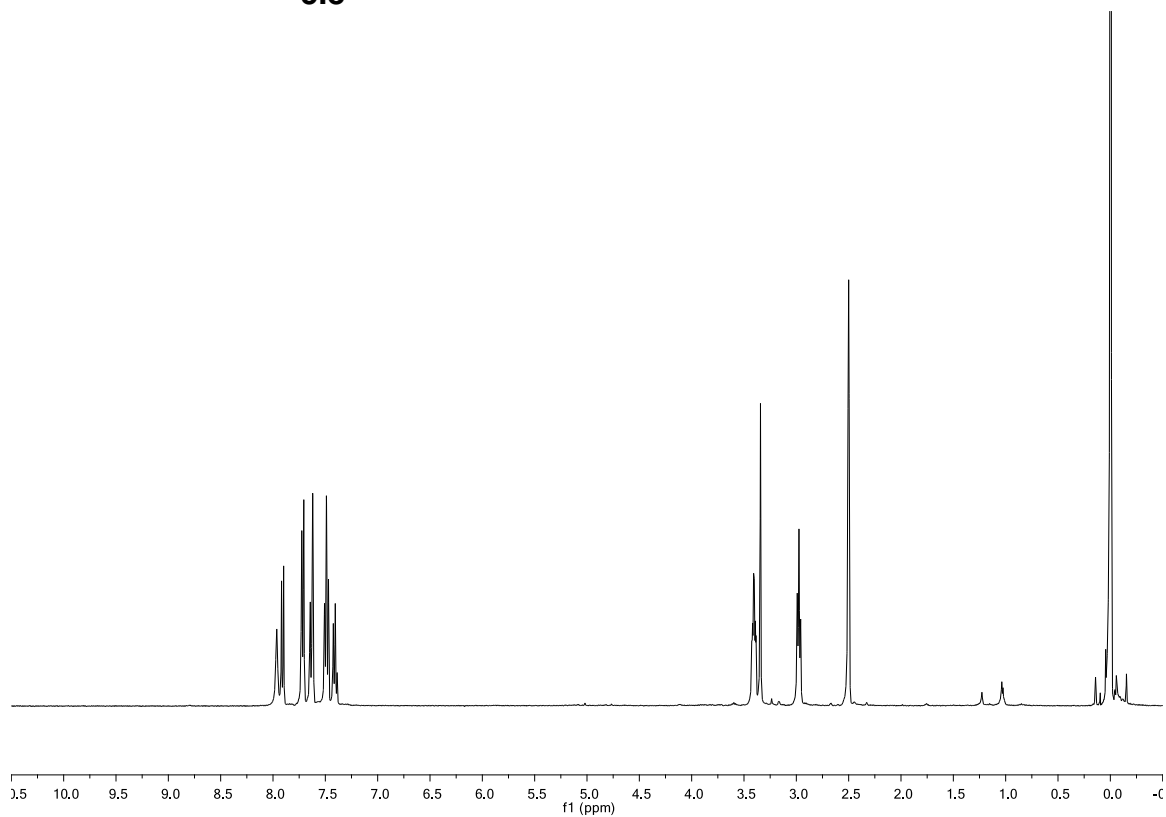


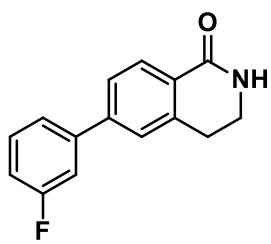
5.7



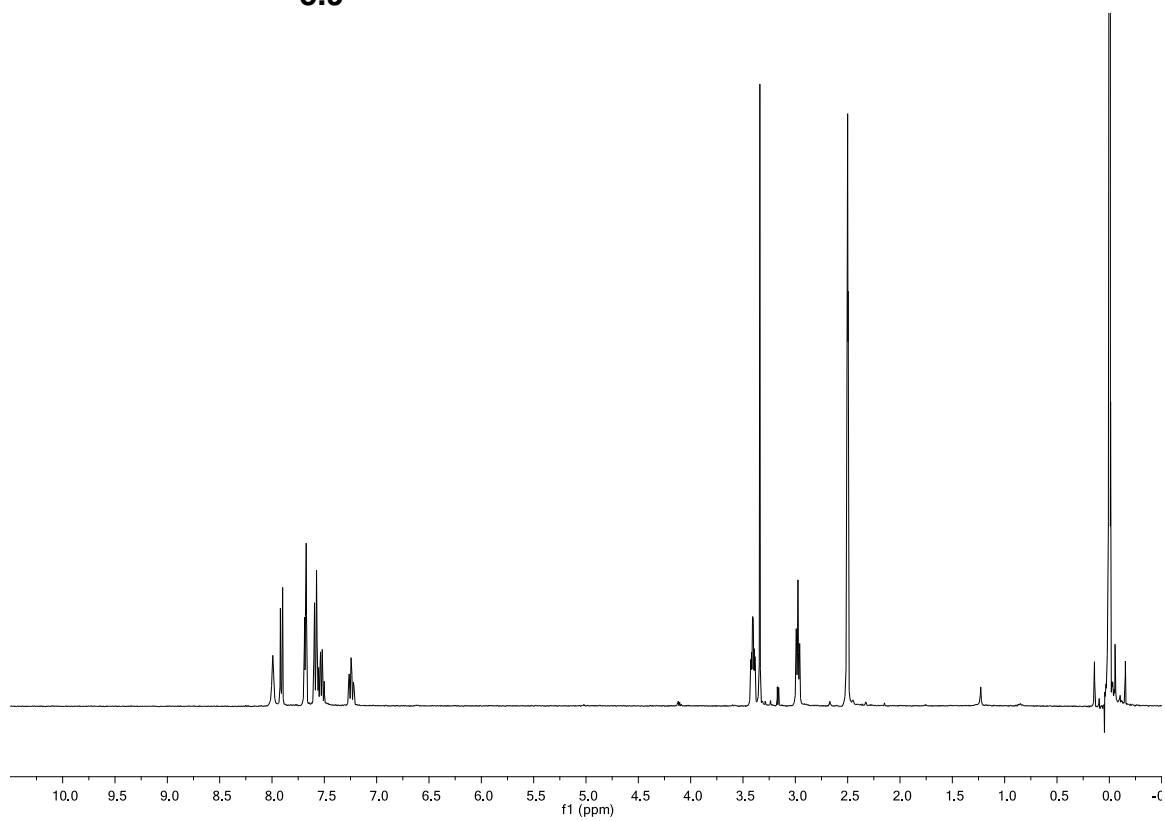


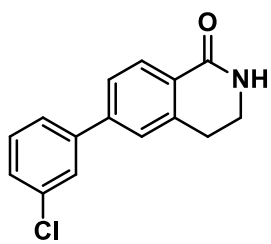
5.8



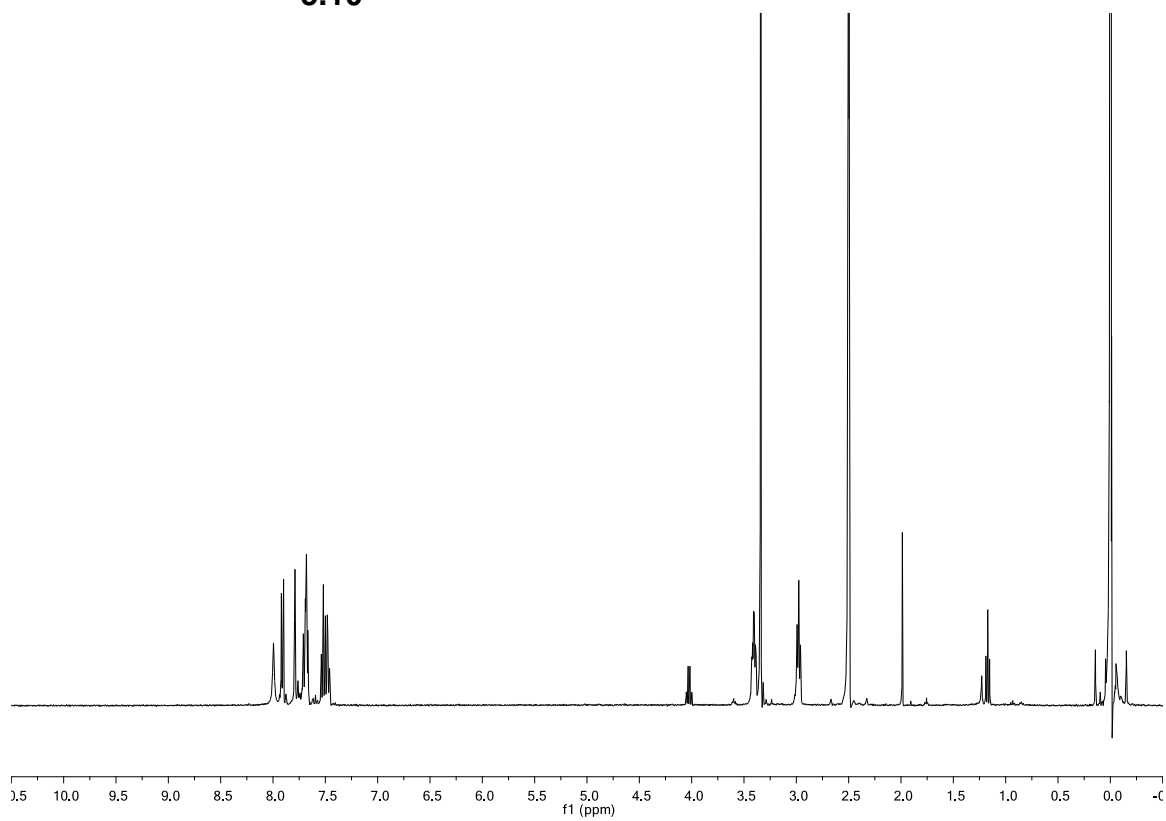


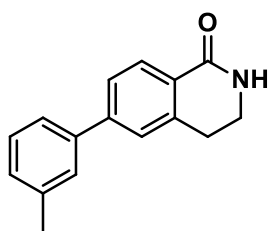
5.9



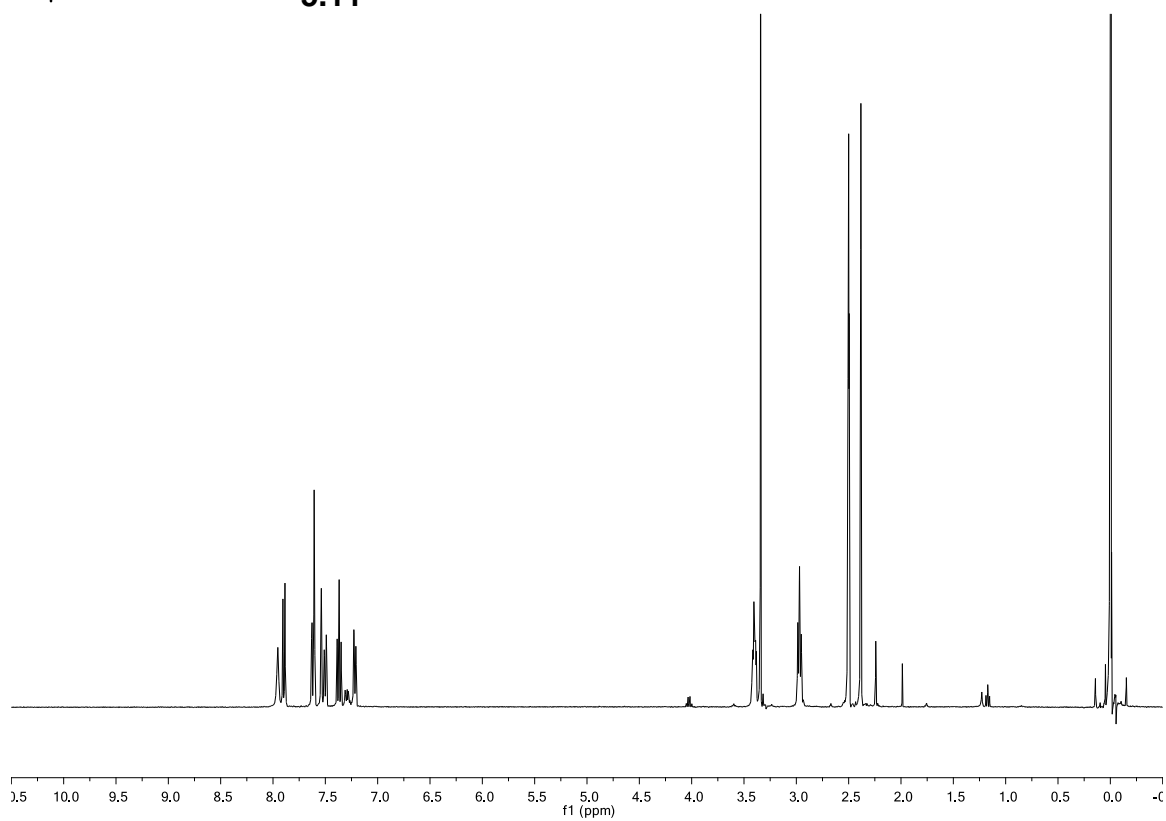


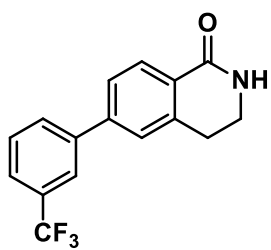
5.10



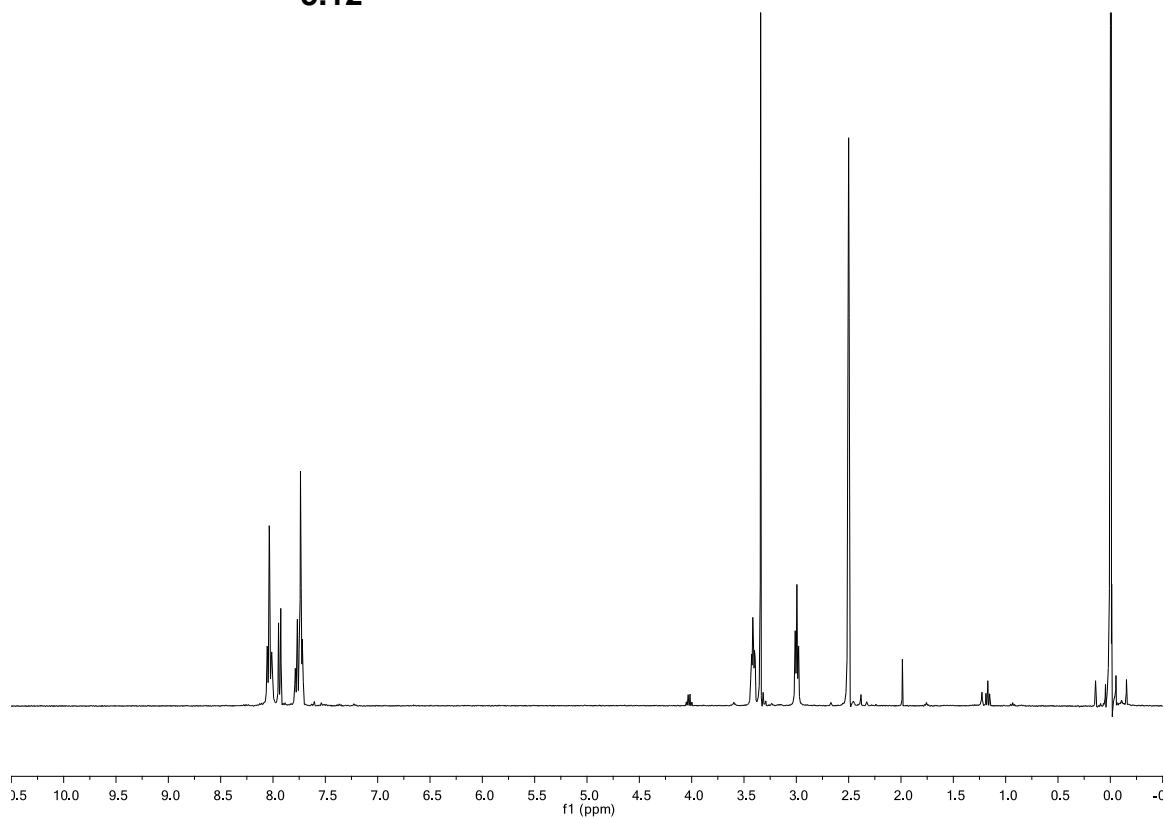


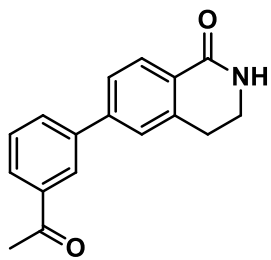
5.11



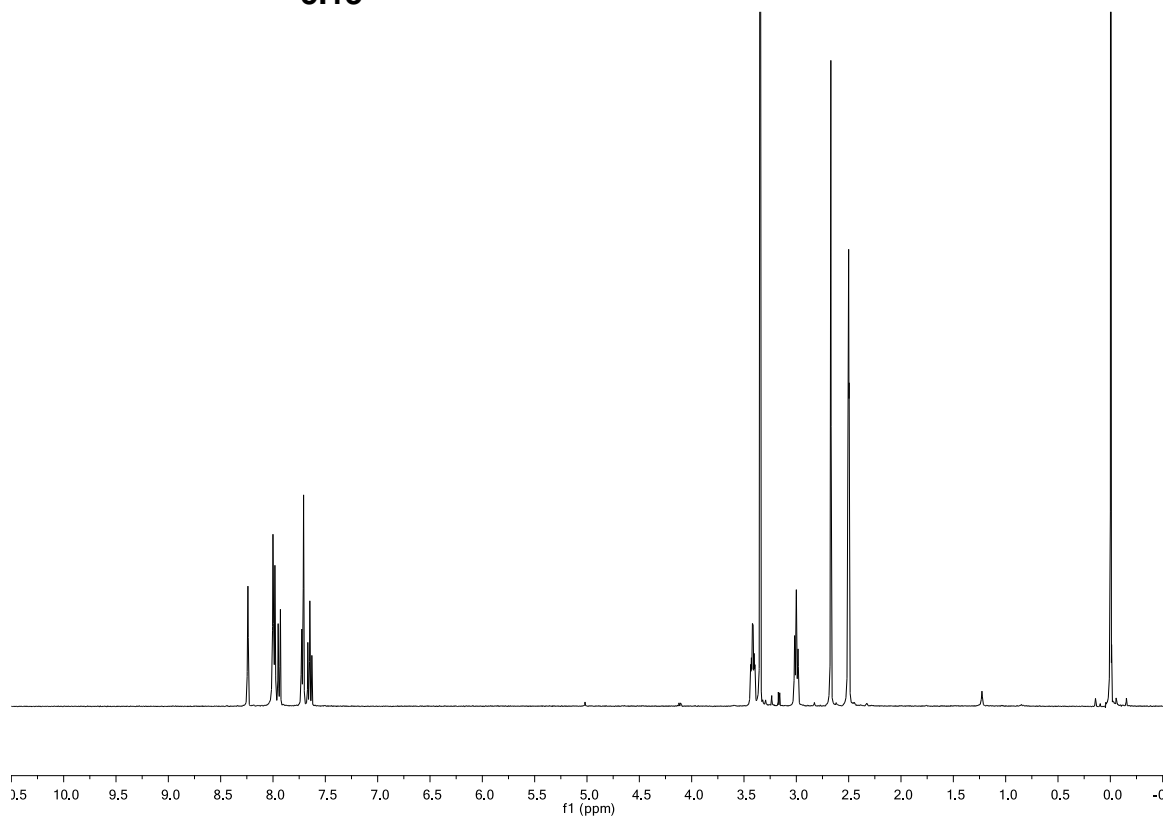


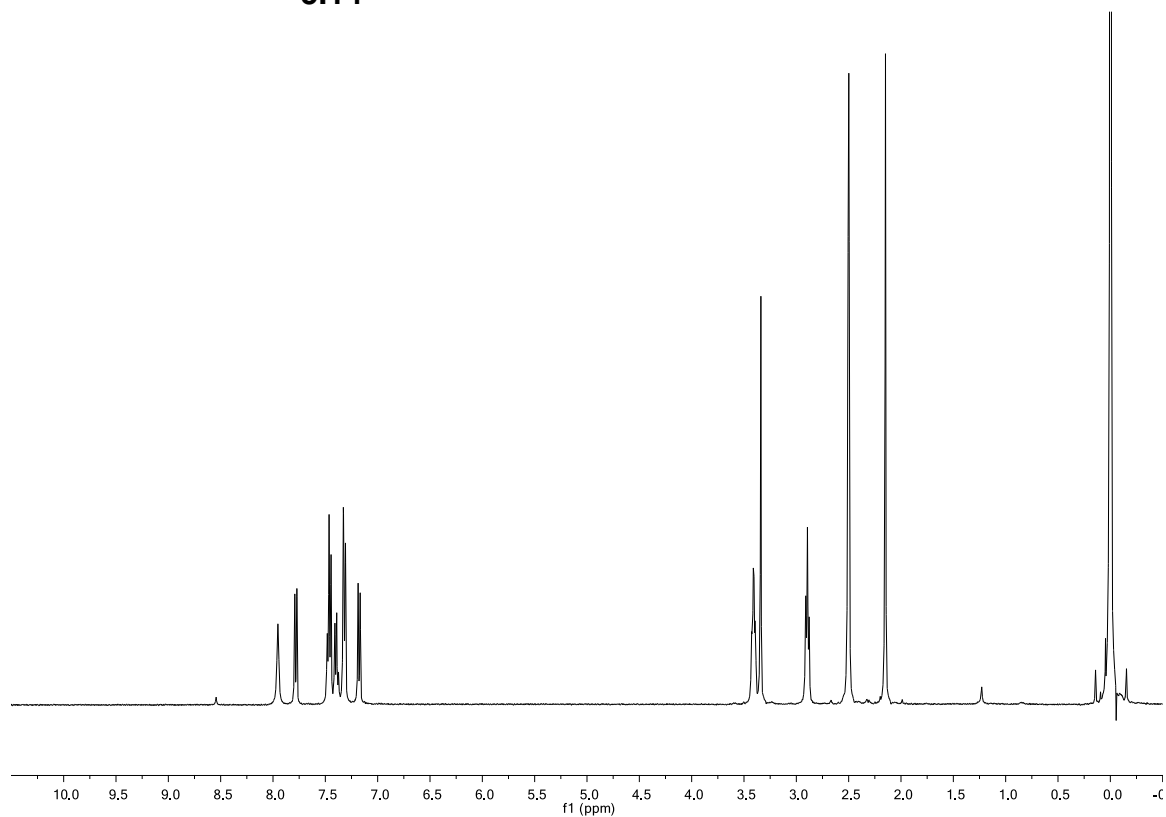
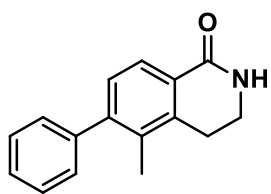
5.12

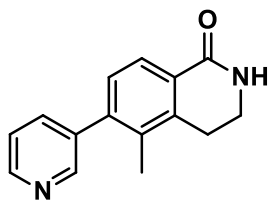




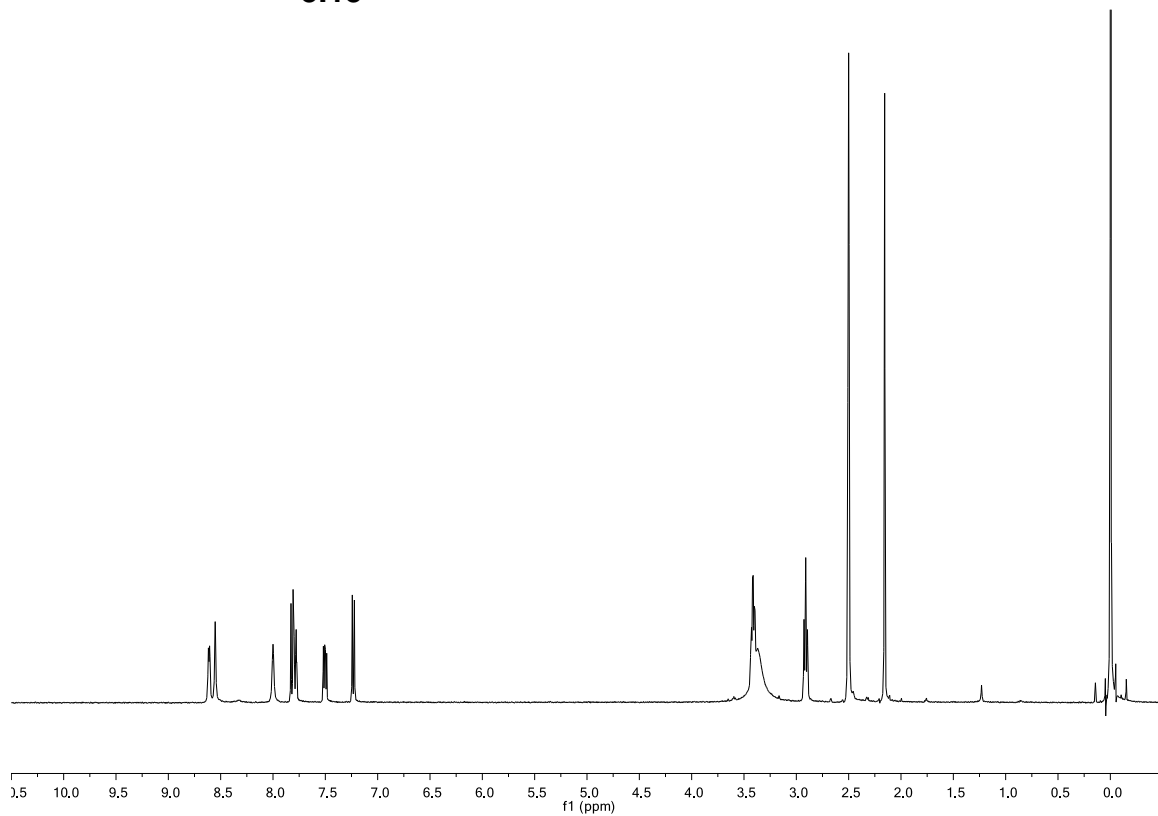
5.13

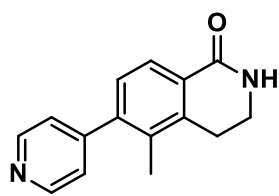




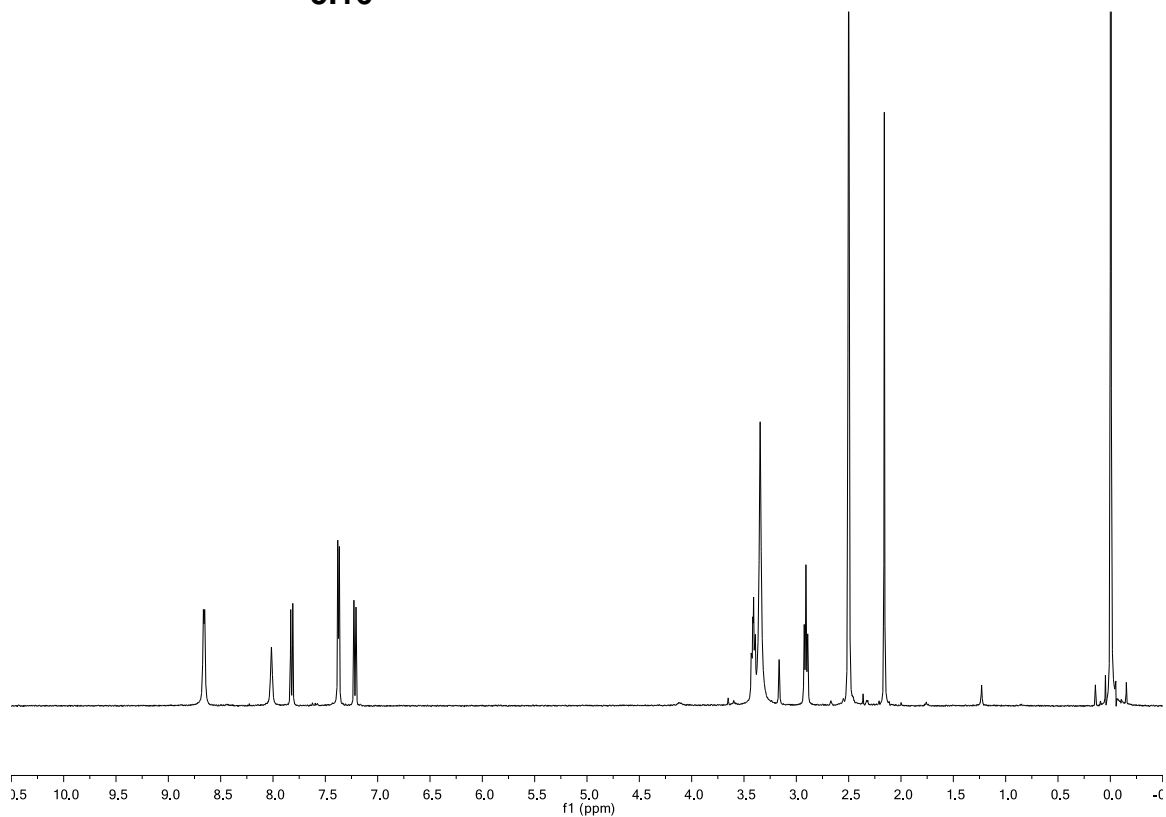


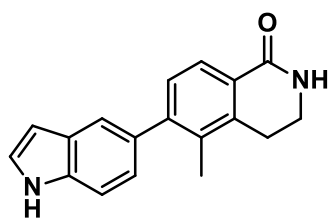
5.15



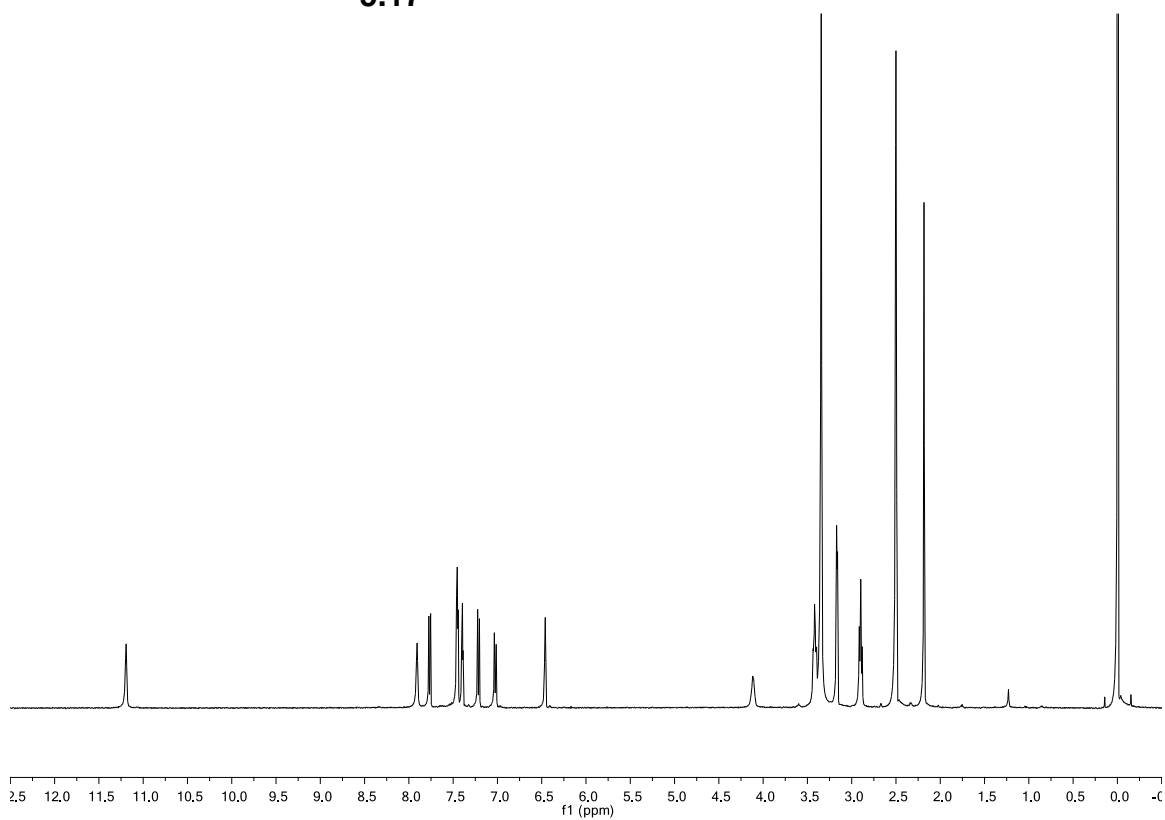


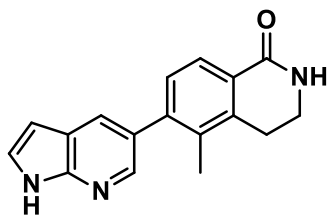
5.16



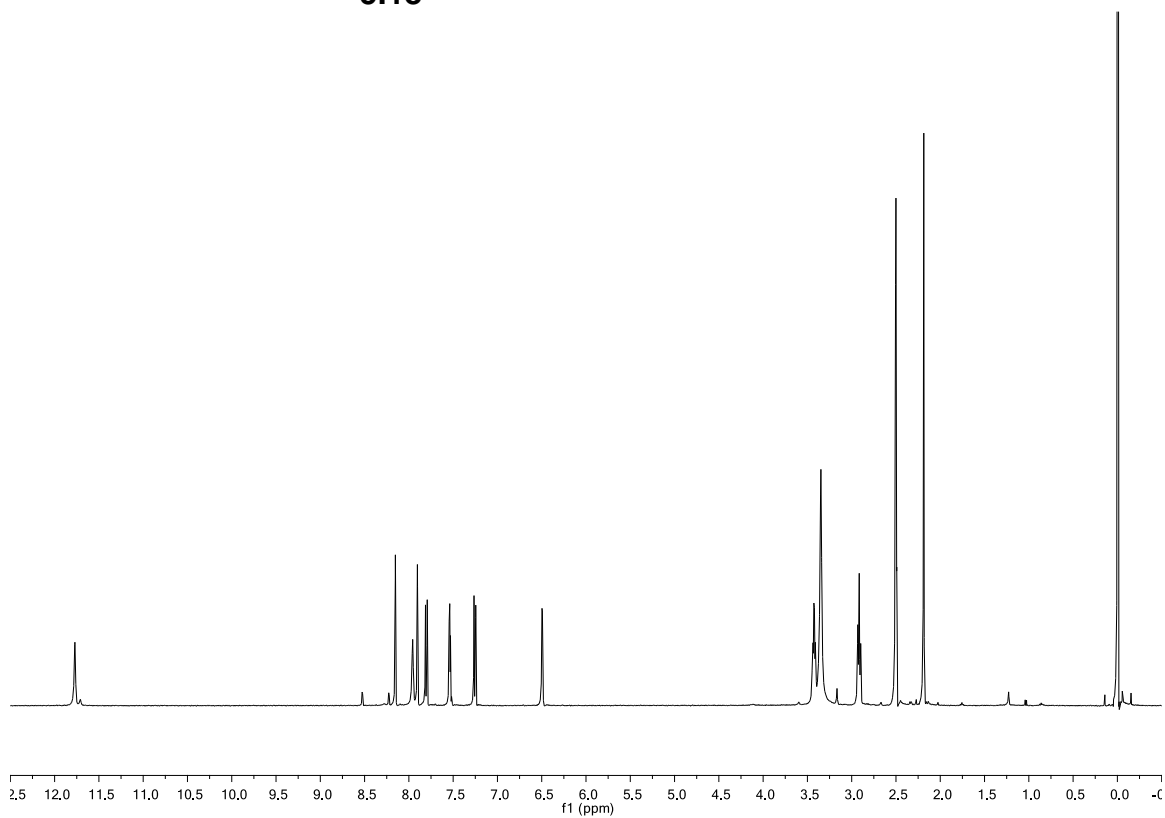


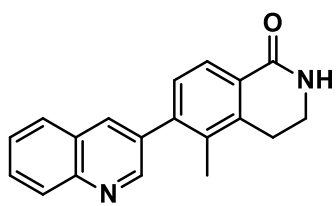
5.17



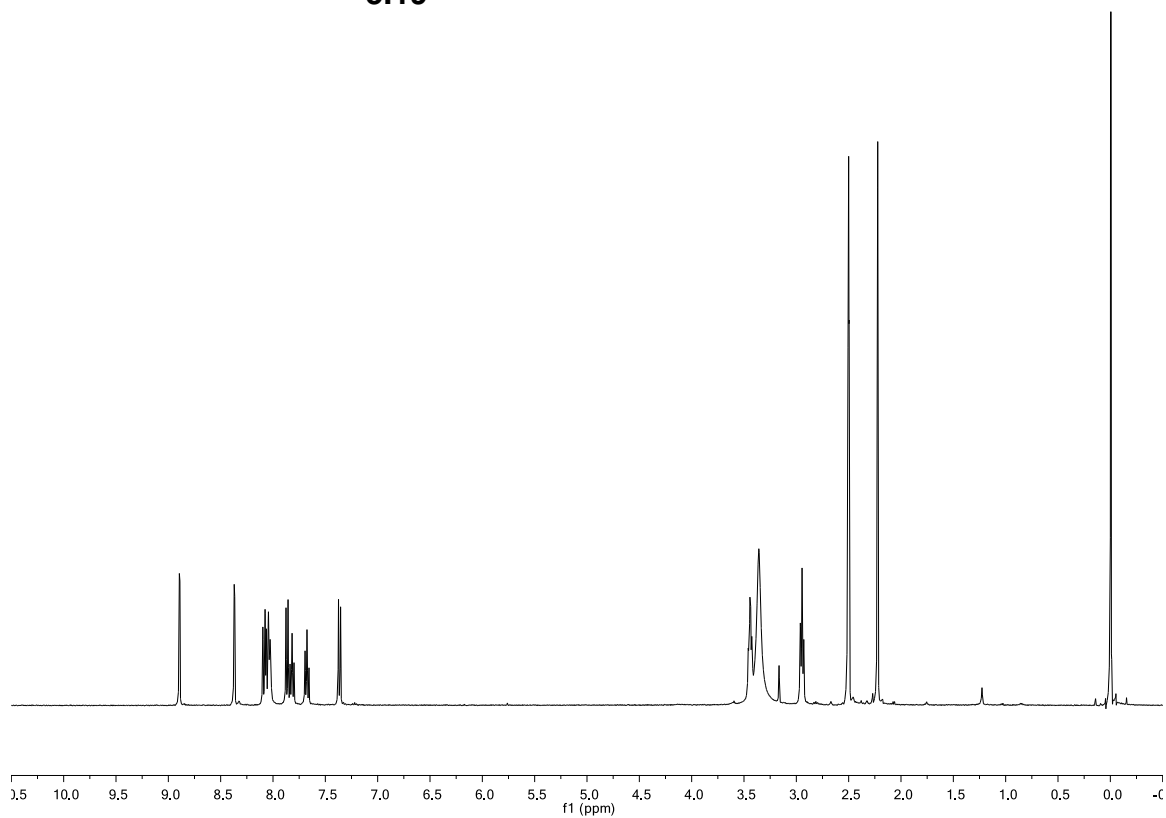


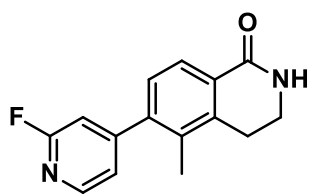
5.18



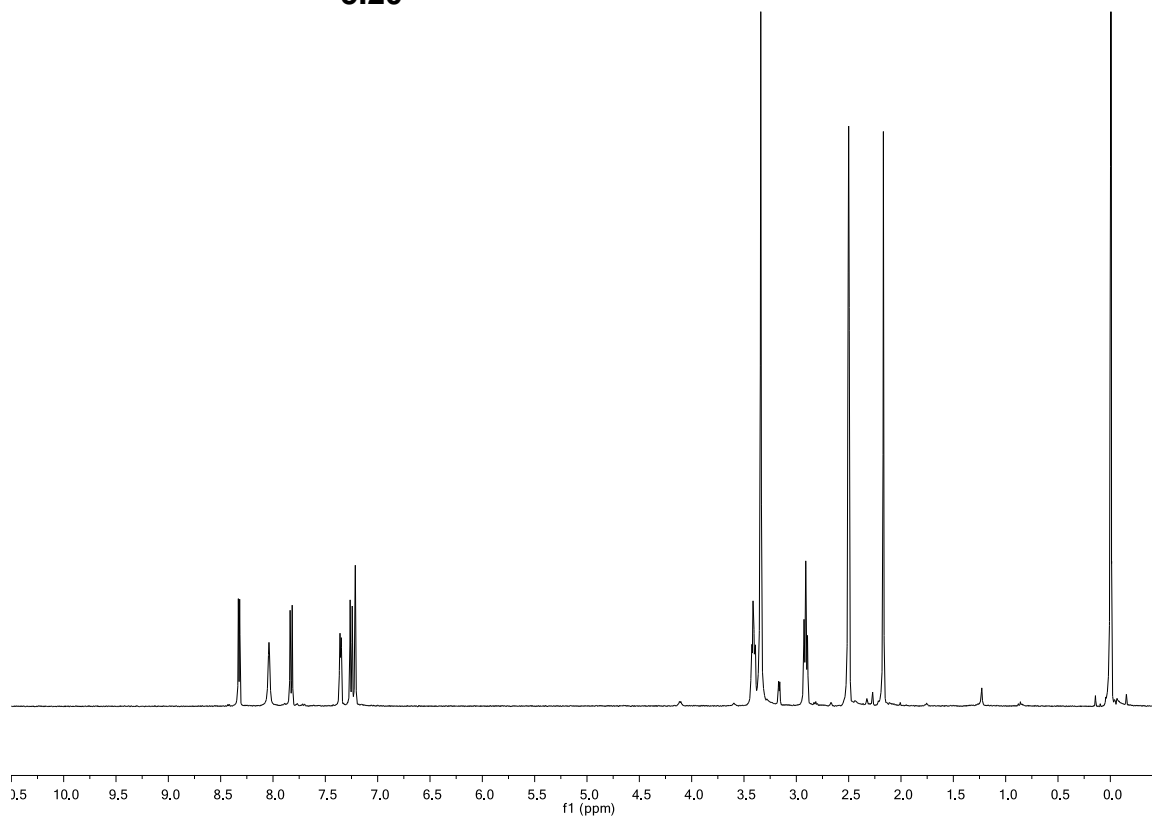


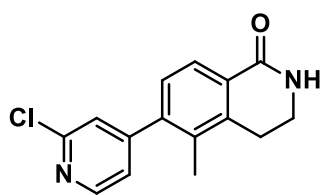
5.19



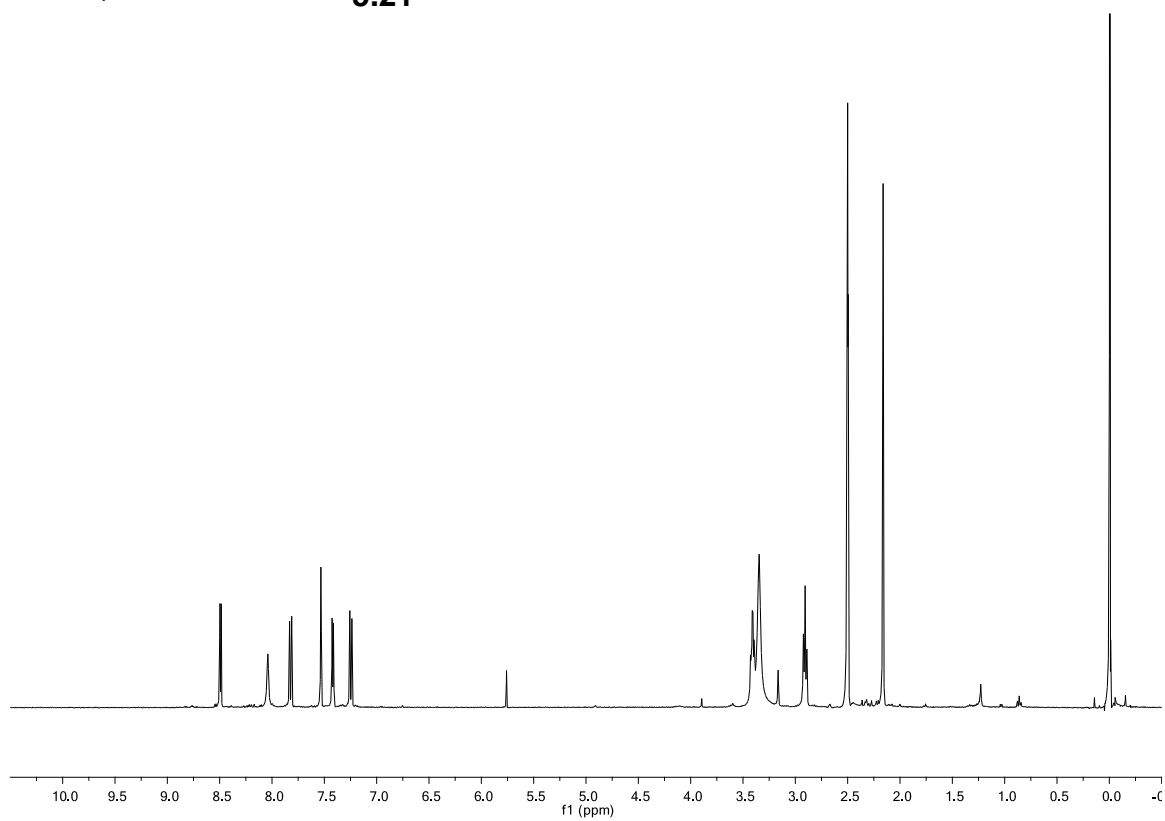


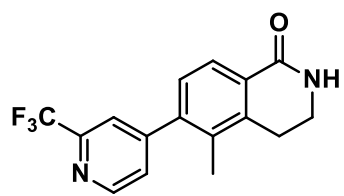
5.20



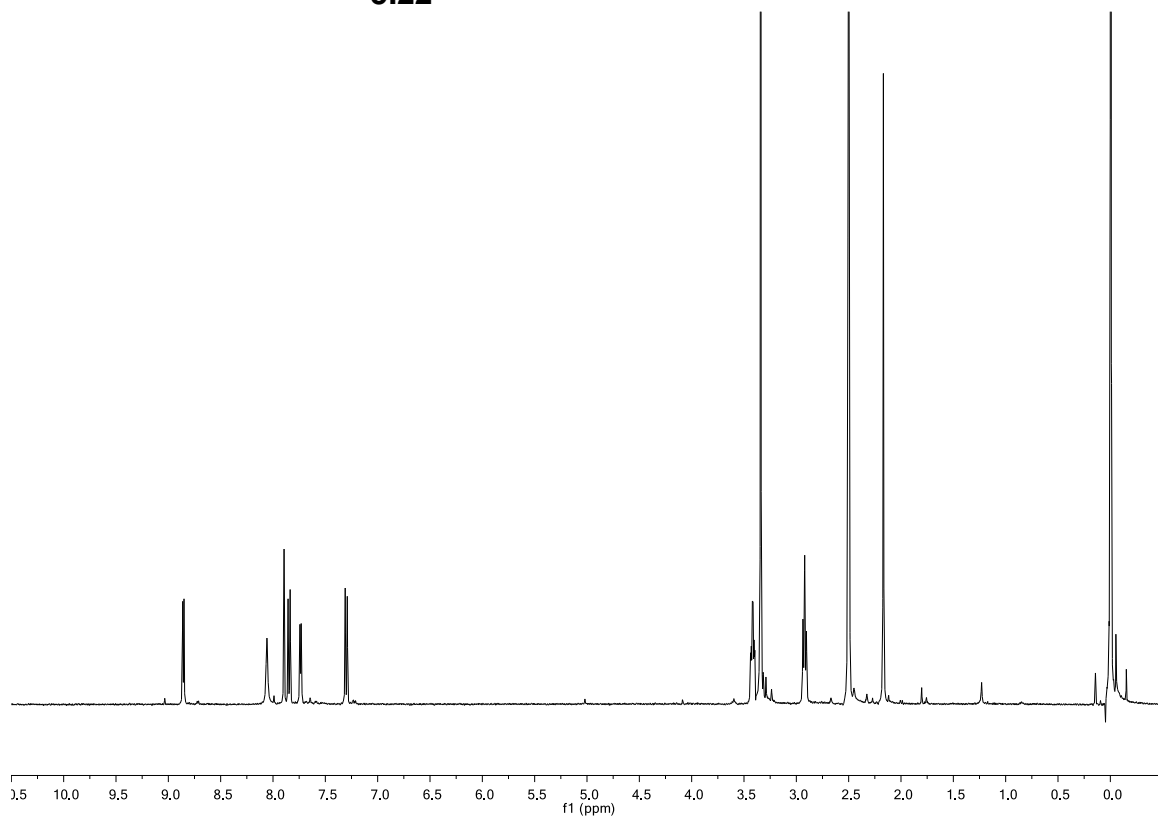


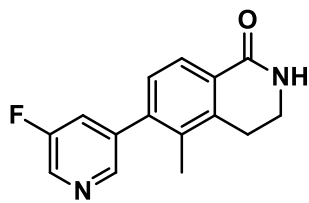
5.21



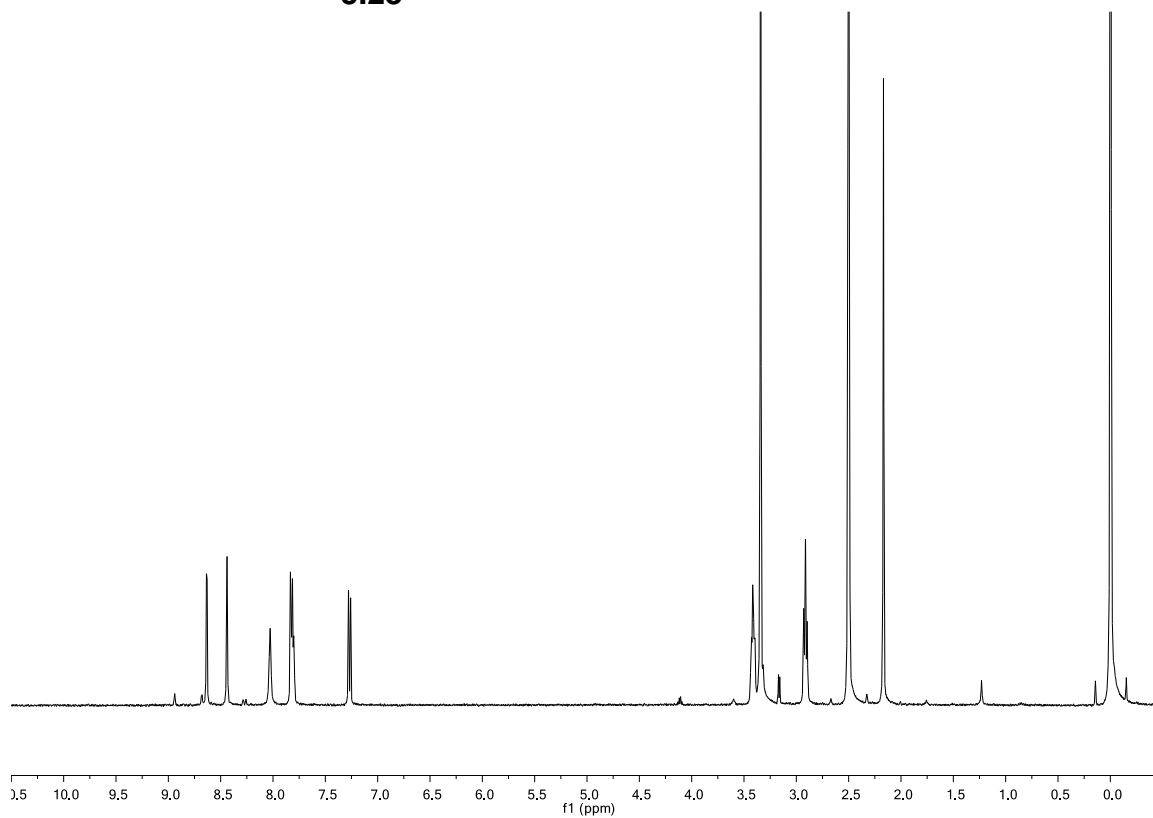


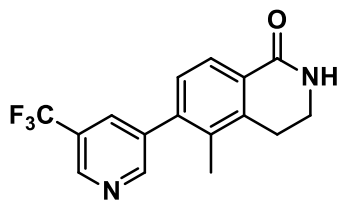
5.22



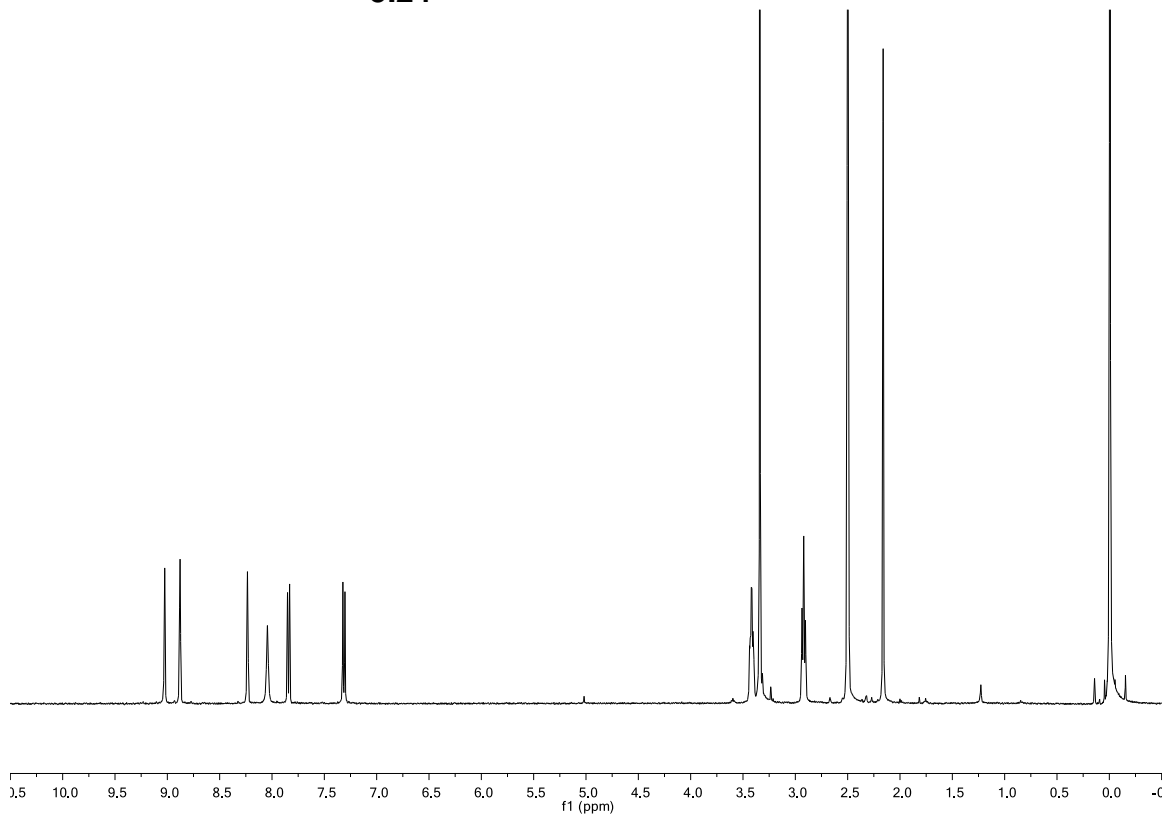


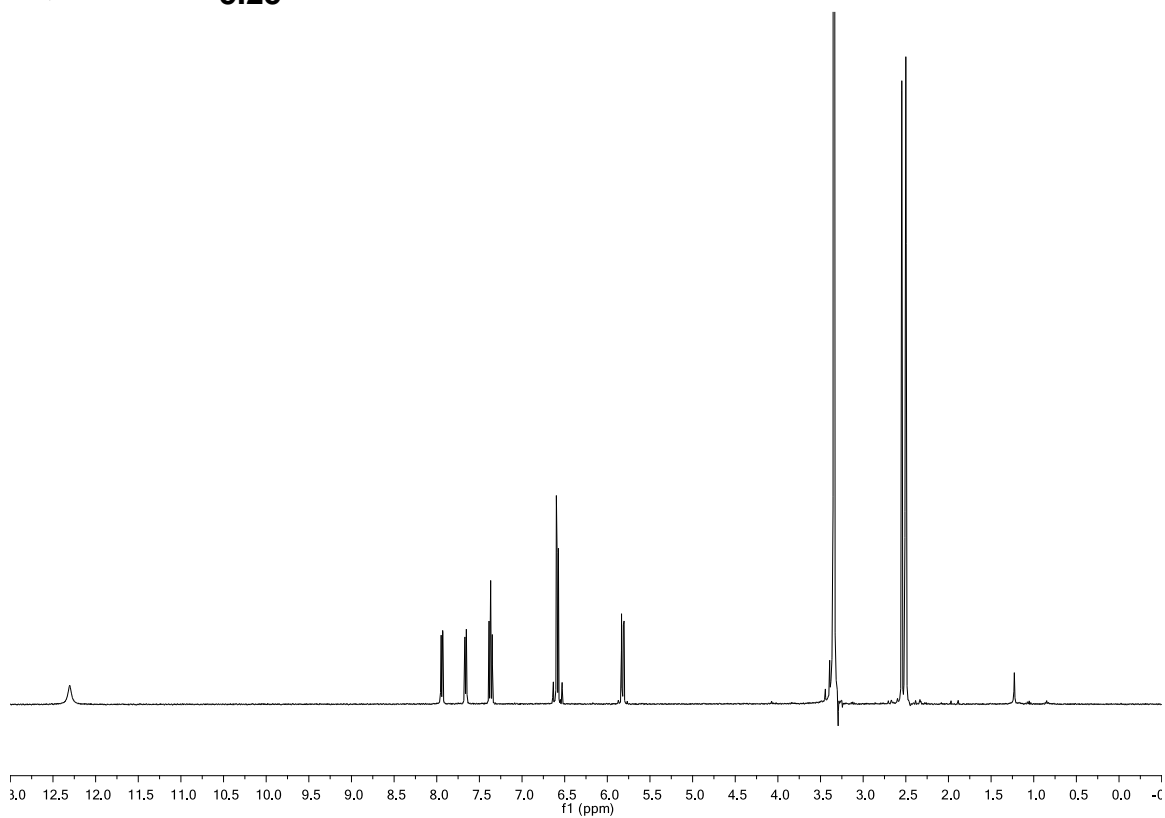
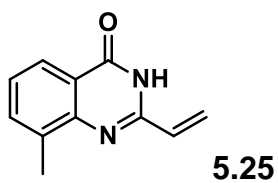
5.23

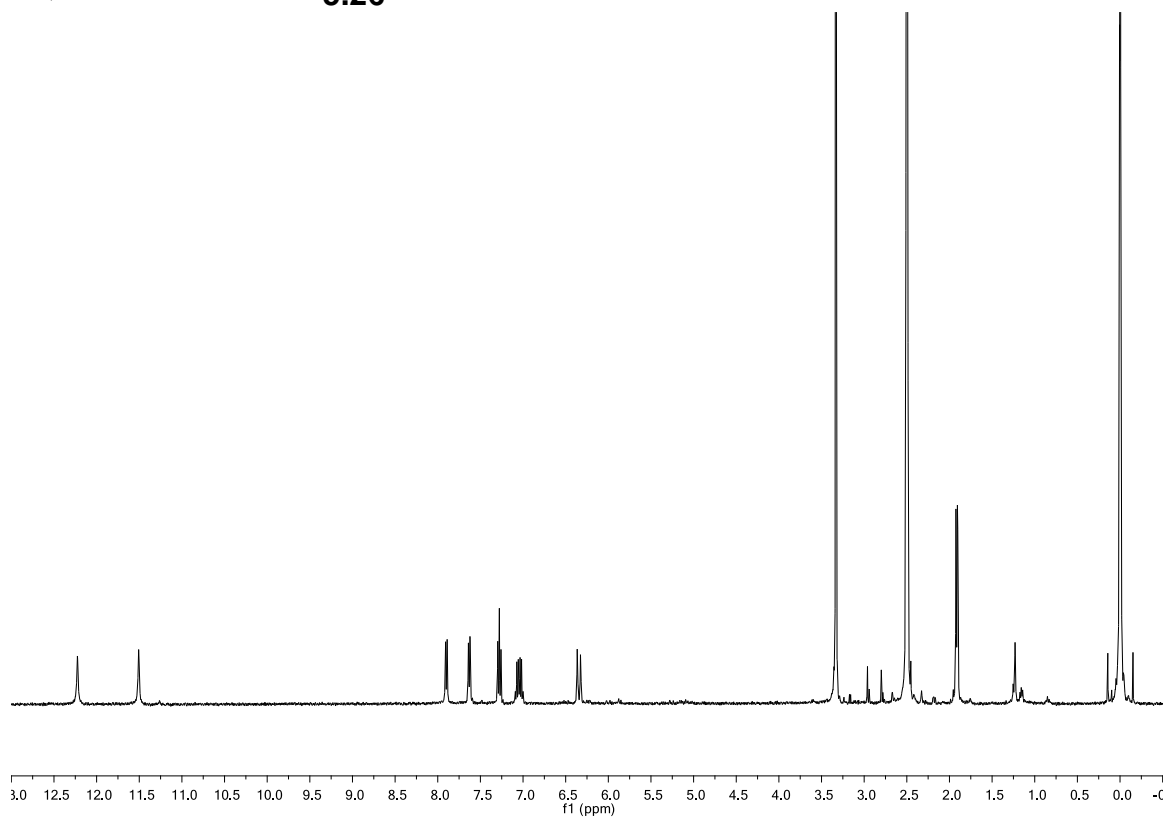
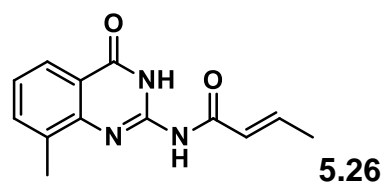


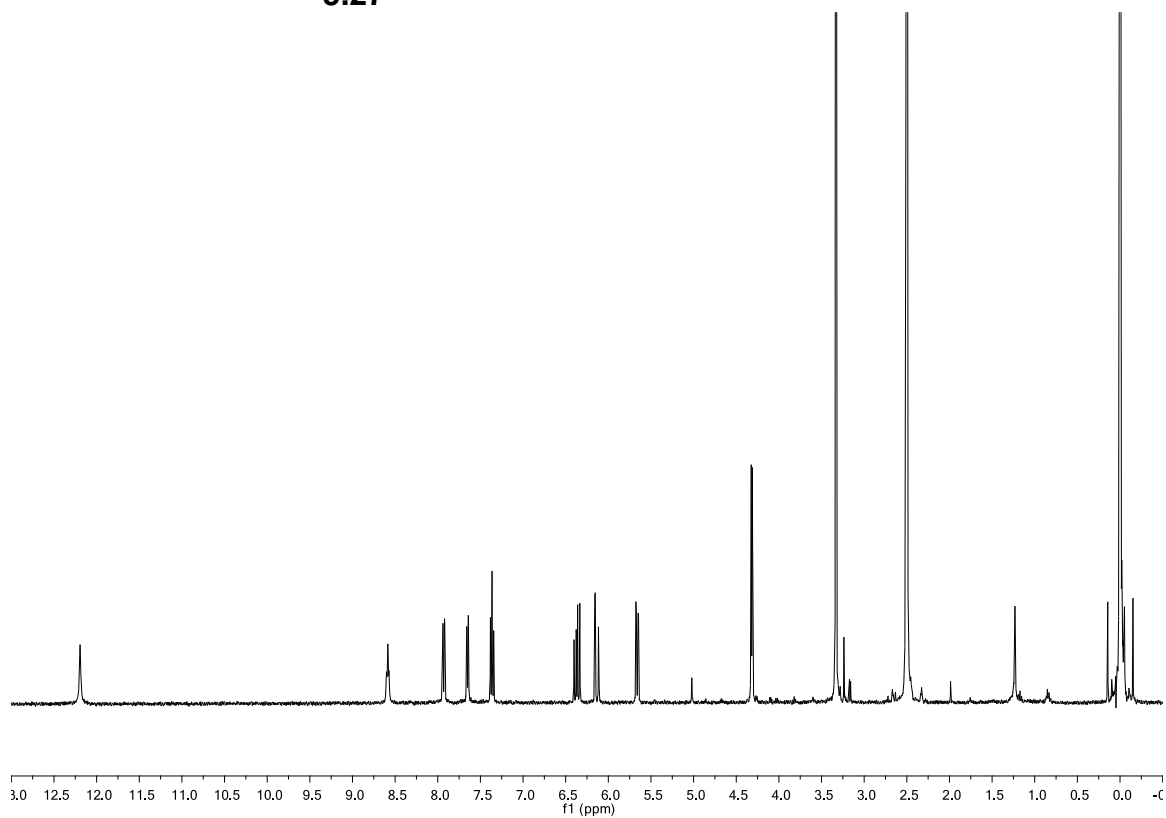
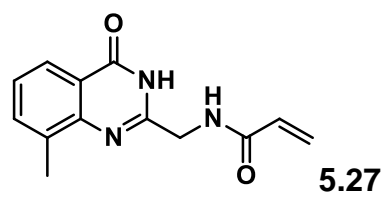


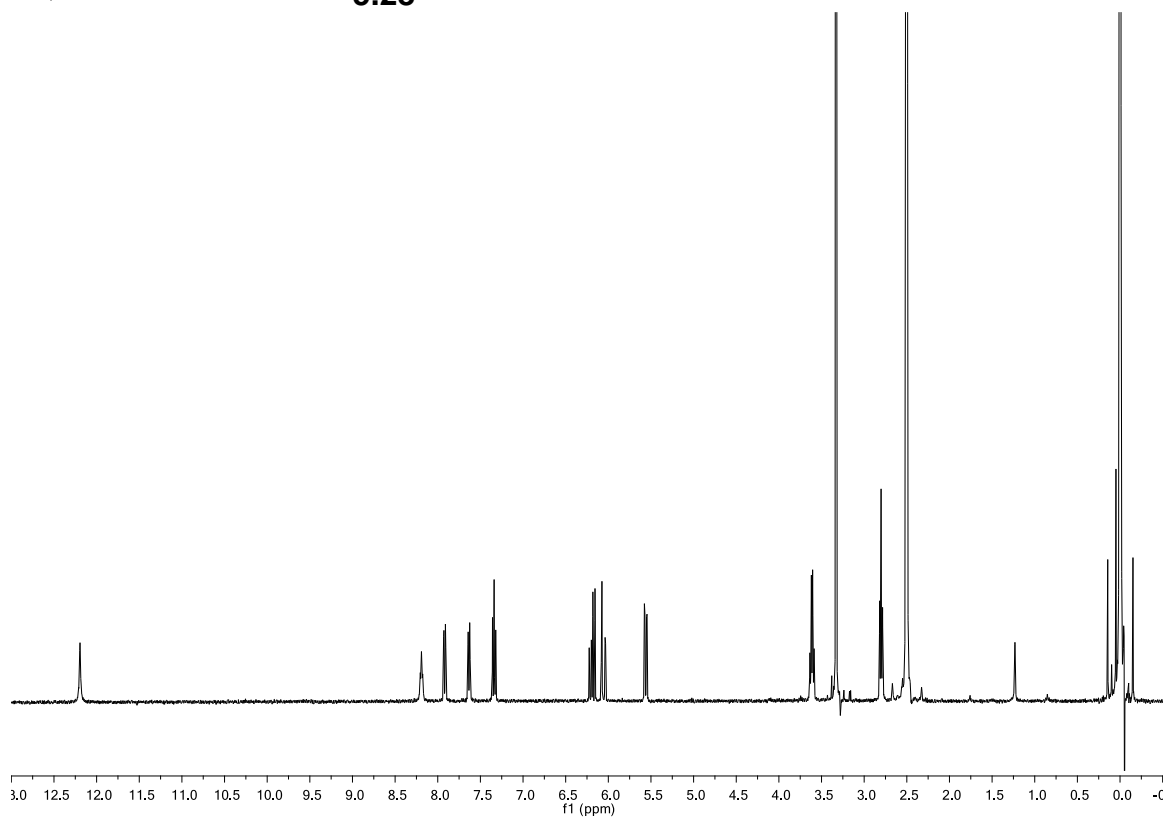
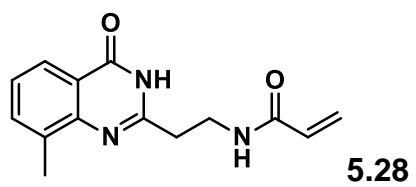
5.24

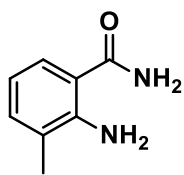




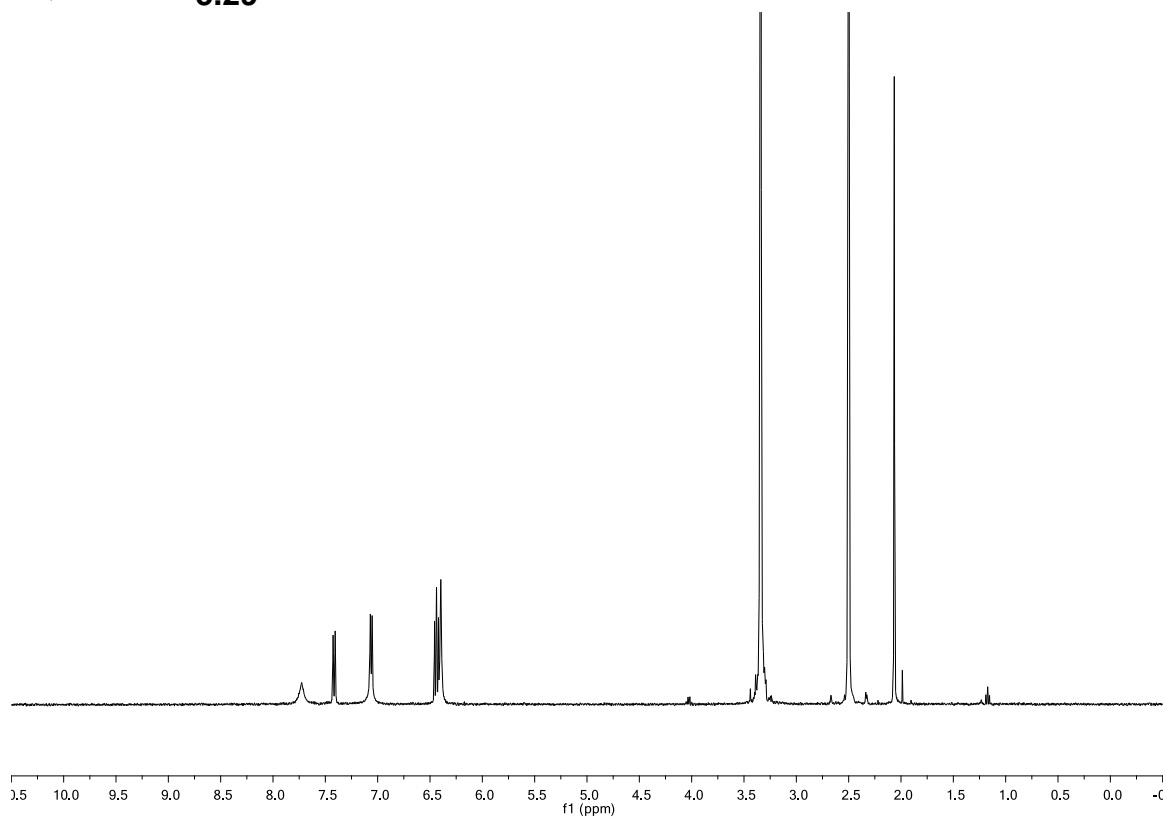


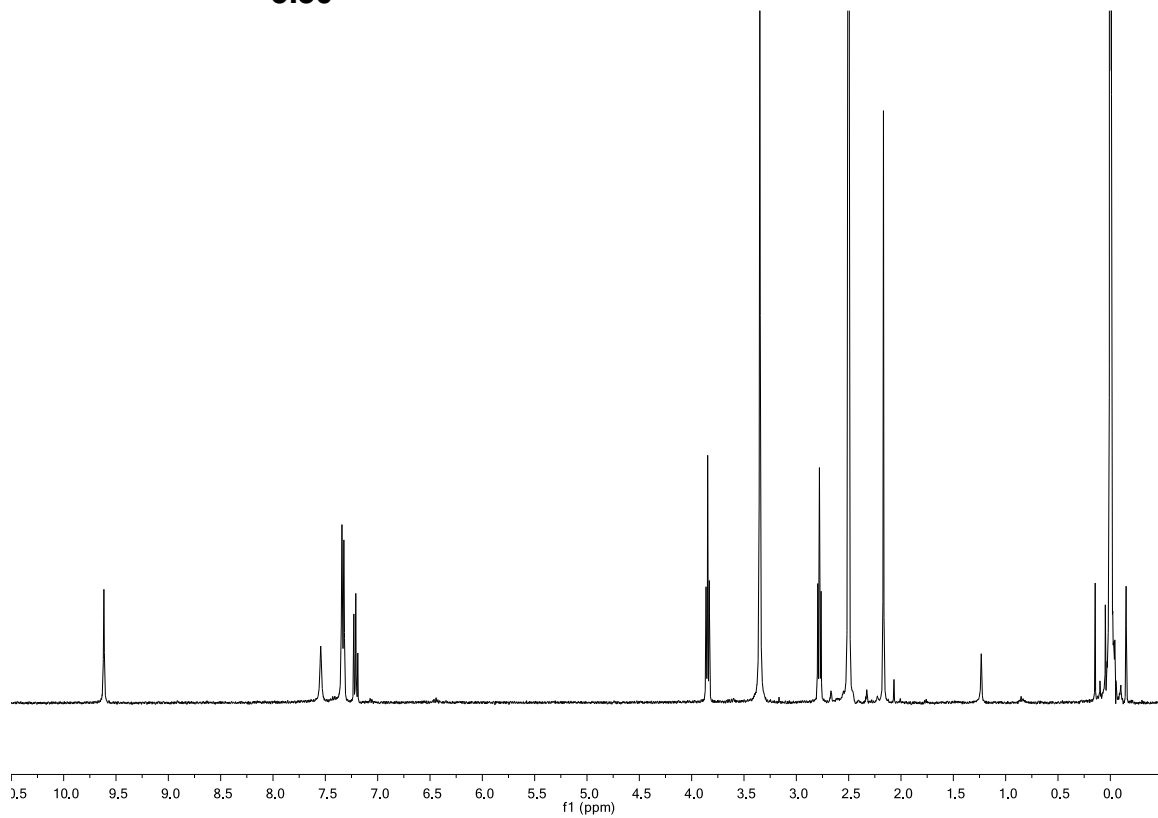
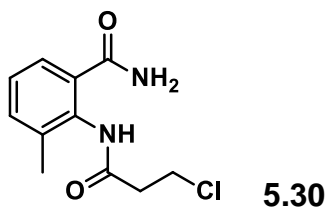


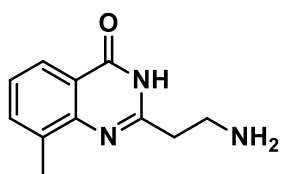




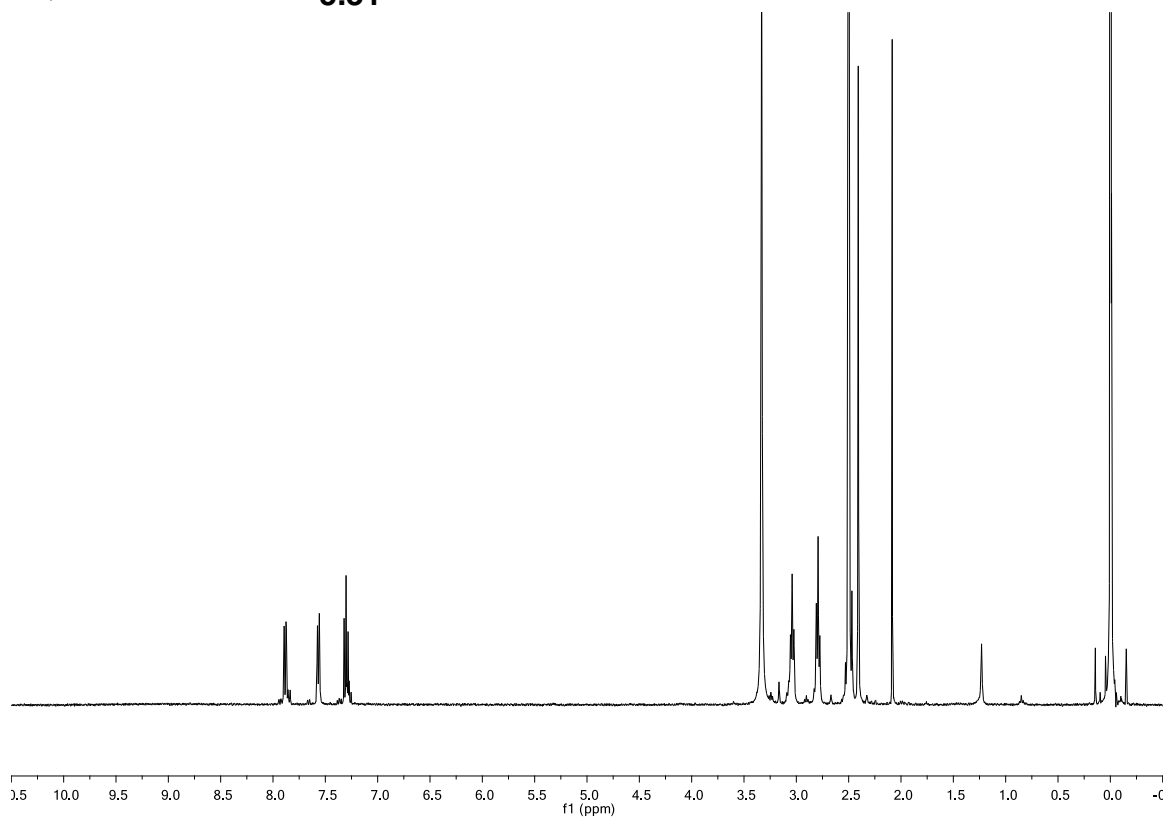
5.29

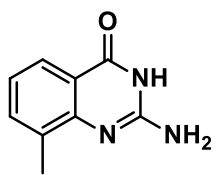




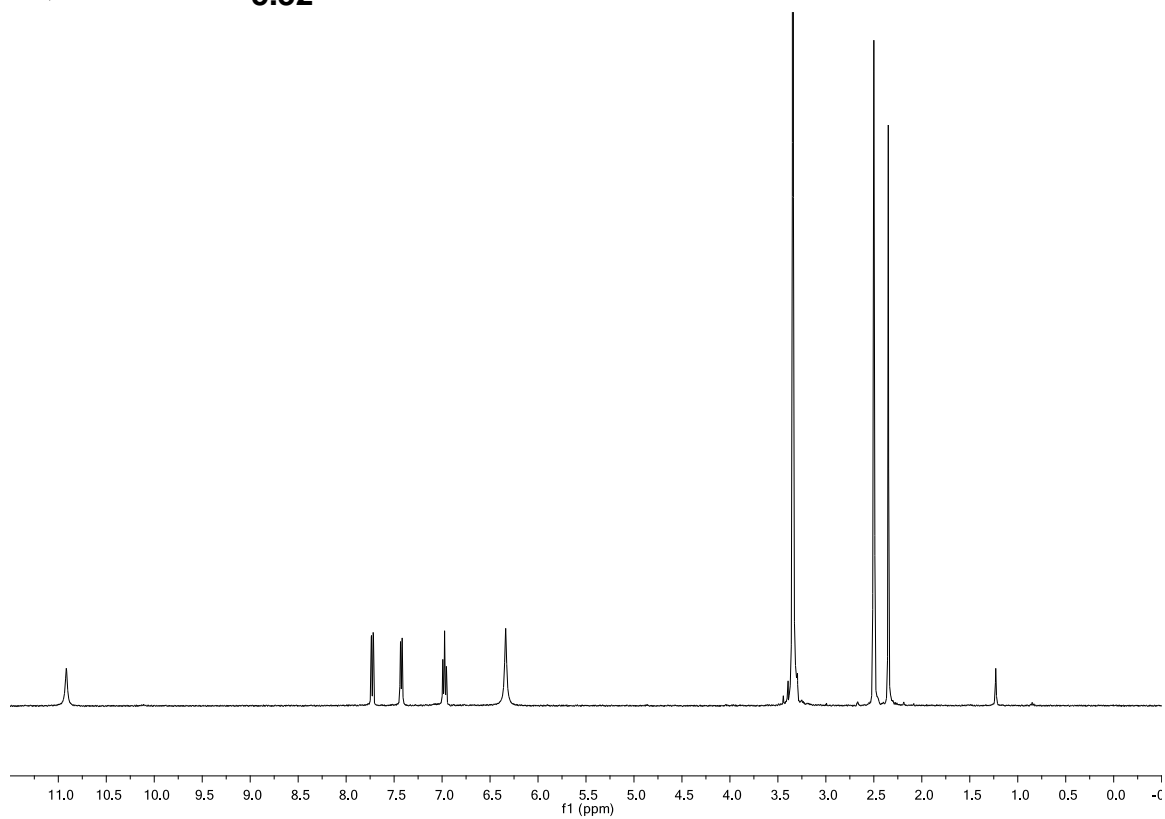


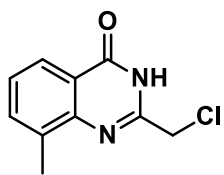
5.31



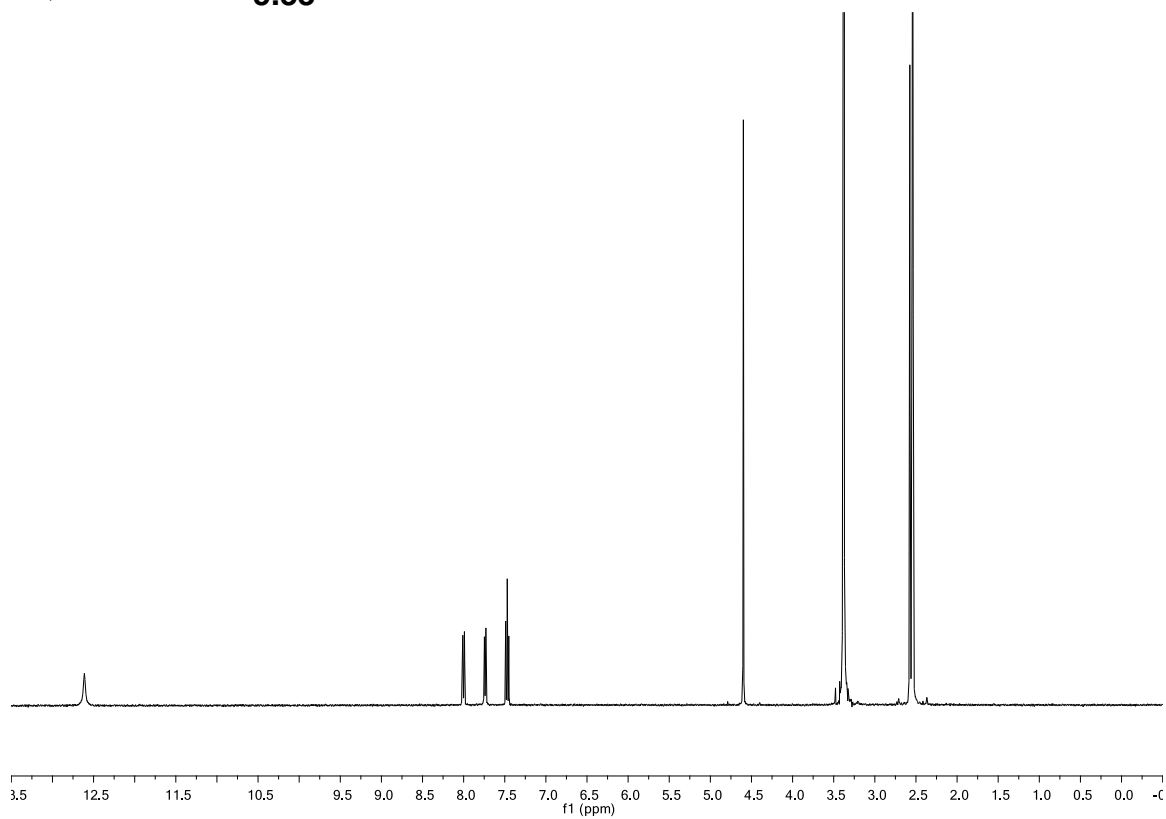


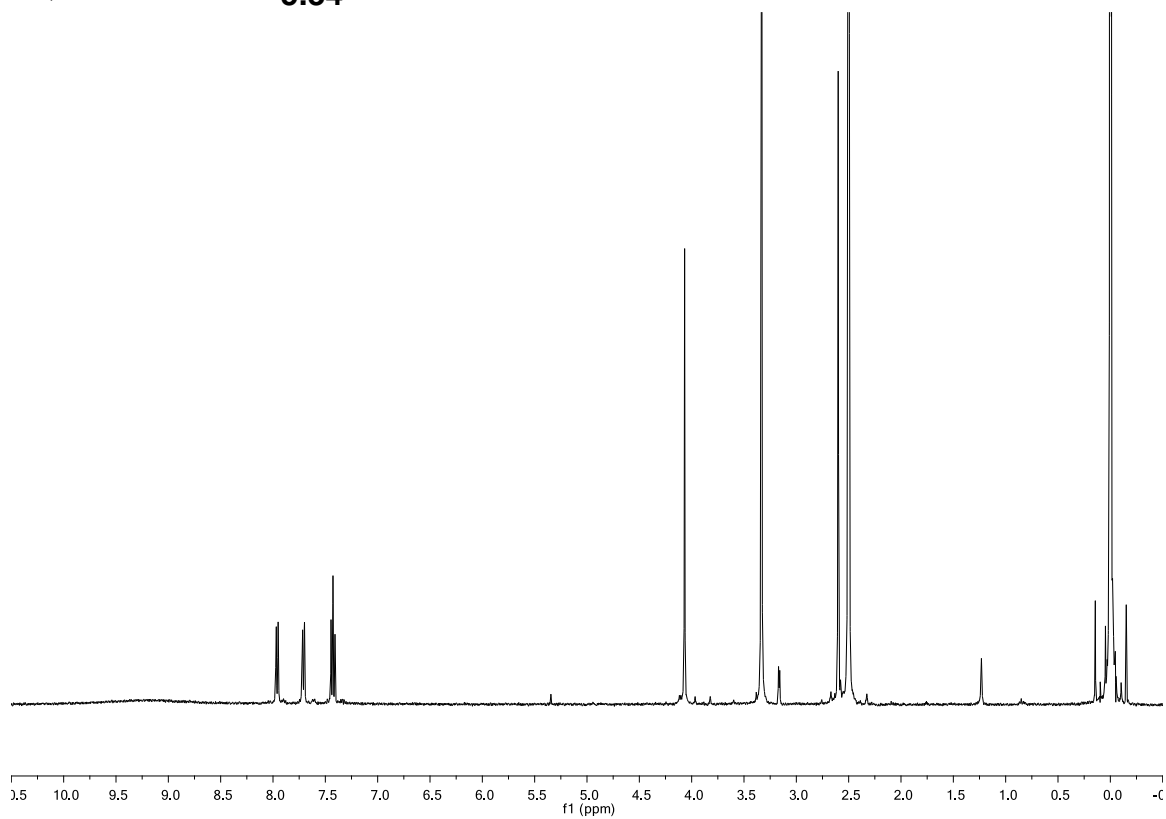
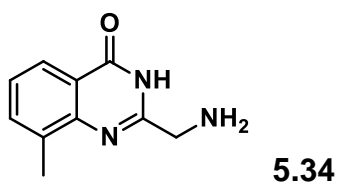
5.32

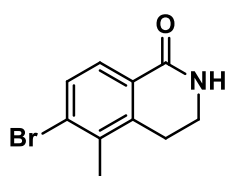




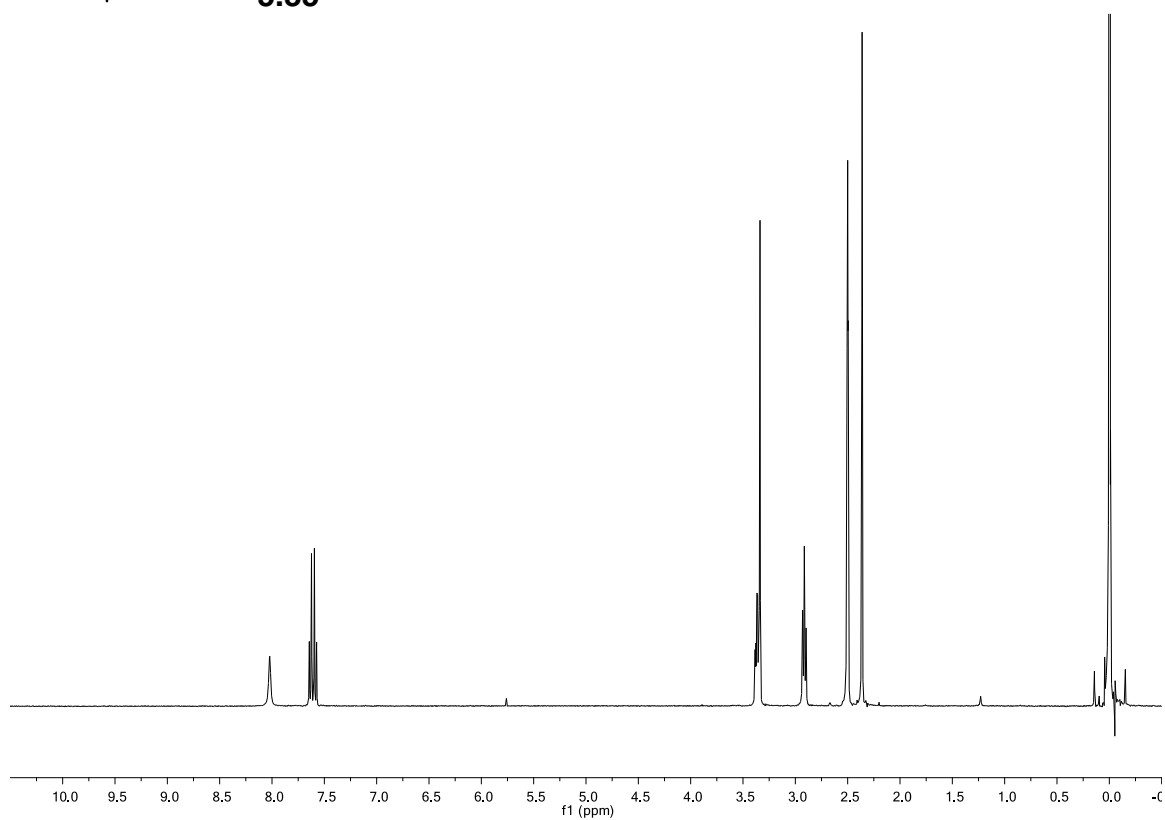
5.33

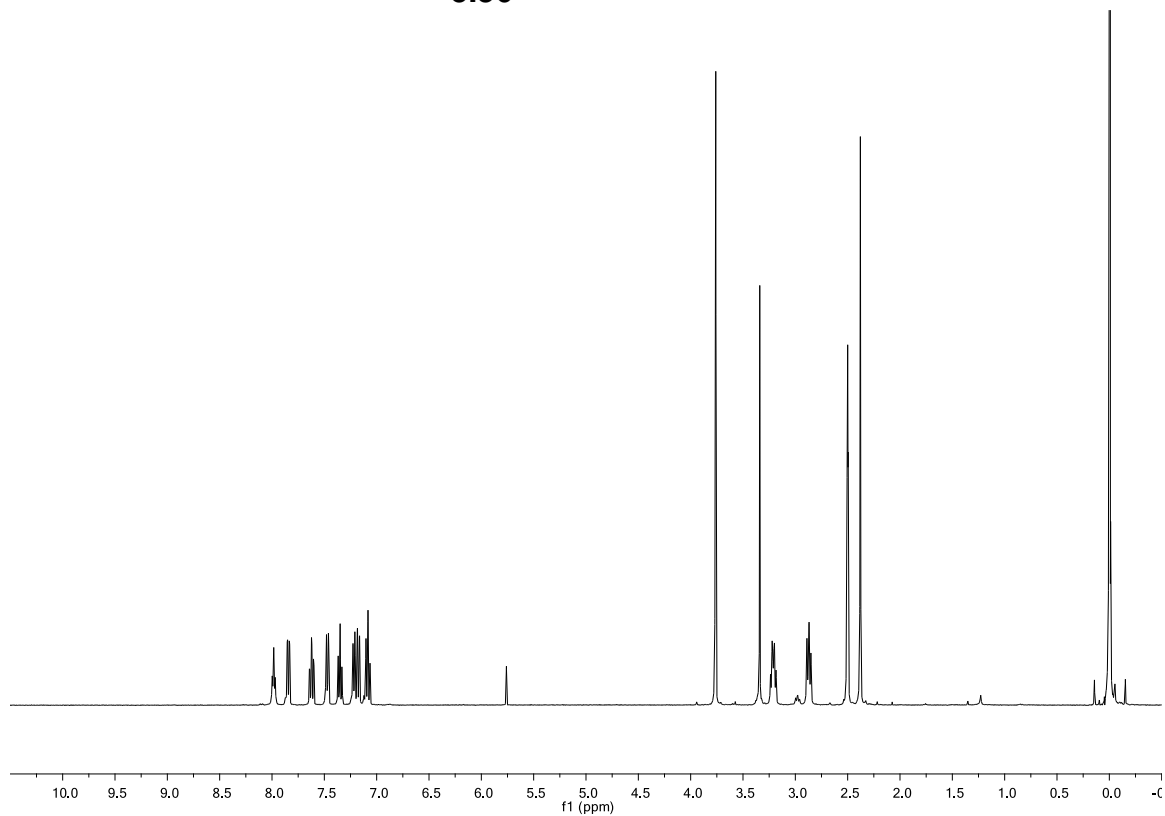
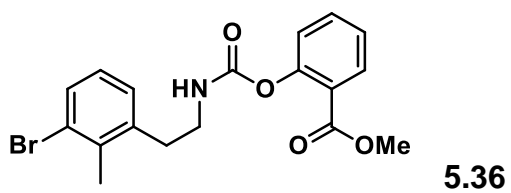


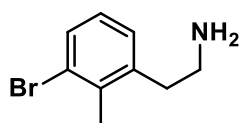




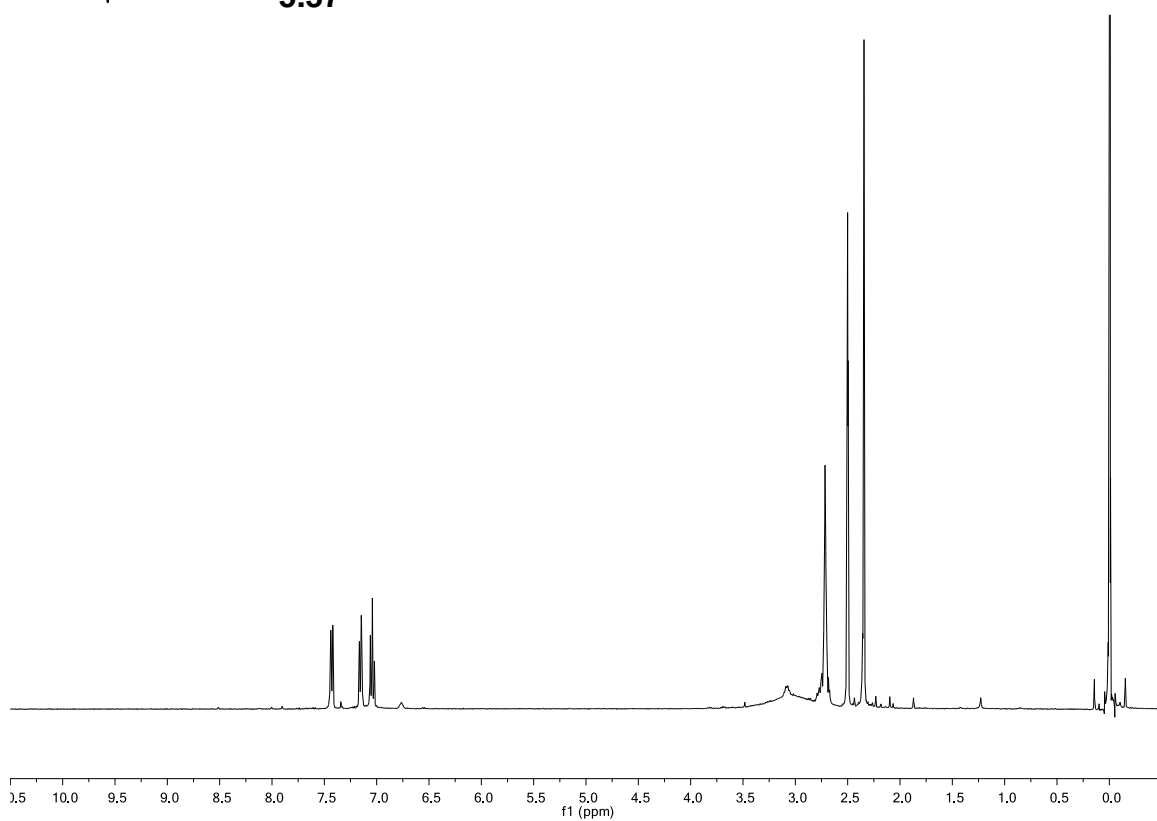
5.35

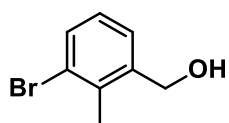




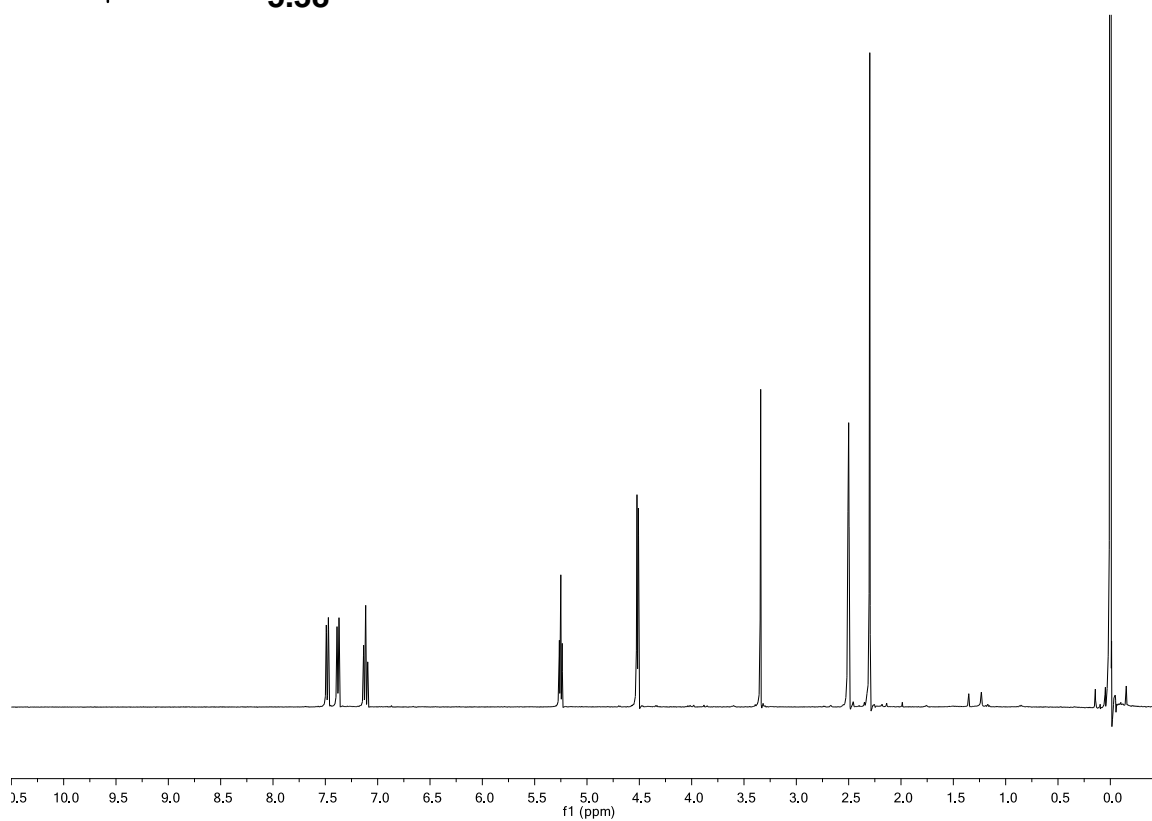


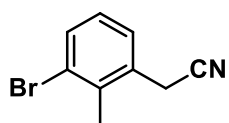
5.37





5.38





5.39

